5-2026

Ontogeny and the Effects of Perinatal Stress in the First Immature Skeleton of Teleoceras aepysoma (Perissodactyla, Rhinocerotidae)

Joe Gajewski

Ontogeny and the Effects of Perinatal Stress in the First Immature Skeleton of *Teleoceras aepysoma* (Perissodactyla, Rhinocerotidae)

A thesis

presented to

the faculty of the Department of Geosciences

East Tennessee State University

In partial fulfillment

of the requirements for the degree

Master of Science in Geosciences

---

by

Joseph A. Gajewski

May 2026

Steven C. Wallace, chair

Joshua X. Samuels

Blaine W. Schubert

Keywords: *Teleoceras*, ontogeny, stress, enamel hypoplasia, growth, subadult, Rhinocerotidae

PLAIN LANGUAGE ABSTRACT

A recently discovered fossil rhinoceros skeleton from the Gray Fossil Site in Tennessee represents the first known immature individual of the species. Comparing the young skeleton with those of adults provides insights into how this extinct animal grew. The present study supports the hypothesis that other rhinos of the same age as the young skeleton are usually of comparable size to adults, typically ~90% of the average adult size. However, the new immature individual from the Gray Fossil Site is considerably smaller than would be expected for its age. Defects found on the teeth, known as enamel hypoplasia, represent periods of severe stress around the time of birth, which is a critical period of bone growth. Such early-life stresses may have slowed or delayed skeletal development, inducing stunted growth and/or reduced size. Other observed abnormalities, such as missing/reduced teeth, may also be attributable to the hypothesized growth complications.

ABSTRACT

Ontogeny and the Effects of Perinatal Stress in the First Immature Skeleton of *Teleoceras aepysoma* (Perissodactyla, Rhinocerotidae)

by

Joseph A. Gajewski

Recovery of an immature fossil rhinoceros (*Teleoceras aepysoma*) skeleton (ETMNH 32999) from the Gray Fossil Site in Tennessee offers the first insights into the ontogeny of the species. ETMNH 32999 is interpreted to be a subadult male in an age class equivalent to ~17-20% of potential lifespan. Comparative analyses support the hypothesis that subadults of related taxa are typically ~91% of average adult size in most dimensions. However, certain cranial dimensions are substantially lower than expected in ETMNH 32999, averaging only ~74% of the average conspecific adult. Such departure from typical growth rates is suggested to be attributable to early-life interruptions in physiological development. Enamel hypoplasia observed on the teeth indicates severe stress during tooth formation, which is proposed to have also disrupted growth during a critical developmental window. The co-occurrence of enamel hypoplasia, reduced dentition, and neotenous skeletal condition suggest a shared etiology.

ACKNOWLEDGEMENTS

I would like to thank my advisor and committee chair, Dr. Steven C. Wallace, for his advice and support, as well as committee members Dr. Joshua X. Samuels and Dr. Blaine W. Schubert for their feedback and encouragement. Thank you to Dr. Luca Pandolfi and Dr. Deng Tao for their assistance in specimen identification. I would like to thank Dr. Matthew Mihlbachler and Dr. Mark Skinner for their helpful conversations and suggestions. A great thanks to Dr. Manon Hullot who offered her expertise in providing valuable information, conversations, and photographs. Thank you to Rachel Narducci and Judy Galkin for providing access to the Florida State Museum and American Museum of Natural History collections, respectively. I would also like to thank Matthew Inabinett for access to the Gray Fossil Site specimens as well as hours of helpful conversations. I extend my thanks to all workers and volunteers of the Gray Fossil Site and Museum for their dedication to excavating, sorting, preparing, and curating the fossils; especially Laura Emmert who dedicated countless hours to the excavation and preparation of "Puddin". I express my gratitude to the Don Sundquist Center for Excellence in Paleontology for research travel funding as well as the East Tennessee State University Department of Geosciences for conference travel funding. Thank you to my family, especially my parents who have supported my career endeavors, and to my cousins, the Isleys, who provided me with lodging when visiting New York City. A great thanks to Skylar Doyle, for her endless support as I pursue my goals. Lastly, I am grateful for the support, comradery, and encouragement of my academic colleagues who saw me through the many ups and downs of this project, and many of whom have become close friends.

TABLE OF CONTENTS

LIST OF TABLES

LIST OF FIGURES

CHAPTER 1. INTRODUCTION

Teleoceras Overview

Teleoceras Hatcher 1894 is a genus of extinct rhinocerotid known from widespread fossil remains and large quarry samples from the Miocene of North America (Prothero 2005). *Teleoceras* lies within the family Rhinocerotidae, but is outside of the subfamily Rhinocerotinae which includes the living rhinoceroses. Rather, *Teleoceras* has been proposed as a member of subfamily Aceratheriinae (Lu et al. 2023a) or Teleoceratinae (Borrani et al. 2025); groups with no extant relatives. *Teleoceras* first appears in the Hemingfordian North American Land Mammal Age (NALMA) (Tedford et al. 2004) as *T. americanum* (Prothero 2005), and its latest occurrence is in the lower Blancan NALMA as *Teleoceras* sp. from the Pipe Creek Sinkhole of Indiana (Farlow et al. 2001), *T. hicksi* from the Ringold Formation of Washington (Gustafson 2012), and *T. aepysoma* from the Gray Fossil Site in Tennessee (Short et al. 2019). First described by Hatcher (1894), the unusual morphology of *Teleoceras* has garnered much interest in its ecology, with the most popular interpretation being that *Teleoceras* lived a semi-aquatic lifestyle comparable to that of the modern *Hippopotamus amphibius* (e.g. Cope 1879; Osborn 1898; Wall and Heinbaugh 1999; Mead 2000; Ward et al. 2024), though this interpretation has been challenged (e.g. MacFadden 1998; Mihlbachler 2001, 2005; Mihlbachler et al. 2004; Clementz et al. 2008; Mallet et al. 2022).

Synapomorphies of *Teleoceras* from Prothero (2005) included: hypsodont teeth, strong antecrochets, loss of dP1/p1, occasional loss of P2/p2, thick cement on teeth, narrow nasals, enlarged premaxilla with I1, broad zygomatic arches, flaring lambdoid crests, barrel-shaped trunk, and lower tusks (i2) that are teardrop-shaped in cross section. Additional generic characters were rejected by Short et al. (2019) with the naming of *T. aepysoma,* including: a

small terminal nasal horn, fused nasals, teleoceratin body proportions, and short, robust limbs. *Teleoceras aepysoma* is distinguished from congeners by its markedly longer forelimb elements, lack of nasal rugosity indicative of nasal horn attachment, unfused nasals, swollen tuberosities superior to the orbits, and slightly exaggerated cranial lengths and widths.

The characters used to define *Teleoceras* species, and many other North American rhinos, would benefit from reexamination, as highlighted by Short et al. (2019). *Teleoceras aepysoma* is not unique in its lack of nasal rugosity, which normally indicates horn attachment; multiple species within the genus have nasal rugosity (or lack thereof) inconsistent with horn attachment in modern rhinoceroses (see Hieronymous et al. 2009). The state of nasal fusion, too, is a poorly defined generic character, as this feature is ontogenetically dependent and variable among *Teleoceras* populations (personal observations), even within the *T. aepysoma* sample. Other species referred to *Teleoceras*, like *T. brachyrhinum*, display characters contrary to the generic diagnoses of Prothero (2005), such as the regular presence of dP1/P1 and flattened, broad nasals. Some *Teleoceras* species are primarily distinguished by the NALMA in which they occur, rather than strong morphological differences (e.g. *T. medicornutum* and *T. major*). Such inconsistencies, among others, highlight the need for reexamination and redefinition of a genus so characteristic of the North American Miocene.

Material of *T. aepysoma* is scarce relative to non-dwarf congeners, as it is currently only known from one locality. Short et al. (2019) described the holotype and paratype specimens in the species' official description. Additional material from the type locality was described by Scaife (2024), and the undescribed remainder mostly consists of fragmentary post-crania. However, recent recovery of partial skeletons with intact crania has enabled a greater

understanding of *T. aepysoma.* Among the new material is ETMNH 33000, a senescent male, and subadult ETMNH 32999, the subject of the present study.

Gray Fossil Site Overview

The Gray Fossil Site (GFS) is a latest Miocene or early Pliocene fossil locality in Washington County, Tennessee, USA. The GFS consists of a series of collapsed sinkholes in the Ordovician-aged Knox Group Limestone infilled by organic-rich, laminated clays (Shunk et al. 2006). Representing the only site of its age in the Appalachian Mountains, the GFS is unique in that it preserves a closed-forest environment, rich in C3 flora and dominated by oak-hickory trees (Wallace and Wang 2004; DeSantis and Wallace 2008; Zobaa et al. 2011; Ochoa et al. 2012). Sedimentological analysis of the clays indicate a calm, anoxic, lacustrine paleoenvironment (Keenan and Engel 2017) in a densely forested setting, supporting a diverse fauna comprised of fish (Woodward 2011; Maden 2023), herpetofauna (Schubert and Mead 2011; Mead et al. 2012; Bourque and Schubert 2015; Jasinski and Moscato 2017; Keenan and Engel 2017; Jasinski 2018; Gunnin et al. 2025a), avifauna (Steadman 2011), and a rich mammalian component including artiodactyls (Doughty et al. 2018; Samuels et al. 2025), glires (Samuels and Schap 2021; Grau-Camats et al. 2025), xenarthrans (McDonald and Wallace 2011), carnivorans (Wallace and Wang 2004; Schubert et al. 2011; Samuels et al. 2018; Bogner and Samuels 2022; Wallace and Lyon 2022), and perissodactyls (Hulbert et al. 2009; Short et al. 2019) including the largest known sample of fossil tapirs (the dwarf *Tapirus polkensis*).

Sedimentary analyses of the GFS have suggested an age range of 6.6 Ma to 4.4 Ma (Odom et al. 2025), while the diverse faunal list has lent itself to biochronologically constraining the age of the site to 4.9 to 4.5 Ma (Samuels et al. 2018), at the boundary of the Hemphillian and Blancan NALMAs. The disappearance of North American rhinos is thought to correlate with the

late Hemphillian (Tedford et al. 2004; Prothero 2005), though some isolated Blancan material of *Teleoceras* challenges this notion (e.g. Madden and Dalquest 1990; Farlow et al. 2001; Gustafson 2012; Samuels et al. 2025). Considering the proposed Hemphilllian-Blancan age, the GFS *Teleoceras* population would be among the latest known occurrences of Rhinocerotidae in North America, rivaled by the Pipe Creek Sinkhole of Indiana (see Farlow et al. 2001; Tucker and Farlow 2025) and the isolated material recovered from the Ringold Formation of Washington (Gustafson 2012).

ETMNH 32999

While rhinocerotids are among the best-studied fossil perissodactyls, little work has been done on immature individuals relative to adults. Preservation biases against juveniles due to their unfused and brittle remains (Klein 1982) likely contribute to this relative scarcity. Disarticulated remains have also contributed to the difficulty in identifying, aging, and describing immature individuals. Nevertheless, immature skeletal material has been discussed for several rhinocerotid taxa. Cranial ontogenetic sequences have been described for *Chilotherium wimani* (Deng 2001), *Teleoceras major*, and the extant rhinoceroses (Hagge 2010). A partial ontogenetic sequence for *Plesiaceratherium gracile* was described by Lu et al. (2023b) and for *Diceros gansuensis* by Deng and Qiu (2007). Dental ontogeny has been documented for *Prosantorhinus* (Böhmer et al. 2015), *Coelodonta* (Garutt 1994; Diedrich 2023) and *Stephanorhinus* (Diedrich 2023). For *Coelodonta antiquitatis,* immature cranial and postcranial remains have been reported (Shpansky 2014; Tong and Wang 2014; Protopopov et al. 2015). Additional immature material has also been reported for *Alicornops simorrense* (Cerdeño and Sánchez 2000), *Acerorhinus yuanmouensis* (Lu 2013; Lu et al. 2021), *Acerorhinus neleus* (Giaourtsakis et al. 2018), *Dicerorhinus cixianensis* (Tong 2012), and *Ceratotherium neumayri* (Geraads and Koufos 1990;

Giaourtsakis et al. 2006). Other studies referencing immature fossil specimens not reported here are listed in Iurino et al. (2020). Regarding the five extant rhinoceroses species, ontogenetic observations have been reported for the black rhino *Diceros bicornis* (Goddard 1970; Hitchins 1978; Hillman-Smith and Groves 1994; Hagge 2010), the white rhino *Ceratotherium simum* (Dittrich 1972; Groves 1972; Hillman-Smith et al. 1986; Hagge 2010), the Indian, or greater one-horned rhino *Rhinoceros unicornis* (Groves 1967; Groves 1982; Laurie et al. 1983; Dinerstein 1991; Dinerstein and Price 1991; Hagge 2010), the Javan rhino *Eurhinoceros sondaicus* (Groves 1982; Groves and Leslie 2011) (recently distinguished from *Rhinoceros* by Nardelli and Heissig 2025), and the Sumatran rhino *Dicerorhinus sumatrensis* (Groves 1967; Groves and Kurt 1972; Hagge 2010; Plair et al. 2012; Roth et al. 2013).

Despite the large samples from quarries across North America, there is scarce data on ontogeny in the North American rhinos. The most comprehensive body of work to date is the unpublished thesis of Hagge (2010), comparing the craniomandibular ontogeny of *Teleoceras major* to the extant rhinoceroses. Within *Teleoceras*, only immature *T. major* specimens have been formally described, due to the pristine state of preservation (articulated, complete, to nearly complete, skeletons) from Ashfall Fossil Beds (AFB) in Antelope County, Nebraska, USA (see Voorhies and Stover 1978; Voorhies and Thomasson 1979; Voorhies 1985). Remains of other *Teleoceras* species are almost always found disarticulated or isolated (Prothero 2005), prohibiting most analyses of post-crania relative to age, but there are enough well-preserved crania in museum collections to document cranial ontogenetic size changes in several other species. A full multi-specific analysis is beyond the scope of this thesis, though here an attempt is made to contribute to filling the literary gap on ontogenetic size changes in fossil rhinocerotids.

Recovery of a partial immature skeleton (ETMNH 32999) from the GFS (Figs. 1-3) has made it possible to compare ontogenetic changes in *Teleoceras aepysoma* with other rhinocerotids. Until the discovery of ETMNH 32999, the GFS *Teleoceras* sample was known only from adult males, including two nearly complete skeletons (ETMNH 609 and 601), a partial skeleton (ETMNH 19280), and isolated elements including mandibles and incisors. Additional postcranial and fragmentary material not assignable to sex has also been recovered, but most of it appears to belong to adult individuals, save for an isolated fetal hindlimb (ETMNH 19025) and a lightly worn dP4-M1 pair (ETMNH 37999). As of 2023, the minimum number of individuals (MNI) for the GFS *T. aepysoma* sample was reported to be 8 based on the juvenile elements and left astragali of adults (Haugrud 2023), though this number continues to increase as yearly excavations continue. ETMNH 32999 is unique among the GFS *Teleoceras* sample for its relatively reduced cranial lengths and widths, unfused longbone epiphyses, and dental features including: absent P2s, abnormally small p3s, reduced dental widths, retention of deciduous premolars, poorly developed tusks, and enamel hypoplasia on the cheek teeth. Of the most interest, the cranium of ETMNH 32999 displays a rather neotenous condition relative to its dental age, possibly of pathological origin or attributable to other developmental abnormalities.

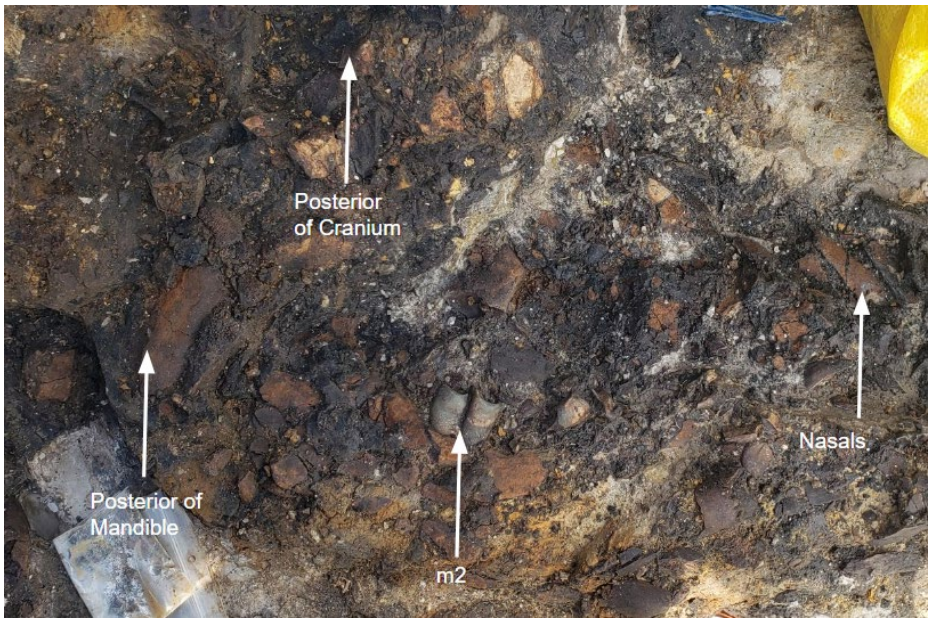

Fig. 1 ETMNH 32999 *in situ* at the Gray Fossil Site Note that the more poorly preserved right side of the cranium is exposed, while the more complete left side remains uncovered in this image. White arrows and text indicate identifiable anatomical landmarks. Photograph courtesy of Laura Emmert.

Fig. 2 Left lateral view of the skull of ETMNH 32999. Note the presence of archival foam between the upper and lower tooth rows to prevent damage from occlusion. Reconstructed areas are represented by white/translucent filler. Note that the premolars in the maxillary crypt, P3 and P4, were removed during preparation and were replaced by replicas. M3 was also removed from the mandible during preparation. Scale bar = 10cm.

ETMNH 32999 is rather poorly preserved when compared with other GFS rhino material, especially relative to the nearly complete holotype and paratype skeletons. This differential preservation is attributable to several factors. From a biological perspective, the unfused/thinner bones of immature individuals face an inherent taphonomic bias, where they are less likely to be preserved than the more robust bones of adults (Klein 1982). From a geological perspective, ETMNH 32999 was found within oxidized layers of the GFS sediments (Fig. 1), where preservation tends to be the poorest. Better preservation seen in other GFS skeletons is largely attributable to their deposition in anoxic conditions, likely at the bottom of the sinkhole pond. Conversely, ETMNH 32999 was recovered from layers where the fine lacustrine clay is interbedded with coarser sediments, suggesting ETMNH 32999 may have been deposited in a shallower part of the pond (see Haugrud 2023). There, ETMNH 32999 could have been exposed to more taphonomic processes like scavenging and more extreme weathering. As a result, the skeleton is more incomplete/damaged than those found elsewhere in the GFS sinkhole pond where taphonomic biases may have been reduced or minimal. ETMNH 32999 is best preserved on its left side; many right-side elements are absent or more severely weathered than their left-side counterparts.

Currently recovered elements of ETMNH 32999 (Fig. 3) include the following: a partial cranium, mostly complete on the left side; complete left maxillary tooth row (dP2-M3) and unerupted P3 and P4; a partial right tooth row (dP2-dP3) with unerupted P3 and M3; both premaxillae; left occipital condyle; palatine fragments; hyoid fragments; a complete mandible with both tooth rows (dp3-m3) and unerupted p3s and p4s; vestigial i1 fragments; partial crowns of both i2s; right humerus with a damaged proximal epiphysis and articular head; both right and left radii and ulnae each with unfused epiphyses; carpal elements (left and right cuneiform, lunar,

scaphoid, unciform, trapezoid; left pisiform); left metacarpals II, III, and IV, each with unfused distal epiphyses; right metacarpals II and III with unfused distal epiphyses; manual proximal and distal phalanges, both medial and lateral; various sesamoids, some associated with the manus; unfused distal epiphysis of right fibula; right patella; right astragalus, left metatarsals II and IV with unfused distal epiphyses; two partial thoracic vertebrae; several rib fragments.

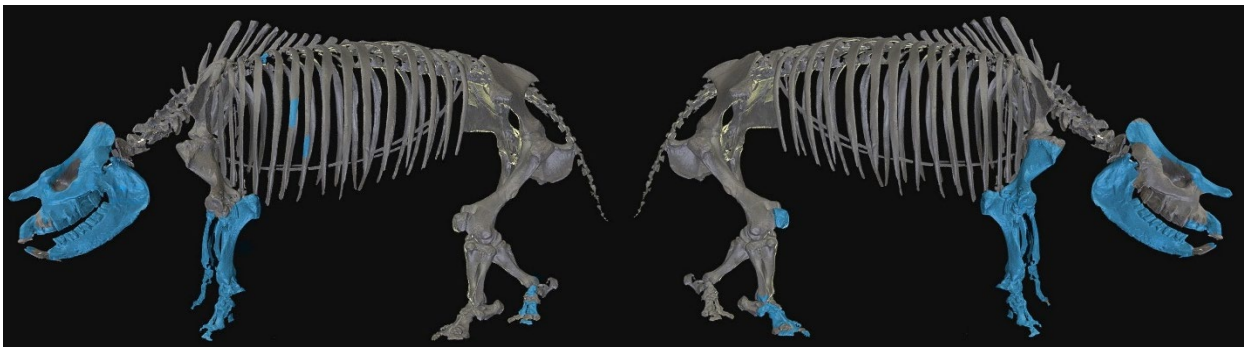

Fig. 3 Currently recovered elements of ETMNH 32999. 3D model of ETMNH 609, *Teleoceras aepysoma* holotype in left (left) and right (right) lateral views, with currently recovered elements of ETMNH 32999 highlighted in blue. Note that the placement of the rib fragments and partial thoracic vertebrae are speculative. Model image courtesy of Gray Fossil Site and Museum on Sketchfab.

Enamel Hypoplasia Overview

Enamel hypoplasia (EH) is a dental defect that indicates a period of nonspecific stress during dental development (Goodman and Rose 1990). Because enamel does not reform throughout life as bone does, hypoplastic defects serve as permanent markers of interruptions in amelogenesis (i.e. enamel secretion) and are used to signify periods of severe physiological stress during tooth formation. Ameloblasts, responsible for enamel secretion, are particularly sensitive to metabolic disruptions, so periods of stress during tooth formation are represented as sections of thin, wavy, or missing enamel, where the ameloblasts struggled or failed to produce normal enamel (Sarnat and Schour 1941; Suckling 1989; Goodman and Rose 1990). Most commonly, EH manifests as linear furrows, grooves, or pits in the enamel. EH is best documented in humans (e.g. Sarnat and Schour 1941; Goodman et al. 1980, 1992; Goodman and

Rose 1990; Goodman and Song 1999; among many others) and other primates (e.g. Lukacs 2001, 2009; Skinner and Newell 2003; Chollet and Teaford 2010; Towle and Irish 2019), but has also been identified in ungulates such as suids (Dobney and Ervynck 2000; Skinner et al. 2014, 2019), giraffids (Franz-Odendaal 2003, et al. 2004), bovids (Niven et al. 2004; Upex and Dobney 2012; Barrón-Ortiz et al. 2019), notoungulates (Braunn et al. 2014), equids (Barrón-Ortiz et al. 2019), tapirs (Bacon et al. 2015), and rhinocerotids (Bratlund 1999; Mead 1999; Antoine et al. 2012; Bacon et al. 2015; Fourvel et al. 2015; Roohi et al. 2015; Böhmer and Rössner 2018; Hullot et al. 2021, 2022, 2023, 2024; Hullot and Antoine 2022).

In investigating probable explanations for the small cranium of ETMNH 32999, Dr. Matthew Mihlbachler (personal communication 2025) suggested that the specimen be examined for physiological signals of growth arrest that may explain the observed size disparity. In analyzing *Teleoceras proterum* assemblages from Florida, Mihlbachler (2005) hypothesized that the relatively reduced sexual size dimorphism observed in *T. proterum*, relative to Great Plains congeners (e.g. *T. medicornutum*: Voorhies 1990; *T. major*: Mead 2000), was possibly attributable to increased ecological pressures on growing males, where they may have been precluded from optimal resources via intraspecific pressures from dominant males. Dinerstein (1991) made similar hypotheses about reduced body size in wild males of the extant *Rhinoceros unicornis*. To this point, Mihlbachler (2005) hypothesized that EH, a dental defect suggesting periods of metabolic upset, observed among the *T. proterum* sample may be indicative of such stress on the population that inhibited the achievement of larger size, though a stress that would have occurred too early in life to be accounted for by competition. Reduced size/delayed growth has also been observed among captive mammals and has been linked to poor nutrition or otherwise inadequate conditions (i.e. nonspecific stress) (e.g. Groves 1966; Dressino and

Pucciarelli 1997; Wielebnowski 2003); most notably, this has been documented in Asian rhinos (Groves 1982). This hypothesized link between reduced body size/delayed growth, EH, and physiological stress warrants the present investigation into the relatively reduced size of ETMNH 32999.

Considering the relatively small size of the cranium of ETMNH 32999 illustrated in the following sections, the correlation between physiological stress and reduced size documented in rhinos (e.g. Groves 1982; Dinerstein 1991; Mihlbachler 2005) is of particular interest. The occurrence of EH on ETMNH 32999 indicates a period of severe physiological stress during tooth formation; pressure that may have been great enough to inhibit skeletal development, leading to its relatively small dimensions. The same disruption may have induced additional abnormalities, including substantial reduction of the anterior premolars and reduced dental widths. Here, the EH on ETMNH 32999 is described in detail and is compared with EH seen on other subadult rhinos. The possible causes of physiological stress are explored, and hypotheses are made about the link between EH-inducing stress and growth arrest in ETMNH 32999.

Accounting for Sexual and Taxonomic Differences

Sexual Dimorphism

Skulls without mandibles are difficult, if not impossible to sex for most rhinocerotid taxa. As a result, the data collected for each age class is sex combined. While this could be troubling in documenting ontogenetic size changes in sexually dimorphic taxa, the small-scale variation in size caused by sex differences is expected to be superseded by the larger-scale ontogenetic size changes. Furthermore, cranial measurements are often conservative in their dimorphism compared to postcranial measurements, at least among *Teleoceras* (Mead 2000; Mihlbachler 2003). Prothero (2005) stated that while size dimorphism is occasionally present among North

American rhinocerotids, it is usually not pronounced enough to warp interpretations. The dimorphism of the AFB *T. major* sample (Mead 2000) is said to be outstanding relative to other rhino samples, including those of other *Teleoceras*, so there is evidently plasticity in size dimorphism within the genus (Mihlbachler 2003). Contrastingly, cranial measurements are rather dimorphic in the fossil species *Menoceras arikarense* (Mihlbachler 2007), though this species has exceptional sexual dimorphism relative to other rhinos and is likely a special case. Gerhold (1992) noted some size differences between males and female *T. fossiger* in cranial length and zygomatic width, but these differences are slight when compared to dimorphism in the mandible, as well as dimorphism in the forelimbs as documented by Voorhies (1990) for *T. fossiger* and *T. medicornutum*. In summary, while dimorphism in cranial dimensions is present among select fossil rhinocerotids, it is typically minute compared to the sexual differences in the mandible and forelimbs. Here it is assumed that minor sexual differences in cranial dimensions are superseded by larger-scale ontogenetic trends.

Among polygynous mammals, sexual size dimorphism is best expressed in mature individuals that continue to exaggerate their craniomandibular dimensions beyond the attainment of sexual/skeletal maturity, such as hippopotamuses (Fidalgo et al. 2025) and walruses (Dierickx et al. 2025); the same pattern is observed in the Sumatran rhinoceros *Dicerorhinus sumatrensis* (Groves and Kurt 1972) and white rhinoceros *Ceratotherium simum* (Groves 1972), where size dimorphism in juvenile or subadult individuals is usually not strongly expressed relative to full adults. Even among extant rhinos which display sexual dimorphism, size dimorphism is typically not very apparent before the onset of adulthood (Hillman-Smith et al. 1986; Dinerstein 1991; Plair et al. 2012). There is some evidence that dimorphism is apparent in the Indian rhinoceros, *Rhinoceros unicornis,* just before the onset of maturity (Dinerstein 1991), but these differences

are related mostly to horn and incisor sizes rather than body size. Among sexually dimorphic fossil rhinocerotids, *Chilotherium wimani* has dimorphism in some cranial dimensions and shapes in adulthood, but cranial length and zygomatic width are not pronounced among these (Deng 2001; Chen et al. 2010), nor are the dimorphic differences readily apparent before maturity (Deng 2001). Among growing *Teleoceras*, dimorphism is most apparent not in size, but in the timing of developmental milestones like tusk eruption (Mihlbachler 2005) or epiphyseal fusion (Mead 2000).

Taxonomic Debates

Many fossil rhinos are a subject of taxonomic contention, including several species included in this study. For example, Borrani et al. (2025) suggest *Aphelops* and *Peraceras* are paraphyletic, and Kampouridis et al. (2023) suggest the same for *Chilotherium*, specifically in the case of *Ch. wimani*. Personal observations suggest potential paraphyly for *Teleoceras* in *T. brachyrhinum*. The rhinocerotine remains recovered from Samos Island, Greece, reported here as *Ceratotherium neumayri*, are a subject of much taxonomic debate (e.g. Koufos et al. 1997; Geraads and Koufos 1990; Giaourtsakis 2021, et al. 2006), as the locality has produced two sympatric two-horned species, *C. neumayri* and *Dihoplus pikermiensis*. *C. neumayri* has been proposed to belong to its own genus, *Miodiceros* (Giaourtsakis 2021), though was recently recovered as sister taxon to the extant *Ceratotherium simum* by Borrani et al. (2025). The specimens examined here are referred to *C. neumayri* partially based on comparisons with *C. neumayri* reported in literature, as well as the distinctions made by Giaourtsakis et al. (2006). It is important to note each of these taxonomic distinctions in making interspecies comparisons, though minor inconsistencies should not greatly influence results as many growth trends observed appear to be consistent across Rhinocerotidae.

Objectives

The goals of the present study are to (1) describe the morphology of ETMNH 32999 in comparison to conspecific adults from the GFS, (2) compare ontogenetic size changes in *Teleoceras aepysoma* with other rhinocerotids, (3) hypothesize about the etiologies of the observed abnormalities in ETMNH 32999 (i.e. reduced anterior dentition, neotenous/stunted skeletal condition, enamel hypoplasia).

CHAPTER 2. MATERIALS AND METHODS

Measurements

Measurements were taken by a single individual with digital calipers to the nearest hundredth of a millimeter. Measurements were taken thrice, and then averaged, to reduce the possibility of error. Damaged, incomplete, or otherwise unstable specimens prevented some measurements from being taken. A digital camera (iPhone 12 rear camera, 12-MP wide-angle lens, f/1.6) was used to photograph specimens. Measurements were documented in Microsoft Excel. Plots were created in Microsoft Excel and were edited in Krita Image Editor. Krita Image Editor was also used to create figures.

Several plots refer to "percentage of average adult" data rather than raw measurements (e.g. Figs. 77, 79, 81, 83, 85, 87). These values refer to the ratio of a given measurement against that of the average conspecific adult for each respective taxon. Measurements for average adults were calculated from the measurements of all individuals $\geq$ Hitchins' (1978) age class XI, considered here to represent mature adults. At this age, the third molar is in occlusion, and sexual maturity, skeletal maturity, and asymptotic/adult size have all typically been achieved, at least in extant species (Groves 1972; Groves and Kurt 1972; Laurie et al. 1983; Hillman-Smith et al. 1986; Hillman-Smith and Groves 1994; Groves and Leslie 2011). Some average adult values, particularly those for the North American rhinoceroses, were taken from Prothero (2005) if available. Craniomandibular measurements (Figs. 4-5) were taken following Guérin (1980), Prothero (2005), and Hagge (2010), and postcranial measurements (Figs. 7-9) followed Prothero (2005) and Short (2013).

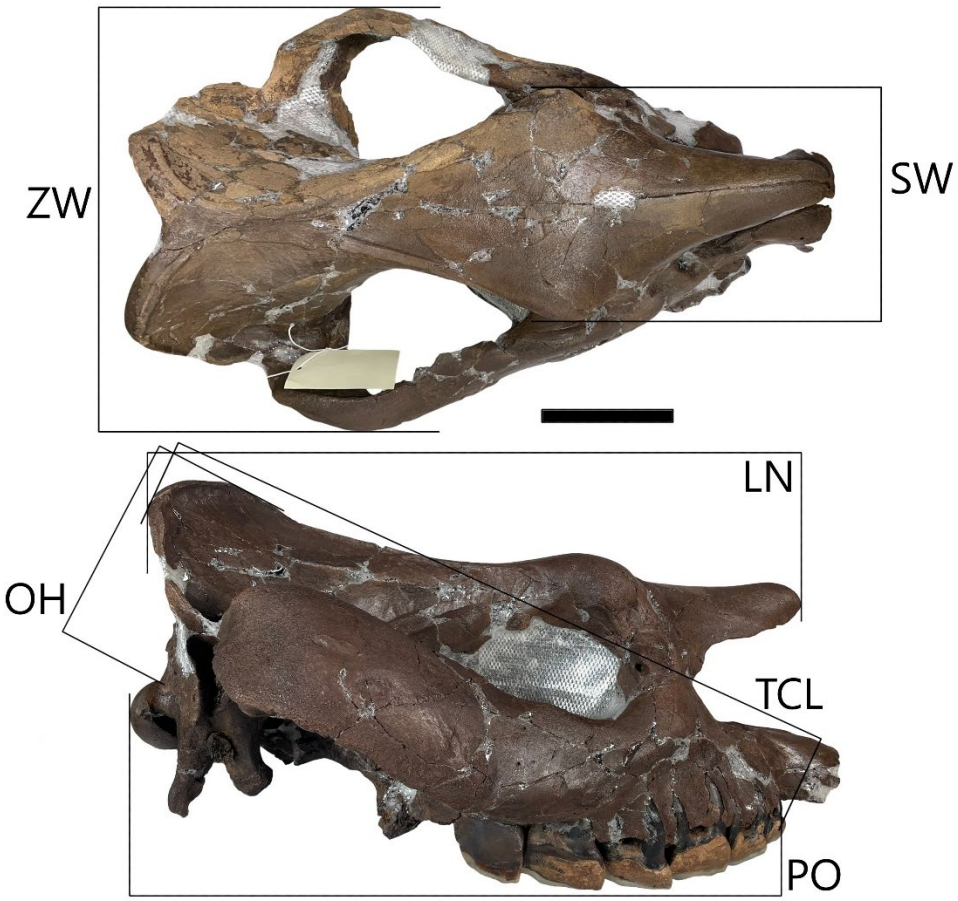

Fig. 4 Cranial measurements used. Measurements are illustrated on the cranium of ETMNH 601, *Teleoceras aepysoma* paratype in (top) dorsal view and (bottom) right lateral view. See "Abbreviations and Nomenclature" subheading for abbreviations. Scale bar = 10cm.

The lambdoid crest was chosen as the posterior landmark for total cranial length (TCL) and the anterior landmark is the crown base of the anteriormost premolar (Fig. 4). Lambdoid crest to nasal tip (LN) and anterior premolar to occiput (PO) measurements were taken for direct comparisons with the same measurements from Prothero (2005). LN measures the anterior tip of the nasals to the posterior extent of the lambdoid crest (Fig. 4). PO measures from the anterior crown base of the anterior premolar to the posterior of the occipital condyle (Fig. 4); in Prothero (2005), this is defined as "P2 to occiput", but the present study also accounts for taxa which

retain a first premolar. PO may be reported as “Basal Length” measurements reported in the literature (e.g. Goddard 1970; Hillman-Smith et al. 1986).

Supraorbital width (SW) and zygomatic width (ZW) measurements (Fig. 4) were taken to examine the growth trajectories in these features relative to other cranial dimensions. Both measurements correspond to notable features of *Teleoceras aepysoma*; the swollen supraorbital boss typical of adults, and the exaggerated zygomatic width relative to congeners (see Short et al. 2019), respectively. SW measures the greatest width of the dorsal skull, from the lateral edge of each frontal supraorbital tuberosity. ZW measures the widest breadth of the skull, from the most laterally extended point of the posterior zygomatic arches (Fig. 4).

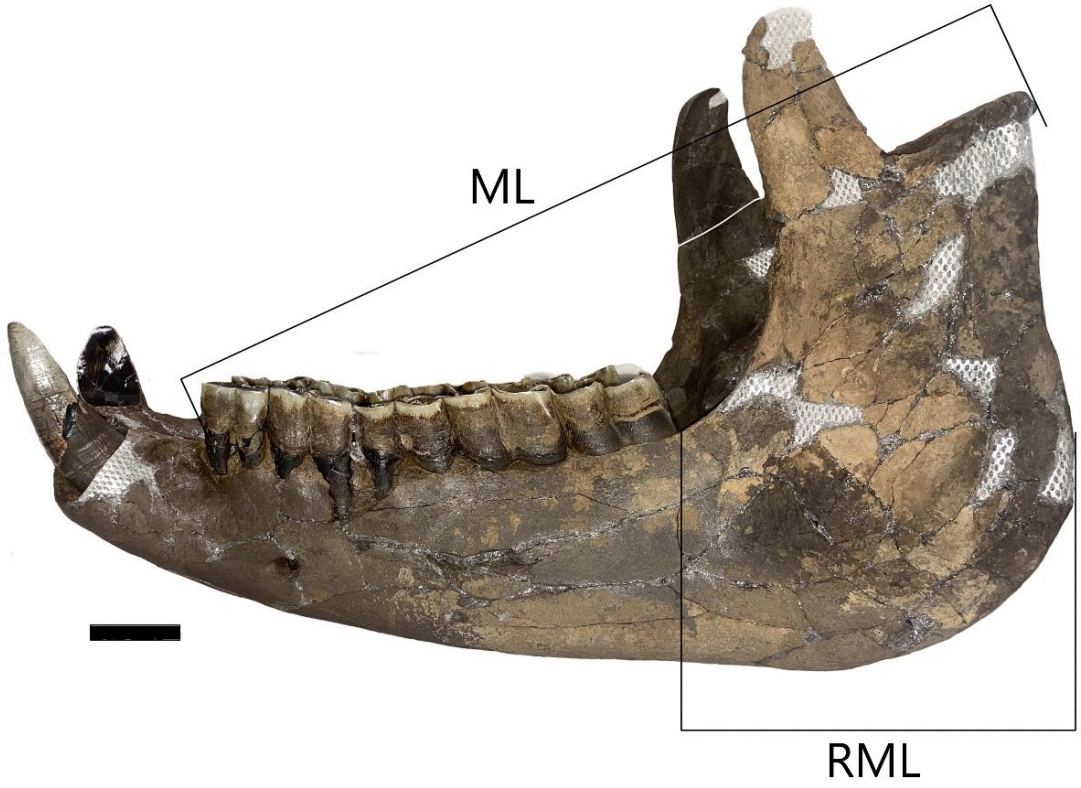

Fig. 5 Mandibular measurements used. Measurements are illustrated on the mandible of ETMNH 601 in left lateral view. Abbreviations can be found under the “Abbreviations and Nomenclature” subheading. Scale bar = 5 cm.

Mandibular length (ML) measures from the base of the anteriormost premolar crown to the posterior edge of the mandibular condyle, with the former landmark modified from Hagge (2010) to account for taxa without mandibular incisors (Fig. 5). Ramus length (RML) measures from posterior m3 alveolus to the posterior edge of the mandibular angle (Fig. 5). Right and left measurements were averaged when available.

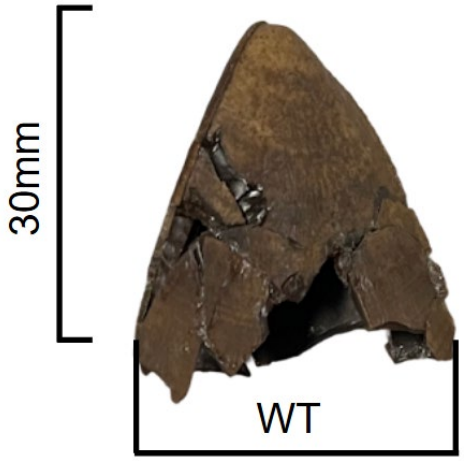

Fig. 6 Tusk measurement used. Mediolateral width of the i2 at 30mm distal to the tip (WT) illustrated on the left i2 of ETMNH 32999 in occlusal view.

Dental measurements for cheek teeth were taken at the base of the crown to account for ontogenetic changes in occlusal surface area. Dental dimensions were only taken if the base of the crown could be accessed for measurement. For incisors, the most relevant measurement for comparison with ETMNH 32999 was mediolateral width across the occlusal surface of the crown measured at 30mm distal to the tip (WT), as the tusk crown is not preserved past this point in ETMNH 32999 (Fig. 6). WT is used here as more traditional tusk measurements (e.g. width at crown base, root diameter; e.g. Mead 2000; Mihlbachler 2005; Chen et al. 2010; Lu et al. 2020) could not be taken due to incomplete formation/preservation in ETMNH 32999.

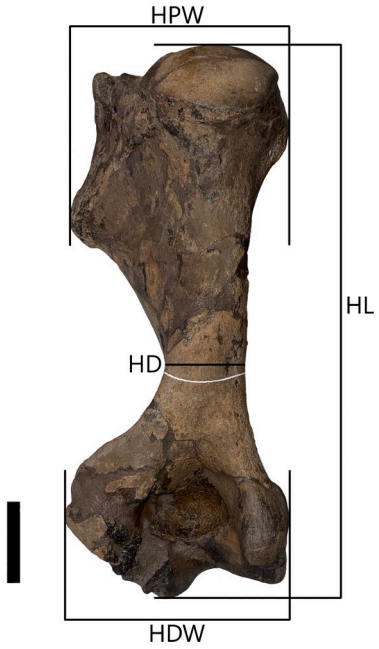

Fig. 7 Humerus measurements used. Measurements illustrated on the left humerus of *Teleoceras aepysoma* holotype ETMNH 609 in posterior view. Abbreviations can be found under the "Abbreviations and Nomenclature" subheading. Scale bar = 5cm.

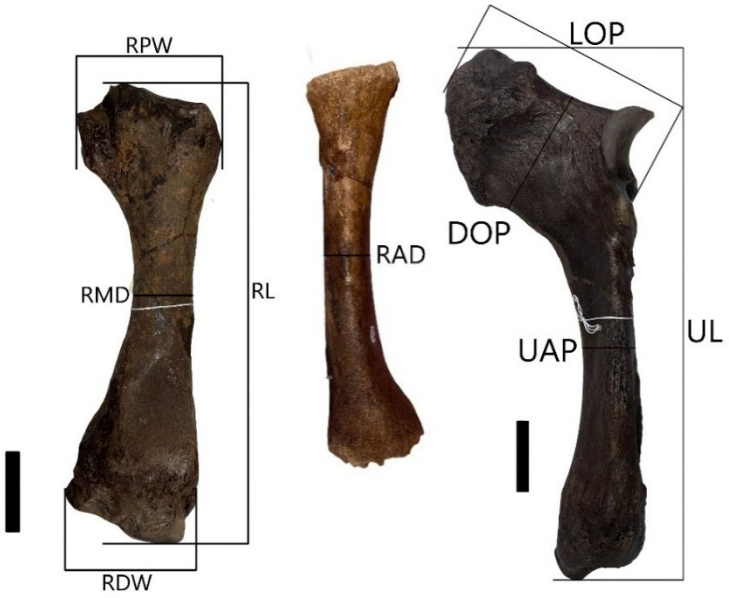

Fig. 8 Radius and ulna measurements used. Measurements illustrated on the left radius of *Teleoceras aepysoma* paratype ETMNH 601 (left) and left radius diaphysis of ETMNH 32999 (middle). Scale bar = 5cm. (Right) Ulna measurements illustrated on the left ulna of ETMNH 601. Abbreviations can be found under the "Abbreviations and Nomenclature" subheading. Scale bars = 5cm.

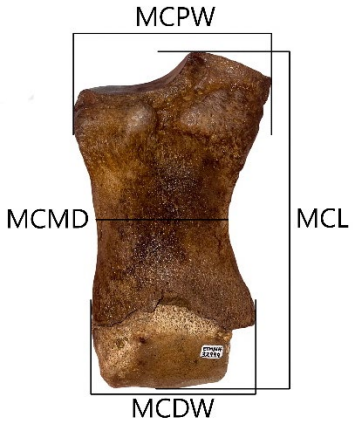

Fig. 9 Third metacarpal measurements used. Measurements illustrated on the right third metacarpal of ETMNH 32999, *Teleoceras aepysoma* subadult. Abbreviations can be found under the "Abbreviations and Nomenclature" subheading. Scale bar = 10cm.

Measurements from Literature

Table 1 Measurements from literature

Taxon	Measurements	Source
Teleoceras americanum	ZW	Prothero (2005)
Teleoceras brachyrhinum	LN, PO, ZW	Prothero (2005)
Teleoceras medicornutum	PO, ZW	Prothero (2005)
Teleoceras major	ZW, ML	Mead (2000), Prothero (2005)
Teleoceras fossiger	ZW, ML	Gerhold (1992), Prothero (2005)
Teleoceras hicksi	LN, ZW	Cook (1927), Prothero (2005), Carbot-Chanona et al. (2009)
Peraceras profectum	ZW, HL	Prothero (2005)
Aphelops mutilus	PO, ZW	Prothero (2005)
Chilotherium wimani	LN, SW, ZW, OH	Deng (2001)
Plesiaceratherium gracile	LN, PO, ML, RML, HL, RL	Lu et al. (2023b)
Acerorhinus yuanmouensis	LN	Lu (2013)
Coelodonta antiquitatis	RL	Shpansky (2014)
Ceratotherium neumayri	TCL, PO, ZW	Geraads and Koufos (1990), Giaourtsakis et al. (2006), Antoine et al. (2012)
Ceratotherium simum	LN, PO	Hillman-Smith et al. (1986)
Diceros gansuensis	LN, PO, SW, ZW, OH	Deng and Qiu (2007)
Diceros bicornis	PO, ZW, ML	Goddard (1970)

Some dental dimensions for *Teleoceras* spp. were also taken from Prothero (2005).

Measurements taken from Gerhold (1992), Mead (2000), Prothero (2005) (Table 1) exclusively refer to average adult values, while all other values were taken for specimens that could be assigned to age and therefore included in the samples for creating subadult-adult ratios and growth curves. For example, as Antoine et al. (2012) provided measurements of an age class XI *Ceratotherium neumayri*, that individual is here included in the *C. neumayri* sample representing an age class otherwise absent from the measurements taken directly. For ageable specimens of taxa that had insufficient data to be included in the growth plots, their measurements were still used in calculating subadult-adult ratios.

Enamel Hypoplasia Methodology

To document enamel hypoplasia (EH) observed on the cheek teeth of ETMNH 32999, ImageJ was used to measure the distance of defects from the dentine-enamel junction (DEJ) (Fig. 10). The affected teeth were observed macroscopically with the naked eye and a handheld jeweler's loupe. Considering the size of rhinocerotid teeth, macroscopic observation, rather than μCT scanning, is considered fit for observing EH in cases where the defects are not heavily obscured by cement, calculus, or sediment (Hullot and Antoine 2022), though requires the declaration of some caveats. Macroscopic observation comes with the inherent risk of under-detecting defects (Hullot and Antoine 2022), though other observational pitfalls include false positives via misidentification of incremental cementum deposition (Kierdorf et al. 2006). Caveats like these were carefully considered when analyzing EH without the aid of μCT.

Fig. 10 Dental defect measurement. Measurement of the distance between enamel defects and the dentine-enamel junction (DEJ) illustrated on the lingual face of the left dp4 of ETMNH 32999. The hypoplastic defect is represented by the pitted furrow running anteroposteriorly along the tooth. Scale bar = 1cm.

Categories for EH utilized here closely follow Fédération Dentaire Internationale (FDI) (1982) and Goodman and Rose (1990): linear EH (FDI type 4), pitted EH (FDI type 3), vertical hypoplasia (type 5) and missing enamel, or aplasia (FDI type 6). For *Teleoceras*, Mead (1999) defined linear EH as "type-M hypoplasia" and pitted EH as "type-G hypoplasia", as well as an additional, less severe enamel defect referred to as "swale hypoplasia", though here these terms are converted to their respective FDI titles. Terminology used here will follow the Fédération Dentaire Internationale (1982) and Goodman and Rose (1990) but will also reference root defects as were documented by Hullot et al. (2019).

Age Determination via Dental Eruption/Attrition

Age determination utilized the seventeen age classes based on dental eruption/attrition in the extant *Diceros bicornis* from Hitchins (1978). Wear on individual teeth was quantified using the wear key of Hillman-Smith et al. (1986). When referencing individuals from other studies that utilized other age determination methods (e.g. Goddard 1970), the classes were converted to their equivalent Hitchins (1978) age class. For consistency, Hitchins' (1978) *D. bicornis* key was

applied to all ageable specimens regardless of taxon, though within Rhinocerotidae, there is some slight variation in the eruption sequence of the second molar and permanent premolars (Böhmer et al. 2015). To account for this, age determination primarily focused on the attrition of P4/M2/M3, as these are always the last teeth to erupt and should give a better indication of age than timing of deciduous premolar replacement (Mihlbachler 2005). A full list of measured specimens and their assigned Hitchins' (1978) age classes can be found in Appendix B.

Abbreviations and Nomenclature

Institutions and Localities

Museum and locality abbreviations: **ETMNH** East Tennessee State University Museum of Natural History collection at the Gray Fossil Site and Museum, Tennessee, USA; **AMNH FM** American Museum of Natural History Fossil Mammal Collections, New York, USA; **AMNH F:AM** Frick Collections of the American Museum of Natural History, New York, USA; **UF** Florida Museum of Natural History, Florida, USA; **UNSM**, University of Nebraska State Museum, Nebraska, USA; **UTK** University of Tennessee Knoxville, Tennessee, USA; **USNM**, United States National Museum, Washington D.C., USA; **FMNH**, Field Museum of Natural History, Illinois, USA; **IVPP** Institute of Vertebrate Paleontology and Paleoanthropology, Beijing, China; **MRG** Museo Regional de Guadalajara, Guadalajara, Mexico; **IGCU** Instituto de Geologia Ciudad Universitaria, Mexico City, Mexico; **MNHN** Muséum national d'Histoire naturelle, Paris, France; **BM** British Museum of Natural History, London, United Kingdom; **NMW** National Museum of Natural Science, Taichung, Taiwan; **NMB** Naturhistorisches Museum Basel, Basel, Switzerland; **GFS** Gray Fossil Site, Tennessee, USA; **AFB** Ashfall Fossil Beds, Nebraska, USA. A full list of specimens can be found in Appendix A. Specimens measured directly for this study include those from ETMNH, AMNH FM/F:AM, and UF.

Anatomical Abbreviations and Nomenclature

Measurement abbreviations include: **TCL** Total Cranial Length, **LN** Lambdoid Crest to Nasal Tip, **PO** Anterior Premolar to Occiput, **OH** Occipital Height, **SW** Supraorbital Width, **ZW** Zygomatic Width, **ML** Mandibular Length, **RML** Ramus Length, **HL** Humerus Length, **HDW** Humerus Distal Width, **HPW** Humerus Proximal Width, **HD** Humerus Diaphyseal Width, **HMC** Humerus Minimum Midshaft Circumference, **RL** Radius Length, **RDW** Radius Distal Width, **RPW** Radius Proximal Width, **RMD** Radius Mediolateral Diaphyseal Width, **RAD** Radius Anteroposterior Diaphyseal Width, **UL** Ulna Length, **UDW** Ulna Distal Width, **UPW** Ulna Proximal Width, **UMD** Ulna Mediolateral Diaphyseal Width, **UAP** Ulna Anteroposterior Diaphyseal Width, **LOP** Length of Olecranon Process, **DOP** Depth of Olecranon Process, **MCL** Metacarpal III Length, **MCDW** Metacarpal III Distal Width, **MCPW** Metacarpal III Proximal Width, **MCMD** Metacarpal III Mediolateral Diaphyseal Width, **MCAP** Metacarpal III Anteroposterior Diaphyseal Width. Measurement landmarks are illustrated in Figures 4-9.

Dental nomenclature follows Antoine et al. (2010) (Fig. 11). Capital letters are used for maxillary teeth (e.g. dP3, M1) and lowercase for mandibular teeth (e.g. dp3, m1). All dimensions are given in mm unless otherwise stated.

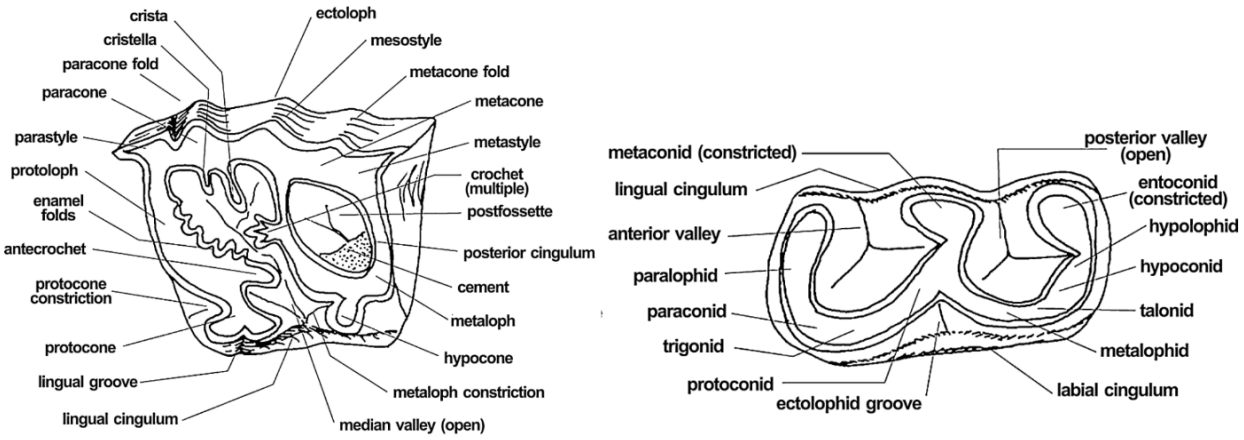

Fig. 11 Rhinocerotid dental nomenclature. Nomenclature illustrated on maxillary (left) and mandibular (right) teeth, figure modified from Antoine et al. (2010). The figured teeth are hypothetical, designed to show as many dental features as possible. Not to scale.

Other Abbreviations

NALMA North American Land Mammal Age, **IQR** Interquartile Range, **EH** Enamel Hypoplasia, **DEJ** Dentine-Enamel Junction, **FDI** Fédération Dentaire Internationale.

Calculations

Interquartile Range

Interquartile range (IQR) is a non-parametric test used to identify outliers by the first and third quartile ranges. Because IQR can be used with smaller sample sizes and bounded or otherwise skewed datasets, the subadult-adult ratio data drawn from the present study was used to illustrate deviations from expectation rather than raw measurements. Subadult-adult ratios were determined by dividing a given measurement for a subadult rhinocerotid by the same measurement of the average conspecific adult. Using subadult-adult ratios, in lieu of raw measurements, corrects for size differences between taxa, enabling direct comparisons and increasing sample sizes used to determine the ratios. One caveat of using the subadult-adult ratios is that the average adult values are treated as static, inflexible values, largely ignoring the potential for variation in adult size. The average adult values used for each respective taxon

should still give some indication of what the expected size for a 'typical' adult should be in each species. Such values are used here only to illustrate the typical proportional differences between subadults and adults.

The first and third quartiles, Q1 and Q3, were determined using the QUARTILE.INC function in Microsoft Excel, and the IQR was defined as Q3 – Q1. The lower fence was set at Q1 – 1.5 * IQR, and the upper fence was set at Q3 + 1.5 * IQR. Values outside of these boundaries were flagged as outliers. Values below Q1 or above Q3 that are not outside of the fences are on the low/high end of variation, respectively. Sample sizes for included subadults (age classes VII-IX) included all species for which ageable specimens were available, so bins may include subadults of up to 15 different rhinocerotid taxa.

Allometric Scaling

The allometric scaling equation is $\mathbf{Y=aX^b}$ following Huxley (1932), modified here to the algebraically equivalent form, $\mathbf{Y = a(X/X_{ref})^b}$ to standardize for size, so that **a** would equal the expected **Y** at the adult reference size metric, $\mathbf{X_{ref}}$. Using this reparameterization, fixed adult reference values can be used to infer the expected adult size of a given measurement for ETMNH 32999, while accounting for difference in size (as inferred from M1 anteroposterior length). The variables are further defined as:

Y = predicted value (expected adult measurement of interest for ETMNH 32999)

a = adult mean value (average GFS adult measurement of interest; fixed value)

X = size metric of specimen of interest (ETMNH 32999 M1 length)

$\mathbf{X_{ref}}$ = size metric of reference (average *T. aepysoma* M1 length)

b = scaling exponent (previously established allometric coefficient)

M1 length was chosen as the size metric of reference because the first molar dimensions are commonly used as a proxy for size in allometric regressions. Despite the known caveats of using dental dimensions as size proxies (e.g. Ungar 2014), M1 dimensions are thought to scale, at least roughly, with body size (Creighton 1980), and when measured correctly at the base of the crown, do not undergo ontogenetic change, so its use as a size proxy is considered fit for the purposes of the present study. One modification had to be made to **Y**; since the immature ETMNH 32999 would not yet be expected to be full adult size, the yielded **Y** values were multiplied by the average subadult-adult ratios for each respective measurement (Table 8) to account for the typical size differences between subadults and adults. For example, the size-corrected allometric scaling equation yielded an expected adult LN measurement of 492.86mm for ETMNH 32999 (Table 11), but since subadults have, on average, 92.35% of adult LN (data from this study; Table 8), the **Y** value was multiplied by 0.9235. Therefore, the expected LN for ETMNH 32999, corrected for age, would actually be 455.15mm. Upper and lower bounds were calculated the same way using the standard deviations of the subadult-adult ratios to partially account for natural variation in ontogenetic size changes, yielding a final expected LN of 455.15mm (± 15.82) for ETMNH 32999.

Allometric coefficients for craniomandibular measurements in *Teleoceras major* (Hagge 2010) and forelimb measurements in *T. proterum* (Santos et al. 2025) were used here to compare ETMNH 32999 with the expected values determined by allometric scaling. Most dimensions from Hagge (2010) and Santos et al. (2025) scaled isometrically or near isometrically in *Teleoceras*, though using allometric coefficients from *T. major* and *T. proterum* for *T. aepysoma* requires the declaration of several assumptions. Despite being closely related, life history and ecology may have effects on developmental timing that could cause ontogenetic inconsistencies

between congeners. Differences in dietary ecology, sexual dimorphism, and developmental timing may contribute to differences in growth between the two species. For example, the three species are thought to differ in feeding ecology, with *T. major* interpreted as a grazer (Voorhies and Thomasson 1979; Wang and Secord, 2020), *T. proterum* as a mixed feeder (MacFadden 1998) and *T. aepysoma* as a browser (DeSantis and Wallace 2008); such dietary differences could influence the development of functional characters related to feeding ecology in ungulates (e.g. Janis 1990; Mendoza et al. 2002; Hagge 2010). Furthermore, sexual dimorphism is pronounced in the AFB *T. major* sample (Mead 2000), more so than in *T. proterum* (Mihlbachler 2005), but sexual dimorphism is not yet known from *T. aepysoma*, so any potential inconsistencies caused by sexual dimorphism cannot be fully accounted for here. Still, the assumption of similar developmental timing between congeners is reasonable considering the similarities found in ontogenetic size change rates in all other rhinocerotid taxa sampled here, but caution should be exercised in assuming identical life-history between the included species.

To investigate whether EH-inducing stress had comparable effects on other subadults in terms of osteological growth arrest, as is hypothesized here for ETMNH 32999, allometric scaling was employed to determine expected sizes for an age class VII *Teleoceras medicornutum* (AMNH F:AM 109518) and an age class VIII *Ceratotherium neumayri* (AMNH FM 20584), both with EH on the same teeth as ETMNH 32999 (dP4, M1). (Table 15). For the allometric equations, *T. medicornutum* used the *T. major* allometric coefficients from Hagge (2010) as was done here for *T. aepysoma*. For *C. neumayri*, the allometric coefficients for *C. simum* from Hagge (2010) were used. Using these coefficients assumes comparable growth trends between closely related taxa. *T. medicornutum* is nearly morphologically indistinguishable from *T. major*

(Prothero 2005), and *C. neumayri* has been recovered as a sister taxon to *C. simum* (Borrani et al. 2025), so comparable allometric trends are considered a reasonable assumption here.

Growth Plots

Measurements were plotted against the dental age classes from Hitchins (1978) to observe ontogenetic size changes. To correct for size differences when comparing multiple taxa, and to better illustrate the achievement of asymptotic/adult size, subadult-adult ratio data is figured in addition to raw mensural data. For species where average adult values were not available in the literature, measurements for all individuals ≥ age class XI were used to calculate average adult value. This methodology assumes that asymptotic size is typically achieved by the full eruption of the third molar, as such is the case for all extant rhinoceroses (Groves 1972; Groves and Kurt 1972; Laurie et al. 1983; Hillman-Smith and Groves 1994; Groves and Leslie 2011). If extant rhinoceroses are a good comparison for their extinct relatives, the same timing of asymptotic size achievement should be applicable. This is a reasonable assumption for *Teleoceras*, considering the growth rate similarities identified in the fossil species *Plesiaceratherium gracile* (Lu et al. 2023b) and *Chilotherium wimani* (Deng 2001), both of which are more closely related to *Teleoceras* than extant species (see Lu et al. 2023a; Borrani et al. 2025). Logarithmic lines of best fit were applied to the data points to illustrate their adherence to typical mammalian growth trends, where the most rapid growth occurs early in life before reaching an asymptotic adult size, or growth plateau (e.g. von Bertalanffy 1957). Data was seldom available for individuals below Hitchins (1978) age class III; therefore, most plots reported here begin with age class III and end at the ultimate age class XVII.

CHAPTER 3. RESULTS

Reported Values

Table 2 Craniomandibular measurements of the GFS *Teleoceras aepysoma* sample

Measurement (mm)	ETMNH 32999 (VIII)	ETMNH 609 (XI)	ETMNH 601 (XIII)	ETMNH 33000 (XVII)	ETMNH 32999 Ratio to Avg. Adult
LN	390.00	460.00	532.31	533.17	0.7670
TCL	390.00	490.96	513.79	532.00	0.7614
PO	405.65	508.78	530.74	523.57	0.7786
SW	124.37	168.82	181.81	202.34	0.6748
ZW	237.58	339.47	376.19	382.30	0.6491
OH	123.33	162.18	157.80	152.76	0.7817
ML	380.60	450.98	495.37	427.90	0.8309
RML	131.57	150.02	169.75	182.92	0.7852

Roman numerals correspond to dental age classes of Hitchins (1978). Abbreviations for measurements can be found under "Abbreviations and Nomenclature".

Table 3 Dental measurements of the GFS *Teleoceras aepysoma* sample

Measurement (mm)	ETMNH 32999 length / width	ETMNH 609 length / width	ETMNH 601 length / width	ETMNH 33000 length / width
(dp3) p3	(27.41 / 16.73) 22.00 / 16.40	38.22 / 26.64	37.00 / 26.78	36.68 / 26.10
(dp4) p4	(38.66 / 22.53) 37.30 / 24.22	46.40 / 32.28	47.60 / 30.85	40.51 / 31.12
m1	45.93 / 26.60	51.50 / 35.50	49.80 / 34.42	47.29 / 30.43
m2	49.23 / 25.60	57.53 / 34.10	58.30 / 34.53	53.67 / 34.80
m3	57.13 / 25.80	51.70 / 31.72	56.00 / 32.09	59.72 / 32.30
m1-m3 length	152.29	160.73	164.10	160.68
(dP2) P2	(21.03 / 13.80) -	36.47 / 34.90	33.00 / 34.53	31.46 / 35.44
(dP3) P3	(30.68 / 33.00) 34.82 / 34.00	43.70 / 54.15	36.45 / 53.33	39.17 / 56.9
(dP4) P4	(41.32 / 44.74) 44.00 / 50.75	47.60 / 67.40	47.65 / 68.14	39.93 / 63.18
M1	47.22 / 46.12	50.90 / 69.24	54.22 / 68.12	41.05 / 69.17
M2	56.80 / 60.84	64.40 / 70.41	63.55 / 65.82	50.36 / 69.66
M3	55.75 / 46.80	52.84 / 59.54	52.43 / 58.81	60.08 / 60.12
M1-M3	159.77	168.14	170.20	151.49
WT	31.55	32.02	34.40	38.15*

Reported values are the anteroposterior length of the base of the crown for each tooth. Right and left averaged when available. P2 was not measurable for ETMNH 32999 as this tooth is absent on both sides.

Table 4 Humerus measurements of the GFS *Teleoceras aepysoma* sample

Measurement (mm)	ETMNH 32999	ETMNH 609	ETMNH 601	ETMNH 33000	ETMNH 32999 Ratio to Avg. Adult
Length (HL)	309.50	392.00	393.00	-	0.7826
Distal Width (HDW)	124.28	146.80	161.50	-	0.8062
Proximal Width (HPW)	-	154.25	161.00	-	-
Diaphyseal Width (HD)	47.00	55.00	66.44	-	0.7741
Minimum Midshaft Circumference (HMC)	152.40	177.80	215.90	214.40	0.7519

Right and left values averaged when available.

Table 5 Radius measurements of the GFS *Teleoceras aepysoma* sample

Measurement (mm)	ETMNH 32999	ETMNH 609	ETMNH 601	ETMNH 32999 Ratio to Avg. Adult
Length (RL)	258.44	296.15	325.05	0.8321
Distal Width (RDW)	83.31	92.55	103.25	0.8510
Proximal Width (RPW)	88.93	98.50	102.40	0.8852
Mediolateral Diaphyseal Width (RMD)	37.46	45.89	52.22	0.7636
Anteroposterior Diaphyseal Width (RAD)	27.09	34.47	40.20	0.7251

Right and left values averaged when available. Average adult values determined from ETMNH 609 and 601.

Table 6 Ulna measurements of the GFS *Teleoceras aepysoma* sample

Measurement (mm)	ETMNH 32999	ETMNH 609	ETMNH 601	ETMNH 32999 Ratio to Avg. Adult
Length (UL)	326.73	375.25	402.25	0.8405
Distal Diaphysis Width (UDW)	59.69	68.08	67.54	0.9002
Proximal Diaphysis Width (UPW)	45.78	48.31	58.12	0.8602
Minimum Diaphyseal Width (UMD)	34.61	40.95	46.64	0.7903
Anterolateral Diaphyseal Width (UAP)	38.98	38.96	46.75	0.9096
Length of Olecranon Process (LOP)	107.15	135.25	144.32	0.7665
Depth of Olecranon Process (DOP)	72.81	86.58	101.93	0.7725

Right and left values averaged when available. Average adult values determined from ETMNH 609 and 601.

Table 7 Third metacarpal measurements of the GFS *Teleoceras aepysoma* sample

Measurement (mm)	ETMNH 32999	ETMNH 609	ETMNH 601	ETMNH 32999 Ratio to Avg. Adult
Length	110.65	118.25	139.65	0.8581
Distal Width	55.14	59.90	73.25	0.8282
Proximal Width	62.43	66.50	76.00	0.8762
Mediolateral Midshaft Width	43.13	48.72	58.29	0.8061
Anteroposterior Midshaft Width	22.20	22.05	22.67	0.9928

Right and left values averaged when available. Average adult values determined from ETMNH 609 and 601.

Table 8 Average subadult-adult ratios for the rhinocerotids sampled

Measurement	Average Subadult: Adult Ratio (± SD)	Subadults Sampled Across Taxa (n)
Lambdoid to Nasals (LN)	0.9235 (± 0.0321)	14
Total Cranial Length (TCL)	0.8901 (± 0.1014)	10
Premolar to Occiput (PO)	0.9374 (± 0.0487)	18
Zygomatic Width (ZW)	0.8980 (± 0.0675)	22
Supraorbital Width (SW)	0.8508 (± 0.0914)	12
Occipital Height (OH)	0.9779 (± 0.0895)	5
Mandible Length (ML)	0.9180 (± 0.0684)	10
Humerus Length (HL)	0.8967 (± 0.0360)	2
Radius Length (RL)	0.9060 (± 0.0062)	3

All craniomandibular ratios were calculated from data collected for this study. *The humerus ratio is that of *Pl. gracile* from Lu et al. (2023b) averaged with the ratio of an associated subadult *P. profectum* humerus (AMNH F:AM 114401). The radius ratio is averaged from that of one *Pl. gracile* radius (Lu et al. 2023b) and two *Coelodonta antiquitatis* radii (Shpansky 2014).

Table 9 Body mass estimations and age classification for the GFS *Teleoceras aeypsoma* sample

Teleoceras aepysoma Specimen	Estimated Body Mass (kg)	Age Class	Age in *Diceros bicornis* Years	% of Potential Lifespan
ETMNH 32999	1330	VIII	7 ± 1	~17-19%
ETMNH 609	1640	XI	10 ± 3	~25-30%
ETMNH 601	2720	XIII	16 ± 3	~35-52%
ETMNH 33000	2630	XVII	37 ± 4	~96-100%

Body mass estimation is based on circumference of the humerus following Anderson et al. (1985). Roman numerals represent Hitchins' (1978) age classes. Ages in *Diceros bicornis* years correspond to data from Hitchins (1978). Percent of potential lifespan is based on Mihlbachler's (2003) correlations between *D. bicornis* and *Teleoceras proterum*.

Interquartile Range Results

Table 10 Interquartile range results of average rhinocerotid subadult-adult ratios

Measurement	Average Subadult-Adult Ratio (± SD)	Q1	Q3	IQR	Low Fence	High Fence	ETMNH 32999 Ratio to Avg. Adult
LN	0.9235 (± 0.0321)	0.8892	0.9390	0.4980	0.8146	1.014	0.7670
TCL	0.8901 (± 0.1014)	0.7843	0.9630	0.1787	0.5163	1.231	0.7614
PO	0.9374 (± 0.0487)	0.8866	0.9750	0.0884	0.7540	1.108	0.7786
ZW	0.8980 (± 0.0675)	0.8330	0.9480	0.1150	0.6605	1.121	0.6491
SW	0.8508 (± 0.0914)	0.7635	0.8988	0.1353	0.5606	1.102	0.6748
OH	0.9779 (± 0.0895)	0.9292	0.1015	0.0861	0.8001	1.144	0.7817
ML	0.9180 (± 0.0684)	0.8844	0.9606	0.0762	0.7701	1.075	0.8309

Subadult-adult ratios are based on data from the present study (Table 8). Samples used to determine IQR consist of subadults of multiple rhinocerotid taxa. Measurement abbreviations can be found above. Highlighted values indicate outlier ratios of ETMNH 32999 that lie below the lower fence.

Allometric Scaling Results

Table 11 Allometric scaling results for craniomandibular dimensions of ETMNH 32999

Measurement (mm)	*Teleoceras major* Allometric Coefficient	ETMNH 32999 Actual Value	Avg. GFS Adult Value	Expected ETMNH 32999 Size (± SD)	Avg. % Deviation from Expectation (Range)
TCL	0.9988	390.00	512.25	441.93 (± 51.52)	-11.75% (-0.41 to -20.78)
LN	0.9988*	390.00	477.76	455.15 (± 15.82)	-14.31% (-11.23 to -17.19)
PO	0.9988*	405.65	521.03	473.39 (± 25.17)	-14.31% (-9.62 to -18.54)
ZW	1.0070	237.58	365.99	318.47 (± 23.94)	-25.4% (-19.34 to -30.12)
SW	0.9775	124.37	184.32	152.10 (± 16.34)	-18.23% (-8.39 to -26.16)
OH	0.8175	123.33	157.58	150.21 (± 13.75)	-17.89% (-9.62 to -24.78)

ML	0.9910	381.07	458.08	407.69 (± 31.08)	-8.76% (-0.87 to -13.12)

Allometric coefficients of congener *Teleoceras major* are from Hagge (2010). For LN and PO length, the allometric coefficient for total cranial length from Hagge (2010) was used. All measurements are reported in millimeters. Measurement abbreviations can be found above.

Table 12 Allometric scaling results for forelimb lengths of ETMNH 32999

Measurement (mm)	Coefficient (b) of *Teleoceras proterum*	ETMNH 32999 Actual Value	Avg GFS Adult Value	Expected ETMNH 32999 Subadult Size (mm)	% Deviation of ETMNH 32999 from Expectation
Humerus Length (HL)	0.8650	309.50	392.50	349.50 (± 14.00)	-11.44% (-7.74 to -14.86%)
Radius Length (RL)	0.9400	258.44	310.60	275.15 (± 1.90)	-7.46% (-6.83 to -8.09)

Allometric coefficients of congener *Teleoceras proterum* are from Santos et al. (2025). All reported measurements are in millimeters.

Descriptions

Osteological Description

Because Short et al. (2019) described the *Teleoceras aepysoma* holotype and paratype specimens in detail, and Scaife (2024) reported additional osteological observations, the following osteological description will focus largely on how ETMNH 32999 differs from conspecific adults rather than again discussing the osteological morphology of *T. aepysoma*. A summary of craniomandibular features of ETMNH 32999 that differ from *T. aepysoma* adults can be found in Table 13. Features considered ontogenetically relevant are prioritized there, rather than differences attributable to taphonomic abrasion (e.g. missing/damaged elements) or pathology (e.g. enamel hypoplasia).

Cranium

Fig. 12 Cranium of ETMNH 32999 in left lateral view. Reconstructed areas are represented by the white/translucent filler. Note the presence of permanent premolars in the maxillary crypt superior to dP2, dP3, and dP4. Note that unerupted P3 and P4 are replicas, and the originals were removed from the cranium during preparation. Note the state of M3 eruption relative to M2. Scale bar = 10cm.

Fig. 13 Cranium of ETMNH 32999 in right lateral view. Reconstructed areas are represented by white/translucent filler. The right teeth (dP4, P4, M1, M2) are mirrored 3D prints of their left-side counterparts. Note that the right side of the cranium is preserved far worse than the left side. A block of archival foam supports the occipital region. Scale bar = 10cm.

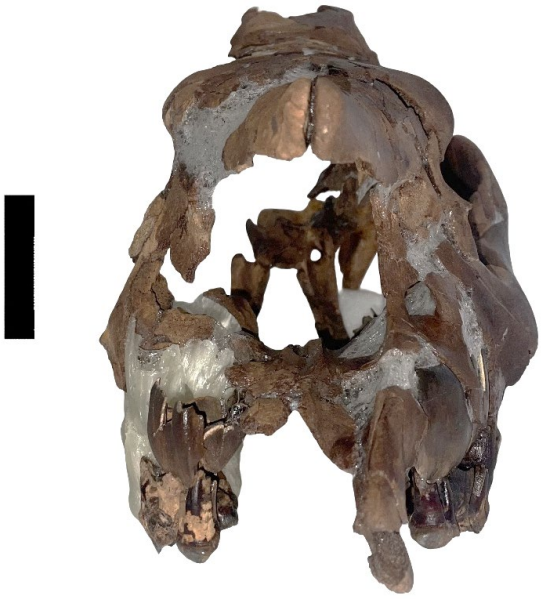

Fig. 14 Cranium of ETMNH 32999 in anterior view. Reconstructed areas are represented by white/translucent filler. Scale bar = 5cm.

Fig. 15 Cranium of ETMNH 32999 in dorsal view. Reconstructed areas are represented by white/translucent filler. Scale bar = 10cm.

Fig. 16 Cranium of ETMNH 32999 in palatal view. Reconstructed areas are represented by white/translucent filler. Scale bar = 10cm.

Nasal. The paired nasal bones are unfused along the medial suture. There is a gap between the nasals at the anterior tip. Lateral edges downturn sharply ventrally. In dorsal view, the anterior is pinched medially so that the tip is slightly narrower. The nasals are absent of any rugosity profile or distribution that would signal attachment of a nasal horn. There is a faint concavity anterior to the nasofrontal suture. The ventral portion of the nasals form the dorsal edge of the nasal cavity (Fig. 14). The nasal notch, which is retracted to the middle of dP4/dp4, is U-shaped with a slight bump at the posterior edge which is horizontally level with the lacrimal process (Fig. 12).

Frontal. The nasofrontal suture is unfused. There are slightly rugose, laterally extending supraorbital tuberosities on the lateral edges of the frontals which form the widest surface of the dorsal skull (Fig. 15). The area between these processes is slightly convex. The lateral expansion of these swellings contributes to the broad, diamond-shaped dorsal surface of the frontals. The anterior portion of the frontal diamond gradually slopes medially to the nasals. The posterior

portion of the frontal diamond constricts to a cylinder-like shape as the temporal crests become more pronounced.

Parietal. The parietals of ETMNH 32999 are weakly concave. The poorly defined temporal crests extend posteriorly from the frontals. The temporal crests are widely separated. Each crest is marked by a relatively weak ventral downturn at the lateral edges. The temporal crests have not merged and remain widely separated by a broad, flat 'sagittal table'. Much of the posterior portion of the skull is missing, but enough of the lambdoid crest remains to indicate a slight concavity as it weakly flares caudolaterally. The parietal slope is weak but present, leading to a slightly concave dorsal skull profile, though not nearly as steep as observed in GFS adults.

Premaxillae. In *Teleoceras*, the premaxilla consists of a narrow projection with two anteroventrally oriented alveoli which contain the chisel-shaped honing incisors that occlude with the lower tusks. In lateral view the premaxillae are cylindrical and pinched lateromedially before the I1 alveolus in ventral view. Both tusk alveoli are preserved in ETMNH 32999, but only the left is attached to the cranium.

Maxilla. Most of the maxilla is not preserved, with the internal maxilla being completely absent. Externally, there is a fragment over the roots of the dP4 that indicates the ventral edge of the maxilla. The missing portion of the anterior maxilla which articulates with the premaxilla reveals the maxillary crypt containing unerupted P3 and P4. The ventral portion of the suture between the posterior maxilla and the jugal is completely fused, but weakly fused dorsally, separating closer to the lacrimal bone.

Lacrimal. The lacrimal tubercle is damaged at the tip. Superior to the tubercle, there is a single lacrimal foramen oriented laterally. Both the frontal and nasal sutures with the lacrimal remain unfused. The suture with the jugal is damaged but is also unfused.

Jugal. The jugal begins gradually above posterior M1. The suture between the jugal and maxilla is evident but mostly fused. In dorsal view, the jugal is straight rather than laterally flared, nearly parallel with the left temporal ridge. The posterior part of the jugal articulates with the squamosal at a weakly fused suture. The postorbital process on the jugal is a weak hillock flush with the jugal-squamosal suture.

Squamosal. The anterior portion of the squamosal forms the posterior zygomatic arch, which flares weakly laterally in dorsal view (Fig. 15), only slightly more laterally flared than the jugal. The concavity on the medial side of the squamosal faces dorsally. The glenoid fossa is concave and faces ventrally. Posterior to the glenoid fossa, the postglenoid process curves slightly anteriorly but is overall directed ventrally. In lateral view, the tip of the postglenoid process is level with the inferior edge of the jugal.

Occipital. Much of the occipital region of ETMNH 32999 is not preserved. The left occipital condyle is preserved but is not attached to the skull. The left paraoccipital process is preserved and, in lateral view, does not extend as far ventrally as the postglenoid process

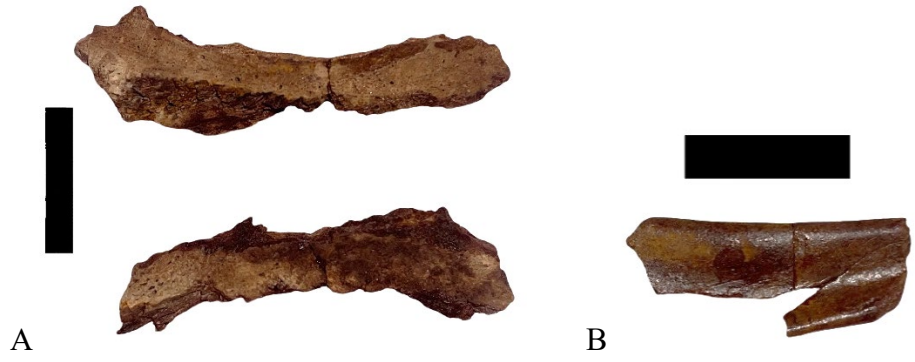

Fig. 17A-B Palatine and hyoid bones of ETMNH 32999. (A) The palatine is represented by two isolated fragments. Scale bar = 2cm. (B) The fragmentary hyoid apparatus of ETMNH 329999 is represented only by a portion of the stylohyoid. Scale bar = 3cm

Palate. The palate of ETMNH 32999 is badly damaged and poorly ossified. In ventral view, the nasal incision is retracted to the middle of dP2. The remainder of the palatine is

represented by two damaged, elongate fragments (Fig. 17A) unattached to the cranium. The vomer and pterygoids are not preserved.

Basicranium. Most of the basicranial region is absent, reconstructed, or badly weathered (Fig. 16), precluding any meaningful comparison with GFS adults; the basicranial regions of GFS adults have similarly poor preservation and/or extreme degrees of fusion, making it difficult to observe individual elements.

Hyoid. The hyoid apparatus is represented only by a flat, checkmark-shaped fragment of the stylohyoid (Fig. 17B). On the dorsal side, a narrow valley runs anteroposteriorly down the middle.

Cranium – Remarks

The cranium is mediolaterally narrower and anteroposteriorly shorter than those of GFS adults. The cranial shape differences are most apparent in the dorsal skull. ETMNH 32999 has a weaker parietal slope and lacks the upturned and laterally flared lambdoid crests typical of adults. Posteriorly, the temporal crests do not meet but remain widely separated by a sagittal table, with the lateral downturn of the weak temporal ridges weaker than in adults. The temporal crests of GFS adults, in dorsal view, meet at the same level as the posterior squamosal, and are sharply laterally downturned. ETMNH 32999 also lacks the dorsally extended nuchal face typical of conspecific adults.

In dorsal view (Fig. 15), the zygomatic breadth of ETMNH 32999 is narrow, flaring only weakly laterally posterior to the jugal-squamosal suture; the same is apparent in anterior view (Fig. 14). The absence of zygomatic arch exaggeration differs from the greatly laterally flared zygomatic arches diagnostic of *Teleoceras*, with *T. aepysoma* displaying the most exaggerated of any species within the genus (Short et al. 2019). The narrow zygomatic arches of ETMNH

32999, in turn, create narrower temporal fossae than those of adults. The slight lateral flare of the zygomatic arch in ETMNH 32999 is parallel with the nasofrontal portion of the frontal diamond that lacks the strong constriction of GFS adults. In adults, the strong zygomatic flare is also parallel with the anterior frontal constriction.

The frontal diamond maintains the typical diamond shape of most other *Teleoceras*, unlike GFS adults where the lateral edges of the frontals medially constrict anterior to the exaggerated supraorbital tuberosities. ETMNH 32999 also lacks the dorsally swollen aspect of the supraorbital tuberosities, which are inflated and rugose in adults, particularly ETMNH 33000; in ETMNH 32999, they swell laterally and only very slightly dorsally (Figs. 14-15). As a result, the area on the frontals between the supraorbital tuberosities is convex in ETMNH 32999 rather than concave as is typical of conspecific adults. Nasals of ETMNH 32999 are slightly pointier than those of GFS adults, with a weak medial constriction proximal to the nasal tip. In both ETMNH 32999 and GFS adults, the nasal notch is retracted to anterior (d)P4 in lateral view (Fig. 12).

Mandible

A

B

Fig. 18A-B Mandible of ETMNH 32999. (A) Left lateral view and (B) occlusal view, with dp3-m2 on the left side and dp4-m2 on the right. Note that the m3s and i2s were removed from the mandible during preparation. Scale bars = 10cm.

Dentary. Symphysis is retracted to anterior dp4 and anteriorly slopes dorsally. In lateral view, the upward inflection of the anterior mandible begins inferior to anterior m2 (Fig. 18A). Upward slope of the mandible begins at p4 in GFS adults but is retracted to the posterior m1 in ETMNH 32999. Mental foramen is inferior to the p4 in GFS adults but is positioned more

anteriorly in ETMNH 32999, inferior to posterior dp3. The angle of the dentary inferior to the coronoid process is not as anteriorly inclined in ETMNH 32999 as it is in GFS adults, creating a slightly obtuse interior mandibular angle relative to the more acute condition in GFS adults. The masseteric fossae are shallow, defined primarily by a weak, laterally oriented rim on the posterior mandibular angle. On the left side, this rim is lined with mildly exposed trabecular bone. On the right side, the rim is rough and irregularly shaped with an undulating profile unlike the more typical morphology of the left side. Ventral to the masseteric fossa on the left side is a damaged, cancellous protrusion, a feature seen in other GFS adults. This protrusion is less expressed on the right side. The m3 alveoli are open, though slightly damaged which makes them appear larger than they likely would have been. In dorsal view, condyle width expands laterally throughout ontogeny, and the mandibular body lengthens.

Maxillary Dentition

Fig. 19 Left maxillary tooth row of ETMNH 32999. dP2-M3 are represented. Scale bar = 5cm.

Fig. 20 Unerupted maxillary premolars of ETMNH 32999. Left P3 (left) and P4 (right) of ETMNH 32999 in labial view. Scale bar = 1cm.

Upper incisors. No upper incisors are preserved on ETMNH 32999, though the premaxillae are preserved with empty alveoli.

Upper deciduous premolars. dP2 is present on both tooth rows and is so heavily worn that nearly no enamel remains, and morphological features are difficult to identify; all lophs are merged with no discernable fossettes. It is subtriangular with the anterior point directed anteromedially. There is a small, rounded bump on the lingual side of the metaloph pointing medially.

dP3 is longer labiolingually than anteroposteriorly. On left dP3, the hypocone is constricted and larger than the protocone. No parastyle is apparent though a paracone fold is present. There is lingual cingulum crossing the lingual valley that connects the hypocone and protocone. Medisinus is interrupted by a weak enamel bridge connecting the antecrochet to an anterolingually oriented fold on the crochet. The crochet has merged with the protoloph and cristae creating two small, elliptical medifossettes. Right dP3 is not as heavily worn, as the crochet merges only with the crista and not with the protoloph. No enamel bridge between the crochet and antecrochet is present on the right dP3 as in the left. The hypocone of the right dP3 is

constricted only anteriorly. The parastyle is visible on the right dP3 but not the left. On both dP3, the teardrop-shaped postfossette is closed.

dP4 is only preserved on the left side. A parastyle is present with a shallow paracone rib. The ectoloph and protoloph are longer than the metaloph. Lingual cingulum connects the hypocone to the protocone but is weaker than that of dP3. The medisinus is interrupted where the crochet merges with the ectoloph. Antecrochet is larger than the crochet and has two enamel folds protruding from the labial face. The protocone is constricted both anteriorly and posteriorly. The hypocone is not as strongly constricted but is pinched into a medially oriented round nub as the constrictions are both pointed labially rather than anteroposteriorly towards each other, as seen on the protocone constrictions. A curved spur protrudes from the posterior hypocone and points lingually.

Permanent upper premolars. Permanent P3 and P4 are unerupted but nearly displacing their heavily worn deciduous counterparts. The original P3 and P4 were removed from the cranium and replaced with replicas. No P2 is present in the maxillary crypt on either side.

In occlusal view, P3 has a mildly undulating ectoloph profile. The ectoloph is longer than the metaloph, which is longer than the protoloph. Cingulum is present on the anterior face from the parastyle to the protocone where it is interrupted. Cingulum crosses the lingual valley, is interrupted by the hypocone, and is pronounced on the anterior face where it runs to the metastyle. There is a V-shaped medial incision lingual to the parastyle. A long, curved crista is present between the metaloph and protoloph. A cingular bridge connects the protocone and hypocone.

P4 is badly damaged and missing most of the occlusal face. Only the ectoloph and a portion of the metaloph are preserved. There is a wide and shallow metacone fold on the

ectoloph. The cingulum on the posterior face is strong. There is a U-shaped medial incision lingual to the parastyle.

Upper molars. M1 is preserved in only the left tooth row. The parastyle is long and curved, hooking over the posterior labial corner of dP4. The ectoloph is longer than both the protoloph and metaloph. The paracone fold is shallow, and a paracone rib is present. Cingulum connects the anterior protocone to the protoloph, forming a shallow cingular basin. The protocone is strongly constricted. The hypocone is not yet extensively worn, but is also constricted, though not as strongly as the protocone. Due to the relatively light wear on the metaloph, it appears to curve posteriorly as does the metastyle. There is a wide and shallow concave metacone fold anterior to the metastyle. The crochet is lentoid and larger than the antecrochet. There are two enamel folds on the labial side of the crochet. There is a faint, reduced crista. The antecrochet is round with a constricted spur on the labial side which is in contact with the lingual face of the crochet, though they are not yet merged enough to close the medisinus. Because it is uninterrupted at this wear stage, the medisinus is highly sinuous. The postfossette is large, U-shaped, and open posteriorly.

M2 is preserved only on the left side. It is lightly worn, only enough to expose dentine on the protoloph and anterior ectoloph. The parastyle, paracone fold, and paracone rib are all apparent. The unworn crochet is long and thin, parallel to the ectoloph, and the antecrochet is smaller than the crochet. A vertical groove can be seen on the lingual face of the hypocone. The hypocone is constricted anteriorly and the protocone is constricted on both sides. Cingulum connects the anterior protocone to the protoloph, forming a shallow cingular basin. The postfossette is U-shaped and open as in M1.

M3 is unerupted and broken, as only the unworn ectoloph, parastyle, and protoloph are preserved. The paracone fold is faint though the paracone rib is apparent. The protocone is constricted, though not as strong as in the other teeth.

Labial view of upper cheek teeth. From left dP2-M1, a band of dental calculus running anteroposteriorly separates the off-white labial face of the enamel crown from the darker brown enamel, and the roots. The fragment of maxilla over left dP4 indicates the ventral edge of the bone surface, dorsal to the band of calculus. As M2 has only erupted relatively recently, the dental calculus band is not present yet, but the off-white, erupted portion of the tooth is still in line with this calculus band. Differential preservation indicates where the tooth was obscured by the bone surface, flush with the ventral edge of the maxilla. The lateral profile of M3 in relation to the dental calculus line indicates that it was likely just above the bone surface but not yet breaching the gum line; differential preservation also denotes the portion of the crown still forming within the crypt as opposed to the crown erupted past the bone. The calculus line is inferred to be subgingival (below the gum line) rather than supragingival, based on the inferred ventral edge of the maxilla. There are linear striations on the roots of the left dP4 and the crown of the left M1, creating visible grooves on the latter. Striae of Retzius are visible on the labial face of the M2 and M3 (Fig. 12).

Mandibular Dentition

Fig. 21 Tusks of ETMNH 32999. (Left) left and (right) right tusks in occlusal (top) and ventral (bottom) views. Scale bar = 10cm.

Fig. 22 Vestigial incisors of ETMNH 32999. Scale bar = 1cm.

Lower incisors. The lower i2s in *Teleoceras* are modified to tusks which are honed via occlusion with the upper incisors. These tusks normally consist of an enamel crown which begins at the tip and ends at the crown base where the root begins to form. In ETMNH 32999, only the anteriormost portion of the enamel crown is preserved (Fig. 21). The remainder of the enamel crown and the root are both absent; the enamel at the proximal portion of the preserved crown is thin, brittle and of a different color than the rest of the tusk, suggesting that the enamel crown was actively forming or recently formed. The occlusal surfaces of the crown face each other medially and have a different, lighter coloration than the lateral and ventrolateral faces. The occlusal faces are convex rather than concave, indicating that they have not yet been extensively

worn by the upper honing incisors. The lateral faces are narrow and meet at nearly a right angle with the ventrolateral face. The ventrolateral faces are slightly curved. On both tusks, all three faces meet at an anterior, rounded point. In life, the tusks would have remained fully or partially unerupted in the alveoli.

Two elongate, narrow fragments of dental material were found associated with ETMNH 32999 (Fig. 22). One is thicker and lentoid in shape, with a distinct cylindrical protrusion on one end that may represent a portion of the root. The other is narrower and pin-shaped, where one end comes to a point and the other ends in a bulbous structure. The narrowness and overall abnormal shape of these fragments suggest that they represent vestigial mandibular incisors.

Fig. 23 Mandibular tooth rows of ETMNH 32999. Occlusal view; left side dp3-m2, right side dp4-m2. Note that the m3s were removed from the mandible during preparation. Scale bar = 10cm.

Deciduous premolars. The lower left tooth row of ETMNH 32999 contains both dp3 and dp4, while the right side is missing dp3 (Fig. 23). Right dp3 is preserved but is too fragmentary to warrant description. The deciduous premolars are so heavily worn that the lingual valleys have merged in dp3 and almost entirely merged in dp4. The labial angle is still visible on both dp4.

Due to heavy wear, the occlusal morphology is mostly unremarkable, as all features have merged.

Fig. 24 Unerupted mandibular premolars of ETMNH 32999. Lingual view. (Left of scale bar) left and right p3s and (right of scale bar) left and right p4s. Note the small size of the p3s relative to the p4s. Scale = 3cm.

Permanent premolars. p3 and p4 (Fig. 24) remain unerupted in the crypt on both sides and were removed from the mandible during preparation. Occlusal morphology does not deviate from what is typical for rhinocerotid premolars, maintaining the characteristic 'm' shape. The most remarkable feature of the permanent premolars is the anomalously small size of both p3.

Fig. 25 Mandibular third molars of ETMNH 32999. Labial view. Note the change in color at the base of the posterior lophids where enamel formation ceased at death. Scale bar = 2cm.

Lower molars. The labial angles of both m1 are defined. The right m1 is slightly more worn than the left, evidenced by greater wear on the ectoconid and the reduction of the lingual valley. On both m1, exposed dentine has merged between cusps. The metaconid curves posteriorly in both teeth. On m2, the crescent-shaped occlusal surfaces of each cusp have not been worn enough to merge as they are in both m1. The wear on the anterior cusp of m2 is

heavier than the posterior. Both unerupted m3s are preserved (Fig. 25), though were removed from the mandible during preparation. There is a distinct change in color and enamel thickness where tooth formation ceased. Based on what is observed in other taxa with comparable m1/m2 wear, the m3 would have been visible through the open alveoli, if not slightly above the bone surface as its maxillary counterpart is interpreted to be.

Dentition – Remarks

Short (2013) described the occlusal morphology of *T. aepysoma* (then *Teleoceras* sp. nov.) in the first body of work addressing the species as distinct from congeners, though less was said for occlusal morphology in the published description (see Short et al. 2019). The occlusal morphology of ETMNH 32999 differs most from conspecific adults in the M1, displaying a lentoid crochet with two enamel folds on the labial face, a weak, rounded crista, and a constricted protrusion on the labial face of the antecrochet (Fig. 19). When compared with an isolated, less worn M1 from the GFS (ETMNH 37999) (Fig. 26), one of the enamel folds on the labial face of the crochet is apparent, though the second enamel fold and the constricted nub on the antecrochet are both absent, suggesting that they may be exclusive to ETMNH 32999. Occlusal morphology, while often considered diagnostic, is highly variable within rhinocerotid populations and throughout their ontogeny (Prothero 2005) (Fig. 26), so these minute differences are not considered here to be taxonomically diagnostic and are instead attributed to intraspecific variation and/or typical ontogenetic wear. On more worn *T. aepysoma* M1s (e.g. ETMNH 601, ETMNH 12487), the crochet is no longer elongate and lentoid as in ETMNH 32999 but is of roughly equal size and shape to the antecrochet; as a result, the medisinus becomes less sinuous. Any cristae, if present, also apparently vanish with wear. The postfosette closes posteriorly and the metacone fold becomes less pronounced (Fig. 26). M1 shortens anteroposterioly throughout

wear as the adjacent P4 and M2 occlude with the anterior and posterior faces, eventually becoming longer mediolaterally than anteroposteriorly.

Fig. 26 Partial left M1 occlusal wear sequence for *Teleoceras aepysoma*. (Left) ETMNH 37999, wear stage 3. (Middle) ETMNH 32999, wear stage 5/6. (Right) ETMNH 12487, wear stage 7. Note that ETMNH 12487 is a right M1 that has been flipped horizontally to appear as left. Wear stages correspond with those depicted in Figure 99. Scale bar = 5cm.

The mandibular dentition of ETMNH 32999 resembles that of conspecific GFS adults. The most marked difference is the small size of the unerupted p3s, with unusually reduced lengths and widths relative to both their deciduous counterparts and to GFS adult p3s. It is also noteworthy that while the dental length measurements of ETMNH 32999 compare favorably with GFS adults, the dental widths are consistently less. ETMNH 32999 also does not retain a vestigial p2 as is present in some *T. aepysoma* adults (e.g. Short et al. 2019). Also of note is the exposed dentine joined between cusps on both m1s, a condition which typically does not occur until later in life based on what is seen in extant taxa (e.g. Hitchins 1978).

The two elongate, abnormal dental fragments found associated with ETMNH 32999 (Fig. 22) are interpreted as possibly being vestigial incisors, as the overall shape resembles the vestigial mandibular incisors observed in *Teleoceras proterum* (personal observations).

Forelimbs

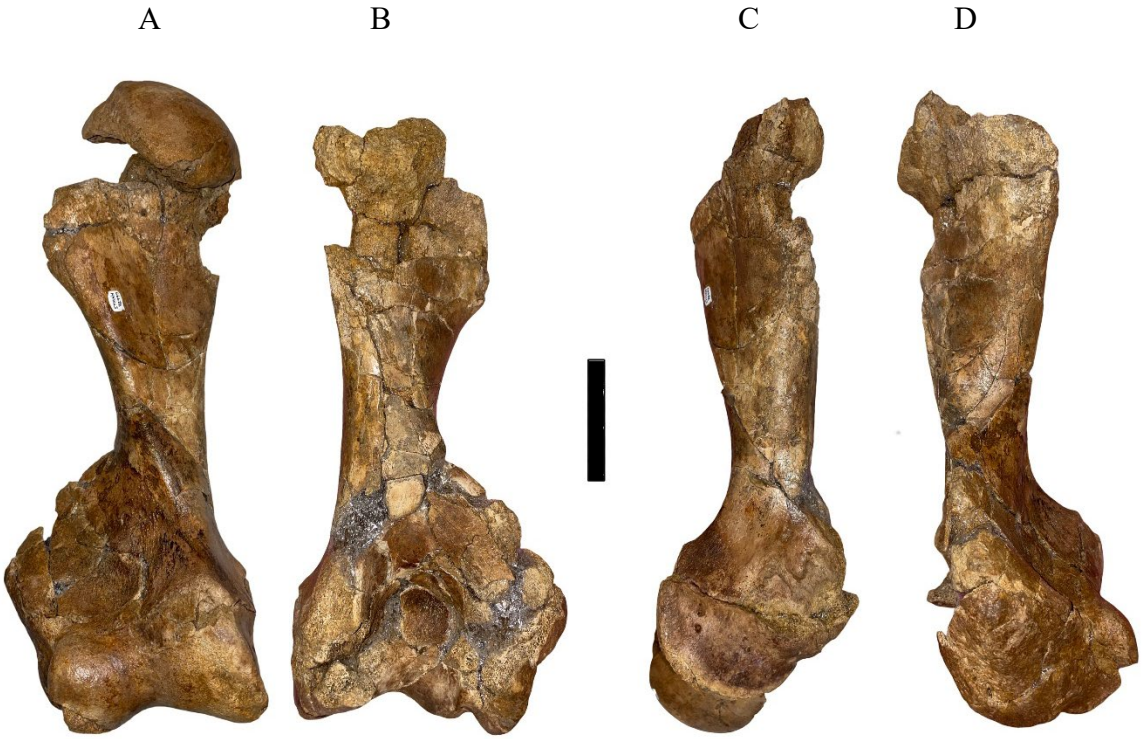

Fig. 27A-D Right humerus of ETMNH 32999. (A) Anterior view, (B) posterior view, (C) medial view, (D) lateral view. The proximal end of the humerus is badly damaged, and the articular head is detached but does loosely articulate with what is preserved of the proximal diaphysis. Note that the articular head is attached only in A, and has been removed in all other views. Scale bar = 5cm.

Humerus. Only the right humerus is preserved (Fig. 27A-D). The distal epiphysis is fused to the shaft. Most of the proximal end is missing, save for the articular head which loosely articulates with the damaged proximal end. Radial and coronoid fossae are shallow. The humeral crest is more strongly pronounced than the epicondylar crest. The deltoid tuberosity is broken away. The diaphyseal width is narrower than that of GFS adults (Table 4).

Fig. 28 Right radius of ETMNH 32999. Anterior (top) and posterior (bottom) views. In anterior view, the unfused epiphyseal plates have been removed from the diaphysis. In posterior view, they are placed in their anatomical position. Scale bars = 5cm.

Radius. Radii of ETMNH 32999 do not differ considerably from those of GFS adults as described by Short et al. (2019). Both epiphyses are unfused. The radial crest is less pronounced than that of GFS adults and the radial neck is narrower. On the proximal epiphysis, the tuberosity between the articular surfaces for the trochlea and ulna is more pronounced than in GFS adults.

Fig. 29 Left ulna of ETMNH 32999. Medial (top) and lateral (bottom) views. In medial view, the unfused epiphyses have been removed from the diaphysis. In lateral view, the epiphyses are placed in their anatomical position. Scale bar = 5cm.

Ulna. Both epiphyses of both ulnae are unfused (Fig. 29). The olecranon process and proximal epiphysis are both absent of the rugose muscle scarring seen in GFS adults. The

articular process proximal to the trochlear notch does not extend as far anteriorly as in adults. Extending from the distal end to halfway up the midshaft is an elongate, triangular section of mildly rugose bone where the radius articulates; said rugosity is not as pronounced as GFS adults but is nonetheless visible. The olecranon process lacks the length and depth seen in adults.

Hindlimbs

Fig. 30 Right fibula distal epiphysis of ETMNH 32999. Scale bar = 2cm.

Fibula. The only portion of the hindlimb longbones that is preserved is the unfused distal epiphyseal plate of the right fibula (Fig. 30). The lateral malleolus is flatter, less concave than what is seen in GFS adults.

Fig. 31 Right patella of ETMNH 32999. Anterior (right) and posterior (left) views. Scale bar = 3cm.

Patella. Only the right patella is preserved (Fig. 31). It is moderately weathered. Concavities on either side of the ridge on the posterior articular surface are slightly shallower than those of conspecific adults.

Carpal Elements

Fig. 32A-B Scaphoids and lunars of ETMNH 32999. (A) Left and right scaphoids of ETMNH 32999 in posterior view. Note the severe taphonomic damage to the right scaphoid relative to the left. Scale bar = 3cm. (B) Left and right lunars of ETMNH 32999 in medial view. The surfaces which articulate with the scaphoid and magnum are broken in the right lunar. Scale bar = 5cm.

Scaphoid. Both left and right scaphoids are preserved, though the right is badly damaged (Fig. 32A). On the left scaphoid, the articular surface for the trapezoid is saddle-shaped as in GFS adults, but is separated from the medial face by a gap which is slightly more pronounced than adults. Scaife (2024) also described the scaphoids of ETMNH 32999 in reference to the suggested presence of pathological 'lipping'.

Lunar. The lunar process of the right lunar is broken. On the left lunar, the articular surface for the unciform is slightly flatter than seen in GFS adults, and the 'lip' between the lunar process and articular surface for the unciform is not as pronounced (Fig. 32B).

Fig. 33A-B Cuneiforms and pisiform of ETMNH 32999. (A) Left and right cuneiforms of ETMNH 32999 in medial view. In the left cuneiform, the inferior surface that articulates with the lunar is damaged, exposing the cancellous bone beneath. Scale bar = 5cm. (B) Partial left pisiform of ETMNH 32999 in dorsal view. The articular surface for the cuneiform is at the top of the image. Scale bar = 1cm.

Cuneiform. The articular surface for the lunar on the left cuneiform is partially broken away, exposing cancellous bone beneath. On both left and right cuneiforms, the articular surface for the ulna is not as deep as seen in GFS adults; it retains the saddle-shape but is not as exaggerated (Fig. 33A).

Pisiform. In dorsal view, the pisiform is pinched medially, though not as strongly as in GFS adults; the pisiform is overall broader. Articular surface for the cuneiform curves, creating a saddle-shape, distinct from the flat surface seen in adults (Fig. 33B).

A B

Fig. 34A-B: Trapezoid and unciform of ETMNH 32999. (A) Left trapezoid of ETMNH 32999 in medial view. Scale bar = 3cm. (B) Left unciform of ETMNH 32999 in dorsal and ventral views. Scale bar = 3cm.

Trapezoid. Both left and right trapezoids are preserved. The articular surface for metacarpal II is broader in GFS adults than in ETMNH 32999.

Unciform. Both left and right unciforms are preserved, but the right is badly weathered. There are no remarkable differences in morphology between ETMNH 32999 and conspecific adults, though ETMNH 32999 lacks the porous protrusion lateral to the articular surface for the cuneiform seen in the holotype.

Fig. 35 Left second metacarpal of ETMNH 32999. Anterior (left) and posterior (right) views with unfused distal epiphyses. Scale bar = 3cm.

Metacarpal II. The articular surface for the trapezoid is not as pronounced in ETMNH 32999 as in conspecific adults. ETMNH 32999 lacks a pronounced posterior ridge as seen on the holotype specimen.

Fig. 36 Left third metacarpal of ETMNH 32999. Anterior (left) and posterior (right) views. In anterior view, the unfused distal epiphysis is placed in its anatomical position. It is removed from the posterior view. Scale bar = 3cm.

Metacarpal III. The articular surface for the unciform is not as distinct from surrounding features as it is in conspecific adults. The nutrient foramen noted on GFS adults by Short et al. (2019) is present. The posterior ridge is not as pronounced. Distal epiphysis is damaged, where

the articular surface for the proximal phalanx is preserved, but the articular surfaces for the sesamoids are not.

Fig. 37 Left fourth metacarpal of ETMNH 32999. Anterior (left) and posterior (right) views. In anterior view, the unfused distal epiphysis is placed in its anatomical position. It is removed from the posterior view. Scale bar = 3cm.

Metacarpal IV. *Teleoceras aepysoma* fourth metacarpals may have an articulation for a vestigial fifth metacarpal, such as ETMNH 601, or a remnant of the fifth metacarpal may be fused to the fourth in place of the articulation, as in the holotype (Short et al. 2019). In ETMNH 32999, there is an articular surface, suggesting the presence of a fifth metacarpal, as in ETMNH 601, though a fifth metacarpal is not preserved in ETMNH 32999. The articular surface for the unciform is slightly shallower in ETMNH 32999 than in adults.

Tarsal Elements

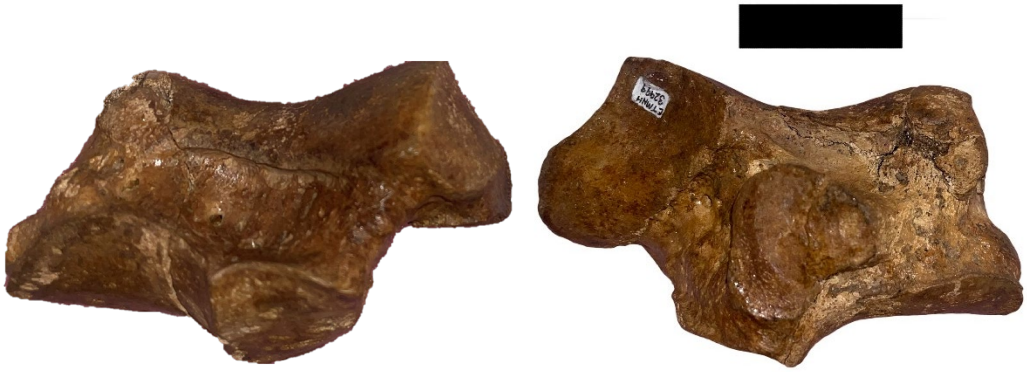

Fig. 38 Right astragalus of ETMNH 32999. Anterior (left) and posterior (right) views. Scale bar = 3cm.

Astragalus. (Fig. 38) The lateral side of the trochlear groove is worn away. Articular surface for the sustentaculum in ETMNH 32999 is shaped differently than in conspecific adults; in adults, it is elliptical in shape, with the long axis running mediolaterally. In ETMNH 32999, it is elliptical, though the long axis runs dorsoventally. The medial side of the articular surface for the sustentaculum is broken.

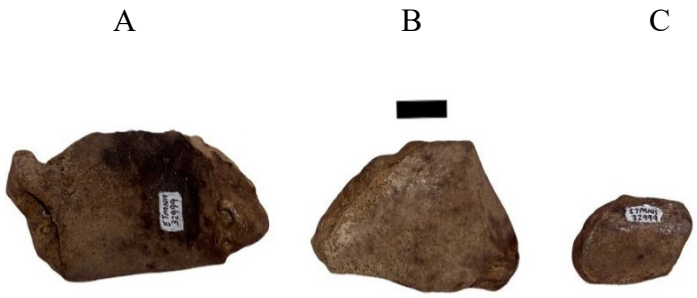

Fig. 39 Right navicular, mesocuneiform, and ectocuneiform of ETMNH 32999. (A) Right navicular, (B) mesocuneiform, and (C) ectocuneiform. Scale bar = 1cm.

Navicular. (Fig. 39A) Only the right navicular is preserved. At the anterior end of the articular surface for the astragalus, there is a projection that is more pronounced than in GFS adults, with larger porosities.

Mesocuneiform and Ectocuneiform. Only the right mesocuneiform (Fig. 39B) and ectocuneiform (Fig. 39C) are preserved. Morphology does not differ considerably from that of GFS adults.

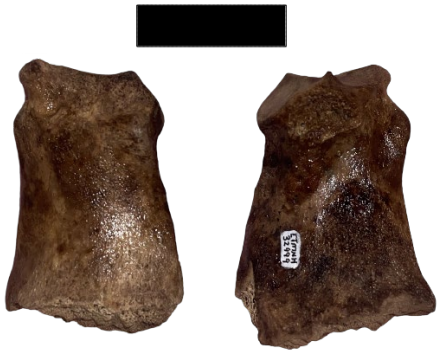

Fig. 40 Left second metatarsal of ETMNH 32999. Anterior (left) and posterior (right) views. Scale bar = 3 cm.

Metatarsal II. Only the left metatarsal II (Fig. 40) is preserved. The distal epiphysis is unfused and is not preserved. In ETMNH 32999, the bone is overall less rugose than GFS adults, but morphology does not differ considerably.

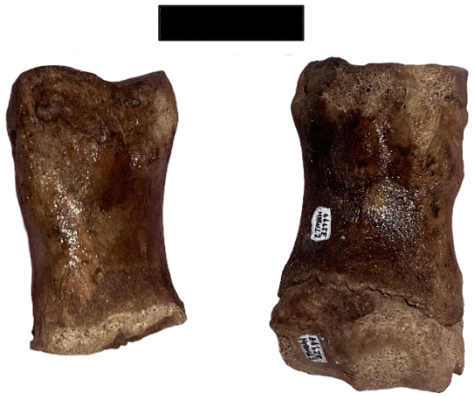

Fig. 41 Left fourth metatarsal of ETMNH 32999. Anterior (left) and posterior (right) views. In posterior view, the unfused distal epiphysis is placed in its anatomical position. In the anterior view, it is removed. Scale bar = 3cm.

Metatarsal IV. Only the left metatarsal IV (Fig. 41) is preserved. The distal epiphysis is unfused. Articular surface for the cuboid is less concave in ETMNH 32999 than in adults. The bone is overall less rugose than that of conspecific adults, but morphology does not differ considerably.

Phalanges and Sesamoids

Fig. 42 Proximal phalanges of ETMNH 32999. In anterior view. (Left) right lateral proximal manual phalanx, (middle) medial proximal manual phalanx, (right) left lateral proximal manual phalanx. Scale bar = 3cm.

Fig. 43 Distal phalanges of ETMNH 32999. In anterior view. (Left) right lateral distal phalanx, (middle) medial distal phalanx, (right) left lateral distal phalanx. Scale bar = 3cm.

Proximal phalanges. Proximal medial and lateral phalanges of ETMNH 32999 are preserved (Fig. 42), and maintain the 'flattened' morphology typical of *Teleoceras* (see Prothero 2005; Short et al. 2019). They do not differ considerably from conspecific adults.

Middle phalanges. No middle phalanges are preserved in ETMNH 32999.

Distal phalanges. Both medial and lateral distal phalanges (Fig. 43) are preserved in ETMNH 32999. Medial phalanges are roughly symmetrical. They are rugose and porous as in GFS adults. Overall, morphology does not differ considerably.

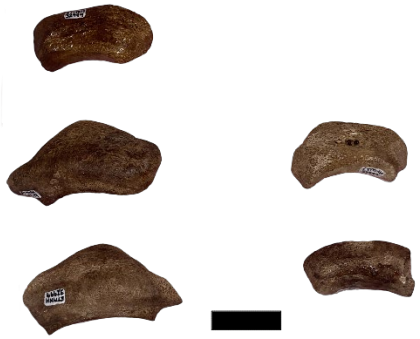

Fig. 44 Sesamoids of ETMNH 32999. Some sesamoids are known to be associated with the third metacarpals, but the exact anatomical locations of the others are unclear. Scale bar = 2cm.

Sesamoids. Various sesamoids are preserved (Fig. 44), but the exact placement is only known for a few which articulate with the right manual third digit. The morphology does not differ considerably from the sesamoids of GFS adults.

Axial Elements

Fig. 45 Partial thoracic vertebra of ETMNH 32999. (Left) posterior and (right) anterior views. Scale bar = 3cm.

Vertebrae. The vertebral column in ETMNH 32999 is represented only by two partial thoracic vertebrae whose exact position in the spine is unclear. On the more complete vertebra (Fig. 45), the anterior centrum is weathered so that cancellous bone is exposed on most of the surface. Neural canal is subcircular, slightly wider mediolaterally than it is dorsoventrally. The dorsal arch is broken away. No apparent zygapophyses are preserved on the anterior side. On the posterior side, the articular face of the centrum is similarly weathered with exposed cancellous bone; the ventral portion is broken away entirely. Both articular rib facets can be discerned, but the left is better preserved, albeit in a porous, weathered condition. Concavity on the left transverse process indicates the caudal notch. The other vertebra consists only of a badly weathered centrum and associated fragment of the neural arch.

Fig. 46 Rib fragments of ETMNH 32999. Scale bar = 5cm.

Ribs. Ribs of ETMNH 32999 are represented by several fragments; only two of them are complete enough to give any indication of morphology (Fig. 46). Both are badly weathered and fragmentary. Overall, morphology is unremarkable and does not differ considerably from conspecific adults. Several fragments of highly porous costal cartilage are also preserved.

Differences from *Teleoceras aepysoma* Adults Summary

Table 13 Ontogenetic morphological differences in the cranium and mandible between ETMNH 32999 and *Teleoceras aepysoma* adults

Craniomandibular Feature	ETMNH 32999	*Teleoceras aepysoma* Adults
Nasofrontal Constriction (1)	In dorsal view, frontal diamond does not constrict anteriorly, slopes gradually to nasals	In dorsal view, abrupt medial constriction of the anterior frontal diamond at the nasofrontal suture
Nasal Upturn (2)	In lateral view, nasals are straight and not upturned	In lateral view, nasals are occasionally upturned as in ETMNH 609 and 33000
Supraorbital Tuberosities (3)	Laterally extending, little to no dorsal expansion	Exaggerated and dorsally swollen, rugose
Frontal Concavity (4)	Region between supraorbital tuberosities is slightly convex	Region between supraorbital tuberosities is concave
Parietal Concavity (5)	Weak concavity	Strong concavity

Temporal Ridge (6)	Weak, barely distinguishable temporal ridges separated by narrow temporal "table"	Temporal ridges are defined and abruptly downturn laterally, in dorsal view the ridges meet at the level of the posterior squamosal, form distinct temporal ridge
Flare of Lambdoid Crest (7)	Weak crest oriented caudally with a very slight lateral flare	Defined crest flares strongly caudolaterally
Lateral Flare of Zygomatic Arches (8)	Posterior zygomatic arches barely flare laterally	Posterior zygomatic arches flare strongly laterally
Upward Slope of Anterior Dentary (9)	Begins at posterior m1	Begins at p4
Mental Foramen (10)	Inferior to posterior dp3	Inferior to p4
Depth of Masseteric Fossa (11)	Shallow	Deep

Numbers for each feature correspond with those shown in Figures 47-48.

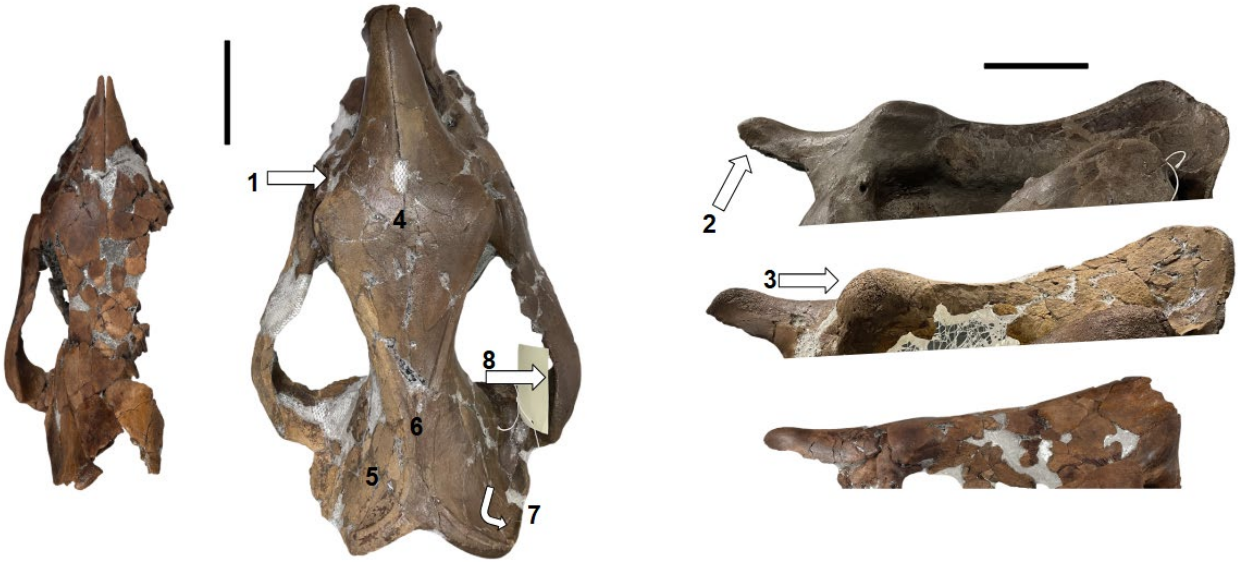

Fig. 47 Cranial ontogenetic features of *Teleoceras aepysoma*. Numbers correspond to Table 13. The skulls shown in dorsal view are ETMNH 32999 (left) and ETMNH 601 (right). The dorsal skull profiles shown in left lateral view are holotype ETMNH 609 (top), ETMNH 33000 (middle), and ETMNH 32999 (bottom). Scale bars =10cm.

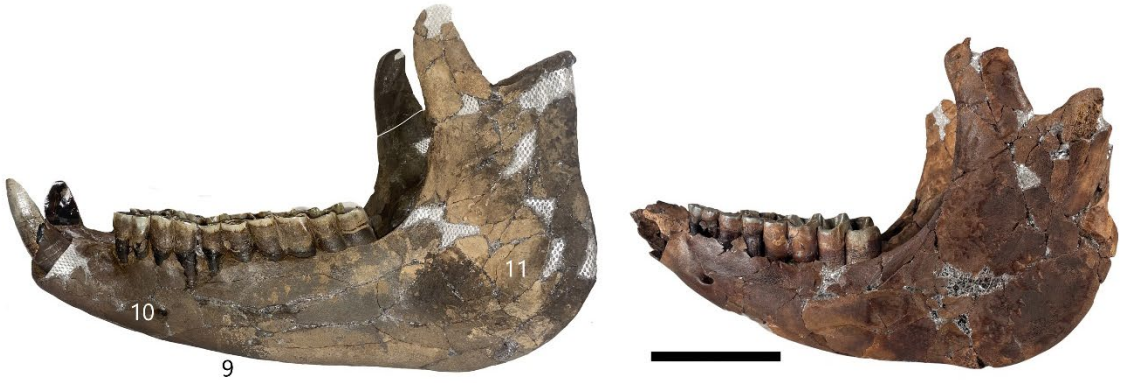

Fig. 48 Mandibular ontogenetic features of *Teleoceras aepysoma*. Numbers correspond to Table 13. (Left) Left lateral view of the mandible of paratype ETMNH 601, flipped laterally. (Right) Left lateral view of mandible of ETMNH 32999. Note that both m3s were removed from the mandible of ETMNH 32999. Scale bar =10cm.

Table 14 Morphological dental differences between ETMNH 32999 and *Teleoceras aepysoma* adults

Dental Feature	ETMNH 32999	*Teleoceras aepysoma* Adults
Upper Second Premolars	No P2 in the crypt on either side overlying dP2	P2 always present
Lower Third Premolars	Atypically small length and width	Length and width do not differ from other *Teleoceras*
Dental Mediolateral Widths	Consistently below those of GFS adults	Of typical mediolateral width for *Teleoceras*
Upper First Molar*	Lentoid crochet with two enamel folds on the labial side, constricted protrusion on labial side of antecrochet. Crochet larger than antecrochet. Postfossette open. Paracone rib present.	Crochet and antecrochet of equal size and lack any extra folds or features. Crochet of typical *Teleoceras* shape. Postfossette closed. No paracone rib.

*See Figures 19 and 26.

Description of Dental Defects

On ETMNH 32999 Mandibular Teeth

A

B

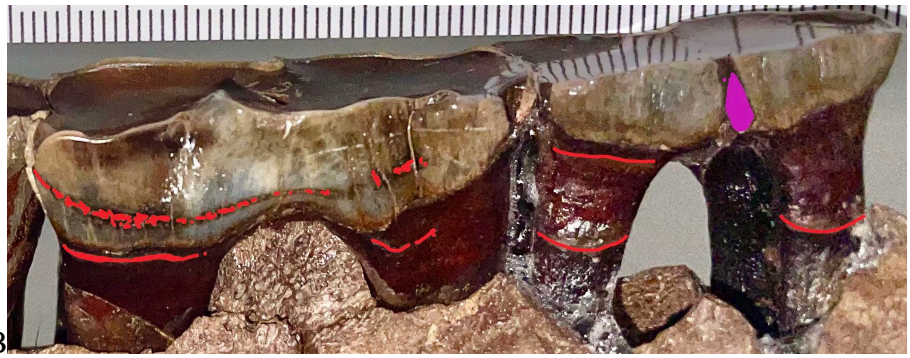

C

D

Fig. 49A-D Hypoplastic defects on the left mandibular teeth of ETMNH 32999. (A) Lingual view of left dp3 and dp4, (B) lingual view of left dp3 and dp4 with hypoplastic defects highlighted. (C) Labial view of left dp3, dp4, and m1, (D) labial view of left dp3, dp4, and m1 with hypoplastic defects highlighted. In B and D, the red coloration indicates defects that follow a roughly linear orientation, and purple coloration indicates an aplastic defect. Areas outlined in purple, but not filled in, represent areas that have irregular enamel distribution/thickness and are likely aplastic in nature.

The most obvious defect is a furrow on the lingual face of the left dp4 (Fig. 49A-B), ranging from ~2-5mm superior to the dentin-enamel junction (DEJ). This furrow extends from where the posterior lophid contacts the anterior lophid of m1, follows the anteroposterior length of the lingual face of the tooth, and tapers off in the middle of the anterior lophid. The entire furrow is distinguished by a darker brown color. The furrow is formed by a linear series of pits; this is not the same as pitted EH, which usually forms in nonlinear clusters (Goodman and Rose 1990; Towle and Irish 2019). Instead, the linear form of this defect reflects the ring-like process of enamel formation and the failure of the ameloblasts during this period of enamel secretion. The lingual face of left dp3 (Fig. 49A-B) has both root striations and a diamond-shaped aplastic defect at the lingual valley.

Much of the labial face of left dp4 (Fig. 49C-D) is obscured by dental calculus, but it is worth noting that immediately superior to the DEJ, especially on the posterior lophid, the color of the enamel beneath the calculus is the deep brown color of the dentine, rather than the off-white enamel color (Fig. 49C-D). A defect of this nature is consistent with aplasia, or total failure of enamel secretion. Matching aplastic enamel defects of lesser severity on the right dp4 and upper left dP4 (Figs. 50 and 55, respectively) support an aplasia diagnosis, as these teeth would have been forming at roughly the same time.

On the anterior and posterior roots of left dp3, there are striations in the enamel at ~3mm inferior to the DEJ, and there are pits/aplasia on the posterior root inferior to the striation at

~6mm inferior to the DEJ (Fig. 49C-D). Defects on the roots of dp3 are visible on both lingual and labial sides. The labial face of the left dp4 roots displays apparent aplastic defects (Fig. 49C-D) ~6mm inferior to the DEJ on both roots. Uniform distribution and identical depth of the defects suggest that they represent failure of dentin formation, rather than an extremely concentrated point of taphonomic weathering. Superior to the missing dentin on left dp4, 1.5mm inferior to the DEJ on both roots, there are pronounced striations where the thickness of the root is altered. Similar root defects have been found in specimens of captive extant rhinos (data from M. Hullot, personal communication 2025).

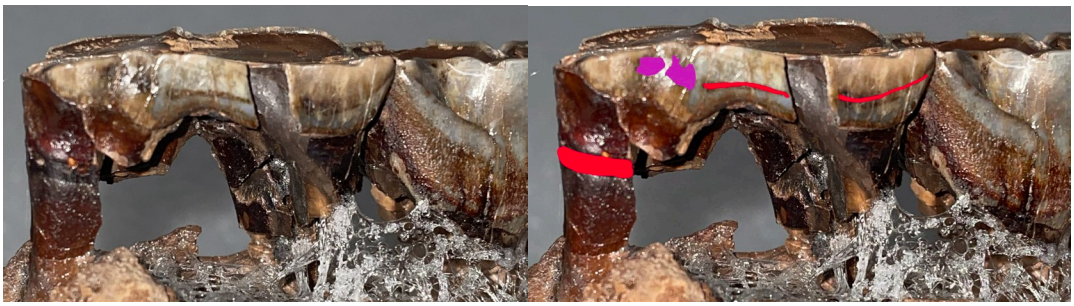

Fig. 50 Hypoplastic defects on the right dp4 of ETMNH 32999. Lingual view of right dp4. Right image shows hypoplastic defects highlighted. Red coloration indicates defects that follow a linear orientation, and purple coloration indicates aplastic defects.

On the lingual face of right dp4 (Fig. 50), there is a linear EH ~1-2mm superior to the DEJ, mirroring the deep furrow on the left dp4. The right dp4 furrow is less severe than that of its left counterpart, though it spans the length of the entire posterior lophid. On the anterior lophid ~2-4mm superior to the DEJ are two aplastic defects (Fig. 50). On the lingual side of the anterior root, there is a thick striation immediately inferior to the DEJ, matching the same defect on left dp4. The posterior root is too damaged to identify any defects with confidence.

On the lower left m1 (Fig. 49C-D), there are two paired defects as observed in its upper counterpart (Fig. 52). The more pronounced one is linear EH ~10.5mm superior to the DEJ and is only expressed on the anterior lophid as a U-shaped groove. The less pronounced one is

largely obscured by cement/calculus buildup. There are faint striations on the posterior lophid which are likely counterparts to the EH on the anterior lophid, but their depth/severity cannot be assessed macroscopically.

Fig. 51 Hypoplastic pits on the right M1 of ETMNH 32999. Pits are highlighted by green dots in the right image.

On the labial face of the anterior lophid of right m1 (Fig. 51), just superior to the DEJ, there is a cluster of pits consistent with pitted EH. Several dozen circular pits are arranged in a rhomboidal area unevenly spaced from each other. Anterior to the pits is a vertical section of dentin uncovered by broken enamel, which spans from the root to the occlusal surface in a semi-elliptical shape. The broken enamel reveals a cross-section of the enamel shell bearing more pits directly adjacent to the PH observed on the labial face. Because of this missing enamel, it is unknown whether the PH defect spanned the entire anterior lophid, but it is not well represented on the posterior. Some have considered PH to have a distinct etiology from linear EH, considering it to be of genetic origin (Towle and Irish 2019) rather than of external stress. Interestingly, the right m1 does not display any obvious linear defects like the left m1 (Fig. 49C-D) or left M1 (Fig. 52).

Striations are visible on the roots of both left and right m1. Left m1 has a striation ~2mm inferior to the DEJ, a series of pits/aplastic defects, and a second striation at ~4mm inferior to the DEJ (Fig. 49C-D).

On ETMNH 32999 Maxillary Teeth

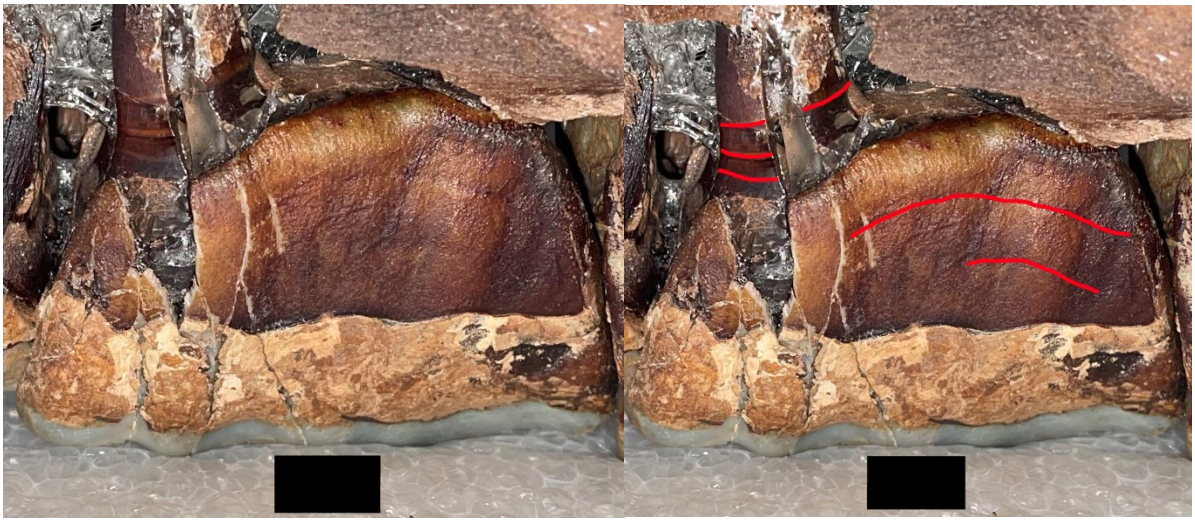

Fig. 52 Linear hypoplastic defects on the right M1 of ETMNH 32999. In the right image, the defects on the enamel and roots are highlighted in red. Scale bar = 1cm.

On the left M1 (Fig. 52), two shallow, parallel linear grooves are visible on the labial face. The superior one is 7.5mm below the DEJ and the inferior one 12.7mm. The groove closer to the DEJ is deeper and more pronounced. It follows the length of the labial face of the tooth from the anterior root to the posterior edge. The inferior groove is parallel to the first but is more difficult to see with the naked eye. A cross-section is visible due to broken enamel inferior to the anterior root (Fig. 53). At the same horizons as the linear grooves, there are visible reductions in enamel thickness revealed by the slightly undulating profile of the enamel cross-section. There are at least three distinct horizons of the cross-section where the enamel thickness narrows and again widens. These are interpreted as reductions in enamel thickness, rather than natural undulations in enamel thickness, due to them being flush with the hypoplastic linear grooves. Notably, the linear EH on the left M1 is less severe than those observed on the dp4. While this pattern is still evidently linear EH, it corresponds more closely with what Mead (1999) described as “swale hypoplasia”, or wavy enamel, rather than a deep furrow as is observed on left dp4. Regardless, these paired defects accurately represent at least a partial failure in enamel formation

where typical enamel thickness was not achieved, as illustrated by the undulating profile of the cross-section (Fig. 53).

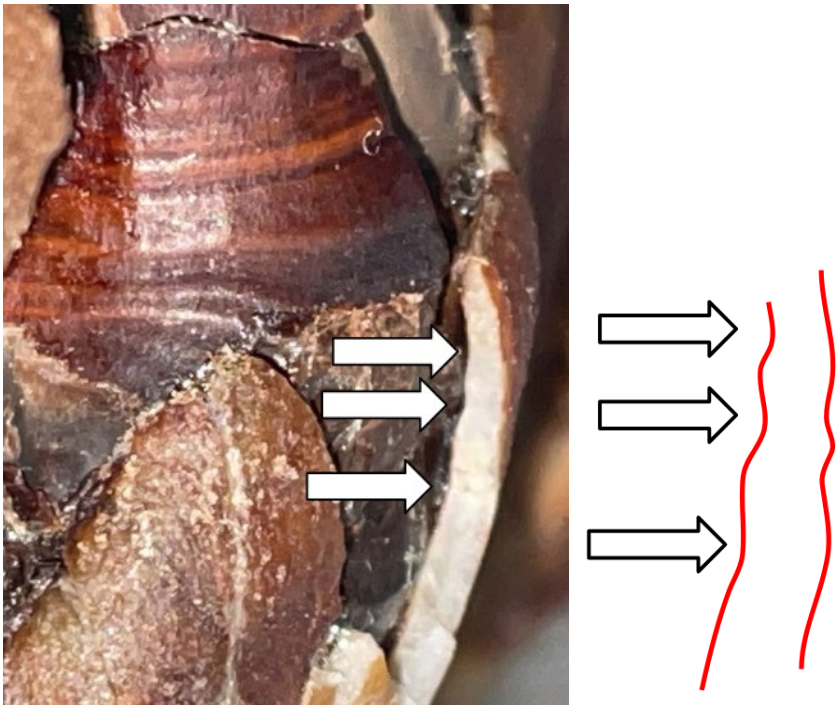

Fig. 53 Enamel cross section of left M1 of ETMNH 32999. (Left) Enamel cross section of left M1 of ETMNH 32999 as revealed by taphonomic damage. White arrows mark visible reductions in enamel thickness level with the hypoplastic linear grooves on the labial face. Note the series of striations visible on the anterior root. (Right) Simplified line drawing of the enamel cross section undulation with white arrows indicating depressions where the enamel thins.

Striations are also visible on the anterior labial root of left M1 (Fig. 52-53); at least six distinct horizontal bands can be found directly superior to the DEJ. The most pronounced of the striations marks an evident change in root thickness. Repetition of the root defects suggests a prolonged period of stress or repeated series of metabolic insults.

Additional defects are visible on the lingual surface of the left M1 metastyle (Fig. 54). On the lingual face of the metastyle, there is a large circular pit. This defect is unlike the other EH types; a similar defect and is referenced and figured by Hullot et al. (2019) as an “unclassified hypoplasia”. Overall shape and depth of the defect suggest it is aplastic in nature, but its circular shape and uniform depth are distinct from the way that aplasia manifests on the other teeth of

ETMNH 32999. Uniformity of the defect resembles what is seen in circular dental caries, which have been associated with typical EH (e.g. Cook and Buikstra 1979; Halcrow and Tayles 2008; Sadida et al. 2021).

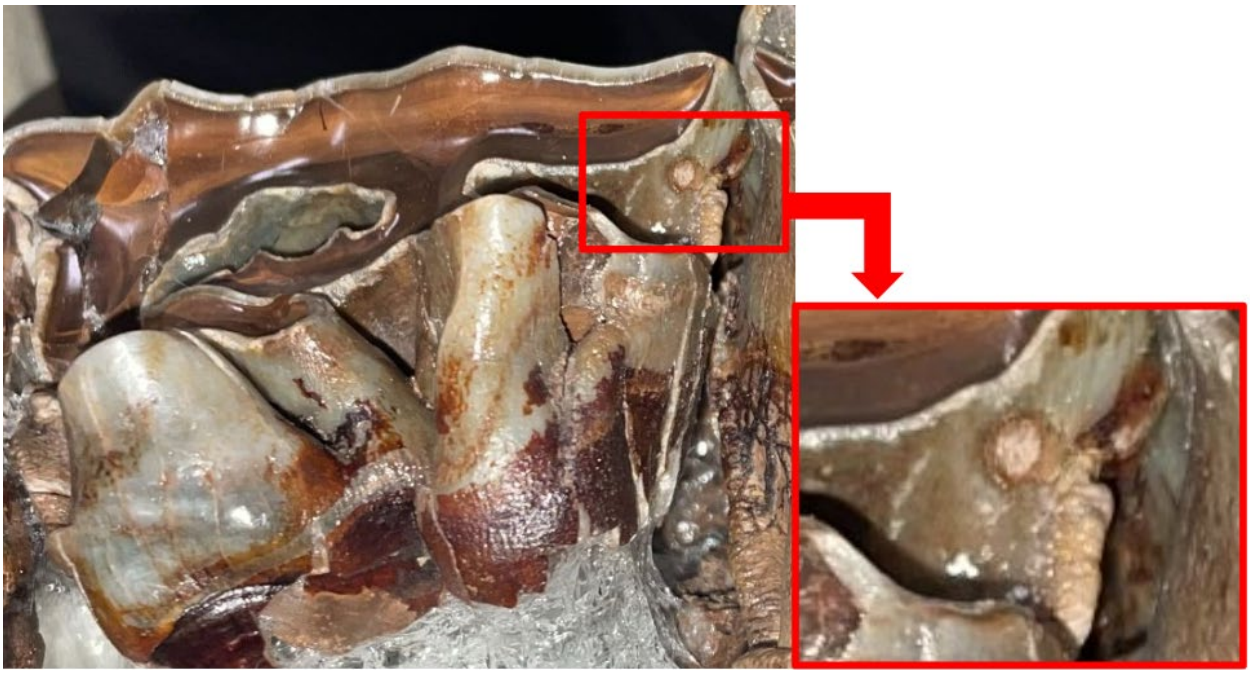

Fig. 54 Circular defect on left M1 of ETMNH 32999. The red box and zoomed-in photo indicate the large circular hypoplastic defect which resembles a dental caries. Not to scale.

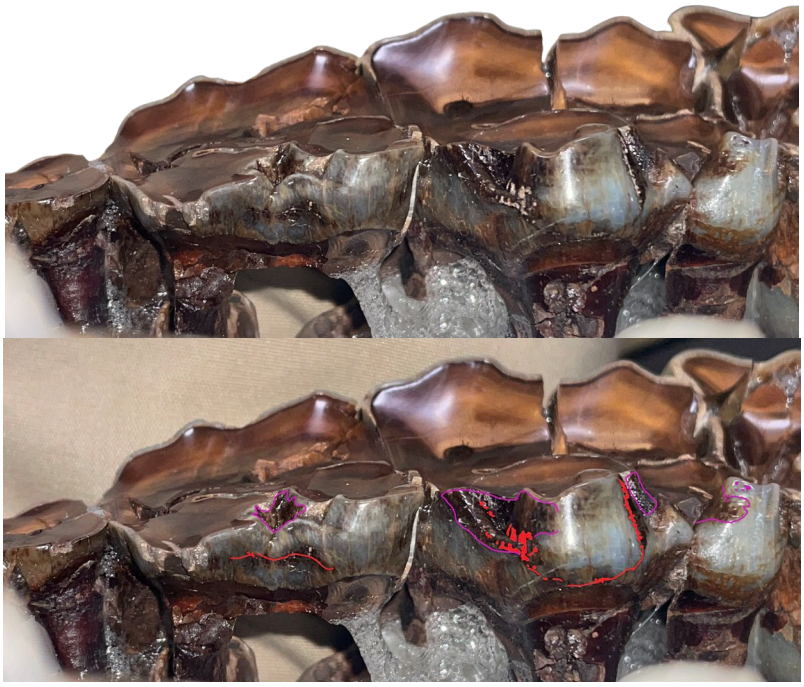

Fig. 55 Hypoplastic defects on the left maxillary premolars of ETMNH 32999. Lingual view of left dP3 and dP4. Red coloration in the bottom image indicates defects that follow a roughly linear pattern. Pink coloration indicates aplastic defects and/or areas of irregular enamel thickness. Note that the photos have been flipped so that the occlusal surface is facing dorsally.

On lingual left dP3, a linear EH furrow originates at the posterior protocone and crosses the lingual valley at 2-2.5mm inferior to the DEJ (Fig. 55). At the same horizon within the median valley, there are aplastic defects on the lingual face of the crochet and anterior face of the metaloph. Roots are too damaged to distinguish breakage and abrasion from defective dentin. Within the fossette, defects on the anterior metaloph and lingual antecrochet appear aplastic in color and distribution.

On the lingual left dP4, there is a pronounced aplastic defect on the anterior protocone constriction (Fig. 55) where the cingulum meets the anterior protocone. On the anterior protocone constriction, posterior to the cingulum, the malformed enamel is thin, discolored, and dotted with pits (though not pitted EH). There is a thin linear EH furrow extending from the aplasia at the cingulum-anterior protocone junction which continues along the lingual protocone, meeting the DEJ at its lowest point. This linear defect curves sharply ventrally at the posterior

protocone and runs up its vertical length to the occlusal surface. While the vertical defect is evidently linked to the preceding linear EH, vertical hypoplasia is distinguished from typical linear EH by the FDI (FDI type 5) as an unusual condition of indeterminate etiology. Adjacent to the vertical furrow is an aplastic patch on the lingual surface of the antecrochet, flush with the aplastic patch on the anterior protocone constriction. There is a faint aplastic defect on the anterior hypocone with small pits nearby (Fig. 55). Most of the roots of left dP4 are too badly damaged to distinguish hypoplastic defects with confidence, aside from the linear root striations on both roots.

On AMNH F:AM 109518, *Teleoceras medicornutum*

Fig. 56 Cranium of AMNH F:AM 109518. (Left) right and (right) left lateral views of AMNH F:AM 109518, subadult *Teleoceras medicornutum*. Scale bar = 5 cm.

Fig. 57 Palatal view of AMNH F:AM 109518. Scale bar = 10cm.

Fig. 58 Hypoplastic defects on the right maxillary teeth of AMNH F:AM 109518. Red coloration in the right image highlights the defects. Scale bar = 1cm.

Fig. 59 Hypoplastic defects on the left maxillary teeth of AMNH F:AM 109518. Red coloration in the right image highlights the defects. Scale bars = 1cm.

AMNH F:AM 109518 (Figs. 56-57) is slightly younger (age class VII) than ETMNH 32999 (age class VIII). While both retain the full deciduous component and share a moderately worn M1 (Fig. 57), the M2 of AMNH F:AM 109518 is unworn (Stage 1), while that of ETMNH 32999 has exposed dentine on the anteriormost lophs (Stage 4) (see Fig. 99 for wear stages). Both the left and right M1 and the left and right dP4 of AMNH F:AM 109518 display linear EH (Figs. 58-59). The labial face of the left dP4 has a deep horizontal furrow ~6-8mm inferior to the DEJ, best pronounced on the posterior loph. A series of pits are visible inferior to the furrow at Xmm inferior to the DEJ. The left M1 has a deep, rounded-M-shaped furrow along the entire labial face of the tooth ~12-20mm inferior to the DEJ. There is also a series of pits inferior to this furrow, though only a few of these pits are visible as much of the tooth inferior to the primary

furrow is obscured by sediment. The defects on the right teeth nearly mirror those on the left in form and distance from the DEJ.

On AMNH FM 20584, *Ceratotherium neumayri*

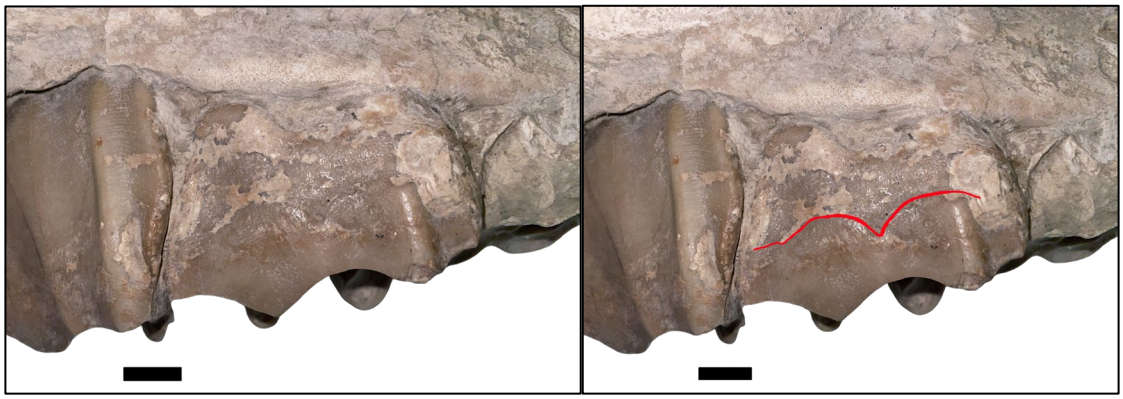

Fig. 60 Hypoplastic defects on the right M1 of AMNH FM 20584. In the right image, the hypoplastic defect is highlighted in red. Scale bars = 1cm.

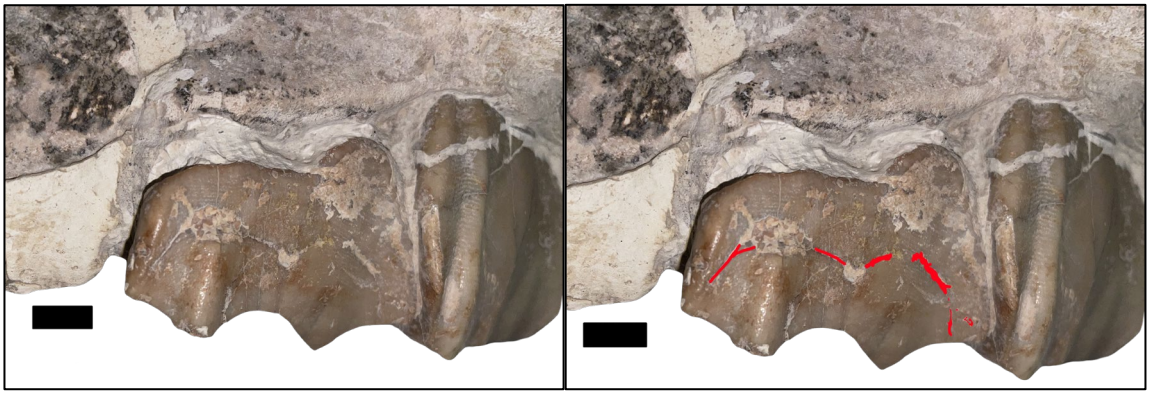

Fig. 61 Hypoplastic defects on the left M1 of AMNH FM 20584. In the right image, the hypoplastic defect is highlighted in red. Scale bars = 1cm.

Scale bar = 10cm.

Fig. 62 Cranium of AMNH FM 20584 in palatal view. AMNH FM 20584 is of nearly identical dental age to ETMNH 32999 (age class VIII). Both individuals retain dP3 and dP4, have moderate wear on the M1, and only the protoloph and anterior ectoloph of M2 are worn enough to expose dentin (Fig. 62); the M3 has also recently breached the bone surface, consistent with what was hypothesized for M3 placement in ETMNH 32999. Both the left and right M1 of AMNH FM 20584 display linear EH; the right dP4 is absent, and the labial face of the left dP4 is too broken to identify any defects. M1 defects are similar in their expression and placement, both appearing as rounded W-shaped furrows ~11-15mm from the DEJ (Fig. 60-61), similar to AMNH F:AM 109518 (Fig. 58-59). The furrows are deep and are found at similar horizons on each tooth, indicating a single, though, severe, metabolic insult.

Subadults with Enamel Hypoplasia Deviation from Expectation

Table 15 Subadult rhinocerotids with enamel hypoplasia deviation from expected size

Specimen	Species (age class)	% Dev LN (Range)	% Dev PO (Range)	% Dev TCL (Range)	% Dev ZW (Range)
ETMNH 32999	*Teleoceras aepysoma* (VIII)	-14.31 % (-11.23 to -17.19%)	-14.31 % (-9.62 to -18.54)	-11.75 % (-0.41 to -20.78)	-25.40% (-19.34 to -30.62)
AMNH F:AM 109518	*Teleoceras medicornutum* (VII)	-18.21% (-15.26 to -20.95%)	-26.26%* (-22.22 to -29.9%)	N/A	-21.43% (-15.04 to -26.92%)
AMNH FM 20584	*Ceratotherium neumayri* (VIII)	N/A	-5.84% (-0.68 to -10.49%)	-2.20% (+10.38 to -12.2%)	+8.81% (+1.20 to +17.65%)

Allometric coefficients used were from Hagge (2010); Calculations for *Teleoceras aepysoma* and *T. medicornutum* used the coefficients determined for *T. major*, and *Ceratotherium neumayri* used those of *C. simum*. *Note that the Anterior Premolar to Occiput Length (PO) for AMNH F:AM 109518 was estimated due to missing occipital condyles, so percent deviation results should be interpreted with caution.

Growth Plots Among Included Taxa

Craniomandibular by Species

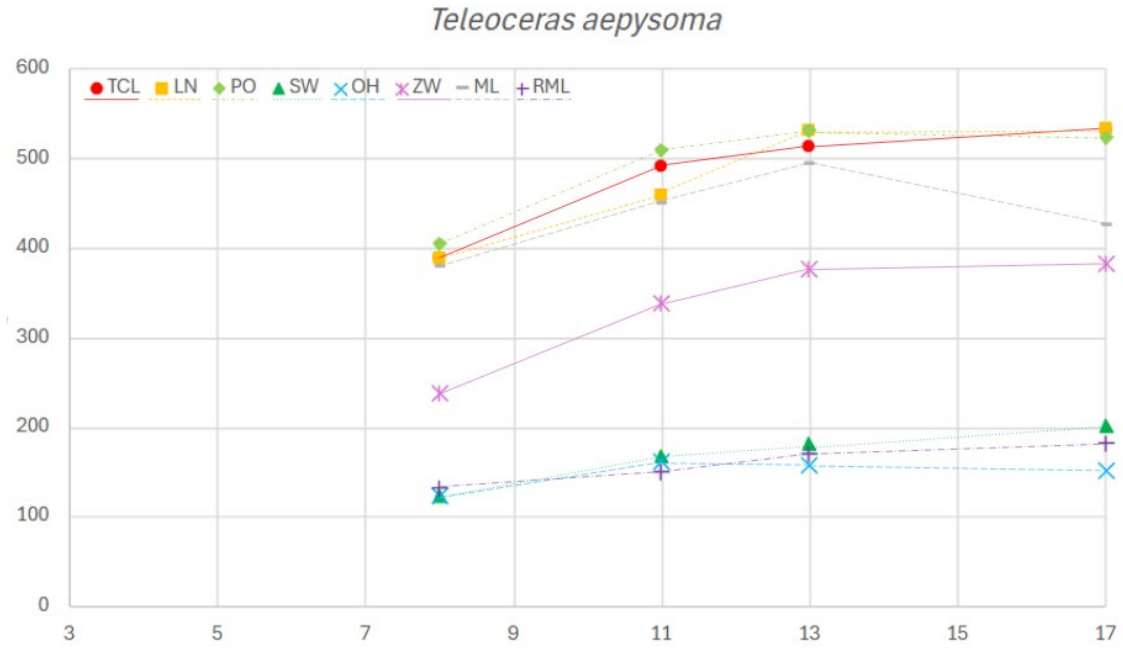

Fig. 63 Raw craniomandibular measurements through ontogeny in *Teleoceras aepysoma*. X-axis values correspond to Hitchins (1978) dental age classes. Y-axis values are in mm. Note the sharp increase in TCL, LN, PO, ZW, and ML from age class 8 to age class 11 relative to the succeeding plots. Abbreviations can be found in the "Abbreviations and Nomenclature" section.

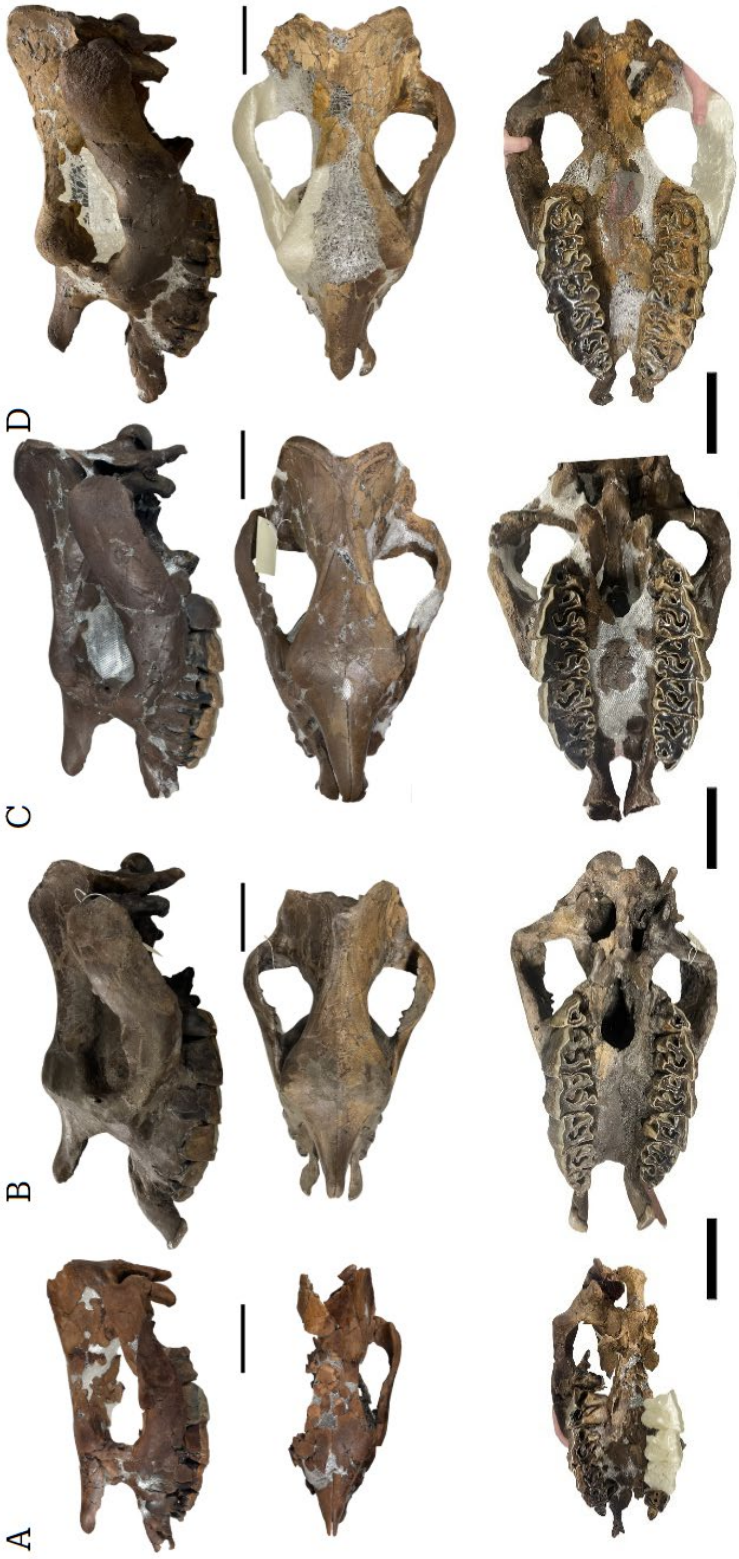

Fig. 64A-D Cranial ontogenetic sequence for *Teleoceras aepysoma*. (Top row) left lateral, (middle row) dorsal, and (bottom row) occlusal views. (A) ETMNH 32999, age class VIII. (B) ETMNH 609, age class XI. (C) ETMNH 601, age class XIII. (D) ETMNH 33000, age class

XVII. Scale bars = 10cm. Note that ETMNH 601 lateral view has been flipped horizontally to figure the better-preserved side. On all but ETMNH 609, reconstructed areas are represented by white or silver filler. In ETMNH 609, the filler is the same color as the bone. Note that the premaxillae of ETMNH 609 are erroneously reconstructed; ETMNH 601 is better representative of premaxilla morphology.

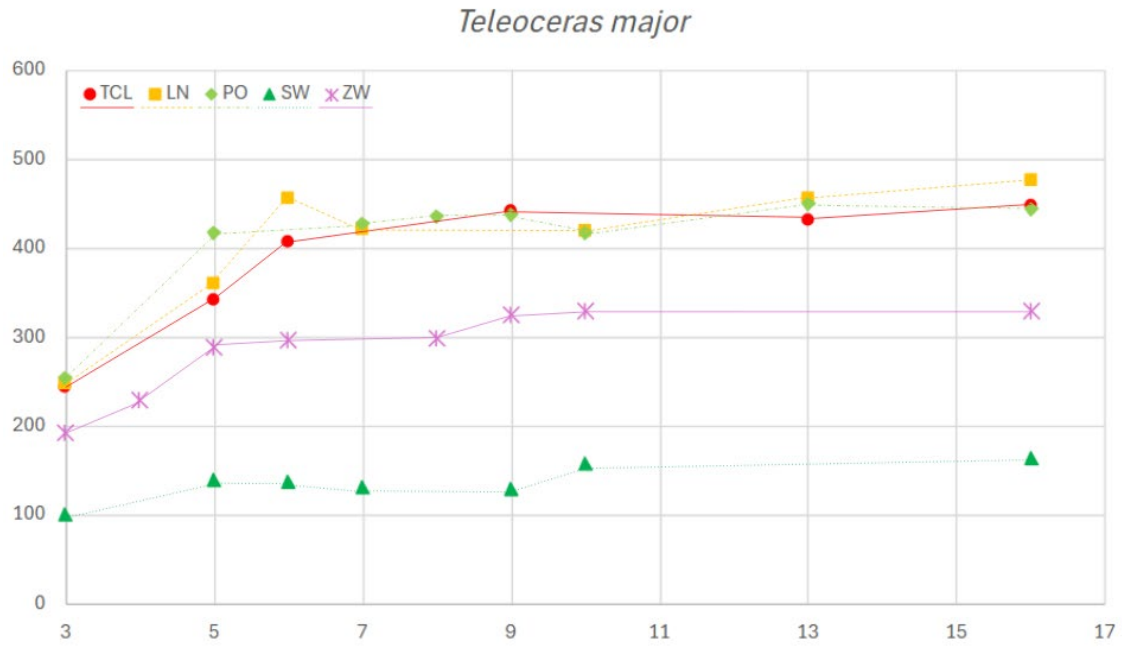

Fig. 65 Raw cranial measurements through ontogeny in *Teleoceras major*. X-axis values correspond to Hitchins (1978) dental age classes. Y-axis values are in mm. Note the achievement/near achievement of asymptotic size in subadulthood. Abbreviations can be found in the "Abbreviations and Nomenclature" section.

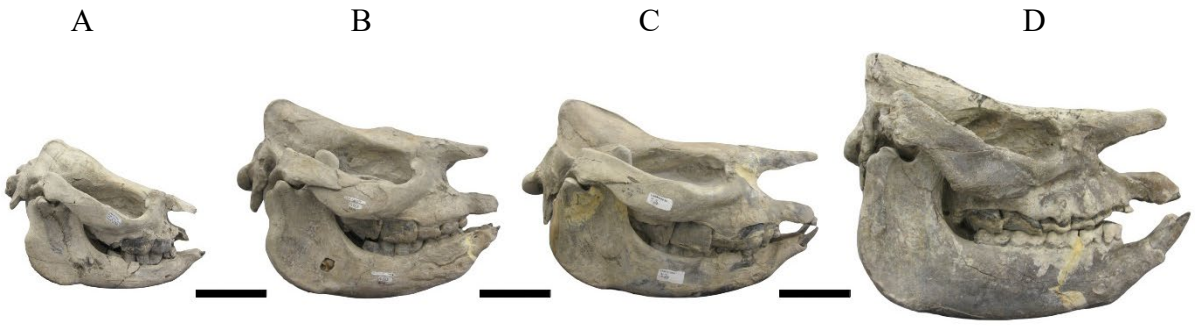

Fig. 66A-D Cranial ontogenetic sequence for *Teleoceras major*. Modified from Hagge (2010). Right lateral view. (A) UNSM 52254, age class II; (B) UNSM 52234, age class V; (C) UNSM 52232, age class VIII; (D) UNSM 52288, age class XVI. Note that, while USNM 52288 appears substantially larger than USNM 52232, the most pronounced size differences are in the mandible rather than the cranium; adult cranial morphology is apparent as early as age class V. Scale bars = 10cm.

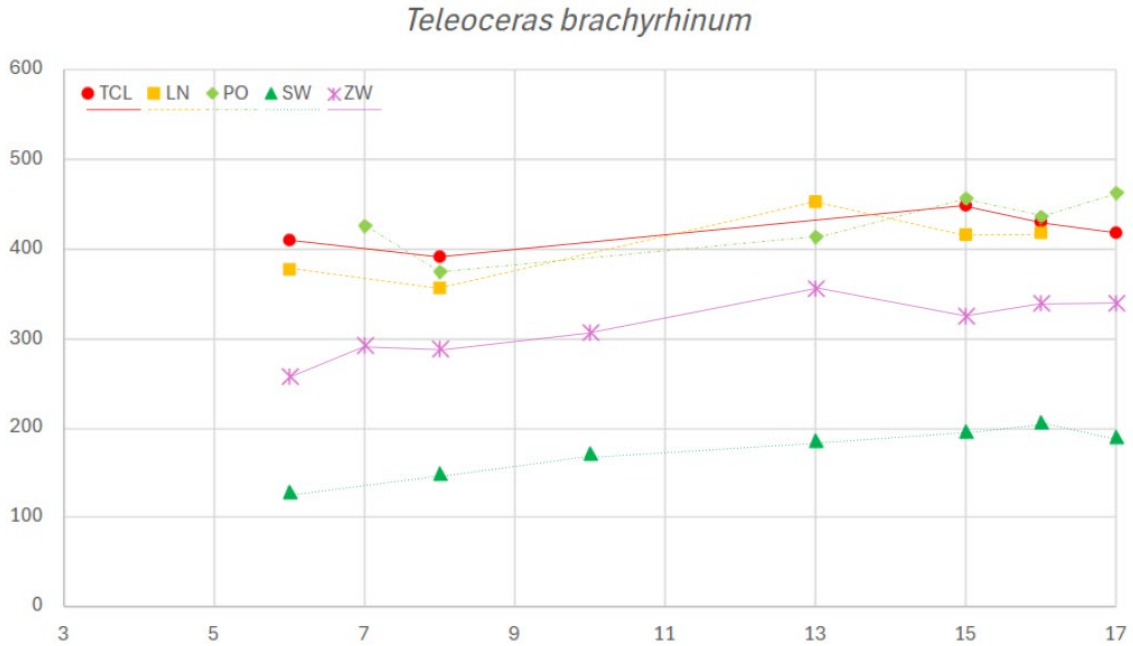

Fig. 67 Raw cranial measurements through ontogeny in *Teleoceras brachyrhinum*. X-axis values correspond to Hitchins' (1978) dental age classes. Y-axis values are in mm. Note the achievement/near achievement of asymptotic size in subadulthood. Abbreviations can be found in the "Abbreviations and Nomenclature" section.

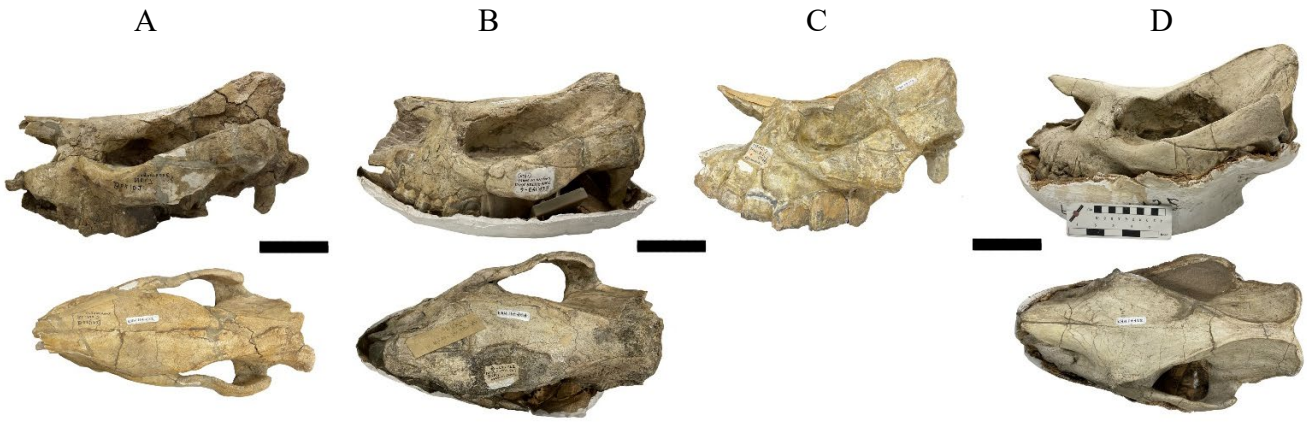

Fig. 68A-D Cranial ontogenetic sequence for *Teleoceras brachyrhinum*. (Top row) left lateral and (bottom row) dorsal views. (A) AMNH F:AM 114455, age class VI; (B) AMNH F:AM 114449, age class VIII; (C) AMNH F:AM 114436, age class XIII; (D) AMNH F:AM 114452, age class XV. Note that all but A have been flipped horizontally. Note the similarities in shape and size between the immature and mature individuals, where A and B display the upright nuchal crest typical of adults and broad zygomatic widths. Dorsal view for C could not be photographed due to the instability of the specimen. Scale bars = 10cm.

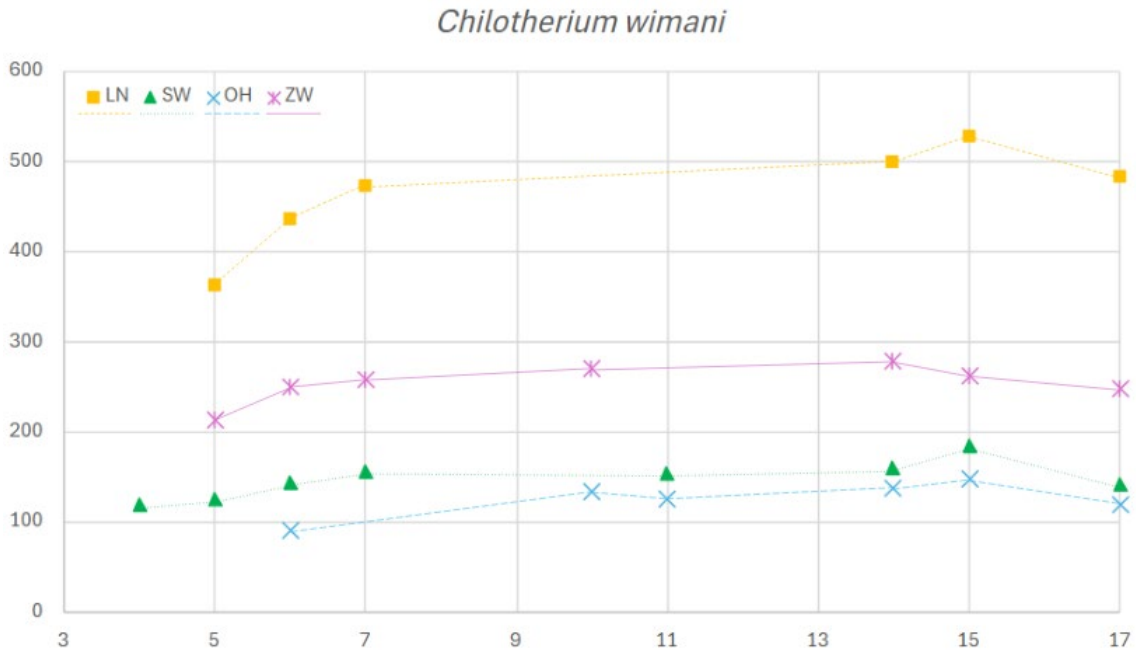

Fig. 69 Raw cranial measurements through ontogeny in *Chilotherium wimani*. X-axis values correspond to Hitchins (1978) dental age classes. Y-axis values are in mm. Data from Deng (2001). Abbreviations can be found in the "Abbreviations and Nomenclature" section.

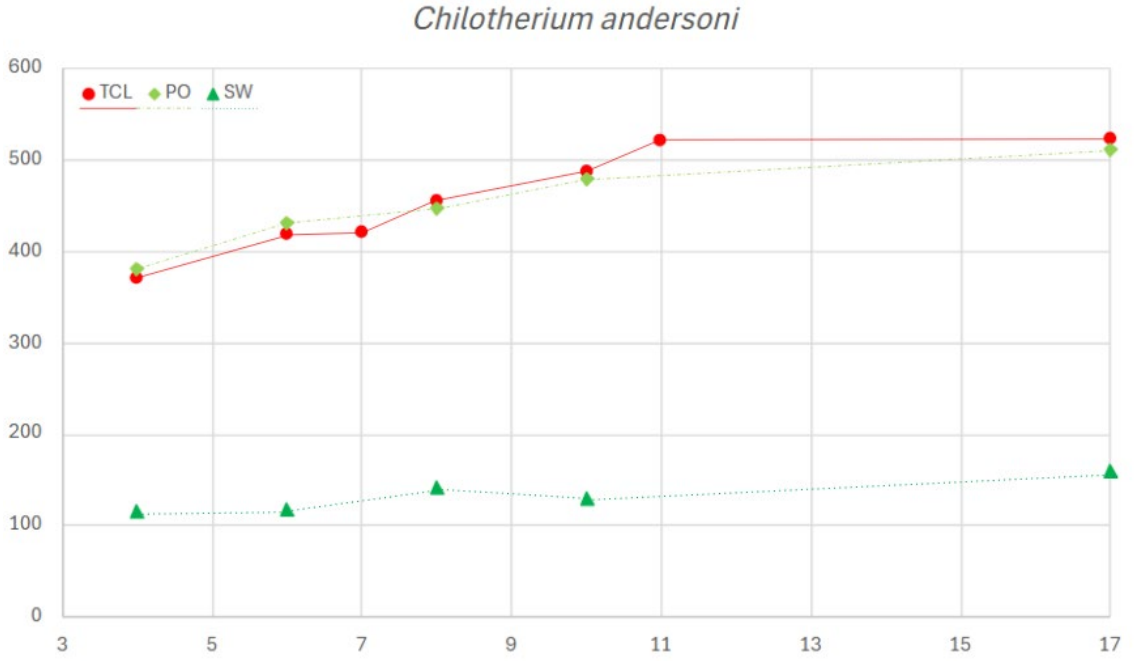

Fig. 70 Raw cranial measurements through ontogeny in *Chilotherium andersoni*. X-axis values correspond to Hitchins (1978) dental age classes. Y-axis values are in mm. Abbreviations can be found in the "Abbreviations and Nomenclature" section.

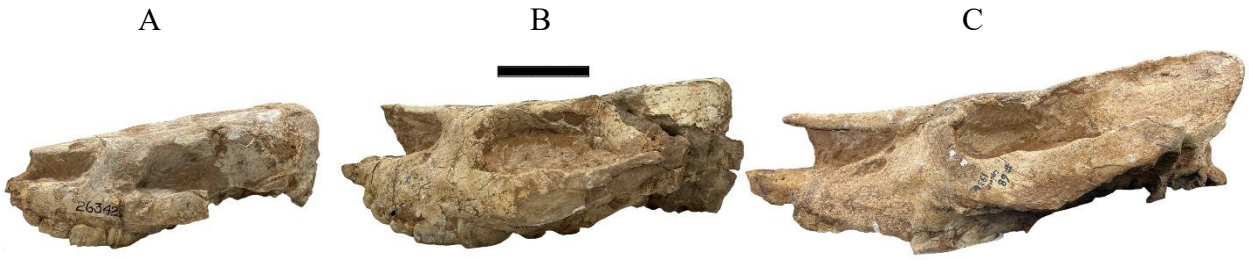

Fig. 71A-C Cranial ontogenetic sequence for *Chilotherium andersoni*. Left lateral view. (A) AMNH FM 26342, age class IV; (B) "CHINA #17", age class VII; (C) AMNH F:AM 147820, age class XVII. Note that B has been flipped horizontally. Scale bar = 10cm.

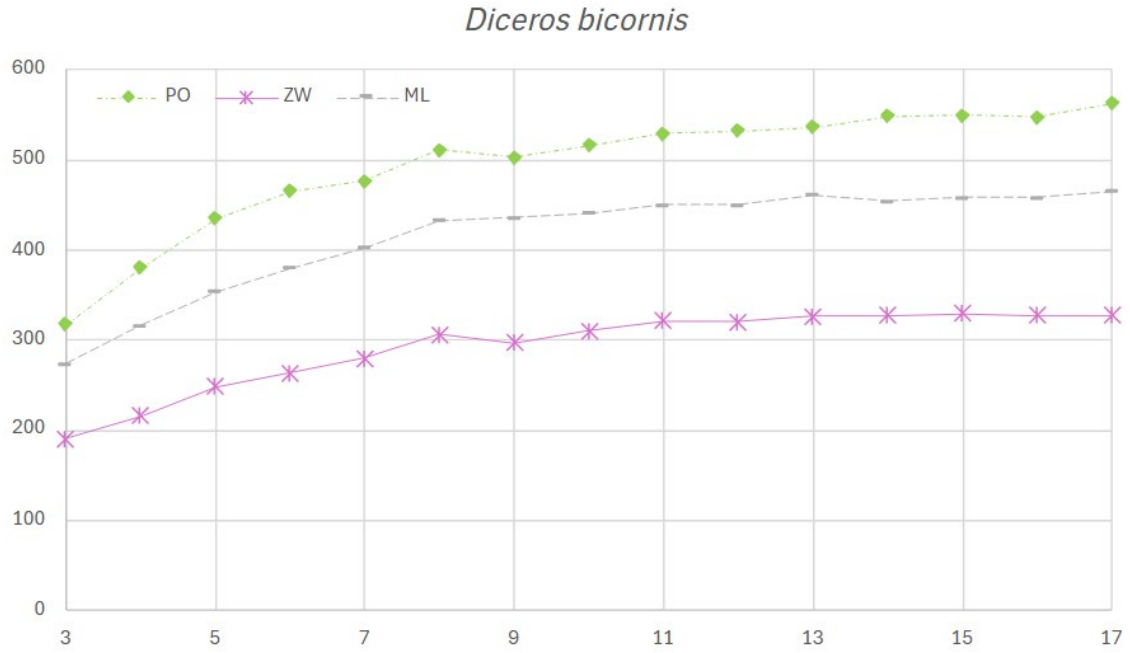

Fig. 72 Raw craniomandibular measurements through ontogeny in *Diceros bicornis*. X-axis values correspond to Hitchins' (1978) dental age classes. Y-axis values are in mm. Data from Goddard (1970). Note the achievement/near-achievement of asymptotic size in subadulthood. Abbreviations can be found in the "Abbreviations and Nomenclature" section.

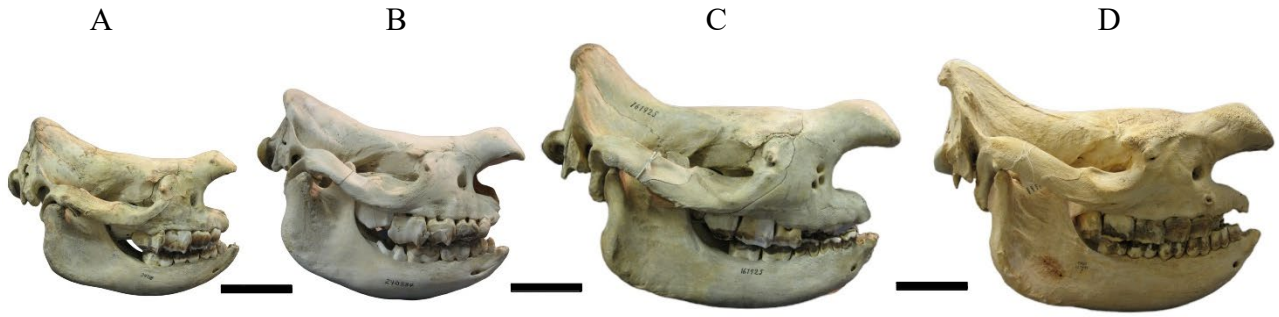

Fig. 73A-D Cranial ontogenetic sequence for *Diceros bicornis*. Right lateral view, all photos modified from Hagge (2010). (A) USNM A34718, age class III; (B) USNM 240884, age class V; (C) USNM 161925, age class VIII; (D) FMNH 127849, age class XII. Scale bars = 10cm.

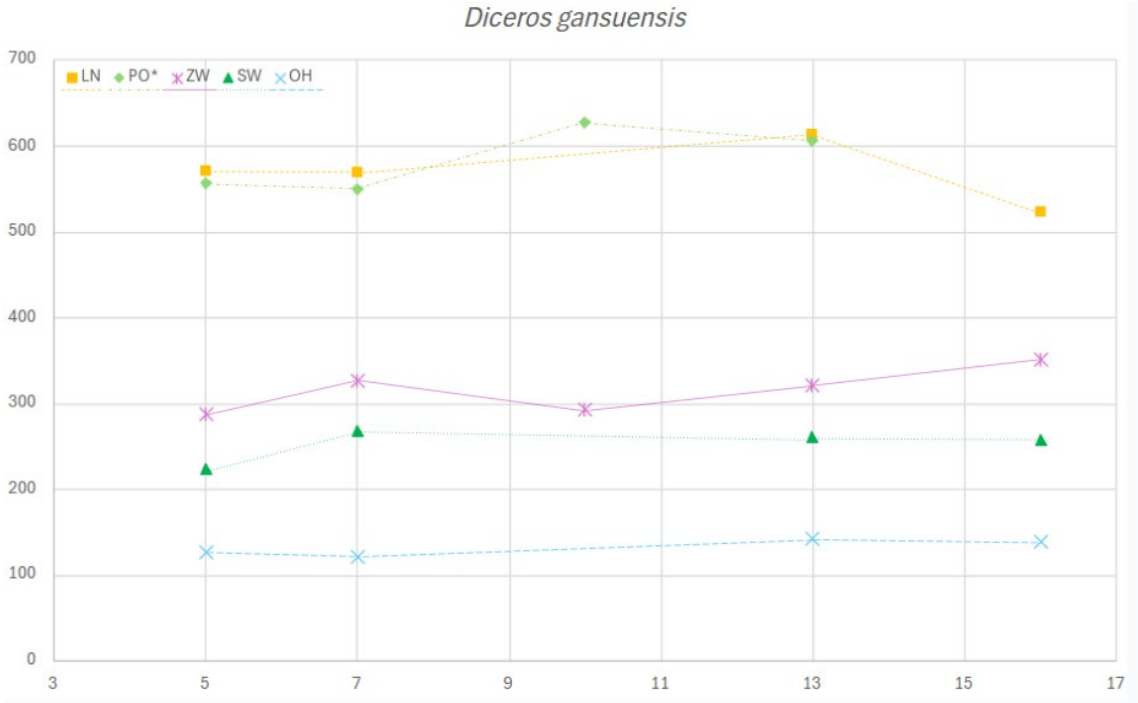

Fig. 74 Raw cranial measurements through ontogeny in *Diceros gansuensis*. X-axis values correspond to Hitchins' (1978) dental age classes. Y-axis values are in mm. Data from Deng and Qiu (2007). Note the size similarities between mature and immature individuals. Abbreviations can be found in the "Abbreviations and Nomenclature" section.

Forelimbs by Species

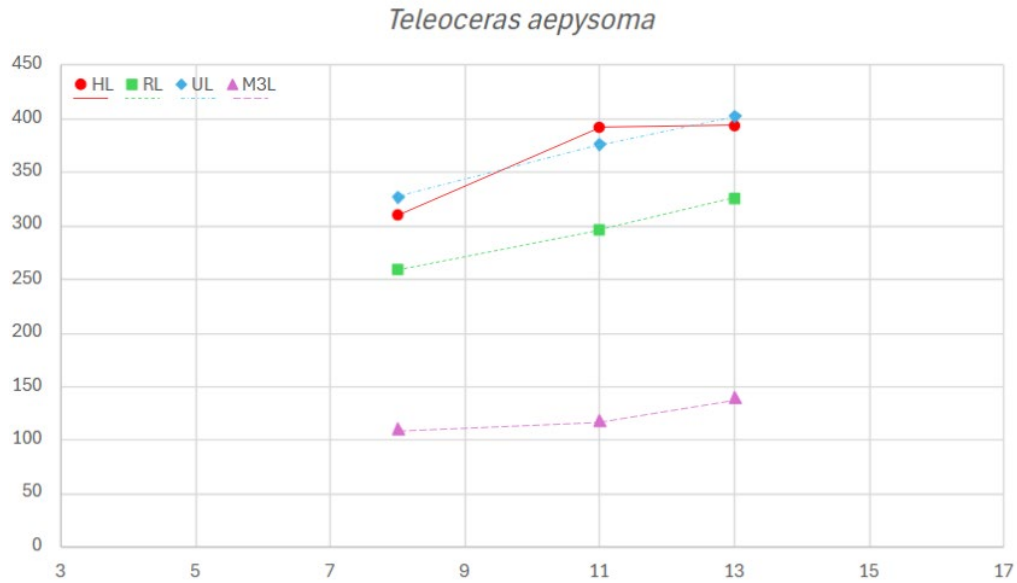

Fig. 75 Raw forelimb lengths through ontogeny in *Teleoceras aepysoma*. X-axis values correspond to Hitchins (1978) dental age classes. Y-axis values are in mm. Abbreviations can be found in the "Abbreviations and Nomenclature" section.

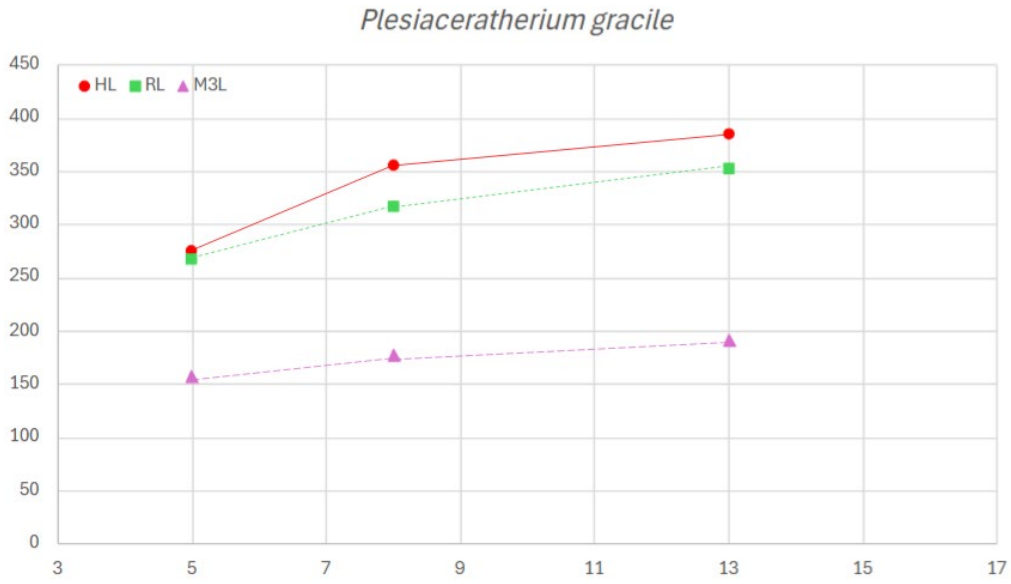

Fig. 76 Raw forelimb lengths through ontogeny in *Plesiaceratherium gracile*. X-axis values correspond to Hitchins (1978) dental age classes. Y-axis values are in mm. Data from Lu et al. (2023b). Mean adult values reported by Lu et al. (2023b) were assigned to age class 13 as this matches the dental age of the adult *Pl. gracile* figured in Lu et al. (2020) from which the values were taken. Abbreviations can be found in the "Abbreviations and Nomenclature" section.

Percent of Average Adult and Raw Measurements Between Taxa

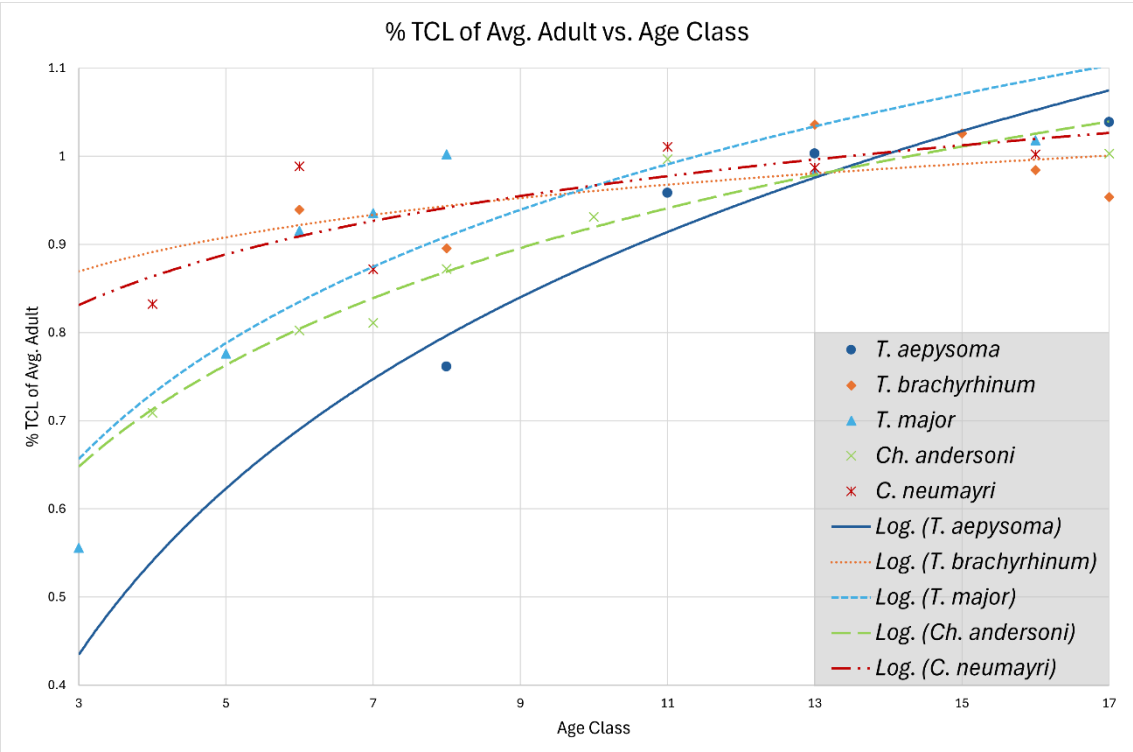

Fig. 77 Percent of average adult total cranial length through ontogeny

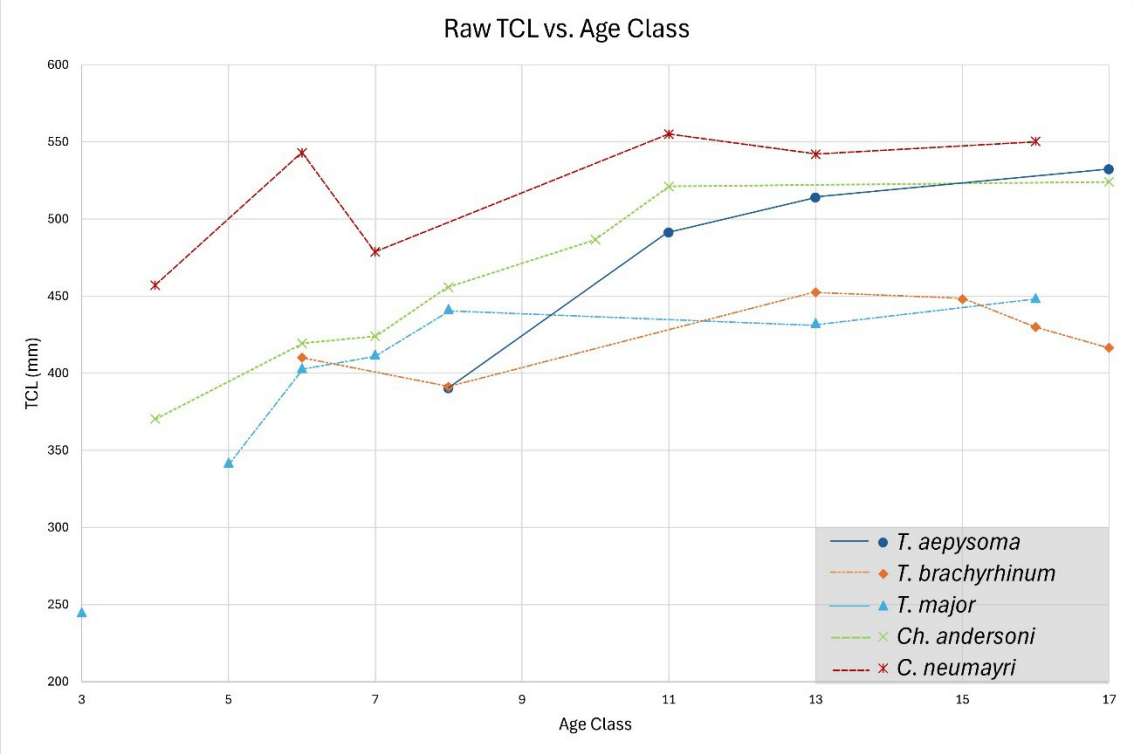

Fig. 78 Raw total cranial length through ontogeny

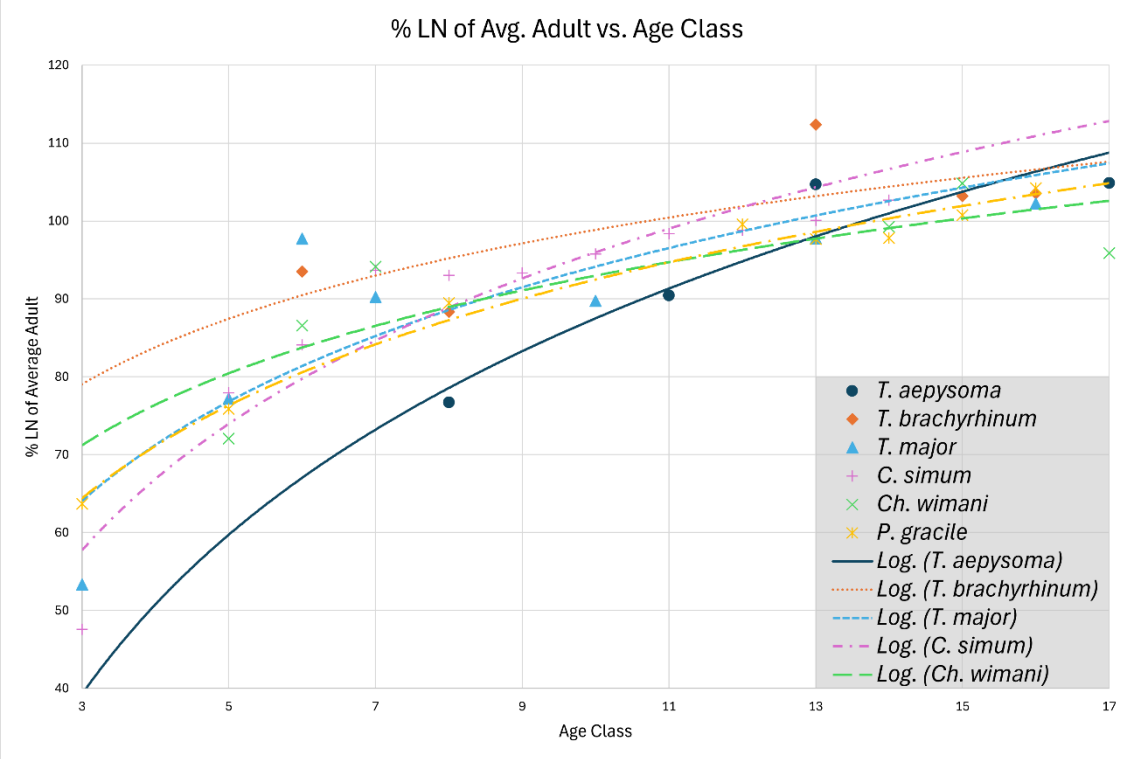

Fig. 79 Percent of average adult lambdoid crest to nasal tip length through ontogeny

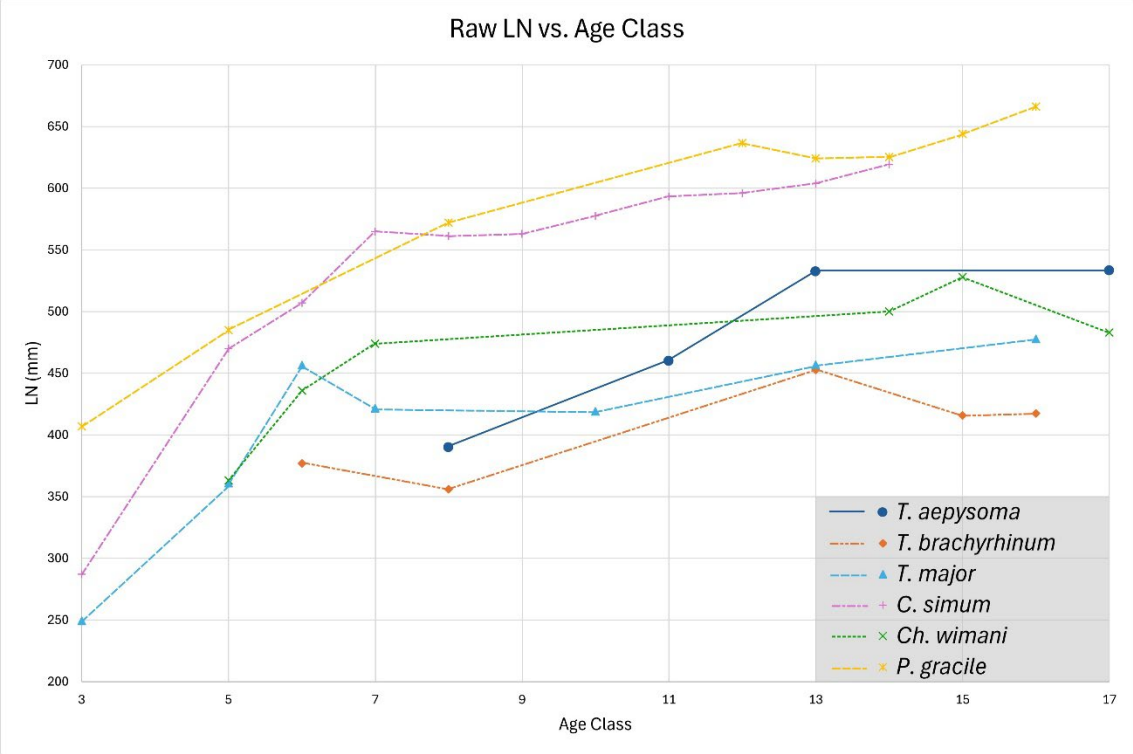

Fig. 80 Raw lambdoid crest to nasal tip length through ontogeny

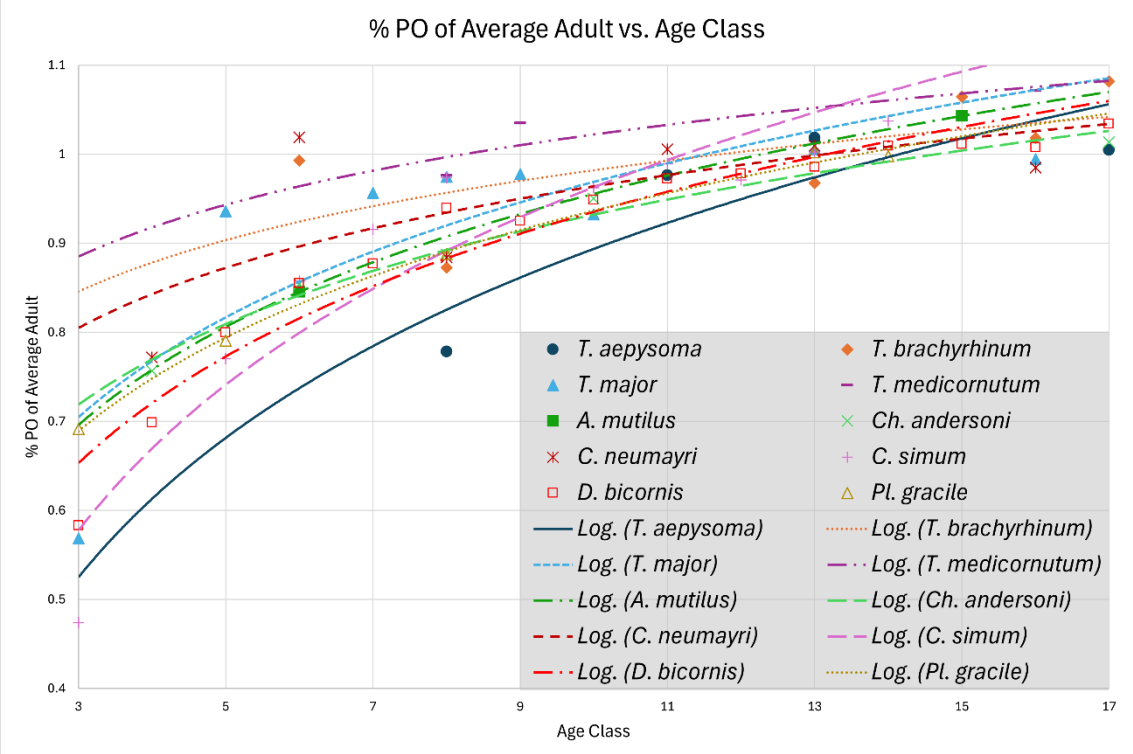

Fig. 81 Percent of average adult anterior premolar to occiput length through ontogeny

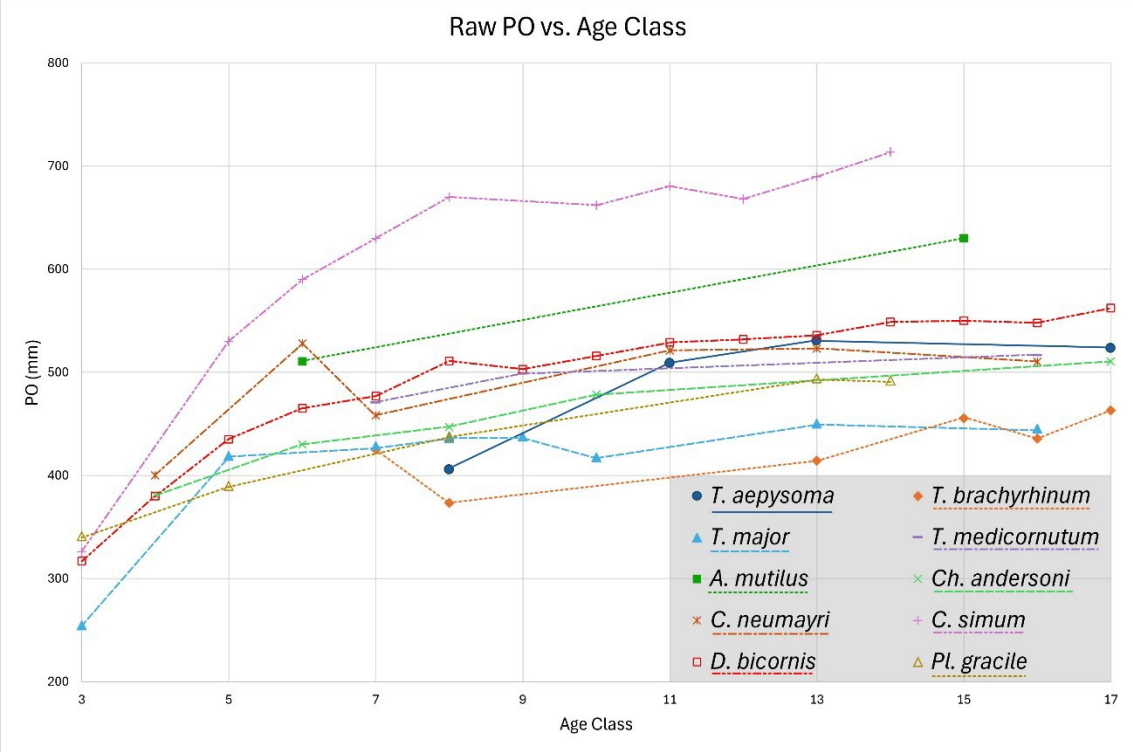

Fig. 82 Raw anterior premolar to occiput length through ontogeny

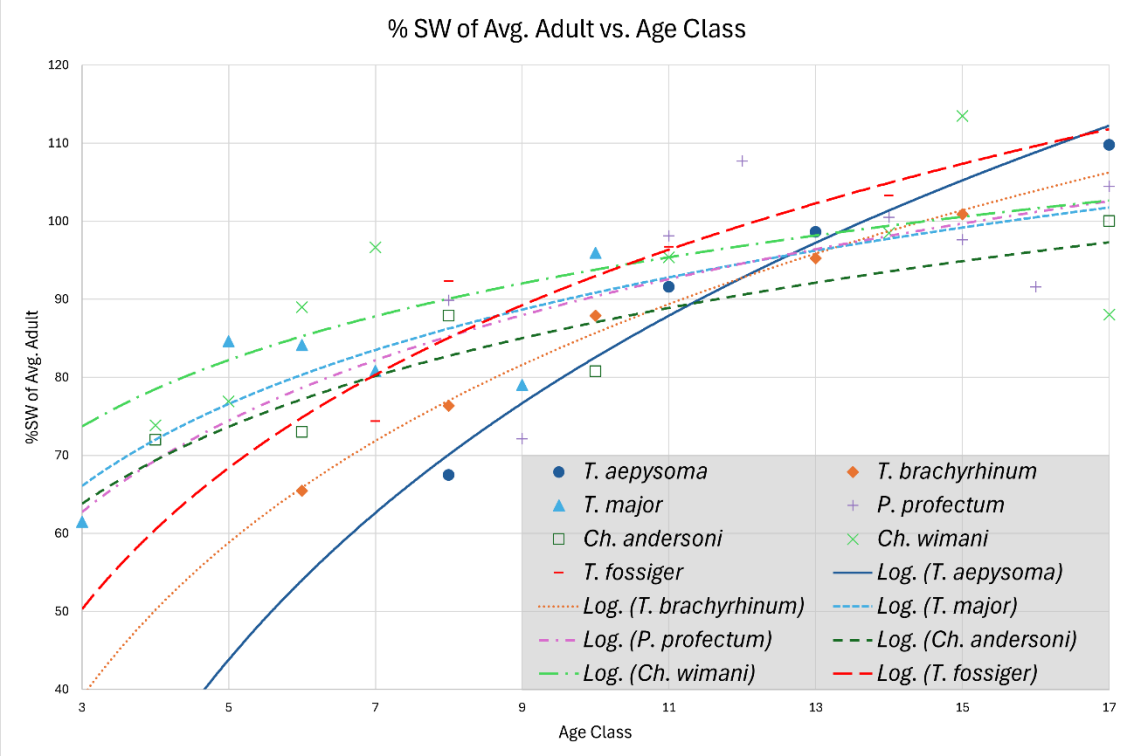

Fig. 83 Percent of average adult supraorbital width through ontogeny

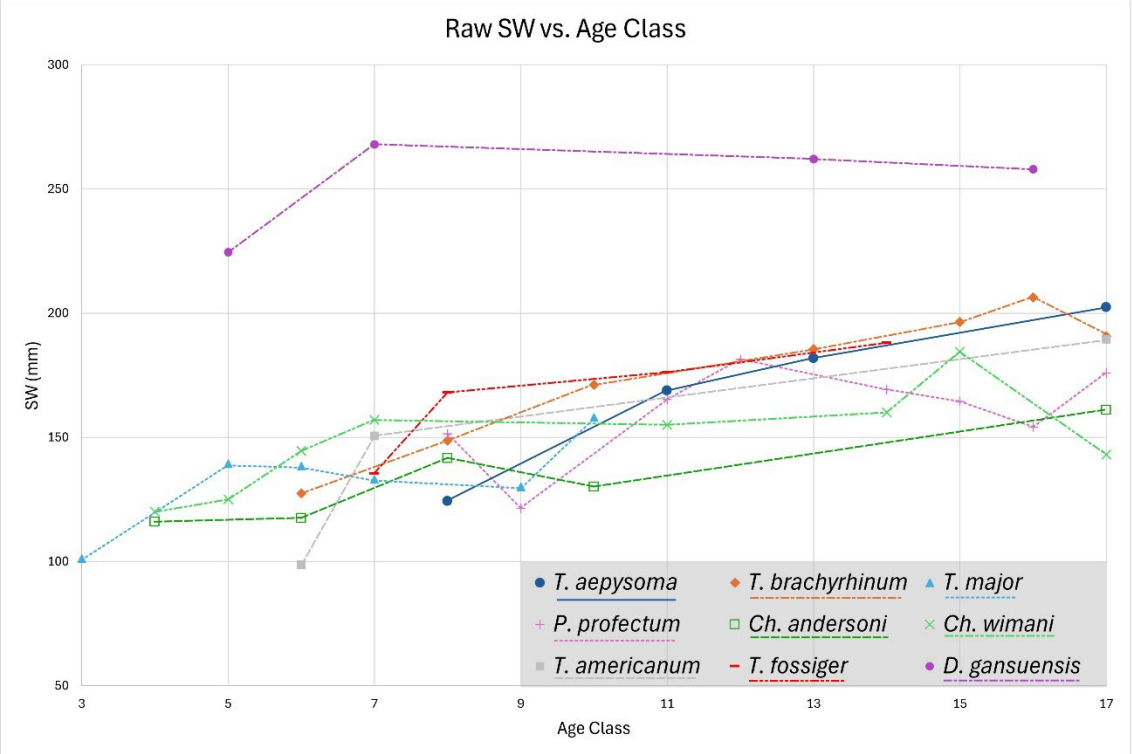

Fig. 84 Raw supraorbital width through ontogeny

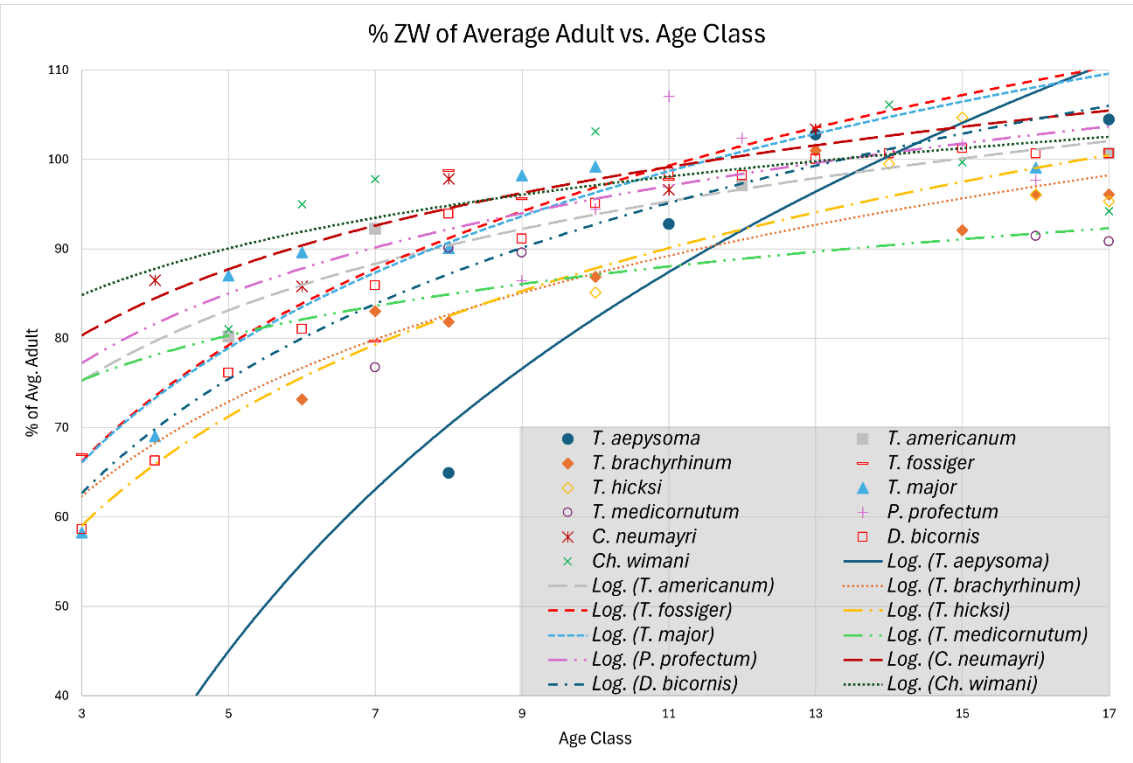

Fig. 85 Percent of average adult zygomatic width through ontogeny

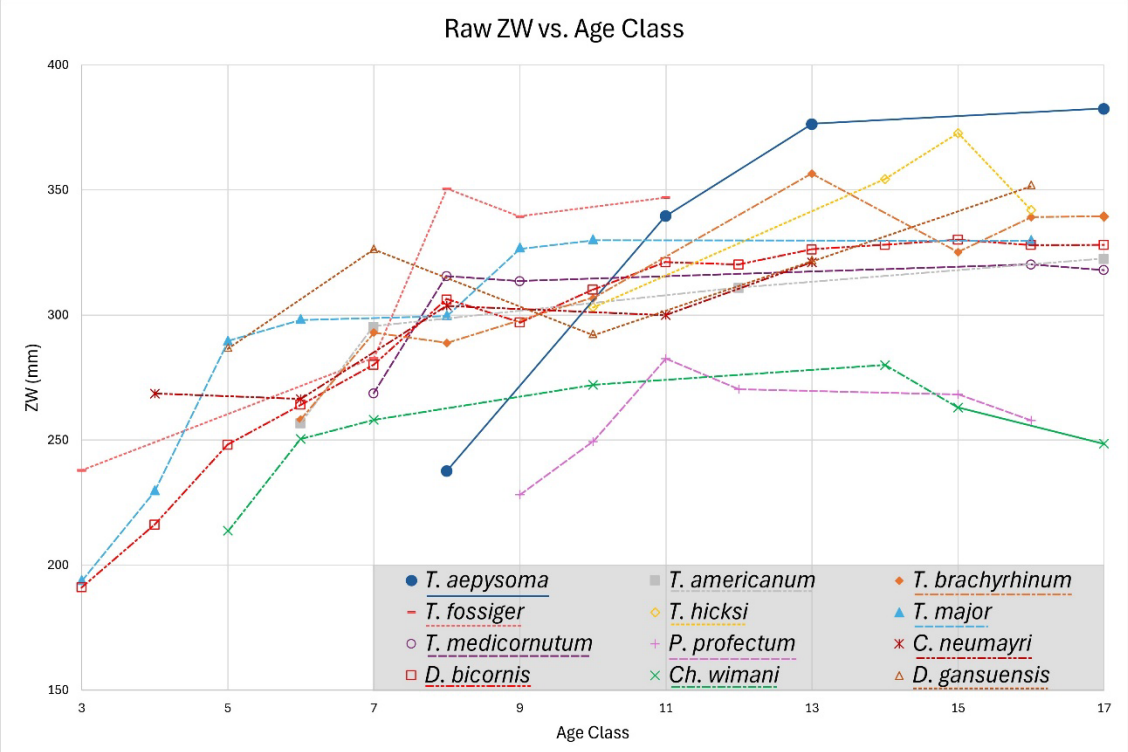

Fig. 86 Raw zygomatic width through ontogeny

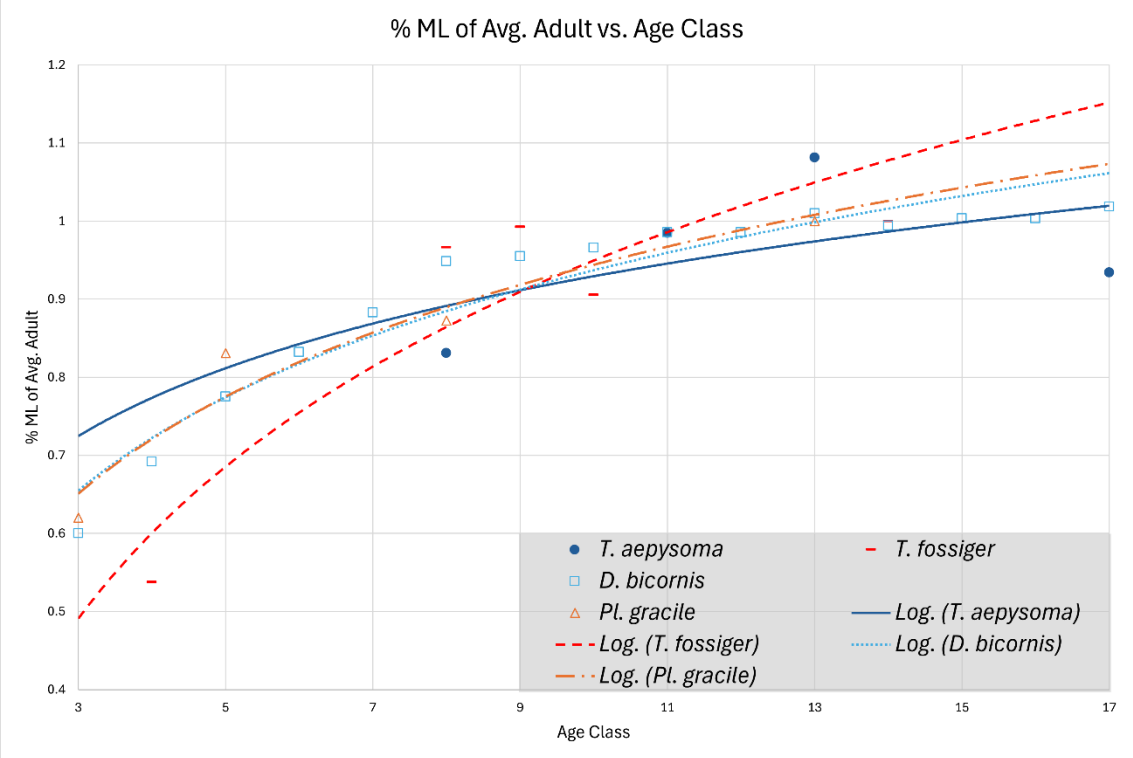

Fig. 87 Percent of average adult mandibular length through ontogeny

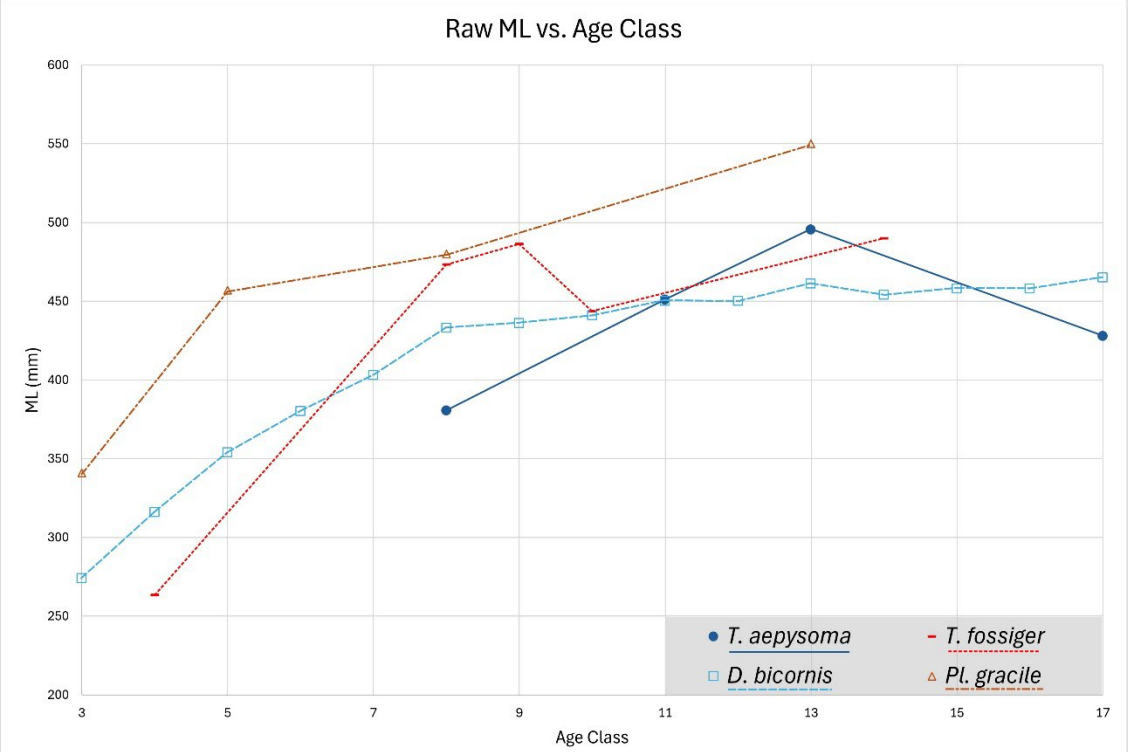

Fig. 88 Raw mandibular length through ontogeny

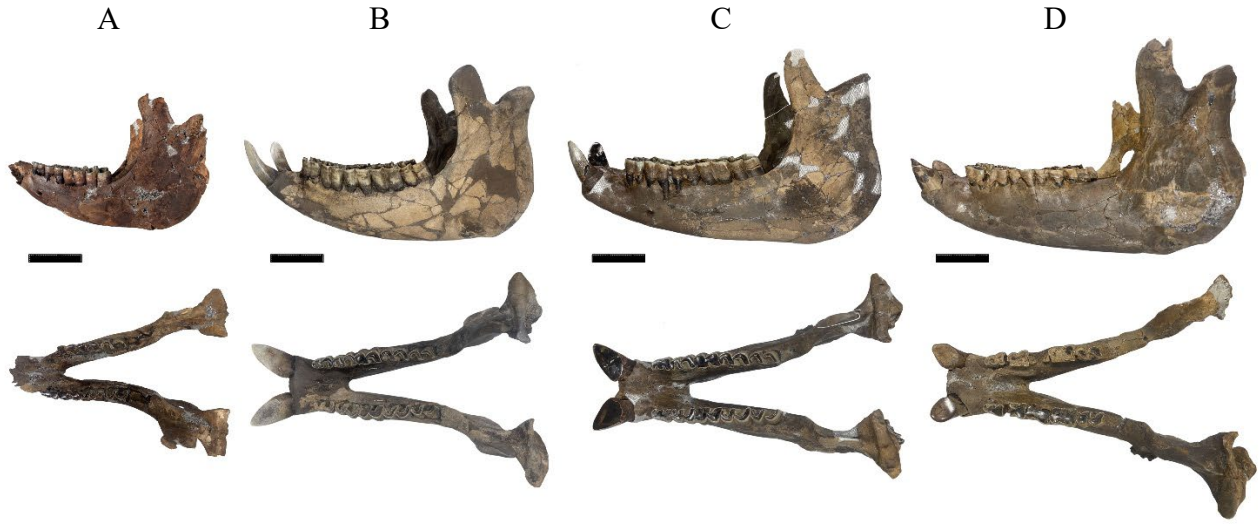

Fig. 89A-D Manidbular ontogenetic sequence for *Teleoceras aepysoma*. (Top row) left lateral view and (bottom row) occlusal view. (A) ETMNH 32999, age class VIII; (B) ETMNH 609, age class XI; (C) ETMNH 601, age class XIII; (D) ETMNH 33000, age class XVII. Scale bars = 10cm.

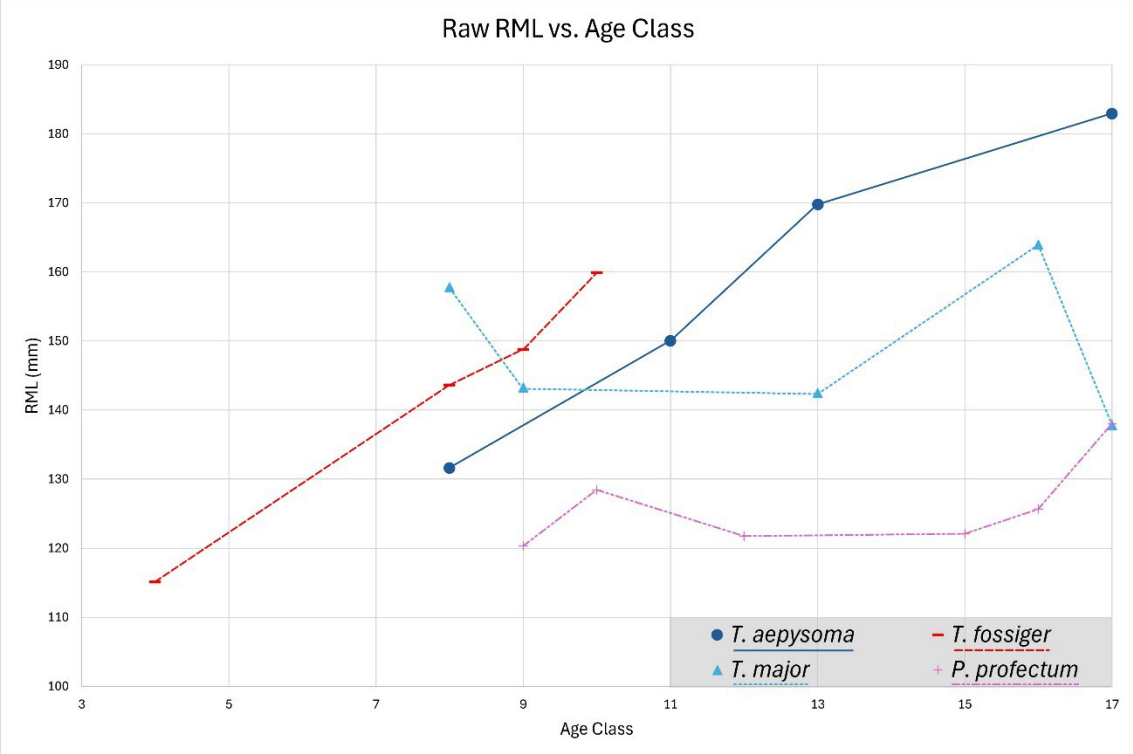

Fig. 90 Raw ramus length through ontogeny

Dental Plots

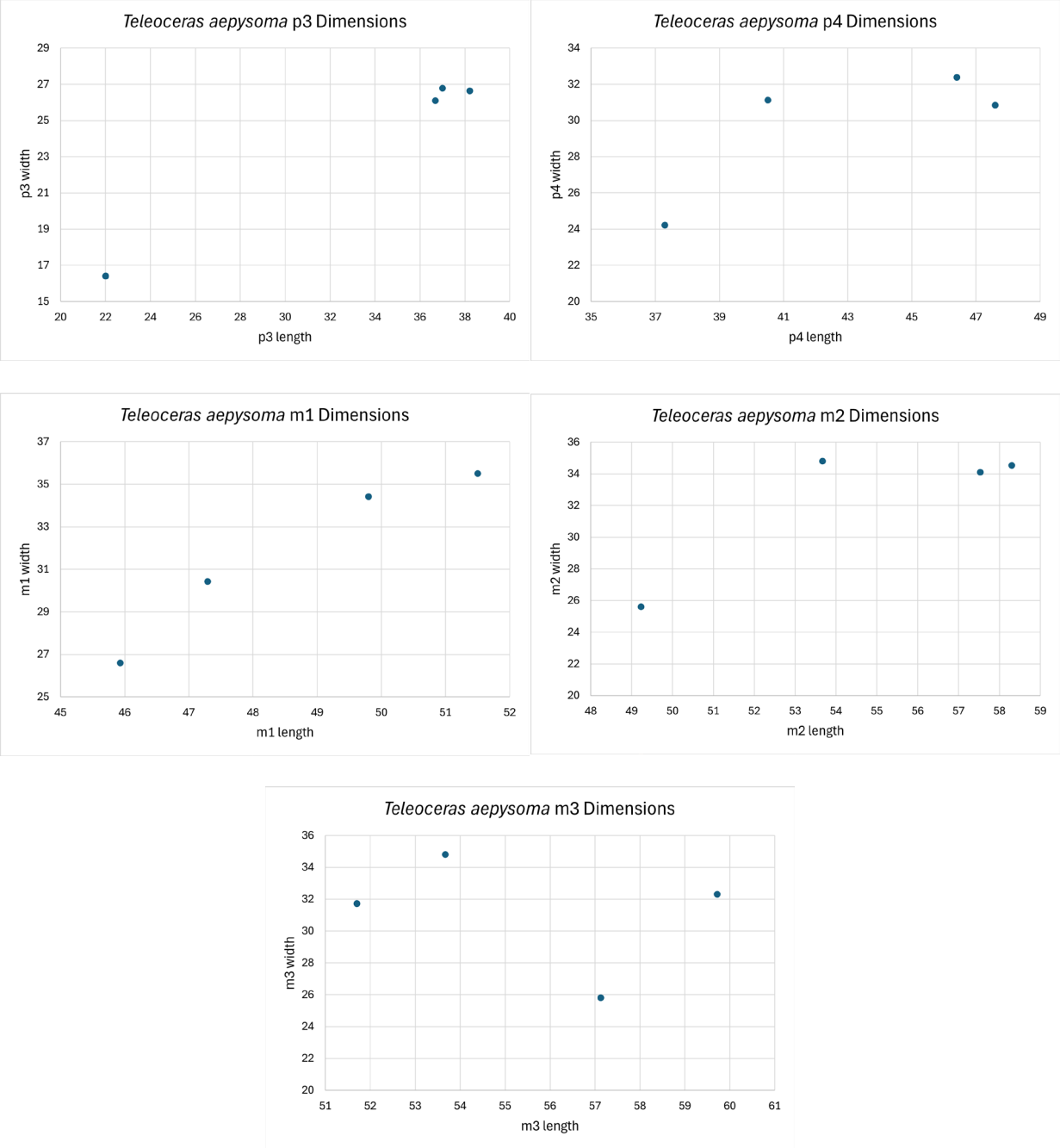

Fig. 91 Dental dimensions of *Teleoceras aepysoma* mandibular teeth. Note that, in all plots, the dental widths of ETMNH 32999 are less than those of conspecific adults.

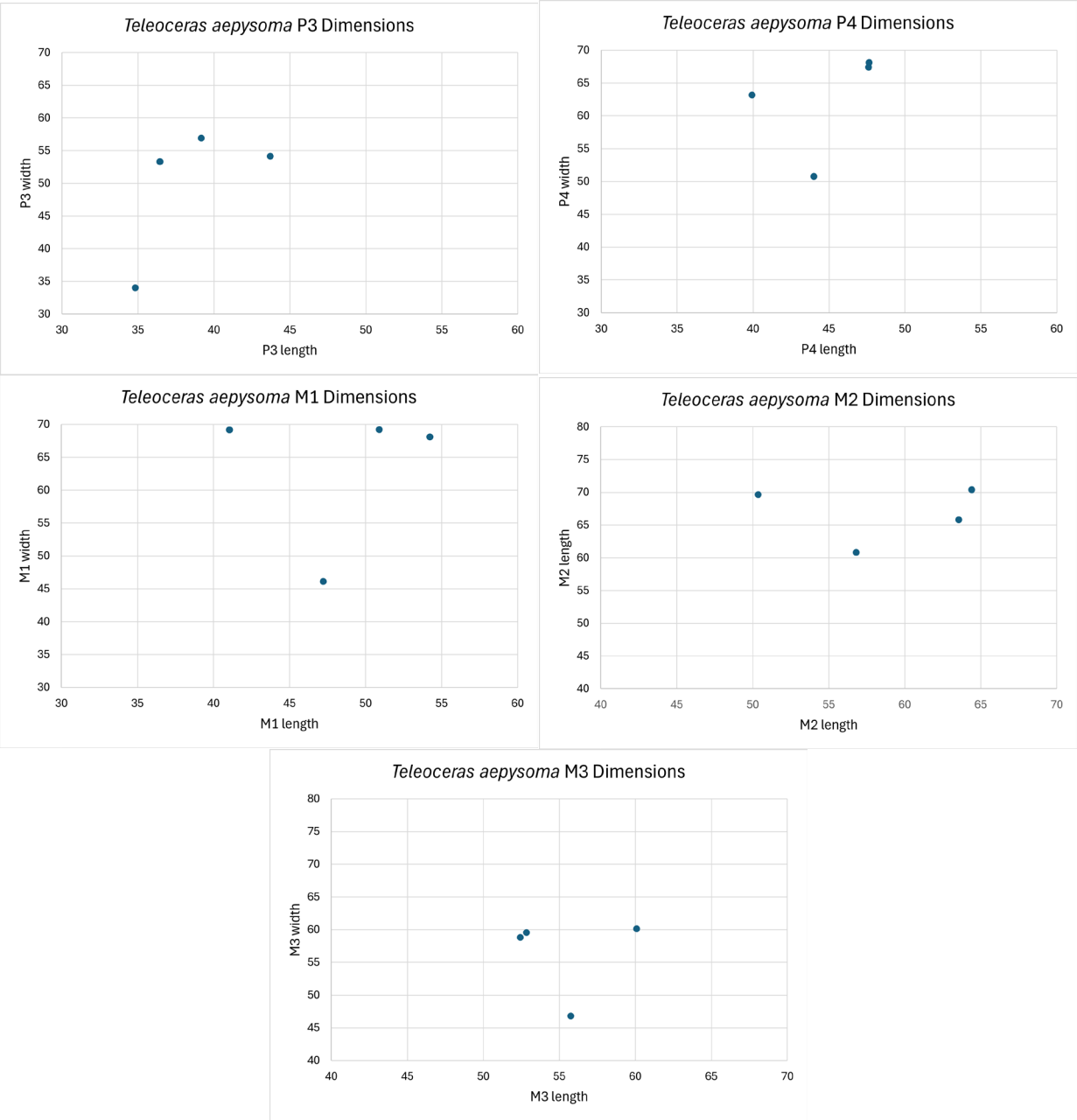

Fig. 92 Dental dimensions of *Teleoceras aepysoma* maxillary teeth. Note that, in all plots, the dental widths of ETMNH 32999 are less than those of conspecific adults.

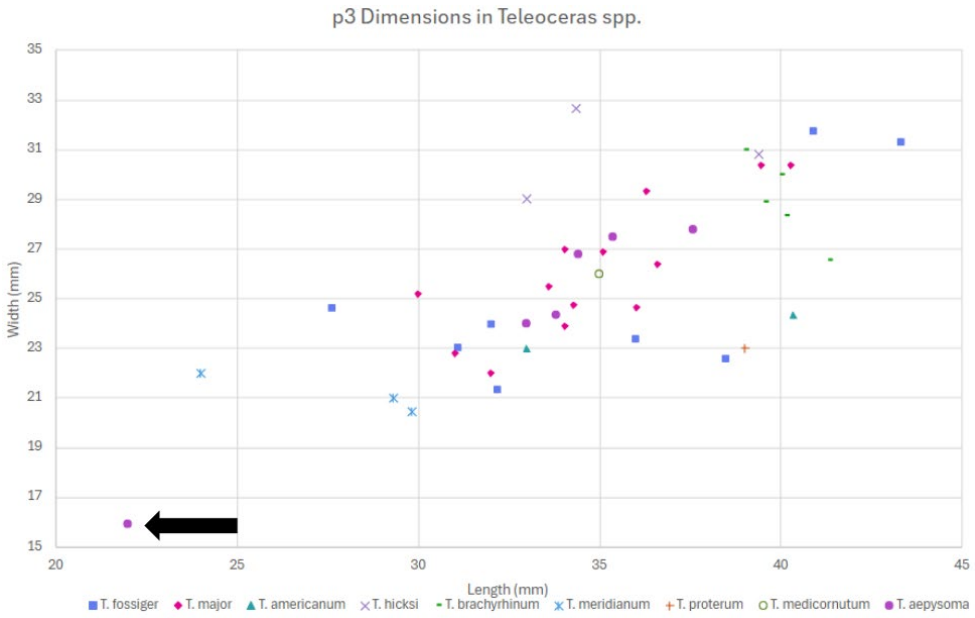

Fig. 93 p3 dimensions in *Teleoceras* spp. The black arrow indicates ETMNH 32999. Note its distance from all other point clusters, even that of the dwarf *T. meridianum*.

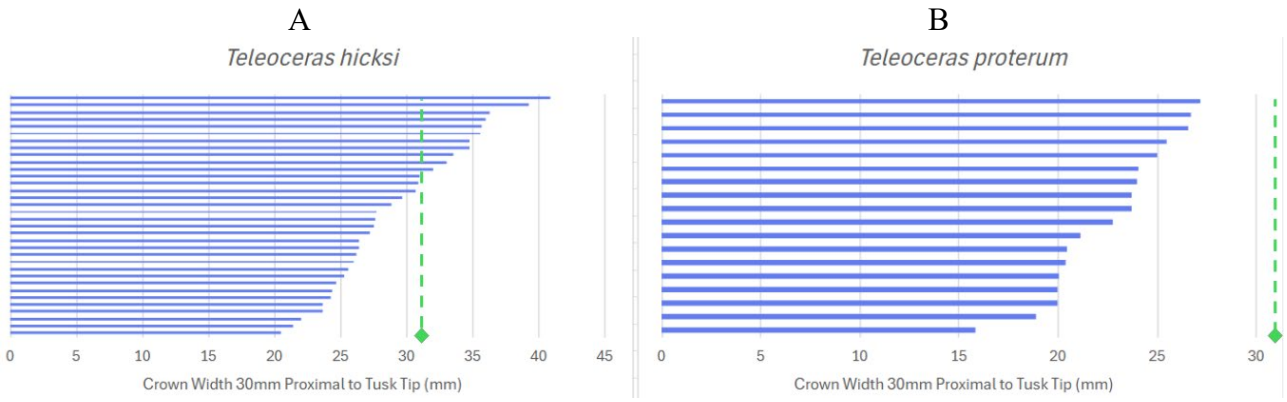

Fig. 94A-B Tusk width at 30mm distal to the tip in *Teleoceras hicksi* and *T. proterum*. Clustered bar plots illustrating the mediolateral width of the tusk (i2) crown at 30mm proximal to the anterior tip (WT) in (A) *Teleoceras hicksi* and (B) *Teleoceras proterum*. The green diamond and dashed line in both figures mark the WT value for *T. aepysoma* subadult ETMNH 32999 (31.6mm). Note that ETMNH 32999 clusters well within the larger, presumably male, measurements of *T. hicksi*.

CHAPTER 4. DISCUSSION

Referral to *Teleoceras aepysoma*

Based on morphology alone, it is difficult to refer ETMNH 32999 to *Teleoceras aepysoma* with confidence. Most diagnostic features of the species (see Short et al. 2019) are based on adults (both the holotype and paratype are identified as adult males) and are therefore not readily applicable to an immature specimen. For example, characters such as "greater zygomatic width" and "greater P2 to occiput length" relative to congeners cannot be used since ETMNH 32999 has not achieved adult size (Table 16).

Table 16 Characters of *Teleoceras aepysoma* and conditions observed in ETMNH 32999

Character of *Teleoceras aepysoma* (Short et al., 2019)	Condition of ETMNH 32999
Greater length from P2 to occiput than congeners	Not comparable; full size not yet achieved
Greater widths across the zygoma and occiput than congeners	Not comparable; full size not yet achieved
Unfused nasals	Unfused, though this character is likely ontogenetically dependent and/or highly variable
No evidence of a nasal horn	No nasal horn evidence, though *T. aepysoma* is not unique in this condition within the genus
Supraorbital tuberosities	Present, albeit reduced relative to adults; extend laterally, but not dorsally as in adults
Greater lengths of the forelimbs and femur	Full lengths not yet achieved, though already in the range of congeneric adults; femur missing
Greater humerus and ulna midshaft and distal widths	Slightly smaller than conspecific adults, likely attributable to ontogeny
More elevated body than is typical of the genus	Full forelimb length not yet achieved, though already within the range of congeneric adults

Outside of size-based characters, *T. aepysoma* is distinguished by its unfused nasals that lack rugosity indicative of a terminal nasal horn (Short et al. 2019), contrary to the generic diagnoses of "a small terminal nasal horn and fused nasals" by Prothero (2005) for *Teleoceras*.

Nasal fusion, however, appears to be variable and largely ontogenetically dependent both within and between species of the genus. ETMNH 609 and 601, the *T. aepysoma* holotype and paratype respectively, have unfused medial nasal sutures (Fig. 97). Conversely, the nasals of the oldest *T. aepysoma* individuals, ETMNH 33000 and ETMNH 19280, as well as an isolated pair of nasals (ETMNH 12175), are completely fused together with the medial suture obliterated (Fig. 97). Plasticity in nasal fusion is apparently also present in congeners: in *T. major*, Hagge (2010) describes some variation in the timing of suture closure, in which the medial nasal suture may be fused or unfused in adult individuals. The nasals of ETMNH 32999 are unfused and are separated anteriorly by a small gap, but this is not atypical of what would be expected of a skeletally immature individual, so it cannot be confidently used here as a feature diagnostic of *T. aepysoma*.

Teleoceras spp. are generally considered to have had a terminal nasal horn (Hatcher 1894; Osborn 1898; Voorhies 1978; Mead 2000; Mihlbachler 2005; Prothero 2005; Hagge 2010), an interpretation usually based on the robusticity and rugosity of the nasals relative to the thin, smooth nasals of hornless species like *Chilotherium* and *Aphelops*. *T. aepysoma*, however, has no rugosity on the nasals consistent with what is seen in modern horned species (Fig. 97) (Short et al. 2019; Scaife 2024). Hieronymous et al. (2009) described the osteological criteria indicative of keratinous nasal horn attachment in *Ceratotherium simum*, which entails irregularly shaped bone spicules that project away from the surface (i.e. projecting rugosity), and are arranged in a ring-like pattern (i.e. annular distribution) (Fig. 98). *T. aepysoma* nasals are generally smooth, with the most rugosity occurring on the anterior nasal tips of very old individuals with no clear distribution pattern (e.g. ETMNH 33000, Fig. 97). Moreover, this rugosity does not differ from that seen elsewhere on the skull, like the zygoma or frontals (Scaife

2024). Rugosity with a uniform, rather than annular, distribution, as seen on some *T. aepysoma* skulls, is more consistent with what Hieronymous et al. (2009) correlated with dermal armor/thickening as seen in *Hippopotamus amphibius*, rather than horn attachment. In other words, it is more reasonable to speculate that the rugosity seen on *T. aepysoma* skulls is indicative of dermal armor/thickening rather than numerous small horns.

Teleoceras aepysoma is not unique among *Teleoceras* for lacking the rugosity indicative of a nasal horn. Several specimens of *T. fossiger* and *T. hicksi* in museum collections lacked nasal rugosity of any kind (Fig. 96), comparable to what is observed in *T. aepysoma*. Conversely, in *T. proterum*, a circular, raised horn boss was present on many isolated nasal bones (Fig. 95), though lacking the projecting rugosity defined by Hieronymous et al. (2009). In *T. major*, Hagge (2010) found little ontogenetic change in nasal rugosity save for a "small rugose patch" that appeared with the onset of adulthood. Evidently, there is variation between species in how the nasal horn boss, if present, is expressed. Projecting rugosity alone is not considered enough to indicate keratinous horn attachment; such reasoning has been applied specifically to *T. aepysoma* (Scaife 2024). It may be that species bearing an annular rugosity distribution on the nasals, like *T. proterum* (Fig. 95), had a very small nasal horn or a calloused knob as proposed for *T. fossiger* by Matthew (1932), but any correlates of such a feature are absent in other Hemphillian *Teleoceras*.

While ETMNH 32999 evidently lacked a horn as in other *T. aepysoma*, this, too, does not appear to be unique to the species. For one of the few genera within Aceratheriinae thought to independently evolve a terminal nasal horn (Lu et al. 2023a), the lack of research and consensus on the eponymous horn of *Teleoceras* is confounding. Future studies should aim to evaluate the

osteological correlates of horn attachment in all extant rhinos and apply the same criteria to their extinct relatives to better understand the evolution of weapon development in Rhinocerotidae.

Fig. 95 Various isolated *Teleoceras proterum* nasal bones. In dorsal view. From Love's Bone Bed, Florida, from the Florida Museum of Natural History (UF) collections. The red arrow and circle on the specimen second to the left indicate the raised, circular boss, which is visible on several other specimens. While this condition is not exactly consistent with the osteological correlates of horn attachment in extant rhinos, it differs from the smooth, level condition seen in other Hemphillian *Teleoceras*. Scale bar =5cm.

Fig. 96 Nasal bones of *Teleoceras fossiger* and *T. hicksi*. (Left) nasal bones of *Teleoceras fossiger* (AMNH FM 8404). (Right) nasal bones of *Teleoceras hicksi* (UF 220373). Note the absence of projecting rugosity, annular distribution, or boss-like structure on the nasals. Scale bars = 5cm.

Fig. 97 Nasals of the Gray Fossil Site *Teleoceras aepysoma* sample. From left to right, ETMNH 19280, ETMNH 12175, ETMNH 32999, ETMNH 609, ETMNH 601, ETMNH 33000. Note the inconsistency in the state of nasal fusion and that pronounced rugosities are present on only individuals thought to be of advanced age. Scale bar = 10cm.

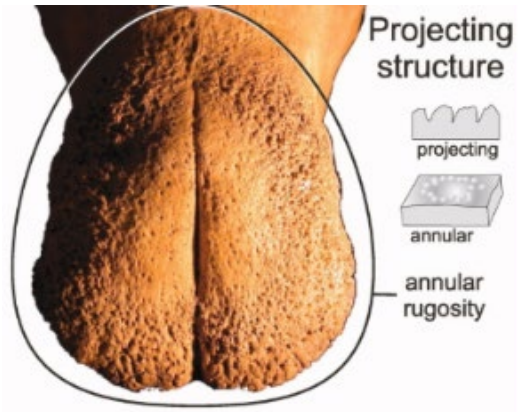

Fig. 98 Rugosity criteria for horn attachment in *Ceratotherium simum*. Modified from Hieronymous et al. (2009). Not to scale.

Despite the absence of diagnostic characters present in ETMNH 32999, there are still some features that are taxonomically diagnostic. Historically, *Teleoceras* species have been differentiated by size as inferred by tooth row lengths (e.g. Prothero 2005). It is worth noting that ETMNH 32999 has comparable tooth row lengths to conspecific adults (Table 3), though tooth row lengths are generally consistent across the genus except for the exaggerated tooth row lengths of *T. fossiger* and *T. proterum* (Prothero 2005; Short et al. 2019). The forelimbs of ETMNH 32999, though still growing, have already achieved lengths typical of other, more brachypodial *Teleoceras* species (listed in Prothero 2005), suggesting that they would be considerably long in adulthood and compare favorably with *T. aepysoma* adults. Allometric

scaling (Table 12) returns expected adult values of 301.6mm and 382.03mm for the radius and humerus lengths of ETMNH 32999, respectively. These estimations alone put ETMNH 32999 well outside of the range of congeneric adults, and into the range of *T. aepysoma*. Other late Hemphillian non-dwarf *Teleoceras* (*T. hicksi*, *T. proterum*, and *T. fossiger*) have remarkably short and stumpy limbs (radius lengths 259, 252, 250mm and humerus lengths 307, 284, and 315mm, respectively; dwarf species *T. guymonense* limbs are even shorter) (Prothero 2005), so it is unlikely that ETMNH 32999 can be referred to any of Hemphillian species other than *T. aepysoma* based solely on its elongate forelimbs.

Referral of ETMNH 32999 to *T. aepysoma* can be supported by a combination of its temporospatial occurrence and its anatomy. *T. aepysoma* is known only from the late Hemphillian to early Blancan-aged Gray Fossil Site (GFS), and to date, its occurrence there is monospecific. *Teleoceras* species rarely co-occur, with the only exceptions being the rare sympatric occurrence of a dwarf and non-dwarf species, such as *T. guymonense* and *T. hicksi* (Prothero 2005). It is unlikely that ETMNH 32999 represents a sympatrically-occurring dwarf species as the dental dimensions of ETMNH 32999 are not proportionally smaller relative to body size, as would be expected based on what is seen in the dwarf *T. meridianum* (e.g. Prothero and Sereno 1982), and again, the limbs are not dwarf. Regarding other North American rhinos, *Teleoceras* often occurs alongside the more slender-limbed *Aphelops* (Matthew 1932; Mihlbachler 2003, 2005; Prothero 2005; Wang and Secord 2020), though no *Aphelops* material is known yet from the GFS. The laterally downturned nasals, hypsodont dentition without cingulum, developed premaxillae, and compressed distal forelimb elements of ETMNH 32999 all disqualify it from referral to *Aphelops* and indicate placement within *Teleoceras.* With referral to *Aphelops* not applicable and referral to a distinct, or dwarf, species unlikely, ETMNH

32999 is here referred to *T. aepysoma*. This diagnosis is also supported by its elongated forelimb elements unique to the species, and its occurrence in the type locality of *T. aepysoma* which, to date, yields no other *Teleoceras*.

SYSTEMATIC PALEONTOLOGY

CLASS Mammalia

ORDER Perissodactyla Owen, 1848

FAMILY Rhinocerotidae Owen, 1845

TRIBE Teleoceratini Hay, 1902

GENUS *Teleoceras* Hatcher, 1894

SPECIES *Teleoceras aepysoma* Short, Wallace, and Emmert, 2019

Holotype: ETMNH 609, a complete skeleton of a young adult male missing only a single ungual.

Paratype: ETMNH 601, a nearly complete skeleton of an adult male, with a better-preserved skull than the holotype, missing a few vertebrae and ribs.

Referred Material: ETMNH 32999, a partial immature skeleton (Fig. 3) consisting of: a partial cranium, mostly complete on the left side; complete left maxillary tooth row (dP2-M3) and unerupted P3 and P4; a partial right tooth row (dP2-dP3) with unerupted P3 and M3; both premaxillae; left occipital condyle; palatine fragments; hyoid fragments; a complete mandible with both tooth rows (dp3-m3) and unerupted p3s and p4s; partial crowns of both i2s; right humerus with a damaged proximal epiphysis and articular head; both right and left radii and ulnae each with unfused epiphyses; carpal elements (left and right cuneiform, lunar, scaphoid, unciform, trapezoid; left pisiform); left metacarpals II, III, and IV, each with unfused distal epiphyses; right metacarpals II and III with unfused distal epiphyses; manual proximal and distal phalanges, both medial and lateral; various sesamoids; right patella; right astragalus, left metatarsals II and IV with unfused distal epiphyses; two partial thoracic vertebrae; two rib fragments.

Description: See "Osteological Description" section above.

Geographic and Stratigraphic Distribution: To date, *Teleoceras aepysoma* is only known from the Gray Fossil Site in Washington County, Tennessee, USA. Late Miocene to early Pliocene.

Diagnosis: (Generic characters from Prothero 2005) Hypsodont teeth (though *T. aepysoma* may be mesodont; Short, 2013), strong antecrochets, dP1 and p2 lost, narrow nasals with downturned lateral edges, i2 teardrop-shaped in cross section. (Specific characters from Short et al. 2019) Pronounced supraorbital tuberosities (present, though reduced in ETMNH 32999), no evidence of a terminal nasal horn, greater forelimb lengths than congeners and therefore, a more elevated stance.

Remarks on Growth: Qualitative

Age Classification

Dental wear. Age determination in fossil rhinoceroses is most frequently based on tooth eruption and wear in *Ceratotherium simum* (Hillman-Smith et al. 1986) and *Diceros bicornis* (Goddard 1970; Hitchins 1978); the extant white rhinoceros and the black rhinoceros, respectively. Hitchins' (1978) study has been the most widely used method, as it used three individuals of known age to verify the classification system with counts of dental cementum lines. Additionally, tooth replacement is assumed to be the same in *Teleoceras* as it is in *D. bicornis* (Mead 1999; Mihlbachler 2003; Böhmer et al. 2015; Short et al. 2019), though there is some variation in the eruption of the second molar and replacement of the deciduous premolars (personal observations). In addition to Hitchins' (1978) classification system, Hillman-Smith et al. (1986) provided a detailed dental wear key for aging *C. simum,* figured by Hullot and Antoine (2020) (Fig. 99). Here, age classification via eruption and attrition will follow Hitchins' (1978)

dental key, though the wear key of Hillman-Smith et al. (1986) and Hullot and Antoine (2020) will be used to assign a wear stage value to each tooth of ETMNH 32999 (Table 17).

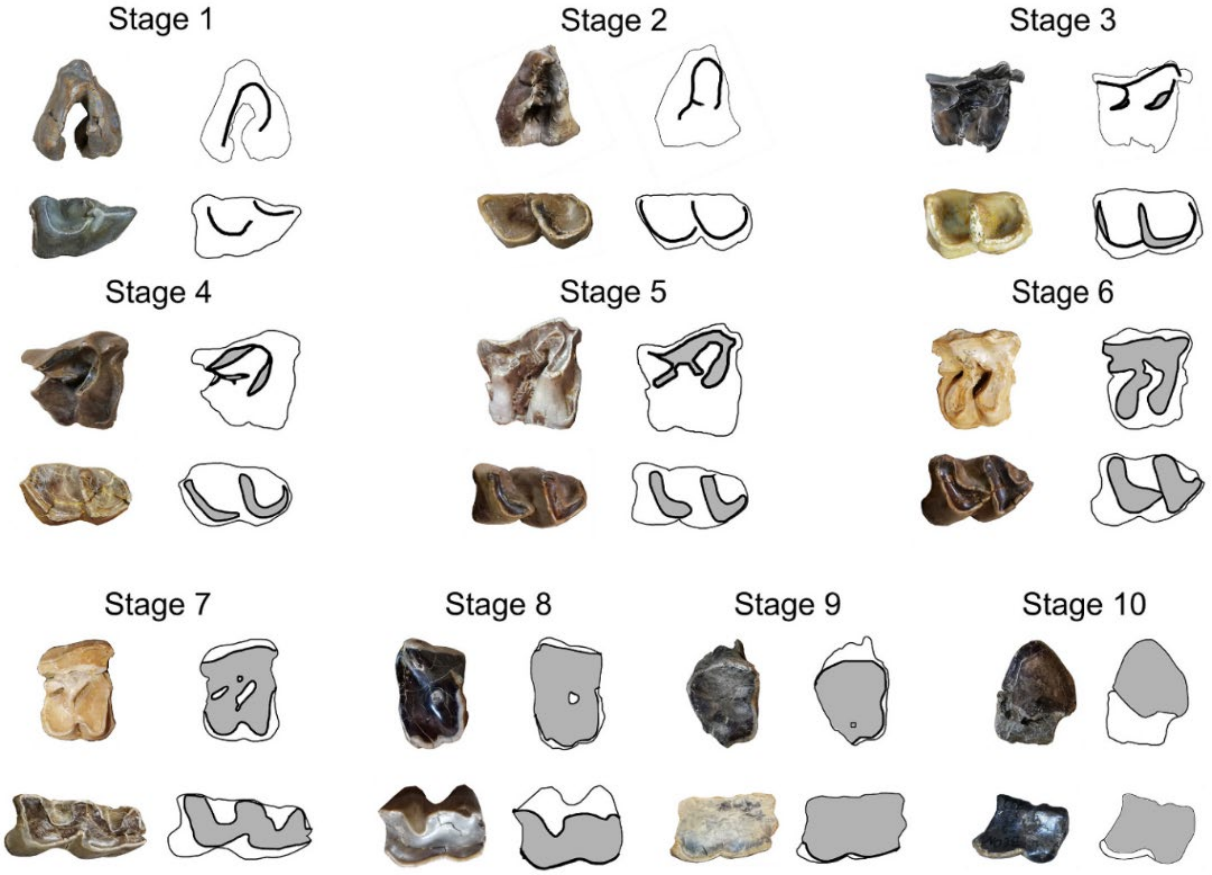

Fig. 99 Ontogenetic wear stages of rhinocerotid teeth. Wear stages are those defined by Hillman-Smith et al. (1986), figure modified from Hullot and Antoine (2020). As the tooth wears and more dentin is exposed, lophs and features merge with each other until no occlusal morphology can be discerned. Not to scale.

Table 17 Dental wear stages of ETMNH 32999

Tooth	dP2	dP3	dP4	M1	M2	M3
Wear stage (upper)	10	7	7	5/6	4	-
Wear stage (lower)	-	9	9	7	5	-

Wear stages follow the classification of Hillman-Smith et al. (1986) and correspond with Figure 99.

Maxillary dentition of ETMNH 32999 (Fig. 100) compares favorably with Hitchins' (1978) age class VIII (Fig. 101), though arguments could also be made for age classes VII and

IX. The lower bracket of this age estimation (VII) reflects the retention of the deciduous premolars, whereas the wear on M1-M2, and the state of the erupting M3, are more consistent with age class IX. Despite the retention of the deciduous teeth, the state of wear and eruption of the molars indicates a slightly older individual. Specifically, the M1 is more heavily worn than it would be in Hitchins' (1978) age class VII (Fig. 101), evidenced by the moderate wear on the crochet, antecrochet, and metastyle, as well as a V-shaped postfosette (Fig. 100) (wear stage 5-6; see Fig. 99). The M2 is usually unworn and just above the gum level in age class VII according to Hitchins (1978); however, light wear on the M2 of ETMNH 32999 is more consistent with age class IX, as there is exposed dentine on the protoloph and anterior portion of the ectoloph (wear stage 4) (Fig. 99). Furthermore, Hitchins' (1978) age class VIII describes the M3 as below the bone surface, while in ETMNH 32999, it is above the estimated horizon of the bone surface, but just below the gum line, consistent with age classes VIII or IX.

Mandibular dentition of ETMNH 32999 returns a similar, if slightly older, age (Fig. 100). Retained deciduous premolars correspond with age class VI-VII, whereas the wear of m1-m2 match that of age class IX (Fig. 101). The m1s of ETMNH 32999 both have dentine joined between the cusps (wear stage 7), a condition which does not occur in *D. bicornis* until age class X. Wear on the m2 is consistent with age classes VIII-IX (wear stage 5). Despite the deciduous premolars being shed most commonly in age classes VI-VIII in *D. bicornis* (Hitchins 1978), the first and second molars of ETMNH 32999 are too worn to indicate an individual younger than age class VII. Superficially, the mandibular dentition resembles that of Hitchins' (1978) age class VI due to the deciduous premolar retention, but the m1 is too lightly worn in class VI to apply to ETMNH 32999, and the m2 is usually not fully erupted, much less in occlusion, at this age.

Fig. 100 Interpretive line drawing of ETMNH 32999 left tooth rows. (Top) left maxillary tooth row (dP2-M3) of ETMNH 32999. (Bottom) left mandibular tooth row (dp2-m2) of ETMNH 32999. Note that m3 was removed from the mandible during preparation and therefore, is not included here in the drawing. Not to scale.

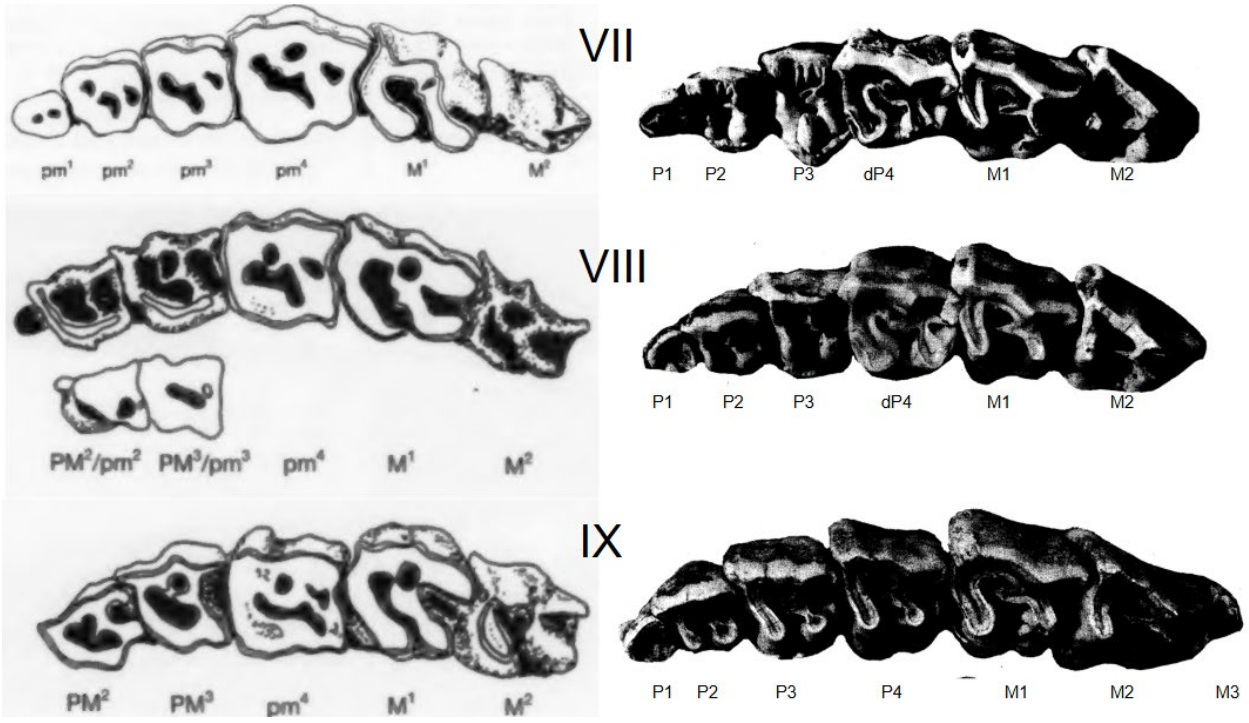

Fig. 101 Subadult maxillary dentition of the extant African rhinos. (Left) Subadult maxillary dentition of *Ceratotherium simum* modified from Hillman-Smith et al. (1986) and (right) the subadult maxillary dentition of *Diceros bicornis* from Hitchins (1978). Roman numerals correspond to dental age classes. ETMNH 32999 is placed in age class VIII based on the attrition of M1 and M2, even though the deciduous premolars are typically fully or partially shed by this life stage in both extant African species. Not to scale.

Tusk (i2) eruption can also be useful in determining age. The state of tusk eruption ETMNH 32999 is consistent with the assigned dental age (age class VIII), as Hagge (2010) found that tusk eruption in *T. major, Rhinoceros unicornis*, and *Dicerorhinus sumatrensis* occurs in age classes VII-VIII, coinciding with the onset of sexual maturity. Findings of the present study corroborate this assumption. Sex-specific trends in the timing of tusk eruption are also a factor, though these are more thoroughly investigated in the "Sex Determination and Sex-Specific Trends" section below. Here, it is worth prefacing that the state of tusk eruption in ETMNH 32999 corresponds more closely with what is observed in male, rather than female *Teleoceras*, in which males have delayed tusk eruption/development (see Mihlbachler 2005).

Age classes VII-IX are encompassed by a broader "subadult" classification, defined here as having a fully erupted second molar, but not yet a third molar. Deciduous tooth retention is more variable than M1-M3/m1-m3 eruption; in *Ceratotherium*, the dP4 can potentially be retained until the M3 is in occlusion, as late as age class XI (Hillman-Smith et al. 1986; Geraads and Koufos 1990), while in *D. bicornis* it is invariably shed before M3 occlusion (Goddard 1970; Hitchins 1978).

Age in years. Percentage of potential lifespan data (%PL) is considered here to be more biologically meaningful than ages in years, primarily because similar lifespans-in-years between extant and extinct taxa cannot be safely assumed. However, Mihlbachler (2005) suggested that the lifespan of *Teleoceras* was comparable to, or possibly slightly shorter than that of extant rhinoceroses at ~40 years, based on counts of annular growth rings observed in *T. proterum* tusks. Hitchins' (1978) age class VIII (Fig. 101), where ETMNH 32999 is placed, corresponds to 7 ± 1 years of age in *Diceros bicornis*. According to Mihlbachler's (2003) conversion to Hitchins' (1978) method, this approximation would equate to ~17-19% of total lifespan in *T.*

proterum (15-19% for combined classes VII and VIII). For age estimation via the method of Hillman-Smith et al. (1986), ETMNH 32999 (Fig. 100) corresponds most closely with age class IX (Fig. 101); 7 to 9 years in *Ceratotherium simum*, or 17.5-22.5% of lifespan. Both lifespan estimations suggest an individual approaching ~20% of potential lifespan, possibly ~7 years old if the lifespan of *Teleoceras* is comparable to those of *D. bicornis* and *C. simum.*

Using the same age determination methods, the adult skeletons from the GFS can be assigned to age (Table 9). Following Hitchins' (1978) dental age classes and Mihlbachler's (2003) lifespan conversions, the holotype of *T. aepysoma,* ETMNH 609, would be 10 ± 3 years old (~25-30% of potential lifespan; age class XI), and paratype, ETMNH 601, would be 16 ± 3 years old (35-52% of potential lifespan; age class XIII). Both senescent individuals ETMNH 33000 and ETMNH 19280 would correspond with 37 ± 4 years old (96-100% of potential lifespan; age class XVII) in *D. bicornis*. If the above calculations are reasonable approximations, then the GFS sample of complete skeletons, though small, appears to include at least three major age classes: subadult, full adults and very old adults. Isolated material, including a fetal tibia-fibula pair (ETMNH 19025) and a lightly worn M1-dP4 pair (ETMNH 37999), suggest the presence of at least two more age classes, natal and juvenile, though these cannot be included in the cranial (Fig. 64A-D) or mandibular (Fig. 89A-D) ontogenetic sequences due to the lack of relevant material.

Eruption sequence. If considered to be a good representative of *Teleoceras aepysoma*, ETMNH 32999 provides valuable information about the dental eruption sequence for the species. The M3 of ETMNH 32999 is nearly fully formed and would likely have been slightly above the bone surface, as inferred by comparisons with subadults of other species. Though the maxilla/palate is not preserved around the M3, its position relative to other teeth can be used to

infer the state of eruption. The anteroventral portion of the ectoloph is flush with the gum line, which is inferred from the superior edge of the horizontal band of dental calculus on the other cheek teeth. While most of the maxilla is missing, the ventral edge is apparent based on a fragment preserved over the dP4. Differential preservation on the M2 appears to denote the extrapolated horizons of the bone surface and gum line (Fig. 12). The dorsal portion of the labial face of M2 is a tan color that defines the portion of the tooth below the bone surface; inferior to this is a gray-colored portion which likely indicates the portion of the tooth within the gum. The ventral edge of this gray horizon is flush with the band of dental calculus/differential coloration on the other cheek teeth, suggesting the point where the gum line is breached.

For determining age in all other specimens used in this study (Appendix B), Hitchins (1978) key was followed to maintain consistency across taxa, requiring the assumption that dental attrition in other taxa is comparable to that of *D. bicornis*. For *Teleoceras* spp., this is a reasonable and tested assumption (e.g. Mihlbachler 2003; Hagge 2010; Short et al. 2019). For other rhinocerotids, there is some degree of variation in the sequence of permanent premolar eruption and eruption of the second molar (Böhmer et al. 2015; personal observations). To account for this variation, age classification for specimens inconsistent with Hitchins' (1978) dental eruption/wear key focused primarily on the attrition of the latest erupting teeth (M2/m2, P4/p4, and M3/m3), as these should be least affected by discrepancies caused by variation in deciduous tooth shedding (Mihlbachler 2005). While there may be some minor misestimations in taxa where the sequence of second molar and permanent premolar eruption differs from *D. bicornis*, these errors should not differ considerably from actual age (±1 age class) and should still be valid representatives of their respective life stage (i.e. juvenile, subadult, adult, old adult).

Full eruption and occlusion of M3/m3 denotes adulthood in rhinocerotids (e.g. Goddard 1970; Groves and Kurt 1972; Hillman-Smith et al. 1986; Hillman-Smith and Groves 1994; Mihlbachler 2003; Hagge 2010; Shpansky 2014; Böhmer et al. 2015; Lu et al. 2023b), which corresponds with Hitchins' (1978) age class X-XI. M3/m3 typically erupts after the replacement of the deciduous premolars, well into the wear of the second molar, though dP4 may be retained while M3 is in early stages of attrition in *Ceratotherium* (e.g. Hillman-Smith et al. 1986; Geraads and Koufos 1990). ETMNH 32999 is atypical for what has been documented in *Teleoceras*, in that the M2/m2 is in active wear prior to dP3/dp3 shedding; P3/p3 generally erupts prior to the second molar, at least in congener *T. proterum* (Mihlbachler 2003). ETMNH 32999, however, retains the entire deciduous component on both the upper and lower tooth rows (Fig. 100); in *D. bicornis*, the oldest age class which includes the full deciduous component is age class VI (Hitchins 1978), though the dP4 is usually retained until M2/m2 is in occlusion (Fig. 101). The M1/m1 and M2/m2 wear (Table 17) of ETMNH 32999 are more consistent with what is described for Hitchins' (1978) age class IX (see Fig. 101), when all deciduous teeth have been shed.

Böhmer et al. (2015) suggests a correlation between tooth crown height and dental eruption sequence in rhinos. Brachydont taxa (e.g. *Diceros bicornis, Aceratherium incisivum, Stephanorhinus hundsheimensis, Prosantorhinus germanicus*) often share the same eruption pattern (m1, m2, p2 and p3, p4, m3); though Goddard (1970) and Hitchins (1978) provide differing accounts of *D. bicornis* p3/p4/m2 eruption sequence. More hypsodont taxa may have the second molar erupt during or after the deciduous premolar replacement (Böhmer et al., 2015) including *T. proterum* (Mihlbachler 2003), *Coelodonta antiquitatis* (Shpansky 2014; Diedrich 2023), and *Ceratotherium simum* (Hillman-Smith et al. 1986). If the dental eruption sequence of

ETMNH 32999 is typical of *T. aepysoma*, the eruption sequence would be more consistent with brachydont, rather than hypsodont, taxa. Short (2013) originally considered *T. aepysoma* teeth to be mesodont, but this notion has yet to be comparatively quantified. It is worth noting that the browsing diet of *T. aepysoma* (DeSantis and Wallace 2008) is thought to have differed from its primarily grazing (Voorhies and Thomasson 1979; Wang and Secord 2020) and mixed feeding (MacFadden 1998) congeners. Whether the slight difference in the eruption sequence of ETMNH 32999 can be attributed to crown height, diet, a species-specific difference, or simply intraspecific variation, requires a larger sample to evaluate.

Observation of *Teleoceras* material from the AMNH FM/F:AM collections revealed possible specific differences in eruption sequence within *Teleoceras*. Subadult specimens of *T. major* (AMNH F:AM 114537; AMNH F:AM 114505) and *T. fossiger* (AMNH FM 8386; AMNH F:AM 104023; AMNH F:AM 115666) shared the eruption sequence of *T. proterum* (P3, M2, P4) as documented by Mihlbachler (2003). In *T. medicornutum* (AMNH F:AM 114474; AMNH F:AM 109518) and *T. aepysoma* (ETMNH 32999), the M2 apparently comes into wear before both dP3 and dp4 replacement (Fig. 100). Because of the small samples, it is unclear whether this difference in eruption sequence is indeed species-specific, or whether it is variable between conspecific individuals. It would be worth investigating the variation in eruption sequence within the genus and its correlation to crown height, diet, or habitat preference to potentially reveal such trends.

There may, however, be other factors that influence tooth eruption sequence: in rhinos, dental pathologies including supernumerary teeth (Garutt 1994; von Koenigswald et al. 2007; Diedrich 2023) and misplaced teeth (Diedrich 2023) have been documented as influencing tooth replacement. Diet, brain/body size (Harvati and Frost 2007), environmental conditions (Harvati

and Frost 2007; De Marinis et al. 2018) and nutritional factors (Alvarez 1995; Chandan and Rao 2023) are found to influence dental eruption timing in other mammals. Delayed dental eruption is also documented in captive rhinos (e.g. Bigalke et al. 1950; Hillman-Smith et al. 1986). Such influences are important to keep in mind, considering the other dental irregularities of ETMNH 32999 (e.g. missing P2s, reduced p3s, narrow tooth widths, enamel/root hypoplasia).

Oddly, ETMNH 32999 also lacks P2 on both sides, though it retains dP2. Though Prothero (2005) states that loss of P2/p2 may occur in *Teleoceras*, observations of *Teleoceras* spp. crania in the AMNH F:AM/FM collections found variation only in the presence of the p2. While occasional P2 loss is listed as a generic character of *Teleoceras*, it is not mentioned in specific diagnoses for any of the other nine species (see Prothero 2005). Unexpectedly, more variation can be seen in the presence of the first maxillary premolar than the second, despite unequivocal dP1 absence being a generic character of *Teleoceras* (e.g. Prothero 2005). For example, multiple specimens listed in the hypodigm of *T. brachyrhinum* (Prothero 2005) regularly retained a dP1/P1 (e.g. AMNH F:AM 114454; AMNH F:AM 114455; AMNH F:AM 114436; AMNH F:AM 114486) (Fig. 102). Furthermore, Hagge (2010) identified several instances of P1 in *T. major* adults, stating that 62% of *T. major* adults observed retained at least one P1.

The implied variation in *Teleoceras* anterior premolars must be addressed to determine whether the missing second premolars of ETMNH 32999 are atypical and/or diagnostic. If Hagge (2010) mistook second premolars for first premolars in *T. major*, the absence of dP1 as a generic character still stands, as does occasional loss of P2; whether the first premolar is deciduous or not is irrelevant, as the presence of any first premolar upsets the generic diagnosis. It is worth noting that, in the AMNH collections, no examined *T. major* crania retained P1 or dP1

(though the list of *T. major* specimens examined for the present study is far from exhaustive). If *T. major* does occasionally retain a P1 (or dP1) as noted by Hagge (2010), total dP1 loss is no longer a reliable diagnostic character of the genus. The placement of *T. brachyrhinum* within *Teleoceras* alone rejects this character, as specimens regularly have P1 (Fig. 102). However, several other features of *T. brachyrhinum* challenge Prothero's (2005) generic diagnoses (e.g. strong labial cingulum on upper and lower teeth; broad, retracted nasals that do not downturn laterally), so the taxonomic status of *T. brachyrhinum* requires reconsideration before its features are used for comparison with congeners; such an investigation lies beyond the scope of this thesis. In summary, it is either the case that 1) at least *T. major* occasionally retains a first premolar, and unequivocal dP1 loss is no longer a valid generic character, 2) occasional loss of dP1 has been mistaken for the occasional loss of P2, or 3) both P2 and dP1 presence are highly variable in *Teleoceras* and are poor diagnostic characters. Whatever the case may be, it can be said that no *Teleoceras* species/specimens documented in the literature or examined for this analysis displayed loss of P2. The presence of dP1/P1 is apparently far more variable in the genus if *T. brachyrhinum* is to be included (see Fig. 102), and if the observations of *T. major* by Hagge (2010) are valid. In any case, it can be said that the absence of both P2s in ETMNH 32999 is indeed atypical of the genus.

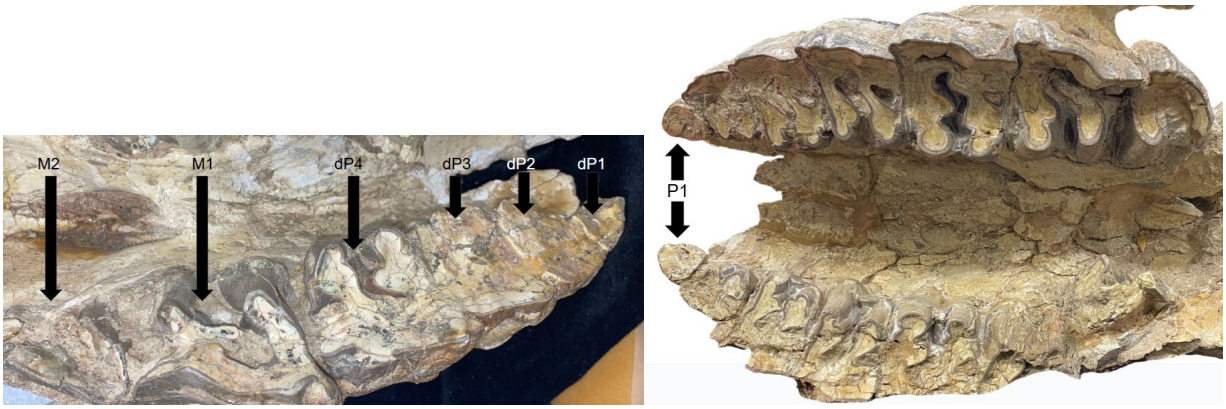

Fig. 102 Maxillary first premolars in *Teleoceras brachyrhinum*. (Left) Left maxillary tooth row (dP1-M2) of AMNH F:AM 114455, juvenile *T. brachyrhinum*. Note the presence of dP1. (Right) Maxillary tooth rows (P1-M3) of AMNH F:AM 114436, adult *T. brachyrhinum*. Note the presence of both P1s, though presence of a first premolar is contrary to the generic diagnosis of *Teleoceras*. Also note the labial cingulum visible on the left tooth row of AMNH F:AM 114436. Not to scale.

All other *T. aepysoma* skulls contain P2, further suggesting a unique condition for ETMNH 32999. ETMNH 32999 also lacks dp2/p2, though this is not as unusual as the absence of the maxillary P2, as p2 has already been documented as variable in *Teleoceras* (Prothero, 2005; Hagge, 2010). Adult *T. aepysoma* individuals often retain a reduced, vestigial p2 (Short et al. 2019); ETMNH 32999 does not, though vestigial incisors (i1) may have been present (see Fig. 22). The presence of both dP2 in ETMNH 32999 implies that this tooth would have been more akin to the persistent dP1 in extant rhinoceroses (e.g. Hitchins 1978; Laurie et al. 1983; Hillman-Smith et al. 1986; Hullot and Antoine 2020), since there is no permanent tooth to replace it. If there were a permanent second premolar, tooth eruption in extant rhinoceroses (e.g. Hitchins 1978; Hillman-Smith et al. 1986) suggests that it would have replaced its deciduous counterpart by this state of M1/M2 attrition (Fig. 101). The persistent dP1 in extant taxa has the potential to be retained late into life, up until age class XV (Hullot and Antoine 2020). The absence of P2 in ETMNH 32999 may also contribute to the difference in eruption sequence from congeners, as additional space in the maxillary crypt may have reduced mechanical pressures

associated with deciduous tooth replacement. Further discussion of the significance of the missing P2s is documented in the "Missing Upper Second Premolars" section below.

Maturity

Sex determination and sex-specific trends. To understand the development of ETMNH 32999, determining the sex is required to interpret features and trends that may be sex specific. Development of female *Teleoceras* is thought to differ from that of males in earlier sexual and skeletal maturity, evidenced by epiphyseal fusion (Mead 2000) and tusk eruption (Mihlbachler 2005). Males are thought to mature later, and often continue to grow well into adulthood, whereas females may reach a growth plateau upon reaching skeletal maturity (Mihlbachler 2005). Bimaturism of this nature is known in extant rhinos as well (e.g. Dinerstein 1991; Hillman-Smith and Groves 1994; Law et al. 2013; Roth et al. 2013).

Teleoceras remains can be sexed based on the size and shape of the tusks, which are modified lower incisors (i2) (Osborn 1898; Voorhies and Stover 1978; Mead 2000; Mihlbachler 2005), as is common for many tusked rhinocerotids (e.g. Mihlbachler 2005, 2007; Chen et al. 2010; Lu et al. 2020). Tusk dimorphism for *Teleoceras* was first hypothesized by Osborn (1898) and was later confirmed upon discovery of a pregnant female *T. major* (Voorhies and Stover 1978). Male tusks are wider and longer than female tusks, with greater diameters, greater widths at the crown base, and longer crown lengths (Mihlbachler 2005). Female tusks are blunter, narrower, and constrict at the base of the enamel crown (Fig. 103). Males occasionally may have a constriction at the base of the crown in earlier stages of wear, like ETMNH 609 (see Short et al. 2019), but this does not occur as consistently as it does in females and is usually worn away relatively early in wear (personal observations).

Fig. 103 Male and female *Teleoceras proterum* tusks. Note that, in the female tusk, the crown constricts at the base, whereas the occlusal surface of the male tusk extends past the base of the crown. Scale bar = 5cm.

Mihlbachler (2005) identified differences in the timing of tusk eruption between male and female *Teleoceras*, so the state of tusk development relative to age can be used to support an assignment to sex, especially if the tusk is found in association with the dentition. Based on observations of Florida samples of *T. proterum*, Mihlbachler (2005) proposed that tusk eruption in males was delayed relative to females. Subadult mandibles with similar dental ages displayed one of two conditions: fully erupted narrower tusks and/or fully developed alveoli (female condition, Fig. 103), or an unerupted larger tusk still within the crypt or only the tip erupted (male condition, Fig. 103). Dinerstein (1991) noted that young adult female *Rhinoceros unicornis* occasionally had longer incisors than similarly aged males, suggesting that similar tusk bimaturism remains present in extant tusked rhinos.

Bimaturism in tusk eruption was corroborated here by observing subadult/young adult mandibles in the AMNH and UF collections (Fig. 104). An unerupted or barely erupted larger, presumably male, tusk was evident in many subadults, including: two age class VIII *T. hicksi* mandibles (AMNH F:AM 114581, AMNH F:AM 115786), an age class VII *T. proterum* mandible (UF 24221), an age class VII *T. proterum* mandible (UF 24234), an age class VIII-IX

partial *T. proterum* mandible (UF 191620), an age class IX *T. major* mandible (AMNH F:AM 114502A), an age class VIII *T. fossiger* mandible (AMNH F:AM 104023), an age class VI *T. fossiger* mandible (AMNH F:AM 115666), and an age class IX *Peraceras profectum* mandible (AMNH F:AM 114401). Conversely, several subadult mandibles displayed fully erupted tusks and/or fully formed alveoli, in which the tusk morphology and/or width of the alveolus compared more favorably with female tusks. Specimens displaying the female tusk condition included: an age class IX *T. major* mandible (AMNH F:AM 104022), an age class IX *T. fossiger* mandible (AMNH FM 2606), an age class IX *T. proterum* mandible (UF 24233), and an age class VIII *T. major* mandible (AMNH F:AM 115509). Unfortunately, this was not a character that could be quantified, as many of the erupted tusks were broken, and many of the unerupted tusks were inside of the bone or embedded in matrix. Still, this bimodal trend in the tusk development is consistent with what has been proposed for *Teleoceras* before (i.e. Mihlbachler 2005) and supports the assertion that ETMNH 32999 is likely a male.

Fig. 104 Sexual bimaturism in *Teleoceras* tusk eruption. In lateral view. (Top) AMNH F:AM 104022, a female *T. major* dentary with a newly emerging m3 (age class VIII) and a fully erupted tusk crown. The erupted extend of the tusk is outlined in red. (Bottom) AMNH F:AM 114581, a male *T. hicksi* dentary with m2 in occlusion and an near fully-erupted m3 (age class IX). The extent of the tusk is outlined in red. Note that, despite being of comparable age, the tusk of the slightly younger female *T. major* has entirely erupted, while the tusk of the male *T. hicksi* remains almost entirely within the alveolus. Note that AMNH F:AM 104022 has been flipped horizontally. Not to scale.

Even without the base of the tusk crown preserved in ETMNH 32999, the width of the preserved crown is still well within the range of male tusks (Fig. 94A-B). Tusks in the AMNH FM/F:AM and UF collections were measured at 30mm distal to the tip (WT), as this is the widest portion of the crown preserved in ETMNH 32999. ETMNH 32999, and all other tusks from the GFS, fell within the range of what is interpreted as male in at least *T. hicksi* and *T. proterum* (Fig. 92A-B).

Because ETMNH 32999 is proposed to have undergone stress-induced growth complications (see Stress and Growth section below), it may be that its poorly developed, unerupted tusks are not indicative of sex, but attributable to delays in maturation. With this in

mind, if sexual bimaturism is disregarded completely, the WT measurement still supports a male sex assignment, since the tusk is already wider than those of congeneric female crowns (Fig. 92A-B), and shows no indication of constricting at the base at this point in development.

Disregarding tusk dimorphism/bimaturism as an indicator of sex, the relatively small size of ETMNH 32999 (Figs. 63, 64A; Tables 10-11) could be argued to resemble the size dimorphism seen in some *Teleoceras* species (e.g. *T. major*, *T. medicornutum*), where males have greater cranial (Mead, 2000) and postcranial (Voorhies 1990; Mead 2000) dimensions. However, in other species, such sexual size differences are either not apparent prior to maturity (e.g. *Dicerorhinus sumatrensis*, Plair et al. 2012; Roth et al. 2013), or subadult females are larger than males due to their accelerated rates of maturation (e.g. *Rhinoceros unicornis*, Dinerstein 1991; *Ceratotherium simum*, Groves 1972). In ETMNH 32999, the most reduced dimensions relative to GFS adult males are cranial lengths and widths (Tables 2, 10, 11), which could potentially be influenced by dimorphism. In the AFB sample of *T. major* (Mead 2000), cranial lengths were somewhat dimorphic, though the ranges for each sex overlapped; zygomatic width and supraorbital width had lower dimorphism ratios with a considerable degree of overlap. However, the sexual dimorphism observed in the AFB sample, and Great Plains *Teleoceras* in general, is said to be exaggerated relative to what is seen in other *Teleoceras* samples, such as Floridian populations of *T. proterum* (Mihlbachler 2005). Plasticity in sexual size dimorphism within the genus suggests that, until an obviously female *T. aepysoma* is discovered (e.g. intact female tusks/narrower tusk alveoli, or a pregnant individual), *T. aepysoma* cannot be assumed to display the same degree of size dimorphism as Great Plains congeners. In summary, with varying factors such bimaturism rates or generic plasticity in size dimorphism confounding sex determination, trends in tusk morphology/eruption are the only features that can be used to

confidently infer sex in immature *Teleoceras*. In both tusk morphology and eruption stage, a male diagnosis is supported for ETMNH 32999, and sexual size dimorphism is considered a highly unlikely cause for its small size relative to age.

Sexual maturity. Timing of sexual maturation in extant rhinoceroses can offer insights into maturation in extinct species. In extant rhinoceroses, females may reach sexual maturity as early as 10% of potential lifespan (Groves 1972; Laurie et al. 1983; Hillman-Smith et al. 1986; Hillman-Smith and Groves 1994; Groves and Leslie 2011; Plair et al. 2012; Law et al. 2013). Sexual maturity occurs later in males; in *Diceros bicornis*, males may be reproductively mature as soon as 12% of potential lifespan, but wild individuals often will not reproduce until later in life, at ~24% of potential lifespan (Hitchins and Anderson 1983) due to extreme intermale competition. Law et al. (2013) consider the subadult-adult transition for male *D. bicornis* to occur at 8 years of age, or ~20% of potential lifespan, while females transition to adulthood sooner, at ~16% of potential lifespan. Similar bimaturism is observed in *Rhinoceros unicornis* (Laurie et al. 1983; Dinerstein and Price 1991) and *C. simum* (Hillman-Smith et al. 1986). Sexual maturity in *Dicerorhinus sumatrensis* is achieved at 6-6.5 years in males, and 5-5.5 years in females (Roth et al. 2013). Assuming a potential life span of 32 years (Groves and Kurt 1972), these ages would correspond with ~18-20% of potential lifespan in males, and ~15-17% in females. Conception in remarkably young individuals has been documented in *Ceratotherium simum* and *R. unicornis*, as young as only 2.7 years of age (Roth et al. 2013 and ref. therein), suggesting that female functional sexual maturity may occur even before ~10% of potential lifespan.

Considering the sex and age classification of ETMNH 32999, sexual maturity may have been imminent or achieved, if said event in *Teleoceras* is comparable to its extant relatives. If

male, it would likely not have been of reproducing age despite its inferred sexual maturity, based on what is observed in *D. bicornis* (Hitchins and Anderson 1983). If female, ETMNH 32999 would likely have been well into sexual maturity based on what is observed in most extant species. In the more closely related *Plesiaceratherium gracile*, females are thought to be sexually mature and fit for parturition by the time the second molar is in occlusion (age class VII), similar to extant taxa (Lu et al. 2023b). Sexual maturation in extinct species, presumably including *Teleoceras*, is apparently somewhat comparable to their extant relatives.

Skeletal maturity. For rhinocerotids, skeletal maturity refers primarily to the fusion of the longbone epiphyses, not necessarily to achievement of asymptotic size; however, based on other rhinocerotid taxa, the two should generally occur in close age-proximity (e.g. Lu et al. 2023b). Epiphyseal fusion is thought to be delayed in male *Teleoceras,* in which two subadult *T. major* males (UNSM 121510 and 121511) from AFB with epiphyses unfused display the same dental age as females with fused epiphyses (Mead 2000). Sex-specific bimaturism in epiphyseal fusion is not uncommon among polygynous, sexually dimorphic ungulates, such as cervids (Flinn et al. 2013; Calderón et al. 2019) and bighorn sheep (Walker 1987).

The scarcity of fossil rhinocerotid skulls with associated post-crania creates difficulty in comparing rates of epiphyseal fusion with other taxa. There are, however, a few examples available for comparison in addition to the two AFB *T. major* subadults described by Mead (2000). A subadult *Plesiaceratherium gracile* (S700017) described by Lu et al. (2023b) aligns most closely with Hitchins' (1978) age class VIII and has all epiphyses fused. A partial skull, right ramus, and associated humerus of *Peraceras profectum* in the AMNH collections (AMNH F:AM 114401) represented an individual in age class IX with an unerupted male tusk in the alveolus; and both epiphyses of the associated humerus fused. A juvenile (age class VI)

Acerorhinus yuanmouensis humerus with an associated cranium (Lu 2013) had at least the distal epiphysis fused (Lu et al. 2021). Young adult individuals of *Coelodonta antiquitatis* had at least proximal longbone epiphyses fused and were of comparable size to conspecific adults (Shpansky 2014) (Fig. 106B), but concise age and sex data could not be correlated.

The sequence of epiphyseal fusion in artiodactyls is thought to be comparable to perissodactyls (Todd and Todd 1938). For the forelimbs, the sequence from Todd and Todd (1938) is as follows: third phalanx, distal humerus, proximal radius, first and second phalanges, metacarpals, distal radius and distal ulna, proximal humerus. ETMNH 32999 appears to mostly follow this pattern, though there are some notable inconsistencies. All phalanges are fused, and the distal humerus is fused, albeit with an evident suture. Proximal ends of the metacarpals and metatarsals are all fused, though the distal ends are unfused. Aside from the unfused proximal radii epiphyses, ETMNH 32999 would place in this sequence after the fusion of the metacarpals, but before that of the distal radius and ulna, possibly in the middle of the stage of metacarpal fusion.

Complete epiphyseal fusion corresponds with skeletal maturity, and therefore, the onset of asymptotic/adult size. Skeletal maturity and/or achievement of asymptotic size may occur anywhere from 4-12 years of age in other rhinocerotids (Groves 1972; Hitchins and Anderson 1983; Laurie et al. 1983; Hillman-Smith et al. 1986; Hillman-Smith and Groves 1994; Groves and Leslie 2011; Roth et al. 2013; Lu et al. 2023b), but may be dependent on sex or species. If extant rhinoceroses are assumed to have an average lifespan of ~40 years, as in *C. simum* (Groves 1972; Hillman-Smith et al. 1986) and *D. bicornis* (Hitchins 1978), male skeletal maturity usually occurs between 20-25% of potential lifespan. Male *R. unicornis* are considered fully grown by age 8, or ~17-20% of potential lifespan (Laurie et al. 1983); *Eurhinoceros.*

sondaicus is fully grown even earlier, at 5.5-6 years of age, or ~15% of potential lifespan (Groves and Leslie 2011). *Dicerorhinus sumatrensis* is considered fully grown "well before" the third molar is in occlusion (Groves and Kurt 1972), which would correspond with a subadult age. While slight differences exist in the timing of skeletal maturity between the sexes, rhinocerotids generally achieve skeletal maturity at ~15-20% of potential life span. This life stage overlaps with the period sexual maturity is usually achieved, especially in females, which mature earlier than males.

Based on annular growth lines observed in the tusks of *T. proterum*, the lifespan of *Teleoceras* may have been comparable to modern taxa at ~40 years, or slightly less (Mihlbachler 2005). If the *D. bicornis* age of 7 ± 1 years old for ETMNH 32999 is applied to this estimation, this would correspond with 15-20% of potential lifespan (consistent with the estimations of Mihlbachler 2003 for *T. proterum*); in other words, skeletal maturity and asymptotic size would likely have been imminent for an individual of the same age as ETMNH 32999. Despite this, ETMNH 32999 remains largely neotenous in both size and shape, evidenced by a seemingly underdeveloped cranium and a mostly unfused appendicular skeleton. While the delay in plate fusion may be partially attributable to sex, as is seen in subadult males of *T. major* (Mead 2000), other factors may affect the timing of epiphyseal plate closure. For example, undernutrition can delay plate fusion by over a year in black-tail deer (Lewall and Cowen 1963). If comparable physiological stress occurred during the development of ETMNH 32999, it may have affected the rate of skeletal maturation or exacerbated the male delay in epiphyseal fusion. The notion of developmental stress in ETMNH 32999 affecting osteological development is expanded on in the "Stress and Development" section below.

Body mass estimates. *Teleoceras aepysoma* is among the larger species of *Teleoceras* (Short et al. 2019), as would be expected from its longer forelimbs and greater cranial dimensions. Mass estimates based on the circumference of the humerus (Anderson et al. 1985) suggested weights of 1640kg for holotype ETMNH 609, 2720kg for paratype ETMNH 601, and 2630kg for ETMNH 33000 (Table 9). The same equation returned a value of 1,330kg for ETMNH 32999. More refined mass estimates for the *T. aepysoma* holotype and paratype used femur and calcaneum measurements (see Short et al. 2019), but as these elements are missing in ETMNH 32999, the same estimates cannot be compared.

When compared to the young adult holotype ETMNH 609, ETMNH 32999 is ~81% of its estimated body mass. However, when compared with the average of all 3 adults, ETMNH 32999 is only ~57% of the average adult body mass. Because of the large discrepancy between the estimated body masses of ETMNH 609 and full adults ETMNH 601 and ETMNH 33000, it is unclear what a typical body mass for an adult *T. aepysoma* is, and therefore, how typical the estimated mass of ETMNH 32999 is.

Mass estimates for the fossil species *Acerorhinus yuanmouensis* (Lu et al. 2021) offer some opportunity for comparison, though because the same body mass estimation equation was not used, proportional differences offer the best comparison rather than raw values. Estimated body mass is reported for a juvenile, though nearly subadult (age class VI) *A. yuanmouensis* (Lu et al. 2021). The juvenile individual (IVPP 18565) was estimated to be 573kg and the estimated adult value was 1544kg (~37% that of the average adult) (Lu et al. 2021). IVPP 18565 is younger than ETMNH 32999, though its skull is already of nearly adult proportions (LN ratio to average adult = 0.9676). It would seem that, for an individual of the same age as ETMNH 32999,

slightly older than IVPP 18565, ~57% of the average adult body mass would be a reasonable expectation.

In the extant Sumatran rhino, *Dicerorhinus sumatrensis*, Roth et al. (2013) reports that captive males reach their adult weight at 6-6.5 years of age (~15-16.25% of potential lifespan, assuming a lifespan of ~40 years) and females at 4 years (~10% of potential lifespan). If similar life histories between *D. sumatrensis* and *Teleoceras* can be safely assumed, a male individual of comparable age to ETMNH 32999 would be expected to be rather close to adult weight, suggesting that the estimated body mass of ETMNH 32999 is lower than would be expected. However, because of the large discrepancy between the body mass estimates for age class XI ETMNH 609 (1640kg) and age class XIII ETMNH 601 (2720kg), it is unclear what a typical adult body mass for *T. aepysoma* is, or how wide the range of variation is in this regard. It must be noted that the mass estimates for *T. aepysoma* are based solely on humeral circumference, so they are directly linked to how robust/gracile the midshaft is, and without more refined estimates, may not best represent mass differences between the GFS skeletons. In other words, it remains to be seen whether the estimated body mass of ETMNH 32999 is typical for an individual of its age, or whether it deviates from expectation based on what is seen in other species.

Remarks on Growth: Quantitative

Growth Plots Discussion

Figures 63, 65, 67, 69-70, 72 and 74 indicate the growth in raw cranial dimensions relative to dental age for best-sampled taxa. A clear trend is apparent in comparing the plot of *Teleoceras aepysoma* (Fig. 63) to all other taxa; in most craniomandibular dimensions, a growth plateau is reached by subadulthood, save for in *T. aepysoma*. Adult or near-adult sizes are achieved in most measurements by the onset of age class VII, if not earlier. The steepest

increases in size always occur prior to age class VII, often from age classes III (or earlier) to V, consistent with the findings of Lu et al. (2023b) for *Plesiaceratherium gracile.* Juvenility apparently entails the most rapid growth rates in extinct species as in extant species (e.g. Dittrich 1972; Hillman-Smith et al. 1986; Plair et al. 2012), especially relative to the attenuated growth rates of subadulthood (Figs. 65-74, 77-88). Though lacking data for juvenile individuals, the slope from age class VIII to age class XI for *T. aepysoma* is rather steep (Fig. 63) relative to what is seen in the other species, more closely resembling the steep growth curves typical of juveniles. *Chilotherium wimani* (Fig. 69), *T. major* (Fig. 65), and *Diceros bicornis* (Fig. 72) are the best examples of a subadult growth plateau, as the datasets for these species include juvenile individuals. ETMNH 32999, then, continues to display juvenile, or otherwise neotenous, cranial proportions relative to subadults of other rhinocerotid taxa.

Comparative data for forelimb lengths was available for *Plesiaceratherium gracile* from Lu et al. (2023b). Unlike cranial measurements, ontogenetic changes in forelimb length are mostly unremarkable in *T. aepysoma* and mostly resemble what is seen in *Pl. gracile* (Fig. 76), though ETMNH 32999 has slightly shorter forelimb lengths proportional to adults (Fig. 75). However, asymptotic size in forelimb lengths is not as clear for *T. aepysoma*, as the holotype ETMNH 609 and paratype ETMNH 601 differ considerably in forelimb lengths despite their close age proximity (Tables 4-7). The forelimbs of ETMNH 32999 are not much shorter than those of the adult ETMNH 609 but are rather short compared to ETMNH 601. Comparatively, asymptotic forelimb size is apparently imminent, if not achieved, for the subadult *Pl. gracile* of comparable age to ETMNH 32999 (Fig. 76).

Lambdoid crest to tip of nasals. LN growth rates across taxa, save for *Teleoceras aepysoma*, appear consistent with each other, though some abnormalities are clear. Despite being

relatively well sampled, *T. brachyrhinum* has the lowest R^2 value (= 0.5616), possibly reflecting the variability of its unique retracted nasals. A *T. major* individual in age class VI is substantially above the line of best fit for the species, larger than a conspecific age class X individual, though otherwise most size change in LN is explained by age for this species (R^2 = 0.7374). Data for *Chilotherium wimani*, *Plesiaceratherium gracile*, and *T. major* are all consistent with the best sampled taxon included, the extant *Ceratotherium simum*, suggesting that these four species represent a consistent LN growth rate despite not being closely related. This consistency suggests that nasal horn presence is also apparently negligible in LN growth rate, as hornless species (*Ch. wimani, Pl. gracile*) grow at a comparable rate to the tandem-horned *C. simum*. If this growth rate is a good representative of how LN develops through ontogeny in rhinocerotids, then ETMNH 32999 represents an outlier among the sample (Table 10), warping the line of best fit for *T. aepysoma.*

It is worth noting that the LN of *T. aepysoma* holotype ETMNH 609 represents an intermediate size between ETMNH 32999 and the other GFS adults (Table 2). This is due in large part to the strong nasal upturn unique to ETMNH 609 among the *T. aepysoma* sample (Fig. 64B); though other adults have upturned nasals, it is not as exaggerated as in ETMNH 609. In other words, the cranium of ETMNH 609 is not abnormally brachycephalic as ETMNH 32999 but has slightly decreased LN due to its snub-nosed condition.

Barring ETMNH 32999, individuals less than 80% of the average conspecific adult LN are only known from much younger juveniles in age class V or below (Fig. 79). Even individuals in age class VI, interpreted here as the onset of subadulthood, are all expected to be above 80% of the average conspecific adult. Though not included in the plots for lack of mensural/complete data, similar trends in occipitonasal length development are reported for *Dicerorhinus*

sumatrensis (Groves and Kurt 1972), *Rhinoceros unicornis* (Laurie et al. 1983), *Eurhinoceros sondaicus* (Groves and Leslie 2011), and fossil species *Diceros gansuensis* (Deng and Qiu 2007) and *Acerorhinus yuanmouensis* (Lu et al. 2013).

Anterior premolar to occiput. Lines of best fit for *T. medicornutum*, *T. brachyrhinum*, and *Ceratotherium neumayri* appear to be higher than expected in the juvenile age classes, likely due to the absence of juveniles sampled for those taxa (Fig. 81). The better sampled taxa, save for *T. aepysoma*, are likely more representative of rhinocerotid growth rates. Much like the trend observed in LN, only individuals in juvenile age classes (age class VI and below) are below 80% of average conspecific adult PO, with most taxa expected to be 80% of average adult PO by the onset of age class VI.

Taxa that could not be included here due to lack of complete/reported mensural data display similar trends in basal length (=PO) growth. Such is the case for the extant rhinos *Dicerorhinus sumatrensis* (Groves and Kurt 1972), *Eurhinoceros sondaicus* (Groves and Leslie 2011), and *R. unicornis* (Laurie et al. 1983). Again, the consistency in growth rates among all taxa sampled, both extant and extinct, suggests common ontogenetic trends that are rooted deep within Rhinocerotidae; similar life history among temporally and phylogenetically distinct rhinocerotoids is consistent with the findings of previous studies (see Lu and Deng 2025). Potential species-specific trends that may influence growth such as diet, body size, and ecology are apparently superseded by the consistency of these broad-scale ontogenetic trends, though larger sample sizes and a greater breadth of taxa diversity would assist in solidifying this assertion.

Total cranial length. ETMNH 32999 deviates much less from expectation in TCL than in other skull length measurements, reflecting that the skull is not as reduced in dorsoventral depth

as it is in anteroposterior length. Scarce sampling for TCL affects the quality of conclusions that can be drawn. The small sample is somewhat attributable to preservation biases in fossil specimens. If a specimen could not be measured for LN due to a distorted or broken lambdoid crest, PO could usually be taken. Conversely, if the occipital region or anterior maxilla was damaged/missing, LN could usually be taken. TCL, on the other hand, requires both an intact, undistorted lambdoid crest and an intact anterior maxilla, which are both regions particularly susceptible to taphonomic breakage. Furthermore, TCL, or a comparable measurement, is not commonly reported for adults in literature like basal length (PO) or LN.

The taxa-combined growth plot for TCL (Fig. 77) suggests a comparable trend to other skull length measurements. Sampled taxa which included juvenile individuals (e.g. *Chilotherium andersoni*, *Teleoceras major*) should be more indicative of how TCL typically develops. Again, ETMNH 32999 is below all other taxa included in the TCL plot, suggesting an additional departure from typical growth, albeit not of the same magnitude as LN and PO.

Zygomatic width. The growth curve for ZW in *T. aepysoma* is one of the most apparently different from other rhinocerotids. It is unlikely that the ZW growth of *T. aepysoma* actually deviates strongly from the normal logarithmic trend observed in other taxa, but instead more likely that the line of best fit is warped by the narrow ZW of ETMNH 32999. Despite being in age class VIII, the ZW of ETMNH 32999 is more equivalent to congeners in age class III, at only 64.74% that of average adult ZW for *T. aepysoma* (Table 10). Similarly, other individuals that measure below 70% of average adult ZW are all younger than age class V. Between age classes VII-IX, only two other subadults score at <80% of average adult ZW: an age class VII *T. medicornutum* specimen (AMNH F:AM 109518) is 76.71% of the average adult ZW, and a *T. fossiger* specimen (AMNH F:AM) in age class VII that scores only slightly below the line of

best fit at 79.67% of the average adult. The *T. fossiger* subadult is too incomplete to make any comparisons, but it is worth noting that the *T. medicornutum* specimen bears a similar series of enamel defects to ETMNH 32999. Developmental interruptions as implied by the enamel defects may be partially responsible for this relatively reduced ZW ratio; this notion is explored further in the "Enamel Hypoplasia" section below.

While specimens from the GFS are often found crushed (Fig. 1), they are rarely distorted (Haugrud, 2023), meaning that the narrow ZW of ETMNH 32999 is not considered here to be attributable to taphonomic deformation. The left zygomatic arch of ETMNH 32999 is intact without any missing pieces, and no other areas of the preserved cranium appear to be taphonomically warped when compared to distorted specimens (e.g. AMNH F:AM 114455, Fig. 68A).

Supraorbital width. Among the diagnostic features of *T. aepysoma*, the most pronounced cranial modification is found in the exaggerated tuberosities superior to the orbits in adults. While the function of this feature is unclear, a preliminary analysis (Gajewski and Wallace 2025) has suggested an independent emergence of this feature among several Aceratheriine taxa, with *T. aepysoma* being the only taxon within Teleoceratini where this feature occurs consistently across specimens. At least one *T. fossiger,* AMNH F:AM 114583, and two *T. hicksi*, MRG-10-295030 figured by Carbot-Chanona et al. (2009) and IGCU-4818 figured by Carranza-Castaneda (1989), also display this condition, but it does not occur as consistently in these species as it does in *T. aepysoma.*

Comparable supraorbital swellings are known from *Peraceras profectum* (Prothero 2005), *Plesiaceratherium tongxinense* (Sun et al. 2024), and *Acerorhinus hezhengensis* (see Lu et al. 2023a; Deng et al. 2023), though only those of *Pl. tongxinense* are as strong as those of *T.*

aepysoma. *Peraceras* and *Plesiaceratherium* have recently been suggested to be more closely related than previously thought, though they are united primarily by characters of the magnum and dentition (Borrani et al. 2025), rather than the supraorbital tuberosities. The small and cryptic *Galushaceras levellorum* is also said to have a slightly swollen frontal region (Prothero 2005), and interestingly, has been proposed to be closely related to *Plesiaceratherium* based on the relatively flat dorsal skull profile (Lu et al. 2023a). Prothero (2005) also considered *Galushaceras* and *Peraceras* to be closely related. If *P. profectum* was included in the phylogenetic analysis of Aceratheriinae (Lu et al. 2023a), one might wonder if it would be grouped away from *P. superciliosum* and closer to *Plesiaceratherium*, as in Borrani et al. (2025); the same question can be raised for *G. levellorum*. The supraorbital swellings of *P. profectum* were briefly mentioned by Prothero (2005) but were considered too variable to be suitable for generic diagnoses. Once the taxonomy of *Peraceras* is better understood, it would be interesting to explore the evolutionary trend of supraorbital swellings and their apparently variable, independent emergences in Aceratheriinae. If *Plesiaceratherium*, *Galushaceras*, and *Peraceras* share some type of phylogenetic affinity in relation to the supraorbital swellings, it is intriguing that the feature emerged again late into the *Teleoceras* lineage.

Ontogenetic trends in the development of the supraorbital boss are variable between groups. *Pl. gracile* displays comparable swellings that extend only laterally (rather than expanding dorsally as in *T. aepysoma* and *Pl. tongxinense*), and a subadult (age class VIII) individual reported in Lu et al. (2023b) (S700017) already bore a pronounced condition comparable to that seen on adults. Conversely, a subadult (age class VIII) *P. profectum* (AMNH F:AM 114379) had no evidence of dorsal swelling in the supraorbital region as seen in adults, though the supraorbital tuberosities extended considerably laterally.

Measurements of SW reported unexpected variation. Adult *Chilotherium wimani* differ wildly from each other (Fig. 69, 84), likely representative of the sexual dimorphism reported for the supraorbital region of this species (see Deng 2001; Chen et al. 2010). The variation observed for this feature in *P. profectum* (Fig. 84) suggests a similar potential for dimorphism, though a larger sample would be needed to identify bimodality. The laterally extended supraorbital tuberosities of *Pl. gracile* are not explicitly stated in the assessment of the species' sexual dimorphism (Lu et al. 2020), though females do appear to lack this feature based on the individuals figured by Lu et al. (2020). Dimorphism in this feature for *T. aepysoma* is also unknown in the absence of a confirmed female specimen.

Mandibular length and ramus length. Data for mandibular length (ML) was not complete enough to create curves for many taxa, but data was available for *Diceros bicornis* from Goddard (1970) and for *Pl. gracile* from Lu et al. (2023b). Unlike the cranial lengths, the ML curve for *T. aepysoma* is not as dissimilar from those of *T. fossiger*, *Pl. gracile*, or *D. bicornis*. Mandibular morphology stabilizes early in life in *T. major* (Hagge 2010), so it is reasonable to expect that a similar ontogenetic trend would be present in congeners. It would seem that whatever factors may have contributed to the small cranium of ETMNH 32999 did not have the same effect on the mandible.

Ramus length (RML) proved to be wildly inconsistent between taxa (Fig. 90), which can likely be attributed to several factors. Sample sizes for RML were small, particularly for juvenile individuals, as usually only the tooth-bearing portion of the dentary is preserved. Even among taxa with more complete sampling, there was a great amount of variation. Sexual dimorphism is the likely cause of this inconsistency, as mandibular dimensions are expected to be more dimorphic than those of the cranium and can be more pronounced within a smaller sample. Tusk

size greatly affects the morphology of the mandible in *Teleoceras* (Mead 2000) as thicker, longer tusks would require deeper and wider alveoli, so it is reasonable to assume that similar variability is at play here.

Dentition. ETMNH 32999 returns dental length measurements comparable to conspecifics, with tooth row lengths well within the range of other *Teleoceras aepysoma* (Table 3). The most abnormal condition is that of both p3s, which in ETMNH 32999, are significantly smaller than any other *T. aepysoma*, or any other *Teleoceras*, even including the dwarf *T. meridianum* (Fig. 93). Z-score calculations on p3 area for all *Teleoceras* spp. sampled implied a significant departure from normality, over three standard deviations from the mean. Interestingly, the dp3s are not as reduced as their permanent counterparts. The anterior P2s are absent altogether. Further exploration into potential etiologies of the reduced dentition observed is provided in the "Reduced Dentition" section below.

The widths of both the maxillary and mandibular teeth of ETMNH 32999 are considerably lower than those of all conspecific adults (Figs. 91-92; Table 3) despite the lengths comparing more favorably. Width discrepancies among the maxillary teeth are more pronounced among those that develop earlier (P3, M1) than those that develop later in life (P4, M2, M3). This difference is unlikely to have any taxonomic significance but is proposed to be more likely attributable to the period of growth arrest evidenced by the EH; this notion is explored further in the "Reduced Dental Widths" section below.

As only the tip of the crown is preserved for both tusks of ETMNH 32999, little is available for measurement or comparison. ~30mm distal to the tip (WT) is the proximalmost extent of the tusk crown of ETMNH 32999, so isolated tusks of other *Teleoceras* species were measured at the same placement to assess if bimodality was present prior to the cessation of

crown formation. Bimodality is present in the plots for *T. hicksi* and *T. proterum* (Fig. 94A-B) but overlap exists between narrower male tusks and thicker female tusks. WT, as measured here, is not as dimorphic as other incisor dimensions, such as width at the base of the crown in *T. proterum* (Mihlbachler 2005) and *T. major* (Mead 2000); rather, there is a weak trend with some overlap between sexes for WT. Regardless, in *T. hicksi*, the group of smaller tusks (i.e. females) seem to rarely, if ever, exceed a WT of 30mm (Fig. 94A); the same is reported for crown base width in *T. major* (Mead 2000). Additionally, the point of measurement for WT was frequently past the base of the crown in narrower, likely female, tusks, which have shorter crowns (Mihlbachler 2005). *T. hicksi* and *T. major* are more comparable in size to *T. aepysoma* than the smaller *T. proterum* (see Short et al. 2019), so if the same WT bimodality seen in *T. hicksi* (Fig. 94A) is applicable to *T. aepysoma*, ETMNH 32999 would fall within the "male" classification, along with ETMNH 601, 609, 33000, 19280, and 21659, who each have a WT exceeding 30mm (Table 3) and a WT that is not past the base of the crown. While this is not as strong of an indicator of sex as the timing of tusk eruption, it still supports the classification of ETMNH 32999, and all other GFS specimens with tusks, as male.

Interquartile Range Discussion

Individuals sampled suggest that, on average, subadult rhinocerotids are 91.3% of adult size in cranial dimensions, ranging from ~85% to 98% (Table 10). Ratios are consistent with what has been reported for both extant (Goddard 1970; Groves 1972; Groves and Kurt 1972; Hillman-Smith et al. 1986; Hillman-Smith and Groves 1994; Groves and Leslie 2011) and extinct (Deng 2001; Deng and Qiu 2007; Lu 2013; Lu et al. 2023b) taxa. Growth rates in some extinct rhinocerotoids, such as *Paraceratherium*, are similar to their extant relatives (Lu and Deng 2025), as subadult individuals are usually rather close to adult size in most dimensions (Lu

et al. 2023b) (Fig. 105). Apparently regardless of size or phylogenetic placement, subadult rhinocerotids have nearly achieved adult or near-adult size in most cranial dimensions by age class VII (Fig. 105), or even earlier.

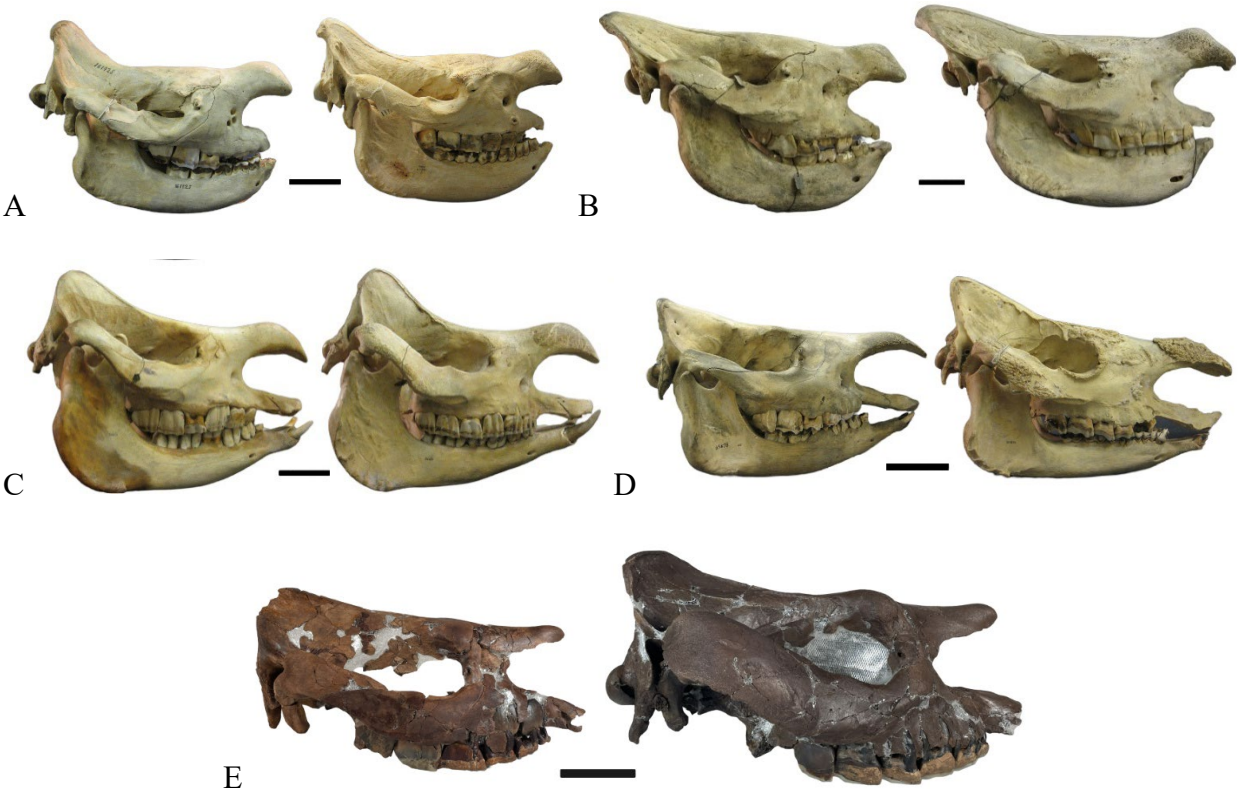

Fig. 105A-E Subadult and adult skulls of the extant rhinos and *Teleoceras aepysoma*. In right lateral view. Photos of extant rhinos modified from Hagge (2010). *Eurhinoceros sondaicus* is excluded. Note that, in the extant taxa, age class VIII individuals are comparable to conspecific adults in shape and size; in *T. aepysoma*, the subadult (ETMNH 32999) retains a largely neotenous condition in both shape and size relative to the adult. (A) *Diceros bicornis*, age classes VIII (USNM 161925) and XII (FMNH 127849). (B) *Ceratotherium simum*, age classes VIII (AMNH 51931) and XII (AMNH 51856). (C) *Rhinoceros unicornis*, age classes VIII (AMNH 54456) and XII (AMNH 54454). (D) *Dicerorhinus sumatrensis*, age classes VIII (FMNH 63878) and XIII (AMNH 81892). (E) *Teleoceras aepysoma*, age classes VIII (ETMNH 32999) and XIII (ETMNH 601). ETMNH 32999 has been flipped horizontally to appear as right. Scale bars = 10cm.

ETMNH 32999 negatively deviates from each of the returned subadult-adult averages, but is flagged as an outlier for only LN, ZW, and OH. Although not an outlier, ETMNH 32999 is at the lower end of variation for PO, TCL, SW, and ML, scoring below Q1 for each; PO was

particularly close to the lower fence (Table 10). On average, ETMNH 32999 is 73.53% of the average adult *T. aepysoma* in cranial dimensions (excluding ML and OH due to poor sampling), contrasting with the average of 91.30% reported for all other sampled subadults. Comparing the geometric means of ETMNH 32999 with the average of GFS adults yields a similar result, suggesting an individual 74.57% that of the average conspecific adult in overall size. Based on the ratio growth plots, a value of ~74% of the average conspecific adult is more consistent with juveniles in age class IV or V, despite the age class VIII assignment of ETMNH 32999.

Overall, the IQR tests support the hypothesis that the cranial dimensions of ETMNH 32999 are quite small relative to subadults of other rhinocerotid taxa. In subadults of all other sampled species, adult/asymptotic size was nearly achieved in most dimensions apparently regardless of phylogenetic or morphological discrepancies. While the subadult-adult ratios would benefit from being refined via larger sample sizes, the relatively low standard deviations reported (Table 8) suggest general consistency in ontogenetic size changes between groups and are consistent with what has been documented in extant species. Therefore, the returned ratios (Table 8) should be a good representation of how large subadult rhinocerotids are relative to conspecific adults (see Fig. 105).

Teleoceras aepysoma Allometric Scaling Discussion

Results suggest that ETMNH 32999 negatively deviates, on average, ~17% from expectation in all cranial dimensions (Table 11). The most affected dimensions are those of ZW, SW, OH, LN, PO, TCL, and ML, in decreasing order of magnitude. Based on the average subadult-adult ratio for ZW, ETMNH 32999 deviates from expectation anywhere from –19.34 to –30.62% ($\bar{x}$ = -25.4%), with the equation returning an expected subadult value of 318.47mm (± 23.94). This is to say, even in the most conservative estimates, the ZW of ETMNH 32999 is at

least 19.34% smaller than would be expected of a subadult of this age, based on M1 anteroposterior length as a size proxy. SW estimates return a deviation of at least –8.39%, though may be as great as –26.16% ($\overline{x}$ = -18.23%); the greater range of deviation reflects greater variance among the subadult sample from which the SW ratio data was drawn. Both LN and PO deviate identically, 14.31% smaller than expected on average. The same dimensions grow at a nearly simultaneous rate in the extant *Rhinoceros unicornis* (Laurie et al. 1983), *Dicerorhinus sumatrensis* (Groves and Kurt 1972), *Diceros bicornis* (Hillman-Smith and Groves 1994) and *Eurhinoceros sondaicus* (Groves and Leslie 2011), so a comparable growth rate for both cranial length measurements is to be expected. ETMNH 32999 deviates less in TCL than in other cranial length measurements. In the most conservative estimates, ETMNH 32999 deviates only ~0.41% from expectation, though may deviate up to –20.78% in TCL ($\overline{x}$ = -11.75%). TCL accounts more for dorsoventral depth than anteroposterior length, so it would appear that the dorsoventral depth of the skull is not as atypical as the exaggerated brachycephaly. TCL ratios were also drawn from smaller sample sizes, as the modifications made to the TCL measurement landmarks in the present study could not be easily compared to measurements reported in the literature for other taxa. Nevertheless, TCL is like the other cranial length dimensions, with rhinocerotid subadult TCL averaging 89.01% that of the average conspecific adult (Table 8), suggesting imminent achievement of adult size.

An average subadult-adult ratio for OH (Table 8) could not be determined with much confidence, considering that the sample size is rather small (n=5) and consists of five different taxa, all measurements taken from literature. Regardless, the average subadult: adult OH ratio ($\overline{x}$ = .9779) suggests that adult OH is nearly achieved at this life stage. Although, it is unclear if the correlation is so simple; the subadults sampled may have simply consisted of large individuals.

Subadults may also have a greater OH than adults as the braincase becomes less globular through ontogeny (e.g. Hagge 2010). In ungulates, OH development may also be influenced by diet (Mendoza et al. 2002) and is variable between rhinocerotid taxa (Hagge 2010), so results here are to be interpreted with caution. ETMNH 32999 is still, however, only 78.27% of the average conspecific adult OH, consistent with its other cranial subadult-adult ratios (Table 10). Results suggest a considerable deviation from expectation ($\overline{x}$ = -17.89%) (Table 11), but this is not considered as informative as the other, better sampled, dimensions due to inherently greater variation in OH. It is noteworthy, however, that ETMNH 32999 lacks the pronounced nuchal crest of conspecific adults (Fig. 64), while this structure is typically well-developed in subadults of other rhinocerotid taxa (e.g. *Teleoceras major*, Fig. 66; *Teleoceras brachyrhinum*, Fig. 68; *Chilotherium wimani*, Fig. 69; *Diceros gansuensis*, Fig. 74; extant species, Fig. 105).

Deviation of ML ($\overline{x}$ = -6.64%) is rather negligible compared to what is observed in the cranium. While ML may deviate up to –13.12%, the most conservative estimate (-0.87%) suggests a mandible of typical length for a rhinocerotid of this age (Table 11). As mandibular morphology is closely linked to the development of the tusks, and therefore, the onset of sexual maturity (Mead 2000; Hagge 2010), the most pronounced growth in ML may have occurred after the period of physiological stress (discussed below) suggested to contribute to the other reduced dimensions. As mentioned earlier, mandible shape and size are also likely to be heavily influenced by sexual dimorphism in *Teleoceras* (Gerhold 1992; Mead 2000) due to the sexual differences in tusk morphology, where males with thicker, longer tusks presumably require much wider, deeper alveoli. Additionally, the sample size for subadult ML was relatively small (n=10). This is not to say that the percent deviation for ML in ETMNH 32999 is entirely inaccurate, only that there are sexual and taxonomic variations that could not be accounted for here that may have

obscured the results. Additionally, the reduced anterior premolars of ETMNH 32999 may provide insight into why ML does not deviate as strongly as cranial lengths. In humans with hypodontia (missing teeth), the length of the maxilla is typically more severely affected than the mandible (Fekonja and Čretnik 2022); cranial lengths of ETMNH 32999 may be more stunted as the anterior maxillary premolar is completely absent, but the anterior mandibular premolar is reduced (Fig. 110), but present.

Forelimb lengths of ETMNH 32999 are apparently not as reduced as cranial dimensions (Table 12), with forelimb lengths roughly ~80% that of an average *T. aepysoma* adult. The humerus length deviates more ($\bar{x}$ = -12.14%) than that of the radius ($\bar{x}$ = -6.07%). Interpretations regarding the forelimb allometry must be made with caution considering the small sample sizes from which the average subadult-adult ratios were drawn; regardless, the ratios used (HL ratio = 0.8967, RL ratio = 0.906) are comparable to what has been recorded for subadult height in extant rhinos (e.g. Hillman-Smith et al. 1986). Immature individuals usually display a shoulder height only slightly below that of conspecific adults in *Rhinoceros unicornis* (Laurie et al. 1983), *Eurhinoceros sondaicus* (Groves and Leslie 2011), and *Ceratotherium simum* (Groves 1972; Hillman-Smith et al. 1986). Specifically, in *C. simum*, individuals of only two years of age are already ~75% of average adult height (Hillman-Smith et al. 1986) (Fig. 106A), and similar rates have been reported for *E. sondaicus* (>75% of adult height when "very young"; Groves and Leslie 2011 and ref. therein) and *R. unicornis* (>80% of adult height before 15% of potential lifespan; Laurie et al. 1983). Fossil species *Pl. gracile* (Lu et al. 2023b), *Alicornops simorrense* (Cerdeño and Sánchez 2000), *Coeldonta antiquitatis* (Shpansky 2014) (Fig. 106B), and *Acerorhinus yuanmouensis* (Lu et al. 2021) differ little from their extant relatives in this regard: a juvenile *A. simorrense* humerus reported by Cerdeño and Sánchez (2000) was >77% of the

average adult length, and a humerus of a juvenile *Pl. gracile* was >70% of average adult length (Lu et al. 2023b). If >70% of average adult height is reached during juvenility as in related taxa, achieving ~90% of average adult height by subadulthood is a reasonable extrapolation. Photographs figured by Hillman-Smith et al. (1986) corroborate this notion, as the *C. simum* subadults pictured are only slightly smaller, if not entirely indistinguishable, from adjacent adults. While the sample sizes used to generate the subadult-adult forelimb ratios are lacking, the resulting ratios are still consistent with growth observations recorded for extant species.

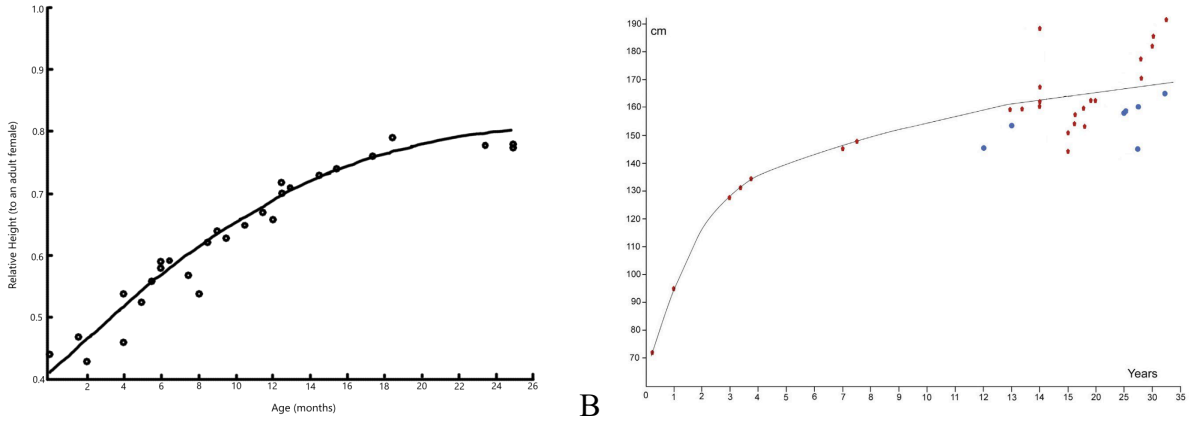

A B

Fig. 106A-B Height through ontogeny in *Ceratotherium simum* and *Coelodonta antiquitatis*. (A) Shoulder height of white rhino (*Ceratotherium simum*) calves relative to an adult female. Note the attenuated growth at ~20 months relative to the prior, more rapid growth. Modified from Hillman-Smith et al. (1986). (B) Body height growth of the woolly rhino, (*Coelodonta antiquitatis*). Note the attenuated growth at only ~7 years of age relative to the rapid growth of juvenility. Modified from Shpansky (2014). Note that the x-axis of the left figure represents months while the x-axis of the right figure represents years.

Why the forelimb lengths appear less affected by the implied growth arrest in the cranium is unclear. Isometric growth in forelimbs is an established trend in many large, graviportal mammals, such as chalicotheres (Potter et al. 2025), proboscideans, hippos, and most notably, rhinocerotids including *Teleoceras proterum*, *Menoceras arikarense* (Santos et al. 2025) and *Diceros bicornis* (Kilbourne and Makovicky 2012; Santos et al. 2025), so there is little reason to assume an ontogenetic departure from isometry in *T. aepysoma.* In other words, there is little

evidence supporting the idea that the forelimbs of *T. aepysoma* have a distinct period of becoming more robust or elongate relative to the rest of the body. Some large-bodied mammals, like elephants and muskox, may have an ontogenetic shift in longbone allometry in the earliest stages of postnatal development (Heinrich et al. 1999; Kilbourne and Makovicky 2012), but such a pattern has not yet been documented in rhinos. If growth delays did afflict ETMNH 32999 (as evidenced by the enamel hypoplasia: see section below), the causative factors may have occurred during a time when skull growth was more critical than the forelimbs. In this same vein, the forelimbs may have better recovered from a period of arrested growth than the cranial bone. If the period of physiological stress was concentrated during a stage of crucial skull development, it would stand to reason that the skull would be more stunted than the forelimbs, which grow slightly later in life. This hypothesis is discussed in greater detail in the "Stress and Growth" section below.

It is noteworthy that, while not as abnormal in length, the midshaft widths of all limb elements in ETMNH 32999 are considerably below those of adults (Tables 4-7). Decreased limb robusticity has been correlated with nutritional stress in early human populations (Cowgill 2010); the severe metabolic upset proposed to have afflicted ETMNH 32999 (see section below) may partially explain the relative gracility of its forelimb diaphyses relative to the more robust condition of conspecific adults.

An alternative hypothesis is that the forelimbs of *T. aepysoma* do not grow at the same rate as other rhinocerotids, representing a heterochronic shift previously undocumented in rhinocerotid ontogeny. Forelimb dimensions of ETMNH 32999 compare more favorably with the young adult ETMNH 609 than they do with the slightly older adult ETMNH 601 (Tables 4-7). In other words, if ETMNH 609 was excluded from the calculations for average adult values,

the forelimbs of ETMNH 32999 would deviate more strongly than they do with its inclusion. With such a small sample of post-cranial elements, an understanding of the variation in the characteristically long forelimbs of *T. aepysoma* is lacking.

Enamel Hypoplasia Discussion

Stress and Growth

The purpose of the investigation into the additional subadult specimens AMNH F:AM 109518 (Figs. 56-59) and AMNH FM 20584 (Figs. 60-62) was to evaluate whether subadult rhinocerotids with EH on dP4/M1 had proportionally smaller cranial dimensions relative to age, as seen in ETMNH 32999. The motivation behind this analysis is the proposed hypothesis that the perinatal physiological stress on ETMNH 32999, as indicated by the EH, was related to its reduced dimensions relative to age. Based on what is known about the timing of dental development in extant rhinos (e.g. Goddard 1970; Hitchins 1978; Hillman-Smith et al. 1986), dP3/dp3, dP4/dp4 and M1/m1 all develop in the perinatal stage: *in utero*, at birth, or slightly thereafter. If extinct rhinos are assumed to have a comparable schedule of dental development to their extant relatives (e.g. Mead 1999; Böhmer et al. 2015; Böhmer and Rössner 2018), it can be inferred that the EH-inducing stresses on the three subadults analyzed here also occurred in the perinatal stage, as these are the same teeth that are hypoplastic in the examined subadults.

It is known that nonspecific physiological stress early in life has the propensity to stunt physical growth and leave lasting osteological (Park 1964; Goodman et al. 1980, 1992; Mousikou et al. 2021) and dental (Cook and Buikstra 1979; Garn et al. 1979; Seow et al. 1984; Lukacs 2001; Christiono et al. 2025; Mountain et al. 2025) indicators. If such stress, regardless of etiology, is severe enough to disrupt amelogenesis, it would be reasonable to expect artifacts of stress elsewhere in the skeleton. In many mammals, the most extreme changes in cranial shape

and size occur in the first years of life, around birth and pre-weaning; large mammals are no exception (e.g. tapirs: Padilla and Dowler 1994; Padilla et al. 2010; rhinos: Groves and Kurt 1972; Groves 1972; Hillman-Smith et al. 1986; Hagge 2010; hippos: Fidalgo et al. 2025; walruses: Dierickx et al. 2025). Based on the findings of the present study (Figs. 63-88) and on what is known about rhino ontogeny (e.g. Dittrich 1972; Hagge 2010; Plair et al. 2012; Roth et al. 2013), early juvenility encompasses the most rapid growth. Therefore, any metabolic disruption(s) in such a critical period, as evidenced by EH, would certainly have the propensity to affect the development of bone as with enamel. In humans, growth stunting and wasting has been correlated with EH and other dental defects (Folayan et al. 2020; Christiono et al. 2025), so it is reasonable to hypothesize a similar association may be present in other mammals.

Examination of the other subadult rhinocerotids with EH (Table 15) returned intriguing results into the potential correlation between EH-inducing stress and reduced size/growth in extinct rhinos. Interestingly, AMNH F:AM 109518 deviates from expected size in a similar fashion to ETMNH 32999. LN of AMNH F:AM 109518 deviates anywhere from -15.26 to -20.95% from expected subadult size ($\overline{x}$ = -18.21%), which overlaps with the deviation range of ETMNH 32999 (-11.23 to -17.19%). PO of AMNH F:AM 109518 deviates more strongly than its LN ($\overline{x}$ = -26.26%), but it must be noted that the measured PO value for AMNH F:AM 109518 was estimated due to the absence of the occipital condyles, so caution must be exercised in interpreting the deviation. ZW of AMNH F:AM 109518 ($\overline{x}$ = -20.95%) deviated only slightly less from expectation than that of ETMNH 32999 ($\overline{x}$ = -25.4%). TCL was measured on AMNH F:AM 109518 but could not be compared due to the absence of an average *T. medicornutum* adult TCL value. Average adult values for LN, PO, and ZW for *T. medicornutum* were taken from Prothero (2005), though it should be noted that these values come from small samples

(n=4). This is to say that though AMNH F:AM 109518 does appear to be smaller than would be expected of a subadult *T. medicornutum*, it is likely not out of the range of variation, but rather falls on the lower end, as does ETMNH 32999 in several measurements (Table 15).

Unlike ETMNH 32999 and AMNH F:AM 109518, AMNH FM 20584 does not appear to deviate from expected subadult *C. neumayri* size (Table 15). On average, the PO of AMNH FM 20584 deviates only -5.84%, with the more conservative estimate suggesting it may only deviate less than one percent (-0.68% to -10.49%). TCL yielded a similar condition, potentially deviating up to –12.2%, though it had the potential to be even 10.38% larger than would be expected of a conspecific subadult. ZW expectations did not negatively deviate from expectation at all, but in fact, may have been 1.2% to 17.65% larger than would be expected of a subadult *C. neumayri*. A slightly younger age class VI *C. neumayri* with EH (AMNH FM 20582) was not included in the allometric calculations here as it is not yet considered a subadult; worth mentioning, however, is that all of its cranial dimensions, save for ZW, were larger than that of AMNH FM 20584, suggesting it, too, would not negatively deviate from expectation despite its EH. While its size supports the assertion that subadult rhinocerotids are generally of comparable size to conspecific adults, allometric scaling results for AMNH FM 20584 do not suggest similar deviation as in ETMNH 32999 and AMNH F:AM 109518.

Without a larger-scale analysis, it cannot be said whether the size discrepancies between the examined subadults are correlated with the stress implied by the presence of EH. Based on allometric scaling (Table 15) AMNH F:AM 109518 and ETMNH 32999 are at least somewhat smaller than would be expected, though the former does not deviate as strongly as the latter. AMNH FM 20584, conversely, is of typical size for a *C. neumayri* subadult. The observed variation is consistent with other studies correlating EH with osteological stress signals (e.g.

Gavrilovic 2023), in that a single osteological parameter is not enough to identify a correlation with EH; this is exacerbated here by the small sample of subadults with EH analyzed (n=3). Establishing such a correlation in fossil rhinos, however, was not the goal of the present study. Rather, examining AMNH F:AM 109518 and AMNH FM 20584 served only to provide preliminary comparisons with ETMNH 32999 since they are all rhinocerotids of comparable subadults age with hypoplastic defects on the same teeth. Considering the similarities observed in the negative deviations of AMNH F:AM 109518 and ETMNH 32999, and since both individuals experienced EH-inducing perinatal stress, some support is lent to the notion that both experienced some degree of growth arrest. Such a hypothesis is tentative but is at least preliminarily supported by the comparisons made here.

Though further analysis is needed, EH alone is apparently too nonspecific of a condition to consistently preclude the achievement of adult size in growing rhinos. Countless factors, including the cause, severity, and duration of stress cannot be accounted for here. Without confident knowledge of the underlying cause, the severity of the EH observed on the subadult rhinos cannot be directly linked to how, if at all, osteological growth was affected. Whether/how growth is inhibited by stress is likely to be variable, as is how such stress presents in the skeleton (Saunders and Hoppa 1993). Each individual also has a different threshold for when stress begins to manifest as EH (Goodman and Rose 1990) (Fig. 107); intense stress may cause severe aplasia in the teeth of one individual, but only shallow grooves in the teeth of another. Such variation may reflect the non-specific nature of EH-inducing stressors; a growing individual with undernutrition-induced EH may be more severely stunted than one with disease-induced EH, for example. Sex may also influence the degree to which physiological stress manifests; for example, growth in male rats and pigs are more adversely affected by undernutrition than

females (Widdowson 1976). In short, a multitude of factors can contribute to whether EH develops at all, and even more factors are at play in determining the effects of stress on growth. This variation, as it applies to rhinos with EH, is exemplified by the comparisons of AMNH F:AM 109518, ETMNH 32999, and AMNH FM 20584 (Table 15).

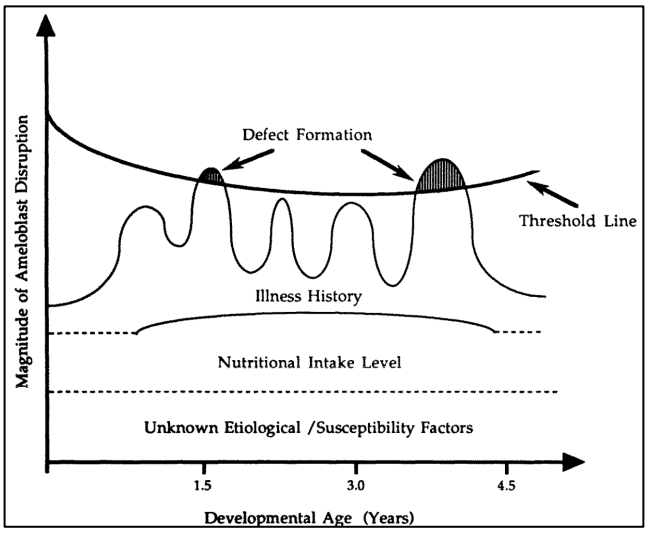

Fig. 107 Variation in the threshold of enamel hypoplasia formation. Modified from Goodman and Rose (1990).

With these caveats in mind, it is still likely that the physiological stress on ETMNH 32999 that disrupted amelogenesis is related to its neotenous/stunted skeletal condition. EH has been correlated with several physiological parameters supporting this hypothesis: reduced height and weight (Goodman et al. 1992; Folayan et al. 2020; Christiono et al. 2025), poor craniofacial bone growth (Skinner 2002; Lukacs 2009; Skinner et al. 2014), thin cortical bone (Goldstein 2018), transverse growth arrest lines in longbones (Clarke 1982), skeletal infection (Cook and Buikstra 1979; Stodder 1997), and other osteological markers of stress (Gavrilovic 2023); all adding credence to the notion that the EH-inducing stress in ETMNH 32999 is at least tangentially related to its neotenous condition, if not directly linked. Other osteological signals of stress have been used to identify periods of growth arrest in skeletal remains, such as Harris lines in longbones (e.g. Clarke 1982; Duckler and Van Valkenburgh 1998) or the presence of porous

bone on the orbital roof (i.e. cribra orbitalia) (e.g. Cook and Buikstra 1979; Mangas-Carrasco and López-Costas 2021; Gavrilovic 2023). In many cases, EH, or other similar dental abnormalities, are found to be correlated with these indicators of poor skeletal growth (e.g. Cook and Buikstra 1979; Goodman et al. 1992; Stodder 1997; Folayan et al. 2020; Salida et al. 2021; Gavrilovic 2023; Christiono et al. 2025), suggesting similar potential for correlation in ETMNH 32999. EH alone is not enough to indicate stunted skeletal growth, but its presence as an indicator of physiological stress supports the notion that the two conditions may occur in tandem and/or share a similar trigger (e.g. Goodman et al. 1992; Folayan et al. 2020; Christiono et al. 2025). Whether ETMNH 32999 is such a case likely requires more data, but at the very least, the stress implied by the EH remains the best explanation for ETMNH 32999's departure from typical rhinocerotid growth rates.

Identifying osteological pathologies in ETMNH 32999 would be helpful in linking EH-inducing stress to other signals of inhibited skeletal growth in rhinos. Unfortunately, the severe taphonomic damage on much of the skeleton precludes confident identification of such conditions. Taphonomic damage and osteopathological features can mimic each other extremely well (de Souza Barbosa et al. 2019), and a combination of both taphonomic and pathological features are present on the GFS *T. aepysoma* skeletons (Scaife 2024), as well as ETMNH 32999. Potential signs of pathology may be obscured or mimicked by taphonomic damage. Confounding such evaluation is the poor preservation of ETMNH 32999 relative to GFS adults, so no attempt is made here to identify osteological correlates of physiological stress such as cribra orbitalia, Harris lines, or abnormal porous bone. Rather, it is proposed that the neotenous skeletal condition of ETMNH 32999, relative to age, is evidence of stress-induced growth complications, possibly the same stress that disrupted amelogenesis. Regardless of etiology, developmental

stress early in life has the potential to inhibit growth as it does enamel formation; this is particularly true in the case of nutritional stressors (e.g. McCance et al. 1961; Park 1964; Lister et al. 1966; Cook and Buikstra 1979; Pucciarelli 1981; Goodman et al. 1980, 1992; Saunders and Hoppa 1993; Lee 1996; Dressino and Pucciarelli 1997; Skinner 2002; Folayan et al. 2020; Sadida et al. 2021; Gavrilovic 2023; Christiono et al. 2025). ETMNH 32999 may provide evidence of stress inducing both EH and growth complications in a fossil rhinocerotid, as has been documented in humans (e.g. Goodman et al. 1992; Folayan et al. 2020; Christiono et al. 2025).

The null hypothesis to the EH investigation of ETMNH 32999 would be that there is no correlation between the EH-inducing stress and the neotenous condition observed in the specimen. Because of the variability and non-specificity in causative factors of EH (Fig. 107), proposing such a correlation is not so simple. Rather, it is hypothesized here that the perinatal stress which induced EH in ETMNH 32999 is related to what may have contributed to a period of growth arrest. Perinatal/early-life stress can induce permanently delayed/stunted growth in many mammals (e.g. McCance et al. 1961; Saunders and Hoppa 1993; Lee 1996; Mousikou et al. 2021; Sadida et al. 2021) as well as cause EH (e.g. Sweeney et al. 1971; Cook and Buikstra 1979; Goodman and Rose 1990; Goodman et al. 1992; Goodman and Song 1999; Dobney and Ervynck 2000; Folayan et al. 2020; Christiono et al. 2025) and reduced dental widths (Garn et al. 1979). Whether these conditions can be definitively proven to share an etiology in the case of ETMNH 32999 is unlikely with the current sample and analytical techniques but is supported by the findings of the present study.

Timing of tooth development may give some indication of EH etiology (Goodman and Song 1999), since the timing of tooth development in rhinos is rather well-documented (e.g.

Goddard 1970; Hitchins 1978; Hillman-Smith et al. 1986). For example, Mead (1999) postulated that stress recorded on *Teleoceras* dp4s was indicative of birth-related stresses, and that stress recorded on the p4 could be attributed to cow-calf separation. EH on second or third molars is thought to indicate external stress induced via environmental fluctuation (Chollet and Teaford 2010; Upex and Dobney 2012; Böhmer and Rössner 2018; Hullot et al. 2021, 2023, 2024). Environmental fluctuation is considered an unlikely factor here because all the subadults investigated (Table 15) have EH on the same teeth (dP4, M1; Figs. 49-55, 58-61), so it is assumed that the EH-inducing event(s) occurred *in utero*, at birth, and/or before weaning. To this point, Mead (1999) suggested that, in temporally and spatially distinct *Teleoceras* populations, birth was consistently an EH-inducing stressor, though it cannot be assumed that the perinatal stress afflicting each individual, or the mother of each individual, was of the same origin (e.g. nutritional stress, juvenile disease, genetic predisposition). For example, Bratlund (1999) considered either malnutrition or fever-inducing disease to be plausible stressors contributing to EH in young rhinos. Nutritional stress concentrated around birth/early juvenility would be consistent with the inherent period of starvation that birth often entails (e.g. Dobney and Ervynck 2000; Langer 2008) and would coincide with the formation of the defected teeth (dP3/dp3, dP4/dp4, M1/m1). If nutritional stress was persistent or repeated throughout development, as is implied by the series of iterative defects on the teeth of ETMNH 32999, it may have slowed or stunted growth considerably as seen in other mammals (e.g. McCance et al. 1961; Park 1964; Dressino and Pucciarelli 1997; Sadida et al. 2021; Folayan et al. 2020; Christiono et al. 2025), causing ETMNH 32999 to retain a neotenous skeletal condition, at least in the cranium, until its death. Studies on undernutrition in other mammals (e.g. suids, McCance et al. 1961; primates, Dressino and Pucciarelli 1997) have shown how early-life nutritional stresses can considerably

stunt cranial lengths and widths, so it is reasonable to expect a similar correlation in ETMNH 32999 if the EH-inducing stress was of nutritional origin.

It is noteworthy that the physiological stress recorded on the teeth of ETMNH 32999 evidently ceased quite some time before death. While the dP3/dp3, dP4/dp4, and M1/m1 are the most severely affected teeth, the teeth that develop later (P3/p3, P4/p4, M2/m2, and M3/m3) do not display any obvious hypoplastic features (Figs. 20A-B, 24-25). A fair assumption would be, then, that ETMNH 32999 persevered through the adverse conditions that caused EH, and survived into a life stage where typical amelogenesis was resumed. The EH-inducing stress most likely did not cause the death of ETMNH 32999, since the teeth that were forming at the time of death are not hypoplastic. In this implied "recovery period", bone growth may have been able to resume typical operations. This may explain why the forelimb lengths do not deviate from expectation as much as the cranium; since forelimb lengths appear to grow more slowly than cranial dimensions in rhinos (see Figs. 76, 106A-B), the growth phase of the forelimbs likely extended past the period of metabolic disruption, allowing them to, at least partially, recover from a stunted condition once the period of stress had ceased. Such is consistent with the findings of Lu et al. (2023b) in assessing the growth of fossil species *Plesiaceratherium gracile*, where rapid limb growth occurred throughout the first five years of life; if the same is applicable to *T. aepysoma*, accentuated forelimb growth likely continued past the cessation of the metabolic disruption period. The most rapid growth phase for the cranium, however, appears to be earlier in life (Figs. 65-74, 77-86), likely in utero and shortly thereafter, with cranial growth becoming attenuated by subadulthood. If the developmental window of critical skull growth was entirely encompassed by the period of stress, it would explain why the skull failed to recover from the growth arrest as the forelimbs may have.

Stress and Growth in Captive Rhinos

Lacking clear data on stress in rhinos aside from studies on EH, zoological data elucidates how captivity/capture-induced stress may impact development. Captivity and its associated stresses can severely affect physiological growth (e.g. Groves 1966, 1982; Dressino and Pucciarelli 1997; Wielebnowski 2003; Hartstone-Rose et al. 2014), which often complicates comparisons between fossil and zoo specimens. In the case of ETMNH 32999, however, the abnormalities imposed by captivity actually provide a unique proxy for how nonspecific stressors manifest in the skull and dentition. Relevant to ETMNH 32999, many stress-induced growth complications have been documented in captive animals; reduced skull size attributed to poor dietary conditions (i.e. nutritional stress) has been reported in captive equids (Groves 1966) and primates (Dressino and Pucciarelli 1997). Of the greatest relevance, however, are the documented effects of captivity on rhinos, in both delayed dental eruption (Bigalke et al. 1950; Schuarte 1966), stunted osteological growth (Groves 1982), and enamel hypoplasia (data from M. Hullot, personal communication 2025).

Groves (1982) described the effects of captivity on the skulls of extant Asian rhinoceroses (*Rhinoceros unicornis*, *Eurhinoceros sondaicus*, and *Dicerorhinus sumatrensis*) and found that the cranial dimensions of captive individuals were frequently lesser than those of their wild counterparts. Two cases of great relevance to ETMNH 32999 are “Bettina”, a captive *D. sumatrensis* adult female (Fig. 108A), and “Mohan”, a wild-caught *R. unicornis* adult male, both described briefly by Reynolds (1961), then more thoroughly by Groves (1982). Even considering the trend of decreased size captive individuals, Bettina stood out for her small size relative to conspecifics, attributed to Bettina being “very sickly from the beginning”, eventually leading to her anemia-induced death (Groves and Kurt 1972; Groves 1982); though it is unclear whether

Bettina originated from captive (Groves 1982) or wild (Reynolds 1961) conditions. Occipitonasal length and basal length were among the most affected measurements in Bettina's skull (NMB 10259) (Fig. 108A) (Groves 1982), as in ETMNH 32999. In life, Bettina stood out for her emaciated condition, reduced height, and low weight (Groves and Kurt 1972). Bettina was also described as having a light, poorly ossified skull lacking the pronounced nuchal crest typical of *D. sumatrensis* adults (Groves 1982; see Fig. 105D); neotenous conditions consistent with what is observed in ETMNH 32999 relative to conspecific adults (Fig. 105E). The cranial bones of ETMNH 32999 remain largely unfused and appear thinner than those of adults, and the nuchal crest does not flare dorsally or laterally as strongly (Figs. 12-16, 64). While some of these conditions can be at least partially explained by ontogeny in ETMNH 32999, they differ from the near-adult condition seen in the skulls of other subadult rhinocerotids (e.g. Deng 2001; Hagge 2010; Lu et al. 2023b; see Fig. 105) but rather resemble what Groves (1982) described of the stunted Bettina.

Mohan presented a similar case, but unlike Bettina, was apparently already stunted at capture, described as "half-grown", suggesting that captivity alone was not the only factor contributing to his stunted growth. Mohan remained "half-grown" throughout his life despite being provided relatively luxurious captive conditions (Groves 1982); it may be that Mohan, too, experienced severe stress during critical developmental windows which contributed to permanently stunted growth, precluding his ability to recover and reach typical size. As with Bettina, the most stunted dimensions of Mohan's skull (BM 1961.5.10.1) included occipitonasal and basal lengths. Reduced cranial length is apparently a relatively common symptom of stress in rhinos; an unnamed captive *E. sondaicus* is also documented as having a small, stunted skull attributable to 'adverse conditions' (Groves and Leslie 2011). Among the similarities between

ETMNH 32999 and the captive specimens, one obvious difference was that of zygomatic width. Zygomatic width is very reduced in ETMNH 32999 (Tables 10-11, Figs. 85-86), but abnormally exaggerated in the captive specimens, which Groves (1982) attributed to a lifetime of feeding from a trough on the floor.

Regarding EH specifically, captive rhino specimens from zoos or circuses frequently have hypoplastic enamel defects (data from M. Hullot, personal communication 2025), presumably due to poor husbandry conditions; the same is documented in captive giraffes (Franz-Odendaal 2004). All of this is to say that, regardless of etiology, stress during development can induce EH, influence dental development, and contribute to poor bone growth. To this point, another captive *D. sumatrensis* skull described by Groves (1982), "Jenny" (NMW 3082), does have EH on the second molars (data from M. Hullot, personal communication 2025) (Fig. 108B); her skull was of typical proportions for a *D. sumatrensis* subadult, as the stress would have occurred during M2 formation, when the skull would have already been well-developed. Reynolds (1961) reported that Jenny died of tuberculosis, a potential etiology for her EH. Bettina's skull (Fig. 108A), on the other hand, had no evident hypoplastic defects, despite her anemic condition and stunted growth. Stress induced via captivity then, regardless of origin (i.e. nonspecific), can evidently induce both stunted growth and EH in rhinos.

Fig. 108A-B Captive *Dicerorhinus sumatrensis* specimens. (A) Palatal view of NMB 10259, "Bettina", a captive *Dicerorhinus sumatrensis* adult female with an abnormally small skull who died of anemia; Scale bar = 10cm. (B) Linear enamel hypoplasia on the left m2 of NMW 3082, "Jenny", a captive *D. sumatrensis* subadult female who died of tuberculosis. Not to scale. Photographs courtesy of Dr. M. Hullot.

Bigalke et al. (1950) and Schuarte (1966) briefly referenced the effects of captivity on the dental eruption sequence in rhinos. In both cases, tooth eruption was delayed; Schuarte (1966) describes a 14-year-old *Diceros bicornis* whose M3 was not yet in occlusion, and Bigalke et al. (1950) describe the deciduous tooth eruption of a *Ceratotherium simum* calf, which is Hillman-Smith et al. (1986) later describe as delayed by ~30 days when compared with the calf reported by Dittrich (1972). Interestingly, Bigalke et al. (1950) references the unusually small size of the *C. simum* calf's anteriormost mandibular premolar, dp1. Both conditions, delayed eruption and reduced anterior dentition, are of relevance to ETMNH 32999, considering its anomalously small p3s (Figs. 24, 110), and to its eruption sequence which differs from congeners. Unlike the captive rhinos described by Groves (1982) whose sicknesses were mostly documented, it is unclear whether the rhinos with delayed eruption were under similar stresses that may have influenced their dental development, though it could be argued that captivity itself represents stressful stimuli of nonspecific origin.

Broader Environmental Implications

For *Teleoceras* ecology. Studies on EH in fossils usually deal with a large number of isolated teeth to make inferences about population-level or species-level stress of environmental origin (e.g. Mead 1999; Franz-Odendaal et al. 2003; Niven et al. 2004; Chollet and Teaford 2010; Upex and Dobney 2012; Roohi et al. 2015; Skinner and Skinner 2017; Hullot et al. 2021, 2022, 2023, 2024), meaning that individual cases of EH occurring on an intact or articulated fossil individual are rare. The relative rarity of intact individuals with EH highlights the significance of ETMNH 32999, enabling exploration into how EH-inducing stress may manifest outside of the dentition.

It is interesting that both the specimens investigated in the present study, as well as the *Teleoceras* analyzed by Mead (1999), regularly displayed EH on the dP4/dp4. Development of these teeth *in utero* provides a relatively stable condition, and because the deciduous teeth are present for a shorter time, EH on deciduous teeth is relatively rare in other rhinocerotid populations (Böhmer and Rössner 2018; Hullot et al. 2021). The prevalence of natal stresses recorded on *Teleoceras* teeth (Mead 1999) may suggest that birth is indeed a more common stressor in *Teleoceras* than in other North American rhinocerotids; though sampling bias may influence this interpretation, as *Teleoceras* is among the best studied North American rhinocerotids (Prothero 2005).

Increased EH frequency observed among samples of Eurasian teleoceratins have been attributed to the group's proposed reliance on water relative to other species (Hullot et al. 2021, 2024). If the 'hippo ecomorph' hypotheses, or at least an aquaphilic lifestyle for *Teleoceras* (e.g. Cope 1879; Osborn 1898; Wall and Heinbaugh 1998; Ward et al. 2024) is assumed correct, an increased reliance on water may have induced stress (i.e. EH susceptibility) in the group more

frequently than in their fully terrestrial relatives, via environmental fluctuation in water availability. It is worth noting, however, that a semi-aquatic, hippo-like lifestyle for *Teleoceras* is not presently supported (e.g. MacFadden 1998; Mihlbachler 2001, 2005; Mihlbachler et al. 2004; Clementz et al. 2008; Mallet et al. 2022). While a reliance on water could account for increased rates of EH, defects would more frequently be found in the permanent, rather than deciduous, dentition, since defects in these teeth are thought to better reflect larger-scale environmental stressors (e.g. Upex and Dobney 2012; Böhmer and Rössner 2018; Hullot et al. 2021, 2023, 2024). A future assessment of EH in *Teleoceras* through time and space may provide insight into the semi-aquatic affinities (or lack thereof) within the group, differing from previous demographic (e.g. Mead 2000; Mihlbachler 2005), morphological (e.g. Wall and Heinbaugh 1999; Mihlbachler et al. 2004; Mallet et al. 2022), or isotopic (e.g. MacFadden 1998; Clementz et al. 2008; Ward et al. 2024) approaches to the *Teleoceras* "hippo hypothesis"; such an analysis, however, is beyond the scope of the present study.

For the GFS paleoenvironment. ETMNH 32999 also represents the first reported case of EH from the GFS, despite the GFS rhino sample to date representing a rather pathological population (see Scaife 2024). Because ETMNH 32999 represents an isolated case of EH from the GFS, and because the affected teeth do not indicate stress via environmental fluctuation (i.e. second or third molars), it is likely that ETMNH 32999 represents stress on only an individual scale, rather than an environmental one applicable to other GFS mammals. The most abundant mammalian component of the GFS is that of the extinct dwarf tapir, *Tapirus polkensis* (Hulbert et al. 2009). Cursory observations of >100 GFS *T. polkensis* specimens found no obvious EH, but the size of the sample warrants a more rigorous look. At least tentatively, there appear to be no large-scale environmental stressors, like seasonal fluctuation, recorded as EH on the

mammals of the GFS. Aseasonality and/or a lack of environmental fluctuation for the GFS is consistent with the findings of isotopic analyses on GFS mammal teeth (DeSantis and Wallace 2008). This interpretation is consistent with the hypothesized timing of the EH-inducing stress on ETMNH 32999 occurring *in utero* or shortly thereafter, rather than being attributable to external environmental factors.

It is worth noting that occupation of environments with limited resources and reduced predation/competition pressures has been correlated with delayed skeletal maturity and slower growth in other ungulates, such as cervids (Snoodijk et al. 2025). If *Teleoceras aepysoma* is a more slowly growing species than other rhinocerotids, it could be due in part to the GFS paleoenvironment. However, to date, there is no reason to assume that resource availability or environmental fluctuation contributed to slow or reduced growth in GFS mammals. Some evidence suggests that the GFS *Alligator* sp. endured periods of slowed or arrested growth (Keenan and Engel 2017; Gunnin et al. 2025b), but the same is likely not applicable to resident GFS mammals which would not have been as impacted by seasonality. The high representation of dwarf tapirs (*Tapirus polkensis*) at the GFS (Hulbert et al. 2009) could suggest that individuals of smaller size thrived under conditions in which resources were not as readily available, so slower growth or smaller size may have been favorable but would require a more rigorous study to properly assess. Scaife (2024) proposed that the GFS represented a "suboptimal" habitat for *Teleoceras*, lending tentative support to the notion that the conditions of the GFS paleoenvironment could have contributed to relatively slow growth in *T. aepysoma*, as is seen in insular cervid populations (Snoodijk et al. 2025). Lacking a larger sample or additional evidence of suboptimal environmental conditions, these postulations are not supported by the present study. The GFS is interpreted to have been abundant in browse and water (DeSantis and Wallace

2008), and most GFS mammal fossils lack evidence of predation pressures (Haugrud 2023), providing little indication of a suboptimal *Teleoceras* habitat. If future analyses of the GFS fauna find evidence of delayed/slowed growth in other mammals, more support can be added to the notion of a slower-growing *Teleoceras* species. Until then, there is sufficient evidence to consider ETMNH 32999 an aberrant individual rather than a representative of environmentally influenced growth trends, or a representative of a species-specific departure from growth trends that appear consistent across the rhinocerotids sampled here, if not superfamily Rhinocerotoidea (see Lu and Deng 2025) as a whole.

Anterior Premolar Reduction

In addition to defective enamel, ETMNH 32999 displays other dental abnormalities including hypodontia (missing teeth) and microdontia (small teeth). ETMNH 32999 lacks both right and left P2, though it retains dP2 on each side. With most of the maxillary bone missing, the state of the unerupted premolars in the maxillary crypt is visible. On the left side, both P3 and P4 are displacing their deciduous counterparts, with P3 closer to full replacement than P4 (Fig. 109). On the right side, only P3 is preserved in the maxillary crypt, and it is in the same state of eruption as its left counterpart. The space within the crypt which would typically be occupied by P2 is mostly occupied by P3, which has shifted forward to lie superior to both dP2 and anterior dP3 on both sides. Upon full eruption, it appears that P3 would displace both dP2 and dP3 (Fig. 109). On the left side, P4 is superior to posterior dP3 and anterior dP4. Upon P4 eruption, a considerable gap between posterior P4 and anterior M1 would be apparent until the molars shift anteriorly upon full eruption of M3.

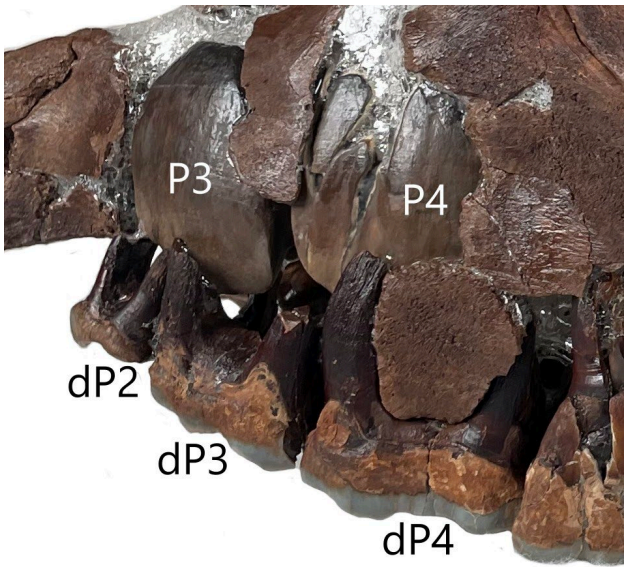

Fig. 109 State of premolar eruption in ETMNH 32999. Note the position of P3 superior to both dP2 and dP3. Note the absence of P2 and the lack of space for its presence. The P3 and P4 in this image are reconstructions, as the actual teeth were removed from the cranium during preparation. Not to scale.

Loss of the anteriormost upper premolars has been described before in rhinocerotids, but has been attributed to an ontogeny-based pathology caused by excessive tooth wear in the oldest individuals of *Diceros bicornis* (Goddard 1970), *Teleoceras* (Gerhold 1992) and *Stephanorhinus* (Diedrich 2023); this is not the case for subadult ETMNH 32999, in which the upper second premolar germ seems to have never developed. Prothero (2005) states that loss of P2/p2 is common in *Teleoceras*, though personal observations of museum collections failed to find a specimen with a complete tooth row that lacked P2; this character is considered questionable. The loss of p2 is certainly common in *Teleoceras*, but this same variability cannot be confidently applied to P2. For *T. aepysoma* specifically, P2 is present among all known skulls, save for ETMNH 32999. As discussed earlier, there appears to be more variation in the presence of dP1/P1 than in P2, at least in *T. brachyrhinum* (personal observations; Fig. 102) and *T. major* (Hagge 2010).

In ETMNH 32999, both p3s were found unerupted in the mandible inferior to corresponding dp3s, though they were later removed during preparation. Both p3 of ETMNH 32999 are conspicuously small when compared to their deciduous counterparts and conspecific adults (Table 3; Fig. 110), and are an extreme outlier for p3 area among a multispecific sample of *Teleoceras* (n=44; all species included save for the dwarf *T. guymonense*) (Fig. 93). Z-scores for p3 area in *Teleoceras* were over three standard deviations from the mean for ETMNH 32999 (Z = -3.56), deviating strongly from normality even when including the values of the dwarf *T. meridianum.*

Fig. 110 Comparison between left p3s of ETMNH 32999 and ETMNH 21659. Both are *Teleoceras aepysoma*. In lingual view. Scale bar = 3cm.

The potential correlation between the anterior premolar reduction and the anteroposteriorly stunted skull is intriguing; the mandible, less stunted in length than the skull (Table 10-11), was able to develop its anteriormost premolar, albeit in a significantly reduced state (Fig. 110). The cranium, with its exaggerated brachycephaly relative to the mandible, did not develop its anteriormost premolar at all. If a correlation is present, it would be that the development of the anterior premolars was linked to the developmental stress proposed to have stunted cranial growth; such growth arrest may have influenced how much space was available in the dental crypts for proper tooth development. The reduction in cranial length may have

caused insufficient room for P2, while more room may have been available in the mandibular dental crypt as the mandibular length was not as severely stunted, so the p3 was able to develop in a reduced state. Supporting this notion is the more typical length of dp3 relative to p3, which apparently developed normally *in utero* in an otherwise uncrowded dentary. P2 and p3 develop before/around weaning in extant African rhinoceroses (Hitchins 1978; Hillman-Smith et al. 1986), around the same time, or slightly after, the EH-inducing stress would have been occurring. Thus, it may be that the poor skull growth in this life stage is related to the anterior premolar reduction.

Reduction of the anterior premolars both reinforces and challenges the previously made hypotheses that the shortened cranium of ETMNH 32999 is attributable to a period of growth arrest. On one hand, in support of the growth arrest hypothesis, the delayed/reduced anteroposterior growth of the cranium may have inhibited anterior premolar development via insufficient room for tooth development within the dental crypt. As the reduced teeth would have been forming around the same time that the EH-inducing stress would have occurred, the metabolic demands required to develop these tooth germs may have been ignored in favor of more critical operations. On the other hand, the inverse may be applicable, where the cranium did not grow to a normal length due to the absence of the anterior teeth. Humans with missing/reduced teeth will often have an abnormally shortened, retrognathic maxilla, though the mandible is not usually affected to this extent (Fekonja and Čretnik 2022; Khalaf and El-Kishawi 2022). Other conditions associated with hypodontia in humans include microdontia of remaining teeth and delayed exfoliation of deciduous teeth; each of these conditions resembles what is seen in ETMNH 32999. If such is the case, it may explain why cranial dimensions depart more from expectation than post-cranial and mandibular dimensions. Challenging this notion is that cranial

lengths are not the only reduced measurements in ETMNH 32999, as zygomatic and supraorbital widths also deviate considerably from expectation (Table 11), which cannot be as easily explained by reduced/absent anterior teeth; the teeth of ETMNH 32999, however, are also atypically reduced in mediolateral width (Table 3; Figs. 91-92), suggesting an additional correlation. Regardless of which hypothesis is more likely, a link between the reduced dentition and the relatively small cranium can be tentatively established, though arguments could be made in either direction for which condition may have contributed to the other.

Reduction/loss of anterior premolars in *Teleoceras* has been attributed to an evolutionary trend in anterior premolar reduction (Prothero 2005). If the anterior teeth were congenitally absent, ETMNH 32999 could represent a variable individual indicative of this trend towards dental simplification. While dental measurements have historically been used to distinguish *Teleoceras* species (e.g. Prothero 2005), it is highly unlikely that the abnormal anterior premolars of ETMNH 32999 are of any valuable taxonomic or evolutionary significance. In artiodactyls, taxonomic splitting based on premolar size variation has largely contributed to over-splitting and consequently, a lack of consensus among researchers (e.g. Emery-Wetherell and Davis 2018). In other words, it would be unwise to assign taxonomic or evolutionary significance to the reduced premolars of ETMNH 32999, especially when coupled with the other abnormalities of ETMNH 32999. Rather, the reduced premolars support the hypotheses of early-life developmental complications associated with tooth formation, and complement the brachycephalic, narrow skull in this regard.

Reduced Dental Widths

In addition to the reduced p3s of ETMNH 32999, the dental widths of all permanent maxillary and mandibular teeth lie beneath those of GFS adults (Table 3; Fig. 91). As is

hypothesized for the p3 reduction, these smaller dimensions may be related to the proposed cranial growth arrest. Adverse perinatal conditions during dental development have been linked with multiple different alterations to odontogenesis (e.g. Shaw and Griffiths 1963; Seow et al. 1984; Mountain et al. 2025), notably including reduced tooth crown sizes (Garn et al. 1979; Buhamer et al. 2021), so it is reasonable to expect a similar association in ETMNH 32999. It is likely that the reduction in dental widths reflects the same perinatal growth disruption that is expressed by the EH and reduced cranial dimensions. The reduced skull widths do not necessarily suggest that there was insufficient space in the dental crypts which induced narrower teeth. Rather, the timing of tooth development and skull development *in utero* coincided with the period of severe systemic stress recorded on the teeth as EH, altering the typical development of the tooth germs. This hypothesis is corroborated by the fact that earlier developing teeth (P3, M1) are more mediolaterally reduced than later developing teeth (P4, M2, M3) (Fig. 92), as P3 and M1 would have been forming during the same period of EH-inducing stress. The recovery period implied by the absence of EH on P4, M2, and M3 may have allowed these later-developing teeth to develop more typically than the earlier teeth which formed under intense stress. Similar reasoning is applied to the forelimb lengths, which are not as proportionally reduced as the cranial dimensions, likely because the limbs continued to develop into the recovery period, allowing them to achieve more typical lengths.

Buhamer et al. (2021) mention a potential correlation between overall head/body growth and crown size determination in humans, which may be relevant to ETMNH 32999. If cellular activity was decreased due to stress while the skull and teeth were forming, both dental and cranial dimensions "missed out" on critical developmental windows; in the case of the cranial dimensions, this precluded their ability to reach full size even during the rehabilitation, or "catch-

up" period. As a result, permanent stunting of both cranial and dental widths may have been disrupted by a shared metabolic insult, likely the same systemic stress(es) that induced the EH. The forelimb lengths and the later developing teeth (P4, M2, M3), however, appear less affected by the hypothesized growth arrest, likely because the formation/growth of these elements took place after the period of severe metabolic disruption.

CHAPTER 5. CONCLUSIONS

- ETMNH 32999 represents the first immature skeleton of *Teleoceras aepysoma* and is a subadult in an age class equivalent to 7 ± 1 years of age in extant African rhinoceroses (see Hitchins 1978), or ~17-20% of potential lifespan. Despite the retention of the deciduous premolars, the state of wear on the first and second molars implies an individual closer to maturity than juvenility, based on what is known about life history in extant rhinos. In extant rhinos of comparable age, sexual and/or skeletal maturity is usually imminent (e.g. *Dicerorhinus sumatrensis* Groves and Kurt, 1972; Roth et al. 2013; *Diceros bicornis*, Hillman-Smith and Groves 1994; *Rhinoceros unicornis*, Laurie et al. 1983; *Ceratotherium simum*, Groves 1972; Hillman-Smith et al. 1986; *Eurhinoceros sondaicus*, Groves and Leslie 2011).
- Sex determination is based on the tusks, which are delayed in their eruption and at their widest preserved extent, are wider than those of congeneric females. Both conditions are consistent with male *Teleoceras* (see Mihlbachler 2005). In ETMNH 32999, the enamel crowns of the tusks are not fully formed, though at their widest extent (30mm proximal to the tip), the mediolateral width (WT) is well within the range of the same measurement on congeneric males (Fig. 94). Though the modified tusk measurement used here, WT, is not as bimodal as those typically taken for more complete tusks, such as root diameter, crown length, or crown base width (e.g. Mead 2000; Mihlbachler 2003; Chen et al. 2010; Lu et al. 2020), it still supports the assignment of ETMNH 32999, and all other *T. aepysoma* tusks to date, as male.
- Other extinct and extant rhinocerotids of the same subadult age as ETMNH 32999, or even younger, are typically ~90% of asymptotic, or average adult size in most cranial

dimensions (Table 8) (e.g. Groves 1972; Groves and Kurt 1972; Laurie et al. 1983; Hillman-Smith et al. 1986; Hillman-Smith and Groves 1994; Deng 2001; Deng and Qiu 2007; Groves and Leslie 2011; Lu 2013; Lu et al. 2023b), an assumption corroborated by the present study. The forelimbs appear to follow a comparable trend (Figs. 75-76, 106), but greater sampling is required. The relatively reduced cranial measurements of ETMNH 32999 (Fig. 63; Tables 10-11) suggest a departure from typical rhinocerotid growth rates. In all other species examined and in those documented in literature, individuals of similar age as ETMNH 32999 are of comparable size and shape to their respective conspecific adults, while ETMNH 32999 retains a neotenous condition.

- Enamel hypoplasia (EH) identified on the dP2, dP3/dp3, dP4/dp4, and M1/m1 of ETMNH 32999 (Figs. 49-55) indicates severe physiological stress during tooth formation. Because the affected teeth develop *in utero*, at birth, and before weaning in extant rhinocerotids (Goddard 1970; Hitchins 1978; Hillman-Smith et al. 1986; Mead 1999; Böhmer and Rössner 2018), it can be inferred that ETMNH 32999 endured stressful conditions in the perinatal stage, possibly due to stress on the mother. Stress concentrated in a period of crucial bone development likely affected the osteological growth of ETMNH 32999 as it did amelogenesis. As a result of this growth delay/arrest, the skull retained a neotenous condition in both shape and size, with thin, poorly ossified cranial bone. Other conditions in ETMNH 32999 potentially attributable to the proposed period of metabolic upset include reduced forelimb midshaft widths, delayed exfoliation of deciduous teeth, reduced dental widths, and the reduction/absence of the anterior premolars.

- Growth arrest of this nature is consistent with the effects of perinatal nutritional stress in other mammals, but a precise etiology for the stress on ETMNH 32999 can only be speculated on. It is noteworthy that the condition of ETMNH 32999, in terms of EH, delayed deciduous tooth replacement, and stunted size, resembles what has been described in captive rhinos (e.g. Groves 1982) that experienced disease, nutritional stressors, or other nonspecific adverse conditions. Such correlation suggests that a multitude of stressful factors can induce EH and/or growth arrest in rhinos.
- The exaggerated brachycephaly of ETMNH 32999 may be related in some way to the reduction of the anterior premolars, where P2 is absent and p3 is significantly reduced. Arrested growth afflicting the cranium may have led to insufficient room in the dental crypts for proper tooth development. Alternatively, congenitally absent premolars may have led to increased brachycephaly via shortening of the maxilla, as is often seen in humans with hypodontia and microdontia. Additionally, ETMNH 32999 returns dental width measurements well below those of conspecific adults, suggesting further complications during dental development, likely linked with the period of severe stress indicated by the presence of EH.
- The forelimbs of ETMNH 32999 were apparently less affected by the hypothesized growth arrest than the cranium. Because the period of stress is proposed to have occurred around birth based on the timing of tooth formation, it may be that the disruption of cranial development permanently stunted the skull, which grows rapidly after birth. The forelimbs, however, likely developed later in life, after the period of severe stress, meaning that they were able to grow to a more typical size in terms of length. In other rhinos, the period of forelimb length growth may extend later into ontogeny than cranial

growth. Corroborating this hypothesis is the absence of hypoplastic defects on the second and third molars, implying a period of recovery after the period of disruption. The midshaft widths of the forelimbs, however, are rather narrow relative to those of adults (Tables 4-7); a condition which can be partially explained by ontogeny but has also been correlated with metabolic upset during growth.

- Other subadult rhinocerotids with enamel hypoplasia on the dP4s and M1s were preliminarily examined to determine if they displayed the same departure from typical rhinocerotid growth rates as ETMNH 32999. In one case, a subadult *Teleoceras medicornutum* (AMNH F:AM 109518) with hypoplastic dentition (Figs. 58-59) was implied to be smaller than expected for an individual of its age (Table 15), suggesting that the amelogenesis-disrupting stress may have been related to some form of growth arrest, as is proposed for ETMNH 32999. Conversely, a subadult *Ceratotherium neumayri* with hypoplastic enamel defects (AMNH FM 20584) (Figs. 60-61), was of typical size for an individual of its age (Table 15), suggesting that the amelogenesis-disrupting stress did not arrest growth considerably in this individual.
- ETMNH 32999 provides valuable information into ontogeny in extinct rhinocerotids. Comparative analyses suggest that achievement of asymptotic or near-asymptotic size in subadulthood is typical of several, if not all, rhinocerotids. Additionally, the occurrence of EH on an individual with an intact skull and associated post-crania provides rare insights into how severe physiological stress manifests in the skeleton and dentition, and how interruptions in development may induce a departure from typical skeletal growth trajectories.

REFERENCES

Alvarez JO. 1995. Nutrition, tooth development, and dental caries. The American Journal of Clinical Nutrition. 61(2):410S-416S

Anderson JF, Hall-Martin A, Russell DA. 1985. Long-bone circumference and weight in mammals, birds and dinosaurs. Journal of the Zoological Society of London. 207(A):53–61

Antoine P-O, Downing KF, Crochet JY, Duranthon F, Flynn LJ, Marivaux L, Metais G, Rajapar AR, Roohi G. 2010. A revision of *Aceratherium blanfordi* Iydekker, 1884 (Mammalia: Rhinocerotidae) from the early Miocene of Pakistan: postcranials as a key. Zoological Journal of the Linnean Society. 160:139–194. doi: 10.1111/j.1096-3642.2009.00597.x

Antoine P-O, Orliac MJ, Atici G, Ulusoy I, Sen E, Cubukcu HE, Albayrak E, Oyal N, Aydar E, Sen S. 2012. A Rhinocerotid Skull Cooked-to-Death in a 9.2 Ma-Old Ignimbrite Flow of Turkey. PLoS ONE. 7(11). doi:10.1371/journal.pone.0049997.

Bacon A-M, Westaway K, Antoine P-O, Duringer P, Blin A, Demeter F, Ponche J-L, Zhao J-X, Barnes LM, Sayavonkhamdy T, Thi Kim Thuy N, Long VT, Patole-Edoumba E, Shackelford L. 2015. Late Pleistocene mammalian assemblages of Southeast Asia: New dating, mortality profiles and evolution of the predator–prey relationships in an environmental context. Palaeogeography, Palaeoclimatology, Paleoecology. 422:101–127. http://dx.doi.org/10.1016/j.palaeo.2015.01.011

Barrón-Ortiz CI, Jass CN, Barrón-Corvera R, Austen J, Theodor JM. 2019. Enamel hypoplasia and dental wear of North American late Pleistocene horses and bison. Paleobiology. 45(3):484–516. doi:10.2307/48574449

Böhmer C, Rössner GE. 2018. Dental paleopathology in fossil rhinoceroses: etiology and implications. Journal of Zoology. 304:3–12. doi:10.1111/jzo.12518

Böhmer C, Heissig K, Rössner GE. 2015. Dental Eruption Series and Replacement Pattern in Miocene *Prosantorhinus* (Rhinocerotidae) as Revealed by Macroscopy and X-ray: Implications for Ontogeny and Mortality Profile. Journal of Mammalian Evolution. https://doi.org/10.1007/s10914-015-9313-x

Borrani A, Mackiewicz P, Kovalchuk O, Barkaszi Z, Capalbo C, Dubikovska, Ratajczak-Shrzatek U, Sinitsa M, Stefaniak K, Mazza PPA. 2025. The evolutionary history of Rhinocerotidae: phylogenetic insights, climate influences and conservation implications. Cladistics. 0:1–17. doi: 10.1111/cla.70015

Bourque JR, Schubert BW. 2015. Fossil musk turtles (Kinosternidae, *Sternotherus*) from the late Miocene-early Pliocene (Hemphillian) of Tennessee and Florida. Journal of Vertebrate Paleontology. 35(1). doi:10.1080/02724634.2014.885441.

Bratlund B. 1999. Taubach Revisited. Jahrbuch des Römisch-Germanischen Zentralmuseums Mainz. 46(1):61–174. https://doi.org/10.11588/jrgzm.1999.1.25776

Braunn PB, Ribeiro AM, Ferigolo J. 2014. Microstructural defects and enamel hypoplasia in teeth of *Toxodon* Owen, 1837 from the Pleistocene of Southern Brazil. Lethaia. 47(3):297–436. doi:10.1111/let.12063

Buhamer SN, Kaklamanos E, Kowash M, Hussein I, Salami A, Al-Habibi M. 2021. What is the effect of preterm birth on permanent tooth crown dimensions? A systematic review and meta-analysis. PLoS ONE. 16(11). doi:https://doi. org/10.1371/journal.pone.0259293.

Grau-Camats M, Casanovas-Vilar I, Crowe CJ, Samuels JX. 2025. Gliding between continents: a review of the North American record of the giant flying squirrel *Miopetaurista* (Rodentia,

Sciuridae) with the description of new material from the Gray Fossil Site (Tennessee). Journal of Mammalian Evolution. 32(1). doi:10.1007/s10914-025-09751-w.

Carbot-Chanona G, Guzman Gutierrez JR, Juarez-Woo J. 2009. Contribution to knowledge of fossil rhinoceroses of the Tecolotlan Basin in the state of Jalisco, Mexico. Boletin de la Sociedad Geologica Mexicana. 61(2):277–286

Carranza-Castaneda O. 1989. Rhinoceros of the fauna of Rancho El Ocote, Late Miocene (Late Hemphillian) of the State of Guanajuato. Geologia. 8(1):88–99

Cerdeño E, Sánchez B. 2000. Intraspecific variation and evolutionary trends of *Alicornops simorrense* (Rhinocerotidae) in Spain. Zoologica Scripta.:275–366. doi:https://doi.org/10.1046/j.1463-6409.2000.00047.x.

Chandan SN, Rao S. 2023. Dietary interventions and nutritional impact on oral health and development: a review. Journal of Food Science and Technology. 60(6):1666–1673. https://doi.org/10.1007/s13197-022-05423-2

Chen S, Deng T, Hou S, Shi Q, Pang L. 2010. Sexual dimorphism in perissodactyl rhinocerotid *Chilotherium wimani* from the late Miocene of the Linxia Basin (Gansu, China). Acta Paleontologica Polonica. 55(4):587–597. doi:10.4202/app.2009.0001.

Chollet MB, Teaford MF. 2010. Ecological Stress and Linear Enamel Hypoplasia in *Cebus*. American Journal of Physical Anthropology. 142(1):1–6. doi:10.1002/ajpa.21182

Christiono S, Pambayn AL, 'Abida AS, Rafika D, Muslimah I, Anwar R. 2025. Analysis of the effect of malnutrition on enamel structure, tooth development, and the risk of malocclusion. Malque Health. doi:1:e2025008.

Clarke SK. 1982. The Association of Early Childhood Enamel Hypoplasias and Radiopaque Transverse Lines in a Culturally Diverse Prehistoric Skeletal Sample. Human Biology. 54(1):77–84. https://www.jstor.org/stable/41463355

Clementz MT, Holroyd PA, Koch PL. 2008. Identifying Aquatic Habits Of Herbivorous Mammals Through Stable Isotope Analysis. PALAIOS. 23(9):574–585. doi:https://doi.org/10.2110/palo.2007.p07-054r.

Commission on Oral Health, Research and Epidemiology. 1982. An epidemiological index of developmental defects of dental enamel (DDE Index). 42:411–426

Cook HJ. 1927. A New Rhinoceros of the Genus *Teleoceras* from Colorado. Proceedings of the Colorado Museum of Natural History. 7:1–5

Cook DC, Buikstra JE. 1979. Health and differential survival in prehistoric populations: prenatal dental defects. American Journal of Physical Anthropology. 51(4):649–664. doi:10.1002/ajpa.1330510415.

Cope ED. 1879. On the Extinct American Rhinoceroses and Their Allies. The American Naturalist. 13(12):771a–771j.

Cowgill LW. 2010. The Ontogeny of Holocene and Late Pleistocene Human Postcranial Strength. American Journal of Physical Anthropology. 141:16–37. doi:10.1002/ajpa.21107

Creighton GK. 1980. Static allometry of mammalian teeth and the correlation of tooth size and body size in contemporary mammals. Journal of the Zoological Society of London. 19

De Marinis AM, Chirichella R, Bottero E, Apollonio M. 2018. Ecological factors affecting eruption timing of mandibular teeth in roe deer. European Journal of Wildlife Research. 64(50) https://link.springer.com/article/10.1007/s10344-018-1211-0

de Souza Barbosa FH, Medeiros da Silva LH, de Araújo-Júnior HI. 2019. Differentiating taphonomic and paleopathological features in Vertebrate Paleontology: a study case with Quaternary mammals. PalZ. 94(3):595–601. https://doi.org/10.1007/s12542-019-00495-6

Deng T. 2001. Cranial Ontogenesis of *Chilotherium wimani* (Perissodactyla, Rhinocerotidae). In: Proceedings of the Eighth Annual Meeting of the Chinese Society of Vertebrate Paleontology.

Deng T, Qiu Z-X. 2007. First Discovery of *Diceros* (Perissodactyla, Rhinocerotidae) in China. Vertebrata Palasiatica. 45(4):287–306.

Deng T, Lu X, Sun D, Li S. 2023. Rhinocerotid fossils of the Linxia Basin in northwestern China as late Cenozoic biostratigraphic markers. Palaeogeography, Palaeoclimatology, Palaeoecology. 614. doi:https://doi.org/10.1016/j.palaeo.2023.111427.

DeSantis LRG, Wallace SC. 2008. Neogene forests from the Appalachians of Tennessee, USA: Geochemical evidence from fossil mammal teeth. Palaeogeography, Palaeoclimatology, Palaeoecology. 266:59–68. doi:10.1016/j.palaeo.2008.03.032

Diedrich CG. 2023. Extinct Eurasian rhinoceros *Coelodonta* and *Stephanorhinus* dental pathologies and tooth change modus. Quaternary Science Reviews. 301. https://doi.org/10.1016/j.quascirev.2022.107922 0277-3791

Dierickx K, Kersten O, van den Hurk Y, Frasier BA, Sabin R, Star B, Barrett JH. 2025. Ontogenetic changes and sexual dimorphism in the cranium and mandible of the Atlantic walrus (*Odobenus rosmarus rosmarus* L.). The Anatomical Record.:1–29. doi:https://doi.org/10.1002/ar.70050.

Dinerstein E. 1991. Sexual Dimorphism in the Greater One-Horned Rhinoceros (*Rhinoceros unicornis*). Journal of Mammalogy. 72(3):450–457

Dinerstein E, Price L. 1991. Demography and Habitat Use by Greater One-Horned Rhinoceros in Nepal. The Journal of Wildlife Management. 55(3):401–411

Dittrich L. 1972. Birth and growth of a male white rhinoceros (*Ceratotherium simum simum*) at Hanover Zoo. International Zoo Yearbook. 12(1):122–125

Dobney K, Ervynck A. 2000. Interpreting Developmental Stress in Archaeological Pigs: the Chronology of Linear Enamel Hypoplasia. Journal of Archaeological Science. 27:597–607. https://doi.org/10.1006/jasc.1999.0477

Doughty EM, Wallace SC, Schubert BW, Lyon LM. 2018. First occurrence of the enigmatic peccaries *Mylohyus elmorei* and *Prosthennops serus* from the Appalachians: latest Hemphillian to early Blancan of Gray Fossil Site, Tennessee. PeerJ 6:e5926.

Dressino V, Pucciarelli HM. 1997. Cranial growth in *Saimiri sciureus* (Cebidae) and its alteration by nutritional factors: A longitudinal study. American Journal of Physical Anthropology. 102(4):545–554

Duckler GL, Van Valkenburgh B. 1998. Exploring the health of late Pleistocene mammals: the use of Harris lines. Journal of Vertebrate Paleontology. 18(1):180–188. https://doi.org/10.1080/02724634.1998.10011042

Emery-Wetherell MM, Davis EB. 2018. Dental measurements do not diagnose modern artiodactyl species: Implications for the systematics of Merycoidodontoidea. Palaeontologia Electronica. 21.2.23A:1–28. https://doi.org/10.26879/748 palaeo-electronica.org/content/2018/2202-dental-variation-of-artiodactyl

Farlow JO, Sunderman JA, Havens JJ, Swinehart AL. 2001. The Pipe Creek Sinkhole Biota, a Diverse Late Tertiary Continental Fossil Assemblage from Grant County, Indiana. American Midland Naturalist. 145(2)

Fekonja A, Čretnik A. 2022. Comparison of craniofacial morphology in individuals with and without hypodontia with a special focus on the number of congenitally missing teeth. Frontiers in Public Health. 10. doi:10.3389/fpubh.2022.1013862.

Fidalgo D, Bibi F, Pandolfi L, Boisserie J-R. 2025. Impact of Life History on Hippopotamus Skull Ontogeny. Evolution and Development. 27. https://doi.org/10.1111/ede.70013

Flinn EB, Strickland BK, Demarais S, Christiansen D. 2013. Age and Gender Affect Epiphyseal Closure in White-tailed Deer. Southeastern Naturalist. 12(2):297–306

Folayan MO, Tantawi ME, Oginni AB, Alade M, Adeniyi A, Finlayson TL. 2020. Malnutrition, enamel defects, and early childhood caries in preschool children in a sub-urban Nigeria population. PLoS ONE. 15(7).

Fourvel J-B, Fosse P, Fernandez P, Antoine P-O. 2015. Large mammals of Fouvent-Saint-Andoche (Haute-Saône, France): a glimpse into a Late Pleistocene hyena den. Geodiversitas. 37(2):237–266. https://doi.org/10.5252/g2015n2a5

Franz-Odendaal TA. 2004. Enamel hypoplasia provides insight into early systemic stress in wild and captive giraffes (*Giraffa camelopardalis*). Journal of Zoology. 263(2):107–218

Franz-Odendaal TA, Lee-Thorp J, Chinsamy-Turan A. 2003. Insights from stable isotopes of enamel defects and weaning in Pliocene herbivores. Journal of Biosciences. 28.

Gajewski JA, Wallace SC. 2025. Convergent and Ancestral Morphology in an Extinct North American Rhinoceros, *Teleoceras aepysoma* (Perissodactyla, Rhinocerotidae). Poster presented at the 104th Annual Meeting of the American Society of Mammalogists, West Lafayette, IN.

Garn SM, Osborne RH, McCabe KD. 1979. The Effect of Prenatal Factors on Crown Dimensions. American Journal of Physical Anthropology. 51:665–678.

Garutt NV. 1994. Dental ontogeny of the woolly rhinoceros *Coelodonta antiquitatis* (Blumenbach, 1799). Cranium. 11(1):37–48

Gavrilovic MK. 2023. Better Teeth, Better Health? The Relationship Between Enamel Hypoplasia and Osteological Stress Markers in EBA Population of Northern Siberia. Archaeology and Science. 19(2):21–37

Geraads D, Koufos G. 1990. Upper Miocene Rhinocerotidae (Mammalia) from Pentalophos-1, Macedonia, Greece. Palaeontographica Abt A. 210:151–168.

Gerhold GJ. 1992. Comparative Morphology and Evolution of *Teleoceras* [Master's Thesis]. Fort Hays State University.

Giaourtsakis I, Svorligkou G, Roussiakis S. 2018. A juvenile skull of the hornless rhinocerotid *Acerorhinus neleus* (Rhinocerotidae, Mammalia) from the Late Miocene locality of Pikermi (Attica, Greece). The Palaeontological Association 62nd Annual Meeting, University of Bristol.

Giaourtsakis I, Theodouru G, Roussiakis S, Athanassiou A, Iliopoulos G. 2006. Late Miocene horned rhinoceroses (Rhinocerotinae, Mammalia) from Kerassia (Euboea, Greece). Neues Jahrbuch für Geologie und Paläontologie. 239(3):367–298

Giaourtsakis IX. 2021. The Fossil Record of Rhinocerotids (Mammalia: Perissodactyla: Rhinocerotidae) in Greece. In: Fossil Vertebrates of Greece. Vol. 2. p. 409–500.

Goddard J. 1970. Age Criteria and Vital Statistics of a Black Rhinoceros Population. African Journal of Ecology. 8(1):105–121

Goldstein J. 2018. The Forensic Application of Skeletal Stress Indicators: A Correlation Study of Linear Enamel Hypoplasia (LEH), Harris Lines, Cortical Bone Loss (CBL), and Stature. In: Anthropology.

Goodman AH, Armelagos GJ, Rose JC. 1980. Enamel Hypoplasias as Indicators of Stress in Three Prehistoric Populations from Illinois. Human Biology. 52(3):515–528

Goodman AH, Pelto GH, Allen LH, Chavez A. 1992. Socioeconomic and Anthropometric Correlates of Linear Enamel Hypoplasia in Children from Solis, Mexico. Journal of Paleopathology. 2:373–380

Goodman AH, Rose JC. 1991. Dental enamel hypoplasias as indicators of nutritional status. In: Advances in Dental Anthropology. Wiley-Liss; p 279–293

Goodman AH, Song R. 1999. Sources of variation in estimated ages at formation of linear enamel hypoplasias. In: Human Growth in the Past. Cambridge University Press. p. 315.

Goodman AH, Rose JC. 1990. Assessment of Systemic Physiological Perturbations From Dental Enamel Hypoplasias and Associated Histological Structures. Yearbook of Physical Anthropology. 33:59–110

Groves CP. 1972. *Ceratotherium simum*. Mammalian Species. 8:1–6

Groves CP, Kurt F. 1972. *Dicerorhinus sumatrensis*. Mammalian Species. 21:1–6

Groves CP, Leslie DM. 2011. *Rhinoceros sondaicus* (Perissodactyla, Rhinocerotidae). Mammalian Species. 43(887):190–208

Groves CP. 1967. On the Rhinoceroses of South-East Asia. Säugetierkundliche Mitteilungen. 15(3):221–237

Groves CP. 1982. The Skulls of Asian Rhinoceroses: Wild and Captive. Zoo Biology. 1(3):251–261

Guérin C. 1980. Les rhinocéros (Mammalia, Perissodactyla) du Miocène terminal au Pléistocène supérieur en Europe occidentale. Comparaison avec les espèces actuelles. Doc Lab Geol Lyon.

Gunnin D, Schubert BW, Samuels JX, Bredehoeft K, Maden S. 2025a. A new plethodontid salamander from the Early Pliocene of northeastern Tennessee, U.S.A., and its bearing on desmognathan evolution. Historical Biology. doi:10.1080/08912963.2025.2501332.

Gunnin D, Schubert B, Woodward H, Samuels, J. 2025b. High levels of histovariability in wild alligators inform the paleobiology of an extinct Appalachian alligator. Geological Society of America Abstracts with Programs. 57(2) doi: 10.1130/abs/2025SE-408972

Gustafson E. 2012. New Records of Rhinoceroses from the Ringold Formation of Central Washington and the Hemphillian-Blancan Boundary. Journal of Vertebrate Paleontology. 32(3):727–731. https://www.jstor.org/stable/41515292

Hagge MD. 2010. A functional and ontogenetic skull analysis of the extant rhinoceroses and *Teleoceras major*. [Master's Thesis]. Louisiana State University.

Halcrow SE, Tayles N. 2008. Stress near the start of life? Localised enamel hypoplasia of the primary canine in late prehistoric mainland Southeast Asia. Journal of Archaeological Science. 35:2215–2222

Hartstone-Rose A, Selvey H, Villari JR, Atwell M, Schmidt T. 2014. The Three-Dimensional Morphological Effects of Captivity. PLoS ONE. 9(11). doi:doi:10.1371/journal.pone.0113437.

Harvati K, Frost SR. 2007. Dental Eruption Sequences in Fossil Colobines and the Evolution of Primate Life Histories. International Journal of Primatology. 28(3). https://doi.org/10.1007/s10764-007-9149-1

Hatcher JB. 1894. On a small collection of vertebrate fossils from the Loup Fork Beds of northwestern Nebraska; with notes on the geology of the region. The American Naturalist. 28:236–238

Haugrud S. 2023. Identifying Taphonomic Distribution Patterns at the Gray Fossil Site [Master's Thesis]. East Tennessee State University Electronic Theses and Dissertations.

Heinrich RE, Ruff CB, Adamczewski JZ. 1999. Ontogenetic changes in mineralization and bone geometry in the femur of muskoxen. Journal of Zoology. 215–225

Hieronymous TL, Witmer LM, Tanke DH, Currie PJ. 2009. The Facial Integument of Centrosaurine Ceratopsids: Morphological and Histological Correlates of Novel Skin Structures. The Anatomical Record. 292(9):1235–1521. https://doi.org/10.1002/ar.20985open_in_new

Hillman-Smith AKK, Owen-Smith N, Anderson JL, Hall-Martin AJ, Selaladi JP. 1986. Age estimation of the White rhinoceros *(Ceratotherium simum*). Journal of Zoology. 210(3):355–377

Hillman-Smith AKK, Groves CP. 1994. *Diceros bicornis*. Mammalian Species. 455:1–8

Hitchins PM. 1978. Age determination of the black rhinoceros in Zululand. South African Journal of Wildlife Research. 8:71–80

Hitchins PM, Anderson JL. 1983. Reproduction, population characteristics and management of the black rhinoceros *Diceros bicornis minor* in the Hluhluwe/Corridor/Umfolozi Game Reserve Complex. South African Journal of Wildlife Research. 13(3)

Hulbert RC, Wallace SC, Klippel WE, Parmalee PW. 2009. Cranial Morphology and Systematics of an Extraordinary Sample of the Late Neogene Dwarf Tapir, *Tapirus polkensis* (Olsen). Journal of Paleontology. 83(2):238–262. https://doi.org/DOI: 10.1666/08-062.1

Hullot M, Antoine P-O. 2020. Mortality curves and population structures of late early Miocene Rhinocerotidae remains from the Beon 1 locality of Montreal-du-Gers, France. Palaeogeography, Palaeoclimatology, Palaeoecology. 558:109938

Hullot M, Antoine P-O. 2022. Enamel hypoplasia on rhinocerotid teeth: Does CT-scan imaging detect the defects better than the naked eye? Paleovertebrata. 45(1). https://doi.org/10.18563/pv.45.1.e2

Hullot M, Antoine P-O, Spassov N, Koufos G, Merceron G. 2022. Late Miocene rhinocerotids from the Balkan-Iranian province: ecological insights from dental microwear textures and enamel hypoplasia. Historical Biology.:1–18. doi:10.1080/08912963.2022.2095910.

Hullot M, Laurent Y, Merceron G, Antoine P-O. 2021. Paleoecology of the Rhinocerotidae (Mammalia, Perissodactyla) from Béon 1, Montréal-du-Gers (late early Miocene, SW France): Insights from dental microwear texture analysis, mesowear, and enamel hypoplasia. Palaeontologia Electronica. 24(2). https://doi.org/10.26879/1163

Hullot M, Merceron G, Antoine P-O. 2019. Dental hypoplasia as a proxy for evaluating environmental constraints on fossil rhinocerotids (Mammalia, Perissodactyla). Poster presented at Ph.D. Students' Day ISE-M.

Hullot M, Merceron G, Antoine P-O. 2023. Spatio-temporal diversity of dietary preferences and stress sensibilities of early and middle Miocene Rhinocerotidae from Eurasia: impact of climate changes. Peer Community Journal. 3(e5). https://doi.org/10.24072/pcjournal.222

Hullot M, Martin C, Blondel C, Becker D, Rössner GE. 2024. Evolutionary palaeoecology of European rhinocerotids across the Oligocene-Miocene transition. Royal Society Open Science. 11(10):240987.

Iurino DA, Conti J, Mecozzi B, Sardella R. Braincase with Natural Endocast of a Juvenile Rhinocerotinae from the Late Middle Pleistocene Site of Melpignano. Earth Sci. 8(94)

Janis CM. 1990. Correlation of cranial and dental variables with dietary preferences in mammals: a comparison of Macropodoids and Ungulates. Memoirs of the Queensland Museum. 28(1):349–366

Jasinski SE, Moscato DA. 2017. Late Hemphillian Colubrid Snakes (Serpentes, Colubridae) from the Gray Fossil Site of Northeastern Tennessee. Journal of Herpetology. 51(2):245–257.

Jasinski SE. 2018. A new slider turtle (Testudines: Emydidae: Deirochelyinae: *Trachemys*) from the late Hemphillian (late Miocene/early Pliocene) of eastern Tennessee and the evolution of the deirochelyines. PeerJ. 6:e4338. doi:10.7717/peerj.4338.

Kampouridis P, Svorligkou G, Kargopoulos N, Spassov N, Böhme M. 2023. Revision of the Late Miocene hornless rhinocerotids from Samos Island (Greece) with the designation of neotypes and implications for the European chilotheres. Journal of Vertebrate Paleontology. 43(1):e225436

Keenan SW, Engel AS. 2017. Reconstructing diagenetic conditions of bone at the Gray Fossil Site, Tennessee, USA. Palaeogeography, Palaeoclimatology, Palaeoecology. 471:48–57. doi:10.1016/j.palaeo.2017.01.037.

Khalaf K, El-Kishawi M. 2022. Craniofacial and Oral Manifestations of Non-Syndromic Hypodontia: A Review. European Journal of General Dentistry. 11(1):17–22. doi:10.1055/s-0042-1742355.

Kierdorf H, Zeiler J, Kierdorf U. 2006. Problems and pitfalls in the diagnosis of linear enamel hypoplasia in cheek teeth of cattle. Journal of Archaeological Science. 33:1690–1695. doi:10.1016/j.jas.2006.03.001

Kilbourne BM, Makovicky PJ. 2012. Postnatal Long Bone Growth in Terrestrial Placental Mammals: Allometry, Life History, and Organismal Traits. Journal of Morphology. 273:1111–1126. doi: 10.1002/jmor.20048

Klein RG. 1982. Patterns of ungulate mortality and ungulate mortality profiles from Langebaanweg (Early Pliocene) and Elandsfontein (Middle Pleistocene), South-Western Cape Province, South Africa. Annals of the South African Museum. 90(2):49–94.

Koufos GD, Syrides GE, Kostopoulos DS, Koliadimou KK, Sylvestrou IA, Seitanidis GC, Vlachou TD. 1997. New excavations in the Neogene mammalian localities of Mytilinii, Samos Island, Greece. Geodiversitas. 19(4):877–885

Langer P. 2008. The phases of maternal investment in eutherian mammals. Zoology. 111:148–162

Laurie WA, Lang EM, Groves CP. 1983. *Rhinoceros unicornis*. Mammalian Species. 211(1):1–6

Law PR, Fike B, Lent PC. 2013. Mortality and female fecundity in an expanding black rhinoceros (*Diceros bicornis minor*) population. European Journal of Wildlife Research. 59:477–485

Lee PC. 1996. The Meanings of Weaning: Growth, Lactation, and Life History. Evolutionary Anthropology. 5(3):87–98

Lewall EF, Cowan IM. 1963. Age Determination in Black-Tail Deer by Degree of Ossification of the Epiphyseal Plate in the Long Bones. Canadian Journal of Zoology. 41:629–636

Lister D, Cowen T, McCance RA. 1966. Severe undernutrition in growing and adult animals 16*. The ultimate results of rehabilitation: poultry. British Journal of Nutrition. 20:633–639

Lu X. 2013. A juvenile skull of *Acerorhinus yuanmouensis* (Mammalia: Rhinocerotidae) from the Late Miocene hominoid fauna of the Yuanmou Basin (Yunnan, China). Geobios. 46:539–548. http://dx.doi.org/10.1016/j.geobios.2013.10.001

Lu X, Deng T, Zheng X-T, Fuchang L. 2020. Sexual Dimorphism and Body Reconstruction of a Hornless Rhinocerotid, *Plesiaceratherium gracile*, From the Early Miocene of the Shanwang Basin, Shandong, China. Frontiers in Ecology and Evolution. 8. doi:10.3389/fevo.2020.544076.

Lu X, Deng T, Pandolfi L. 2023a. Reconstructing the phylogeny of the hornless rhinoceros Aceratheriinae. Frontiers in Ecology and Evolution. 11. https://doi.org/10.3389/fevo.2023.1005126

Lu X, Deng T, Rummy P, Zheng X-T, Zhang Y-T. 2023. Reproduction of a fossil rhinoceros from 18 mya and origin of litter size in perissodactyls. iScience. 26. doi:https://doi.org/10.1016/ j.isci.2023.107800.

Lu X, Deng T, Zheng X-T, Fuchang L. 2020. Sexual Dimorphism and Body Reconstruction of a Hornless Rhinocerotid, *Plesiaceratherium gracile*, From the Early Miocene of the Shanwang Basin, Shandong, China. Frontiers in Ecology and Evolution. 8. https://doi.org/10.3389/fevo.2020.544076

Lu X, Deng T, Ji X. 2021. Postcranial bones of *Acerorhinus yuanmouensis* from the Late Miocene of the Yuanmou Basin, China, and body reconstruction. Chinese Science Bulletin. 66(12):1516–1526. https://doi.org/DOI: 10.1360/TB-2020-0743

Lu X, Deng T. 2025. Life history of a new Paraceratheriid from the Early Oligocene of Northwest China. Scientific Reports. 15(1). doi:10.1038/s41598-025-13365-w.

Lukacs JR. 2001. Enamel hypoplasia in the deciduous teeth of early Miocene catarrhines: evidence of perinatal physiological stress. Journal of Human Evolution. 40:319–329. https://doi.org/10.1006/jhev.2000.0458

Lukacs JR. 2009. Markers of Physiological Stress in Juvenile Bonobos (*Pan paniscus*): Are Enamel Hypoplasia, Skeletal Development, and Tooth Size Interrelated? American Journal of Physical Anthropology. 139(3):279–446

MacFadden BJ. 1998. Tale of two Rhinos: Isotopic Ecology, Paleodiet, and Niche Differentiation of *Aphelops* and *Teleoceras* from the Florida Neogene. Paleobiology. 24(2):274–286

Madden CT, Dalquest WW. 1990. The last rhinoceros in North America. Journal of Vertebrate Paleontology. 10(2):266

Maden S. 2023. An early Pliocene fish assemblage from the southern Appalachians: Ichthyofauna of the Gray Fossil Site [Master's Thesis]. East Tennessee State University Electronic Theses and Dissertations.

Madhusudhan KS, Pallavi MR. 2022. Perspective Chapter: Effects of Malnutrition on Pediatric Oral Health - A Review. In: Pediatric Dentistry - A Comprehensive Guide.

Mangas-Carrasco E, López-Costas O. 2021. Porotic hyperostosis, cribra orbitalia, femoralis and humeralis in Medieval NW Spain. Archaeological and Anthropological Sciences. 13(10). https://doi.org/10.1007/s12520-021-01432-y

Mallet C, Houssaye A, Cornette R, Billet G. 2022. Long bone shape variation in the forelimb of Rhinocerotoidea: relation with size, body mass and body proportions. Zoological Journal of the Linnean Society. 196(3):1201–1234.

Matthew WD. 1932. A review of the rhinoceroses with a description of *Aphelops* material from the Pliocene of Texas. University of California Publications Bulletin of the Department of Geological Sciences. 20(12):411–482.

McCance RA, Ford EHR, Brown WAB. 1961. Severe undernutrition in growing and adult animals 7. Development of the skull, jaws and teeth in pigs. British Journal of Nutrition. 15:213–224

McDonald HG, Wallace SC. 2011. The Timing of the First Appearance of Sloths in North America: What Do We Really Know? In Gray Fossil Site: 10 Years of Research.

Mead AJ. 2000. Sexual Dimorphism and Paleoecology in *Teleoceras*, A North American Miocene Rhinoceros. Paleobiology. 24(4):689-706

Mead AJ. 1999. Enamel Hypoplasia in Miocene Rhinoceroses (*Teleoceras*) from Nebraska: Evidence of Severe Physiological Stress. Journal of Vertebrate Paleontology. 19(2):391–397

Mead JI, Schubert BW, Wallace SC, Swift SL. 2012. Helodermatid lizard from the Mio-Pliocene oak-hickory forest of Tennessee, eastern USA, and a review of monstersaurian osteoderms. Acta Palaeontologica Polonica 57(1):111−121.

Mendoza M, Janis CM, Palmqvist P. 2002. Characterizing complex craniodental patterns related to feeding behavior in ungulates: a multivariate approach. Journal of Zoology. 258(2):139–278.

Mihlbachler, M. C. 2001. Was *Teleoceras* a semi-aquatic hippo ecomorph? Journal of Vertebrate Paleontology, 22(3, supplement):80

Mihlbachler MC. 2003. Demography of Late Miocene Rhinoceroses from Florida. Paleobiology. 29(3):412–428

Mihlbachler MC, Lucas SG, Emry RJ, Bayshashov BU. 2004. A New Brontothere (Brontotheriidae, Perissodactyla, Mammalia) from the Eocene of the Ily Basin of Kazakstan and a Phylogeny of Asian "Horned" Brontotheres. American Museum Novitiates. 3439:1–43. doi:10.1206/0003-0082(2004)439<0001:ANBBPM>2.0.CO;2.

Mihlbachler MC. 2005. Linking Sexual Dimorphism and Sociality in Rhinoceroses: Insights from *Teleoceras proterum* and *Aphelops malacorhinus* from the Late Miocene of Florida. Bulletin Florida Museum of Natural History. 45(4):495–520

Mihlbachler MC. 2007. Sexual Dimorphism and Mortality Bias in a Small Miocene North American Rhino, *Menoceras arikarense*: Insights into the Coevolution of Sexual Dimorphism and Sociality in Rhinos. Journal of Mammalian Evolution. 14:217–238. https://doi.org/DOI 10.1007/s10914-007-9048-4

Mountain RV, Zhu Y, Pickett OR, Lussier AA, Goldstein JM, Roffman JL, Bidlack FB, Dunn EC. 2021. Association of Maternal Stress and Social Support During Pregnancy With Growth Marks in Children's Primary Tooth Enamel. Jama Network Open. 4(11). doi:10.1001/jamanetworkopen.2021.29129.

Mousikou M, Kyriakou A, Skordis N. 2021. Stress and Growth in Children and Adolescents. Hormone Research in Paediatrics. 96(1). doi:10.1159/000521074.

Nardelli F, Heissig K. 2025. A taxonomic review of the genus *Rhinoceros* with emphasis on the distinction of *Eurhinoceros* (Perissodactyla, Rhinocerotidae). ZooKeys. 1230:303–333. doi:10.3897/zookeys.1230.127858.

Niven LB, Egeland CP, Todd LC. 2004. An inter-site comparison of enamel hypoplasia in bison: implications for paleoecology and modeling Late Plains Archaic subsistence. Journal of Archaeological Science. 31:1783–1794

Ochoa D, Whitelaw M, Yu-Sheng CL, Zavada M. 2012. Palynology of Neogene sediments at the Gray Fossil Site, Tennessee, USA: Floristic implications. Review of Palaeobotany and Palynology. 184:36–48

Odom WE, Granger DE, Wallace SC. 2025. 10Be/9Be and 26Al/10Be Support a Late Miocene Burial Age for Basal Gray Fossil Site Sediments. Pan-American Paleontology.(1).

Osborn HF. 1898. A Complete Skeleton of *Teleoceras* the True Rhinoceros from the Upper Miocene of Kansas. Science.

Osborn HF. 1904. New Miocene rhinoceroses with revision of known species. Bulletin of the American Museum of Natural History. 20(27):307–326

Padilla M, Dowler RC. 1994. *Tapirus terrestris*. Mammalian Species. 481:1–8.

Padilla M, Dowler RC, Downer CC. 2010. *Tapirus pinchaque* (Perissodactyla: Tapiridae). Mammalian Species. 42(863):166–182.

Park EA. 1964. The imprinting of nutritional disturbances on the growing bone. Pediatrics. 33(5):815–861. doi:10.1542/peds.33.5.815.

Plair BL, Reinhart PR, Roth TL. 2012. Neonatal Milestones, Behavior and Growth Rate of Sumatran Rhinoceros (*Dicerorhinus sumatrensis*) Calves Born and Bred in Captivity. Zoo Biology. 31:546–560

Potter T, Prothero DR, Welsh E. 2025. Allometric trends in growth of the chalicothere *Moropus elatus* (Mammalia: Perissodactyla: Chalicotheriidae). New Mexico Geology. 100:171–174.

Prothero DR, Manning EM. 1987. Miocene rhinoceroses from the Texas Gulf Coastal Plain. Journal of Paleontology. 61(2):388–423

Prothero DR, Sereno PC. 1982. Allometry and Paleoecology of Medial Miocene Dwarf Rhinoceroses from the Texas Gulf Coastal Plain. Paleobiology. 8(1):16–30

Prothero, DR., 2005. The Evolution of North American Rhinoceroses. Cambridge University Press, Cambridge.

Protopopov A, Potapova O, Valerievich PV, Mashchenko EN, Boeskorov G, Klimovsky AI, Banderov A, Ivanov S, Kolesov S, Pavlov I. 2015. The frozen mummy of the woolly rhinoceros, *Coelodonta antiquitatis* Blum., 1799 calf: a new data on early ontogenesis of the extinct species. Programs and Abstracts of the 75th Annual Meeting of the Society of Vertebrate Paleontology, Dallas TX, USA.

Pucciarelli HM. 1981. Growth of the functional components of the rat skull and its alteration by nutritional effects. A multivariate analysis. American Journal of Biological Anthropology. 56(1):33–41.

Reynolds RJ. 1961. Asian rhinos in captivity. International Zoo Yearbook. 2:17–42.

Roohi G et al. 2015. Enamel Hypoplasia in Siwalik Rhinocerotids and its Correlation with Neogene Climate. Pakistan Journal of Zoology. 47(5):1433–1443

Roth TL, Reinhart PR, Romo JS, Candra D, Suhaery A, Stoops MA. 2013. Sexual Maturation in the Sumatran rhinoceros (*Dicerorhinus sumatrensis*). Zoo Biology. 32:549–555. doi:https://doi.org/10.1002/zoo.21089.

Sadida ZJ, Indriyanti R, Setiawan AS. 2021. Does Growth Stunting Correlate with Oral Health in Children?: A Systematic Review. European Journal of Dentistry. 16(1).

Samuels JX, Bredehoeft K, Wallace SC. 2018. A new species of *Gulo* from the Early Pliocene Gray Fossil Site (Eastern United States); rethinking the evolution of wolverines. PeerJ. 6

Samuels JX, Schap J. 2021. Early Pliocene Leporids from the Gray Fossil Site of Tennessee. Eastern Paleontologist. 8:1–23

Samuels JX, Williams OR, Maden S, Schubert, BW. 2025. Early Pliocene Deer from the Gray Fossil Site, Appalachian Highlands, Tennessee, USA. Palaeontologia Electronica, 28(2):a36.https://doi.org/10.26879/1560

Santos SM, Prothero DR, Watmore KI, Welsh E. 2025. How did extinct rhinoceros limbs grow? Allometric growth in rhinoceros limbs. New Mexico Geology. 207–211

Sarnat BG, Schour IS. 1941. Enamel Hypoplasia (Chronologic Enamel Aplasia) in Relation to Systemic Disease: A Chronologic, Morphologic, and Etiologic Classification. The Journal of the American Dental Association. 28(12):1989–2000

Saunders SR, Hoppa RD. 1993. Growth deficit in survivors and non-survivors: Biological mortality bias in subadult skeletal samples. American Journal of Physical Anthropology. 36(S17):127–151.

Scaife T. 2024. Pathology and Osteological Observations of Early Pliocene Rhinoceros, *Teleoceras aepysoma* from Gray Fossil Site, Tennessee. East Tennessee State University.

Schaurte, WT. 1966. Beitrage zur Kenntnis des Gebisses und Zahnbaues der afrikanischen Nashorner. Saugetierkundliche Mitteilungen, 14:327-341

Schubert BW, Mead JI. 2011. Alligators from the Gray Fossil Site. In Gray Fossil Site: 10 Years of Research.

Schubert BW, Wallace SC, Soibelzon LH. 2011. A Small Bear from the Mio-Pliocene of Gray, Tennessee, and Its Role in Determining the Age of the Fossil Site. In Gray Fossil Site: 10 Years of Research.

Seow WK, Brown JP, Tudehope DA, O'Callaghan M. 1984. Dental defects in the deciduous dentition of premature infants with low birth weight and neonatal rickets. Pediatric Dentistry. 6(2):89–92.

Shaw JH, Griffiths D. 1963. Dental Abnormalities in Rats Attributable to Protein Deficiency during Reproduction. The Journal of Nutrition. 80(2):123–141

Short RA. 2013. A New Species of *Teleoceras* from the Late Miocene Gray Fossil Site, with Comparisons to Other North American Hemphillian Species [Master's Thesis]. Electronic Theses and Dissertations, East Tennessee State University.

Short RA, Wallace SC, Emmert, LG. 2019. A New Species of *Teleoceras* (Mammalia, Rhinocerotidae) from the Late Hemphillan of Tennessee. Florida Museum of Natural History Bulletin. 56(5):183–260

Shunk AJ, Driese SG, Clark GM. 2006. Latest Miocene to earliest Pliocene sedimentation and climate record derived from paleosinkhole fill deposits, Gray Fossil Site, northeastern Tennessee, U.S.A. Palaeogeography, Palaeoclimatology, Palaeoeology. 231:265–278

Shpansky AV. 2014. Juvenile remains of the "woolly rhinoceros" *Coelodonta antiquitatis* from the Tomsk Priob'e area. Quaternary International. 333:86–99

Skinner MF. 2002. 4. Myopia and nutritionally inhibited cranio-facial growth: a theoretical model based on localised hypoplasia of the primary canine tooth in orangutans and bonobos. In: Bones and the man: studies in honour of Don Brothwell. Oxbow Books

Skinner MF, Imbrasas M, Byra C, Skinner M. 2019. Growth response of dental tissues to developmental stress in the domestic pig (*Sus scrofa*). American Journal of Physical Anthropology.

Skinner MF, Rodrigues AT, Byra C. 2014. Developing a Pig Model for Crypt Fenestration-Induced Localized Hypoplastic Enamel Defects in Humans. American Journal of Physical Anthropology. 154(2):239–250

Skinner MF, Skinner MM, Pilbrow VC, Hannibal DL. 2016. An enigmatic hypoplastic defect of the maxillary lateral incisor in recent and fossil orangutans from Sumatra (*Pongo abelii*) and Borneo (*Pongo pygmaeus*). Journal of Primatology. 37(4):548–567

Skinner MF, Newell EA. 2003. Localized Hypoplasia of the Primary Canine in Bonobos, Orangutans, and Gibbons. American Journal of Physical Anthropology. 120:61–72

Snoodijk F, Calderon T, Lyras GA, van der Geer AE. 2025. Delayed skeletal maturity in dwarf, medium and giant Pleistocene insular deer (*Candiacervus*) indicating a slower life history regardless size shift. Swiss Journal of Palaeontology. 144(1). doi:10.1186/s13358-025-00413-1.

Steadman, DW. 2011. A Preliminary Look at Fossil Birds from the Gray Fossil Site, Tennessee. In Gray Fossil Site: 10 Years of Research.

Stodder ALW. 1997. Subadult stress, Morbidity, and Longevity in Latte Period Populations on Guam, Mariana Islands. American Journal of Physical Anthropology. 104(3):363–380. https://doi.org/10.1002/(SICI)1096-8644(199711)104:3<363::AID-AJPA6>3.0.CO;2-W

Sun D, Deng T, Wang S. 2024. New materials of plesiacerathere (Perissodactyla, Rhinocerotidae) from the late Early Miocene of Northern China. PeerJ. https://peerj.com/articles/16822/#

Sweeney EA, Saffir AJ, de Leon R. 1971. Linear hypoplasia of deciduous incisor teeth in malnourished children. The American Journal of Clinical Nutrition. 24

Tedford RH, Albright III LB, Barnosky AD, Ferrusquia-Villafranca I, Hunt Jr. RM, Storer JE, Swisher III CC, Voorhies MR, Webb SD, Whistler DP. 2004. Mammalian Biochronology of the Arikareean Through Hemphillian Interval (Late Oligocene Through Early Pliocene Epochs). In: Late Cretaceous and Cenozoic Mammals of North America: Biostratigraphy and Geochronology. Columbia University Press. p. 269–343.

Todd TW, Todd AW. 1938. The epiphyseal union pattern of the ungulates with a note on Sirenia. American Journal of Anatomy. 63(1):1–36

Tong H-W. 2012. Evolution of the non-*Coelodonta* dicerorhine lineage in China. Comptes Rendus Palevol. 11:555–562.

Tong H-W, Wang X-M. 2014. Juvenile Skulls and Other Postcranial Bones of *Coelodonta nihowanensis* from Shanshenmiaozui, Nihewan Basin, China. Journal of Vertebrate Paleontology. 34(3):710–724

Towle I, Irish JD. 2019. A probable genetic origin for pitting enamel hypoplasia on the molars of *Paranthropus robustus*. Journal of Human Evolution. 129:54–61

Tucker ST, Farlow JO. 2025. Carnivorans from the late Neogene Pipe Creek Sinkhole (lower Blancan), Grant County, Indiana, U.S.A. Journal of Vertebrate Paleontology. 45(4). doi:https://doi.org/10.1080/02724634.2025.2566982.

Ungar PS. 2014. Dental allometry in mammals: a retrospective. Annales Zoologici Fennici. 51(1/2):177–187.

Upex B, Dobney K. 2012. Dental enamel hypoplasia as indicators of seasonal, environmental, and physiological impacts in modern sheep populations: a model for interpreting the

zooarchaeological record. Journal of Zoology. 287:259–268. https://doi.org/10.1111%2Fj.1469-7998.2012.00912.x

Verme LJ, Ozoga JJ. 1980. Effects of Diet on Growth and Lipogenesis in Deer Fawns. The Journal of Wildlife Management. 44(2):315–324

von Bertalanffy L. 1957. Quantitative Laws in Metabolism and Growth. The Quarterly Review of Biology. 32(3):217–231

von Koenigswald W, Smith HB, Keller T. 2007. Supernumerary teeth in a subadult rhino mandible (*Stephanorhinus hundsheimensis*) from the middle Pleistocene of Mosbach in Wiesbaden (Germany). Palaeontological Journal. 81(4):416–428. doi:10.1007/BF02990253.

Voorhies MR, Stover SG. 1978. An articulated fossil skeleton of a pregnant rhinoceros, *Teleoceras major* Hatcher. Proceedings- Nebraska Academy of Sciences and affiliated societies. 88:47–48

Voorhies MR, Thomasson JR. 1979. Fossil Grass Anthoecia Within Miocene Rhinoceros Skeletons: Diet in an Extinct Species. Science. 206:331–333

Voorhies MR. 1985. A Miocene rhinoceros herd buried in volcanic ash. National Geographic Society Research Reports. 19:671–688.

Voorhies MR. 1990. Vertebrate Paleontology of the Proposed Norden Reservoir Area: Brown, Cherry, and Keya Paha Counties Nebraska. Lincoln, NE: University of Nebraska Department of Anthropology Division of Archeological Technical Report No.: 82–09.

Walker DN. 1987. Sequence of Epiphyseal Fusion in the Rocky Mountain Bighorn Sheep. The Great Basin Naturalist. 47(1):7–12

Wall WP, Heinbaugh KL. 1999. Locomotor adaptations in *Metamynodon planifrons* compared to other amynodontids (Perissodactyla, Rhinocerotoidea). National Parks Paleontological Research. 4:8–17.

Wallace SC, Wang X. 2004. Two new carnivores from an unusual late Tertiary forest biota in eastern North America. Nature. 431. doi:10.1038.

Wallace S, Lyon L. 2022. Systemic revision of the Ailurinae (Mammalia: Carnivora: Ailuridae): with a new species from North America. In: Red Panda: Biology and Conservation of the First Panda. 2nd ed. 10.1016/B978-0-12-823753-3.00011-9.

Wang B, Secord R. 2020. Paleoecology of *Aphelops* and *Teleoceras* (Rhinocerotidae) through an interval of changing climate and vegetation in the Neogene of the Great Plains, central United States. Palaeogeography, Palaeoclimatology, Palaeoecology. 542

Ward CT, Crowley BE, Secord R. 2024. Home on the range: A multi-isotope investigation of ungulate resource partitioning at Ashfall Fossil Beds, Nebraska, USA. Palaeogeography, Palaeoclimatology, Palaeoecology. 6504

Widdowson EM. 1981. The role of nutrition in mammalian reproduction. In: Environmental Factors in Mammalian Reproduction. Palgrave Macmillan

Widdowson EM. 1976. The response of the sexes to nutritional stress. Proceedings of the Nutritional Society. 35:175–180

Widdowson EM, Kennedy GC. 1962. Rates of Growth, Mature Weight and Life-Span. Proceedings of the Royal Society of London Series B, Biological Sciences. 156(962):96–108

Widyanti SP, Andrew E, Tantiana. 2024. The effect of Vitamin D deficiency on the occurrence of enamel hypoplasia in babies: A review article. World Journal of Advanced Research and Reviews. 21(2):2019–2026. https://doi.org/10.30574/wjarr.2024.21.2.0684

Woodward AB. 2011. Fishes of the Mio-Pliocene Gray Fossil Site. In Gray Fossil Site: 10 Years of Research.

Zobaa MK, Zavada MS, Whitelaw MJ, Shunk AJ, Oboh-Ikuenobe FE. 2011. Palynology and palynofacies analyses of the Gray Fossil Site, eastern Tennessee: Their role in understanding the basin-fill history. Palaeogeography, Palaeoclimatology, Palaeoecology. 308:433–444. doi:doi:10.1016/j.palaeo.2011.05.051.

APPENDICES

Appendix A: Directly Observed Museum Specimens

Teleoceras aepysoma: ETMNH 601, ETMNH 609, ETMNH 32999, ETMNH 19280, ETMNH 21659, UTK 10.08, ETMNH 37999, ETMNH 12175, ETMNH 33000, ETMNH 12487, ETMNH 780

Teleoceras americanum: AMNH F:AM 115022, F:AM 115023, F:AM 114417, F:AM 114414, F:AM 114416, F:AM 114419

Teleoceras medicornutum: F:AM 114474, AMNH FM 9832, F:AM 109518, F:AM 114462, F:AM 115186, uncatalogued tusks

Teleoceras meridianum: F:AM 108839, F:AM 108306, F:AM 108351, F:AM 108342, uncatalogued mandible

Teleoceras brachyrhinum: F:AM 114486, F:AM 114449, F:AM 114452, F:AM 114454, F:AM 114471, F:AM 114477, F:AM 114439, F:AM 114438, F:AM 114436, F:AM 114455, F:AM 114437

Teleoceras major: F:AM 114523, F:AM 114503, F:AM 114505, F:AM 114526, F:AM 42980, F:AM 114533, F:AM 114502, F:AM 114543, F:AM 114514, F:AM 115613, F:AM 114494, F:AM 114500, F:AM 114508, F:AM 104209, F:AM 115425, F:AM 115547, F:AM 115583, F:AM 11504, F:AM 114513, F:AM 114493, F:AM 104022, F:AM 115509; uncatalogued skull and mandible

Teleoceras fossiger: AMNH FM 8384, AMNH FM 8386, AMNH FM 8391, AMNH FM 8404, AMNH FM 2606, F:AM 104023, F:AM 114570, F:AM 114566, F:AM 115666, F:AM 115667, F:AM 115701, F:AM 115717, F:AM 115729, F:AM 115730, uncatalogued mandible and isolated tusks

Teleoceras hicksi: F:AM 114589, F:AM 114590, F:AM 114598, F:AM 114599, F:AM 114575, F:AM 114588, F:AM 115783, F:AM 115786, UF 220373, uncatalogued isolated tusks

Teleoceras proterum: UF 9078, UF 41376, UF 24229, UF 24233, UF 24230, UF 24235, UF 24221, UF 24213, UF 24214, UF 24218, UF 191620, UF 40058, isolated teeth

Teleoceras guymonense: F:AM 115994, F:AM 115997

Aphelops mutilus: UF 115631, UF 115633, F:AM 114368, AMNH 9832

Peraceras profectum: AMNH F:AM 109360, F:AM 114401, F:AM 114359, F:AM 114381, F:AM 114384, F:AM 108338, F:AM 114382, F:AM 114379, F:AM 114390, F:AM 114378, F:AM 114395; F:AM 114928; F:AM 114923

Ceratotherium neumayri: AMNH 20584, AMNH 22964, AMNH 20679, AMNH 20582

Chilotherium andersoni: AMNH 26342, AMNH 22506, “CHINA #74”, “CHINA #12”, F:AM 147820, “CHINA #61”

Chilotherium habereri: “CHINA #17”, “CHINA #41”, AMNH FM 22508

Appendix B: Specimen Age Classification

*Only specimens that were able to be assigned to one of Hitchins' (1978) age classes are listed here (i.e. crania and/or mandibles with complete enough dentition). Includes all specimens figured in the present work as well as all specimens from which mensural data was collected.
**Data for *Ceratotherium simum* (Hillman-Smith et al. 1986) and *Diceros bicornis* (Goddard 1970) did not have associated specimen numbers.
***Specimens from other literature are tagged with their associated work

II
Teleoceras major: UNSM 52245 (Hagge 2010)

III
Teleoceras major: AMNH F:AM 115613
Teleoceras fossiger: AMNH F:AM 115730
Plesiaceratherium gracile: S700016 (Lu et al. 2023b)
Diceros bicornis: USNM A34718 (Hagge 2010)

IV
Chilotherium andersoni: AMNH FM 26342
Chilotherium wimani: HMV 0770 (Deng 2001)
Ceratotherium neumayri: AMPG: K3.111 (Giaourtsakis et al. 2006)

V
Teleoceras major: AMNH F:AM 114500, 115583; UNSM 52234 (Hagge 2010)
Teleoceras medicornutum: AMNH F:AM 115186
Teleoceras meridianum: AMNH F:AM 108341
Chilotherium wimani: HMV 0381 (Deng 2001)
Diceros gansuensis: HMV 1447 (Deng and Qiu 2007)
Diceros bicornis: USNM 240884 (Hagge 2010)

VI
Teleoceras americanum: AMNH F:AM 114417
Teleoceras brachyrhinum: AMNH F:AM 114455
Teleoceras major: AMNH F:AM 114543, 114514
Teleoceras meridianum: AMNH F:AM 108342
Aphelops mutilus: UF 115631
Acerorhinus yuanmouensis: IVPP V 18565 (Lu 2013)
Chilotherium andersoni: AMNH FM 22506, "CHINA #61"
Chilotherium wimani: HMV 0675 (Deng 2001)
Ceratotherium neumayri: AMNH FM 20582

VII
Teleoceras americanum: AMNH F:AM 115022, 115023, 114419
Teleoceras fossiger: AMNH FM 8404
Teleoceras major: AMNH F:AM 114505

Teleoceras medicornutum: AMNH F:AM 109518
Teleoceras proterum: UF 24230
Chilotherium wimani: HMV 0380 (Deng 2001)
Aphelops mutilus: AMNH F:AM 114368
Diceros gansuensis: HMV 1443 (Deng and Qiu 2007)

VIII
Teleoceras aepysoma: ETMNH 32999
Teleoceras brachyrhinum: AMNH F:AM 114449
Teleoceras fossiger: AMNH FM 8384, AMNH F:AM 104023
Teleoceras hicksi: AMNH F:AM 115786
Teleoceras major: AMNH F:AM 114494, 115509; UNSM 52232 (Hagge 2010)
Teleoceras medicornutum: AMNH F:AM 114474, 114462
Teleoceras proterum: UF 24221
Chilotherium andersoni: CHINA #74
Peraceras profectum: AMNH F:AM 114359
Plesiaceratherium gracile: S700017 (Lu et al. 2023b)
Ceratotherium neumayri: AMNH FM 20584
Rhinoceros unicornis: AMNH 54456 (Hagge 2010)
Dicerorhinus sumatrensis: FMNH 63878 (Hagge 2010)
Ceratotherium simum: AMNH 51931 (Hagge 2010)
Diceros bicornis: USNM 161925 (Hagge 2010)

IX
Teleoceras fossiger: AMNH FM 8386, 2606,
Teleoceras hicksi: AMNH F:AM 114575
Teleoceras major: AMNH F:AM 114533, 114502, 104022
Teleoceras proterum: AMNH F:AM 141390
Peraceras profectum: AMNH F:AM 114401, 114928

X
Teleoceras brachyrhinum: AMNH F:AM 114486
Teleoceras fossiger: AMNH FM 114570, AMNH F:AM 115667
Teleoceras hicksi: AMNH F:AM 114598
Teleoceras major: AMNH F:AM 114503, 42980,
Chilotherium wimani: HMV 0363 (Deng 2001)
Diceros gansuensis: HMV 1421 (Deng and Qiu 2007)

XI
Teleoceras aepysoma: ETMNH 609
Teleoceras fossiger: AMNH FM 8391
Teleoceras hicksi: AMNH F:AM 115783
Peraceras profectum: AMNH F:AM 114382
Ceratotherium neumayri: HU-2011-1 (Antoine et al. 2012)

XII
Teleoceras americanum: AMNH F:AM 114416
Teleoceras brachyrhinum: AMNH F:AM 114439, 114471
Peraceras profectum: AMNH F:AM 114390
Rhinoceros unicornis: AMNH 54454 (Hagge 2010)
Ceratotherium simum: AMNH 51856 (Hagge 2010)
Diceros bicornis: FMNH 127849 (Hagge 2010)

XIII
Teleoceras aepysoma: ETMNH 601
Teleoceras brachyrhinum: AMNH F:AM 114436
Teleoceras major: AMNH F:AM 11504,
Teleoceras meridianum: AMNH F:AM 108306
Ceratotherium neumayri: AMNH FM 22964
Diceros gansuensis: HMV 1446 (Deng and Qiu 2007)
Plesiaceratherium gracile: Values reported by Lu et al. (2020)
Dicerorhinus sumatrensis: AMNH 81892 (Hagge 2010)

XIV
Teleoceras hicksi: AMNH F:AM 114588, 114590
Teleoceras major: AMNH F:AM 104209; UNSM 52288 (Hagge 2010)
Teleoceras meridianum: AMNH F:AM 108839
Peraceras profectum: AMNH F:AM 114379
Chilotherium wimani: HMV 0060 (Deng 2001)

XV
Teleoceras brachyrhinum: AMNH F:AM 114477, 114452
Teleoceras hicksi: AMNH F:AM 114589; MRG-10-295030A (Carbot-Chanona et al. 2009)
Teleoceras major: AMNH F:AM 114508
Peraceras profectum: AMNH F:AM 114381, 114384, 114923
Aphelops mutilus: AMNH FM 17584

XVI
Teleoceras brachyrhinum: AMNH F:AM 114438, 114454
Teleoceras fossiger: AMNH FM 114566, AMNH F:AM 114526
Teleoceras hicksi: DMNH 309 (Cook 1927)
Teleoceras major: AMNH F:AM 115425, 114513
Teleoceras medicornutum: AMNH F:AM 115297
Peraceras profectum: AMNH F:AM 114378, 109360
Chilotherium wimani: HMV 0063 (Deng 2001)
Ceratotherium neumayri: AMNH FM 20679
Diceros gansuensis: HMV 1442 (Deng and Qiu 2007)

XVII
Teleoceras aepysoma: ETMNH 33000, 19280
Teleoceras americanum: AMNH F:AM 114414

Teleoceras brachyrhinum: AMNH F:AM 114437
Teleoceras fossiger: AMNH F:AM 115729
Teleoceras hicksi: AMNH F:AM 114599
Teleoceras major: AMNH F:AM 115547, 114493
Teleoceras medicornutum: AMNH FM 9832
Chilotherium andersoni: AMNH F:AM 147820, CHINA #12
Chilotherium wimani: HMV 0094 (Deng 2001)
Peraceras profectum: AMNH F:AM 108338, 114398

VITA

JOSEPH A. GAJEWSKI

Education:

M.S. Geosciences, Paleontology Concentration, East Tennessee State University, Johnson City, Tennessee, 2026

B.A. Geological Sciences, University at Buffalo SUNY, Buffalo, New York, 2023

St. Joseph's Collegiate Institute, Buffalo, New York, 2018

Professional Experience:

David B. Jones Paleontology Intern, Ashfall Fossil Beds, Royal, Nebraska, 2021

Geology/Paleontology Collections Intern, Buffalo Museum of Science, Buffalo, New York, 2022-2024

Field Crew, Elevation Science Institute for Natural History Exploration, Red Lodge, Montana, 2023

Field and Laboratory Assistant, Gray Fossil Site and Museum, Gray, Tennessee, 2025-2026

Graduate Teaching Assistant, East Tennessee State University, Johnson City, Tennessee, 2024-2026

Honors and Awards:

First Place Scholarship, 3MT Competition, East Tennessee State University, Johnson City, Tennessee, 2025

Outstanding Graduate Student in Paleontology, East Tennessee State University, Johnson City, Tennessee, 2026

Collins Chew Student Research Award, Don Sundquist Center for Excellence in Paleontology, Johnson City, Tennessee, 2025